THE INTERNATIONAL FOOD OPERATIONS & PROCESSING SIMULATION WORKSHOP

SEPTEMBER 21-23 2015
BERGEGGI, ITALY

EDITED BY
AGOSTINO BRUZZONE
FRANCESCO LONGO
RUBEN MERCADÉ – PRIETO
GIUSEPPE VIGNALI

PRINTED IN RENDE (CS), ITALY, SEPTEMBER 2015

ISBN 978-88-97999-55-3 (Paperback)
ISBN 978-88-97999-64-5 (PDF)

ISBN 978-88-97999-55-3 (Paperback)
ISBN 978-88-97999-64-5 (PDF)

THE INTERNATIONAL FOOD OPERATIONS & PROCESSING SIMULATION WORKSHOP, FOODOPS 2015

SEPTEMBER 21-23 2015, BERGEGGI, ITALY

ORGANIZED BY

DIME – UNIVERSITY OF GENOA

LIOPHANT SIMULATION

SIMULATION TEAM

IMCS – INTERNATIONAL MEDITERRANEAN & LATIN AMERICAN COUNCIL OF SIMULATION

DIMEG, UNIVERSITY OF CALABRIA

MSC-LES, MODELING & SIMULATION CENTER, LABORATORY OF ENTERPRISE SOLUTIONS

UNIVERSITY OF PARMA

MODELING AND SIMULATION CENTER OF EXCELLENCE (MSCOE)

LATVIAN SIMULATION CENTER – RIGA TECHNICAL UNIVERSITY

LOGISIM

LSIS – LABORATOIRE DES SCIENCES DE L'INFORMATION ET DES SYSTEMES

MIMOS – MOVIMENTO ITALIANO MODELLAZIONE E SIMULAZIONE

MITIM PERUGIA CENTER – UNIVERSITY OF PERUGIA

BRASILIAN SIMULATION CENTER, LAMCE-COPPE-UFRJ

MITIM - MCLEOD INSTITUTE OF TECHNOLOGY AND INTEROPERABLE MODELING AND SIMULATION – GENOA CENTER

M&SNET - MCLEOD MODELING AND SIMULATION NETWORK

LATVIAN SIMULATION SOCIETY

ECOLE SUPERIEURE D'INGENIERIE EN SCIENCES APPLIQUEES

FACULTAD DE CIENCIAS EXACTAS. INGEGNERIA Y AGRIMENSURA

UNIVERSITY OF LA LAGUNA

CIFASIS: CONICET-UNR-UPCAM

INSTICC - INSTITUTE FOR SYSTEMS AND TECHNOLOGIES OF INFORMATION, CONTROL AND COMMUNICATION

NATIONAL RUSSIAN SIMULATION SOCIETY

CEA - IFAC

UNIVERSITY OF BORDEAUX

UNIVERSITY OF CYPRUS

I3M 2015 INDUSTRIAL SPONSORS

CAL-TEK SRL

LIOTECH LTD

MAST SRL

SIM-4-FUTURE

I3M 2015 Media Partners

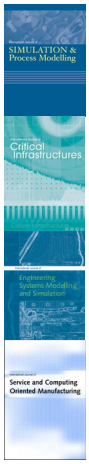

Inderscience Publishers – International Journal of Simulation and Process Modeling

Inderscience Publishers – International Journal of Critical Infrastructures

Inderscience Publishers – International Journal of Engineering Systems Modelling and Simulation

Inderscience Publishers – International Journal of Service and Computing Oriented Manufacturing

IGI GLOBAL – International Journal of Privacy and Health Information Management

Halldale Media Group: Military Simulation and Training Magazine

Halldale Media Group: The Journal for Healthcare Education, Simulation and Training

SAGE
Simulation Transaction of SCS

EUROMERCI

DE GRUYTER

DE GRUYTER
INTERNATIONAL JOURNAL OF FOOD ENGINEERING

EDITORS

AGOSTINO BRUZZONE
MITIM-DIME, UNIVERSITY OF GENOA, ITALY
agostino@itim.unige.it

FRANCESCO LONGO
DIMEG, UNIVERSITY OF CALABRIA, ITALY
f.longo@unical.it

RUBEN MERCADÉ – PRIETO
SOOCHOW UNIVERSITY, CHINA
ruben@suda.edu.cn

GIUSEPPE VIGNALI
UNIVERSITY OF PARMA, ITALY
giusppe.vignali@unipr.it

.

THE INTERNATIONAL MULTIDISCIPLINARY MODELING AND SIMULATION MULTICONFERENCE, I3M 2015

GENERAL CO-CHAIRS

AGOSTINO BRUZZONE, *MITIM DIME, UNIVERSITY OF GENOA, ITALY*
YURI MERKURYEV, *RIGA TECHNICAL UNIVERSITY, LATVIA*

PROGRAM CO-CHAIRS

FRANCESCO LONGO, *DIMEG, UNIVERSITY OF CALABRIA, ITALY*
EMILIO JIMÉNEZ, *UNIVERSITY OF LA RIOJA, SPAIN*

THE INTERNATIONAL FOOD OPERATIONS & PROCESSING SIMULATION WORKSHOP, FOODOPS 2015

GENERAL CO-CHAIRS

GIUSEPPE VIGNALI, *UNIVERSITY OF PARMA ITALY*
RUBEN MERCADÈ - PRIETO, *SOOCHOW UNIVERSITY, CHINA*

PROGRAM CHAIR

FRANCESCO LONGO, *DIMEG, UNIVERSITY OF CALABRIA, ITALY*

FoodOPS 2015 International Program Committee

Eleonora Bottani, *University of Parma, Italy*
Agostino Bruzzone, DIME, *University of Genoa, Italy*
Xiao Dong Chen, Soochow University, China
Andrea Grassi, *University of Modena and Reggio Emilia, Italy*
Michel Havet, *GEPEA research unit, France*
Francesco Longo, *MSC-LES, University of Calabria, Italy*
Marina Massei, *Liophant Simulation, Italy*
Francesco Marra, *University of Salerno, Italy*
Ruben Mercade Prieto, *Soochow University, China*
Roberto Montanari, *University of Parma, Italy*
Letizia Nicoletti, *Cal-Tek Srl, Italy*
Tomas Skoglund, *Tetrapak, Sweden*
Giuseppe Vignali, *University of Parma, Italy*
Jack Vander Vorst, *ORL Group - Wageningen Universiteit, NL*
Mustafa Tahsin Yilmaz, *Yildiz Teknik Üniversitesi, Turkey*

Tracks and Workshop Chairs

Liquid Food Processing
Chairs: Tomas Skoglund, Tetrapak, Sweden

Simulation of Food Supply Chain
Chairs: Jack Vander Vorst, ORL Group - Wageningen Universiteit, NL

Modelling and Simulation of food processing
Chairs: Michel Havet, GEPEA research unit, France

Modelling and Simulation of food properties
Chairs: Mustafa Tahsin YILMAZ, Yildiz Teknik Üniversitesi, Turkey

Sustainability of Food processes
Chairs: Giuseppe Vignali, University of Parma, Italy

Modelling and simulation of food fouling and cleaning techniques
Chairs: Ruben Mercade Prieto, Soochow University, China

Modeling of transport phenomena in food processes assisted by microwaves and radio-frequencies
Chairs: Francesco Marra, University of Salerno, Italy

CHAIRS' MESSAGE

On behalf of the Organization Committee, we would like to welcome and thank all the people who have contributed to the First edition of "The international Food Operations & Processing Simulation Workshop" (FoodOPS 2015). In this first edition FoodOPS workshop is intended to extend a track we managed in last years for the I3M conference on "Modelling and Simulation of Food Processing and Operations" bringing new ideas, solutions, approaches and plenty more. The aim of this initiative is to promote the particular nature of the food sector, being able, at the same time, to integrate new perspectives and raise new challenges.

FoodOPS Workshop offers the possibility to present results and critical issues concerning processes design and operations management in food industry using Modeling and Simulation as methodological approach. Nevertheless, different topics concerning processes and operations management in food industry has been well-accepted. We received high-quality, original scientific contributions and we will also consider them for publication in a Special Issue on the ISI indexed Journal "International Journal of Food Engineering". To this end, we would like to thank you the Editor in Chief of this prestigious Journal, Prof. Dong Chen, who agreed to support this workshop on this particular field also by contacting the Associate editor Ruben Mercade Prieto, who agreed to be here as "General Co-Chair" of the workshop.

Based on the peculiarities of the Food modelling and simulation sector, the scientific committee structured the workshop on 4 tracks dealing with:

1. Simulation of Food Supply Chain
2. Modelling and Simulation of food processing
3. Modelling and Simulation of food properties
4. Sustainability of Food processes

As regard to these topics, FoodOPS 2015 is an opportunity to meet and discuss and create new opportunities for cooperation and also joint research projects. FoodOPS 2015 is co-located with the I3M 2015 multi-conference, that includes 8 additional international conferences, in the wonderful location of Bergeggi, Italian Riviera. We would like to wish to all the FoodOPS and I3M attendees a fruitful conference and a wonderful stay in Bergeggi.

Giuseppe Vignali
University of Parma
Italy

Rubers Mercadé-Prieto
Soochow University
China

Francesco Longo
University of Calabria
Italy

ACKNOWLEDGEMENTS

The FoodOPS 2015 International Program Committee (IPC) has selected the papers for the Conference among many submissions; therefore, based on this effort, a very successful event is expected. The FoodOPS 2015 IPC would like to thank all the authors as well as the reviewers for their invaluable work.
A special thank goes to all the organizations, institutions and societies that have supported and technically sponsored the event.

I3M 2015 INTERNAL STAFF

AGOSTINO G. BRUZZONE, *DIME, UNIVERSITY OF GENOA, ITALY*
MATTEO AGRESTA, *SIMULATION TEAM, ITALY*
TERESA BARBIERI, *CAL-TEK SRL, ITALY*
CHRISTIAN BARTOLUCCI, *SIMULATION TEAM, ITALY*
LUIGI BRUNO, *DIMEG, UNIVERSITY OF CALABRIA*
ALESSANDRO CHIURCO, *DIMEG, UNIVERSITY OF CALABRIA, ITALY*
MARIO COSENTINI, *CAL-TEK SRL, ITALY*
RICCARDO DI MATTEO, *SIMULATION TEAM, ITALY*
CATERINA FUSTO, *DIMEG, UNIVERSITY OF CALABRIA, ITALY*
FRANCESCO LONGO, *DIMEG, UNIVERSITY OF CALABRIA, ITALY*
GIANLUCA MAGLIONE, *CAL-TEK SRL*, ITALY
MARINA MASSEI, *LIOPHANT SIMULATION, ITALY*
LETIZIA NICOLETTI, *CAL-TEK SRL*
ANTONIO PADOVANO, *DIMEG, UNIVERSITY OF CALABRIA, ITALY*
ALBERTO TREMORI, *SIMULATION TEAM, ITALY*
MARCO VETRANO, *CAL-TEK SRL, ITALY*

This International Workshop is part of the I3M Multiconference: the Congress leading **Simulation around the World and Along the Years**

Index

CFD ANALYSIS OF COFFEE PACKAGING IN CAPSULES USING GAS FLUSHING MODIFIED ATMOSPHERE PACKAGING

Simone Spanu[(a)], Giuseppe Vignali[(b)]

[(a)]CIPACK Interdepartmental Center, University of Parma, Parco Area delle Scienze 181/A, 43124 Parma (Italy)
[(b)]Department of Industrial Engineering, University of Parma, Parco Area delle Scienze 181/A, 43124 Parma (Italy)

[(a)]simone.spanu@nemo.unipr.it, [(b)]giuseppe.vignali@unipr.it

ABSTRACT

The aim of this work is to analyze, by means of CFD, the gas flow in a packaging machine used to fill polymeric capsules with coffee. The final goal is to optimize the geometric shape of some of the mechanical components in the machine's sealing station in order to reduce inert gas consumption (N_2 in this case) and, at the same time, achieve an O_2 residual which is constantly equal or below 1% by mass in the center of the capsule.

The fluid domain has been obtained starting from the 3D CAD model of the sealing station of the packaging machine. The CAD software SolidWorks (version 2014) has been used to design the system, while Ansys CFX 14.5 software has been used for the CFD analysis.

The CFD model has been validated by comparing the simulation results with those obtained by experimental tests. The modified solution allows reducing the O2 residual from almost 3% to less than 1%.

Keywords: CFD, Food Packaging, Modified Atmosphere Packaging, Gas Flushing

1. INTRODUCTION

Modified Atmosphere Packaging (MAP) is a packaging technique which implies the addition (or removal) of gases from storage rooms, transportation containers or packages in order to manipulate the level of gases such as oxygen, carbon dioxide, nitrogen, ethylene etc., and achieve an atmospheric composition different to that of normal air around the food (Floros 1990). This technique is used generally to enhance the shelf-life of food products or to preserve their organoleptic features.

Nowadays MAP is an important part of food industry and it is used especially in the processing of fresh products such as fruits and vegetables, fish and fresh meat, or in the processing of products which have to maintain unaltered for a long period of time their aromatic features such as coffee, tea or spices.

MAP is nowadays frequently used in the packaging of coffee in capsules. Today, in fact, the demand of coffee packaged in capsules is constantly increasing, enhancing the attention in product quality. To fulfill the coffee quality requirements, producers started to ask for coffee packaging lines, which are able to minimize the O_2 residual inside the capsules. A low oxygen level in capsules help limiting the oxidation process of the final product, thus enhancing its shelf-life and reducing the organoleptic alteration of coffee. Some systems could be used to achieve this goal, such as: vacuum filling, vacuum filling with inert gas injection and many others. Among these techniques the most used is the gas flushing Modified Atmosphere Packaging. According to this method the capsule is fluxed with an inert gas before the filling phase until the sealing phase, to remove air from the inner side of the capsule itself and consequently reducing the O_2 residual in the closed package. The inert gases usually used for these purposes are N_2, CO_2, Argon or mixtures of them.

To make modified atmosphere packaging effective, three conditions must be satisfied:

1. the packaging phase must be preceded by a correct coffee degassing process, in order to minimize the quantity of air blocked in the coffee itself;
2. the packaging phase needs a very effective monitoring to be sure that air is completely removed by the capsules and Nitrogen is instead inside them;
3. the capsule and closing material must have a low permeability, in order to limit the permeation of the inert gas through the package wall (aluminium or multilayer polimeric films are usually used in this case).

The third point attends to technological aspects of the container manufacturers, while the first one attends to the food equipment manufacturer, whilst the second one is on the responsibility of food packaging manufacturer.

Considering its importance, MAP is now studied in a more methodical way, also by means of advanced techniques as CFD (Computational Fluid Dynamics). This tecnique was in particular adopted in the design of postharvest facilities or cooling facilities for the storage of fruits and vegetables (Delele et al., 2011 and Ferrua et al., 2008); recently it has also been used to investigate mass and heat transfer of bio-substrates in modified atmosphere packaging (De Bonis et al., 2013) or to

evaluate the losses of CO_2 through a PET bottle containing a carbonated beverage (Carrieri et al., 2011). Nevertheless, CFD has never been used to evaluate the flow of gas in packaging machines and as a tool to optimize the packaging process.

Aim of this work is then to analyze, by means of CFD, the gas flushing of N_2 on a coffee in capsules packaging machine in order to optimize the geometric shape of some of the mechanical components in the sealing station of the machine itself. The new configuration should allow reducing inert gas consumption and, at the same time, achieving an O_2 residual in the center of the container which is constantly equal or below 1% by mass.

2. MATERIALS AND METHODS

Based on what stated in the introduction about the influence of the coffee degassing phase, both in the simulation and in the subsequent experimental phase the capsules were left empty in order to avoid the influence of the coffee degassing process on the results (since its accuracy could not be monitored).

2.1. Equipment

The coffee packaging machine is made by a conveyor belt which moves in a discontinuous way (one step every 0.4s). On all the elements composing the conveyor belt are present four holes and in every hole is housed a little basket which contains a capsule. The conveyor belt advances and stops at every station present on the packaging line. In particular, four station are present:

1. a filling station, where the capsules are filled with coffee;
2. an aspiration station, where coffee powder is aspirated from the edge of every capsule in order to facilitate the following sealing operation;
3. a station where a micro-perforated film is placed on the "free surface" of coffee;
4. a sealing station, where the capsules are closed with a polymeric or aluminium lid.

The second station is not always activated, depending on coffee granulometry.

From immediately before the filling station, to the sealing station, there is a tunnel where it is fluxed nitrogen gas in order to saturate the environment and remove air that may cause an excessive O_2 residual inside the closed package.

This packaging lines can produce more than 340 capsules per minute. The overall dimensions of the packaging machine are 4690 x 555 x 1340 mm.

Figure 1 shows a block diagram which resumes the functioning of the previously described packaging line.

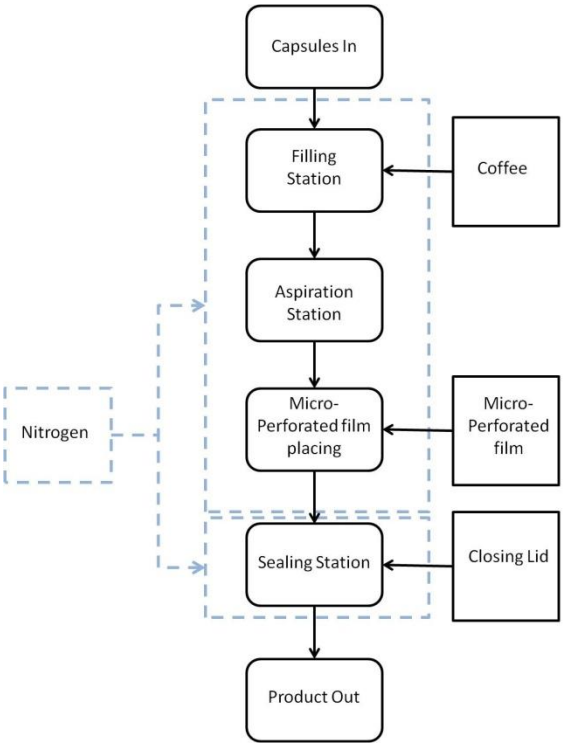

Figure 1:block diagram of the coffee packaging line considered in this study

As previously explained, the CFD analysis has been focused only on the sealing station of the packaging machine. The reason is that this is the area where the N_2 flow rate is higher. In Figure 2 is shown a 3D simplified geometry of the capsules' sealing station.

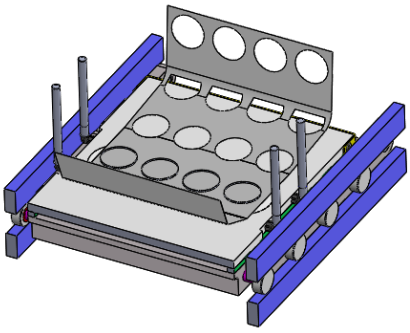

Figure 2: capsules' sealing station

The main components present in this station are: a stainless steel plate, within which a groove for the distribution of gaseous N_2 is formed by milling, four diffuser rings, which address N_2 inside the capsules, four small pipes (internal diameter equal to 8 mm) which direct N_2 flow inside the groove realized in the plate, the closing lid and, finally, four electric heaters welding the lid on the capsules' edge. Figure 3 shows a section of the stainless steel plate.

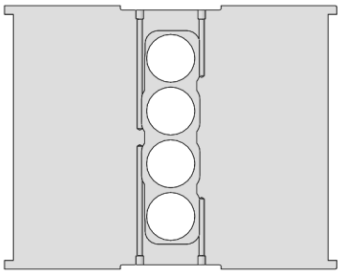

Figure 3: plate section

The one just outlined is the original configuration of the sealing station, which is currently installed on the packaging line. In addition to this, a modified station has been analyzed.

After the modeling phase, the simulations will be validated with an experimental phase. Both in the simulations and in the experimental phase. The considered capsule is the model "Blue", made by Lavazza, which has a truncated-cone shape, with a maximum diameter of 40 mm, a minimum diameter of 32 mm and an overall height of about 26 mm. It is important to specify the capsule's model because from it depends the kind of diffuser ring that has to be mounted.

After the validation of the CFD model some simulation with other two kind of capsule that the packaging line can process have been performed. The involved capsules model are "A Modo Mio", made by Lavazza and a Nespresso-Like capsule. The first one has a maximum diameter of 40 mm, a minimum diameter of 32 mm and an overall height of 17 mm, while the second one has a maximum diameter of 30 mm, a minimum diameter of 15.7 mm and an overall height of 28 mm.

Based on the obtained results some changes in the shape of the plate will be made and tested.

2.2. CFD Modelling

To set up the physics and solve the calculation, Ansys CFX version 14.5 has been used, because this software allows to simulate multi-component fluids. In fact, a 3D multi-component simulation has been set up, considering a gas mixture of Argon, N_2 and O_2.

In a mixture each component has its own equation for conservation of mass. After Reynolds-Averaging it can be expressed as:

$$\frac{\delta\tilde{\rho}_i}{\delta t} + \frac{\delta\left(\tilde{\rho}_i\,\tilde{U}_j\right)}{\delta x_j} = -\frac{\delta}{\delta x_j}\left[\rho_i\left(\tilde{U}_{ij} - \tilde{U}_j\right) - \overline{\rho_i'' U_f''}\right] + S_i \quad (1)$$

where:

$\tilde{\rho}_i$ is the mass-average density of fluid component i in the mixture

$\tilde{U}_j = \sum \frac{\left(\tilde{\rho}_i\,\tilde{U}_{ij}\right)}{\bar{\rho}}$ is the mass-average velocity field,

$\tilde{U}_{ij}$ is the mass-average velocity of fluid component i,

$\rho_i\left(\tilde{U}_{ij} - \tilde{U}_j\right)$ is the relative mass flux,

S_i is the source term for component i which includes the effects of chemical reactions.

The mixture, instead, is generally treated as an "Ideal Mixtures", meaning that its properties are calculated directly by means of a mass averaging of the component materials properties. Thus, for instance, the mixture density ρ can be calculated from the mass fraction Y_i and the thermodynamic density of each component ρ_i by means of equation 2.

$$\frac{1}{\rho} = \sum_{i=A,B\ldots}^{N_C} \frac{Y_i}{\langle\rho_i\rangle} \quad (2)$$

In the mixture, N_2 has been considered as constraint component, meaning that its mass fraction is calculated to ensure that all the component mass fraction sum to unity in every instant. This means that the mass fraction of nitrogen is set equal to the total mass fraction of the other components in the Ideal Mixture subtracted from unity.

The full buoyancy model has been implemented in the domain, to consider motion due to density differences and a heath exchange model has been considered, to take account of the heath generated by the electrical resistances used to fix the closing lid over the capsules. In particular, the "Total Energy" model has been adopted, which is usually recommended by Ansys CFX solver theory guide and Ansys CFX solver modeling guide when dealing with flow of compressible substances.

Furthermore, the Shear Stress Transport turbulence model has been adopted. The SST model, proposed by Menter (1994), is an eddy-viscosity model, which is a combination of a k-ω model and k-ε model. The first is used in the inner boundary, while the second in the outer region and outside of the boundary layer (Bottani et al, 2008). The SST model has been used in order to overcome the problems of both the methods. These features make the SST model more accurate and reliable for a wider class of flows than the standard k-ω and k-ε models.

2.2.1. Mesh setting for the fluid domain

The fluid domain has been obtained starting from the 3D CAD model of the sealing station by means of the CAD software SolidWorks (version 2014), while the discretization of the fluid domain has been performed using the software Icem CFD version 14.5.

The mesh was initially set by creating a uniform subdivision, and then thickened in the critical areas of the fluid volume. In particular, a finer mesh was used near the capsules, in the groove realized inside the stainless steel plate and near the diffuser rings which address the N_2 flow inside the containers.

At the end of the operation, an unstructured grid with a total of 4,700,000 nodes and 27,600,000 tetrahedrons was obtained.

Figure 4 shows a section of the obtained volume mesh.

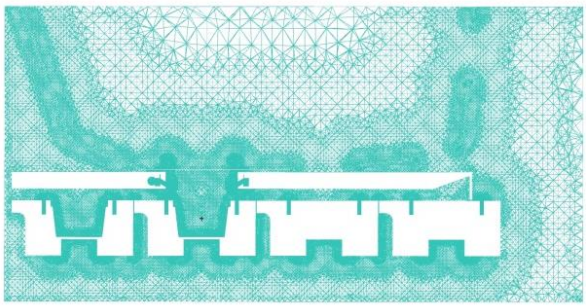

Figure 4: section of the fluid domain volume mesh

2.2.2. Simulation setting

A 3D multi-component simulation has been set up considering a gas mixture of Argon, N_2 and O_2. These three substances were considered as ideal gases, while the mixture has been set as "Ideal Mixture". N_2 has been used as constrain component, meaning that its mass fraction is set equal to the total mass fraction of the other components in the Ideal Mixture subtracted from unity.Since Argon Ideal Gas is not present in Ansys CFX material library it has been created using the settings showed in Table 1.

Table 1: Argon ideal gas settings

Argon Ideal Gas Settings	
Thermodynamic State	Gas
Equation of State	Ideal Gas
Molar Mass	$39.948 \frac{g}{mol}$
Specific Heat Capacity	$520 \frac{J}{kg\,K}$
Specific Heat Type	Constant Pressure
Reference Temperature	25 °C
Reference Pressure	1 atm
Dyamic Viscosity	2.217e-05 Pa·s
Thermal Conductivity	$0.016 \frac{w}{m\,K}$

At the beginning of the simulation the fluid domain has been considered, in order to simulate air presence, as composed by 21% of O_2, 1% of Argon and 78% of N_2, while on the inlets only nitrogen was considered.

The boundary and initial condition for the original case are shown in Table 2.

Table 2: boundary and initial conditions for original case

Original Case Buondary Conditions	
Inlet_1; Inlet_2; Inlet_3; Inlet_4	Volumetric Flow-Rate = 20 l/min T = 25°C
Opening	Composition: 1% Ar, 78% N_2, 21% O_2 T = 25°C p = 1 bar
Resistenze	Free Slip Wall T = 90°C
Wall	Free Slip Wall Adiabatic
Original Case Initial Conditions	
Domain Composition	1% Ar, 78% N_2, 21% O_2
Velocity	0 m/s
T	25°C
p	1 bar

The simulations have been performed both in steady state and both in transient mode because the flow of N_2 is not time dependent but the capsules stay in the sealing station only for a fixed period of time (0.4s). In particular, in transient mode, 4s have been simulated with a time step of 0.02 s. The results have been checked at 0.4s.

2.3. Experimental Method

To validate the CFD model some experimental tests have been performed on the packaging machine object of this study. In particular, the machine with the new plate has been tested.

As previously stated, the capsules considered during experimental phase were the "Blue" model and they were left empty, so the coffee dosing system has been excluded from the machine configuration. Furthermore also the tunnel has been excluded, in order to evaluate only the effects of gas flushing in the sealing station.

The sensor used in the tests was Dansensor CheckPoint, especially created to evaluate O_2 or CO_2 concentration in the headspace of containers processed in modified atmosphere. This sensor has a needle which must be inserted in the closed package. From the needle a small quantity of the internal gas mixture is aspired and then the probe evaluates the O_2 concentration in the mixture.

Before the test, few packaging cycles have been performed, in order to reach steady state condition in the flux of N_2.

The respected experimental procedure is the following:

1. execution of the packaging cycle;
2. taking of the capsules coming out from the packaging line;
3. placing on the capsules closing lid of a small piece of adhesive rubber, so to avoid the flow

of external air in the container during the perforation;
4. introduction of the sensor's needle;
5. test execution;
6. writing of the value of O_2 residual showed by sensor's monitor.

Before tests' execution is important to check the correct calibration of the sensor, measuring various time the O_2 concentration of the air around the sealing station and verifying that the showed value is always close to 21%.

3. RESULTS AND DISCUSSION

3.1. CFD simulation of the original case

With the "probe" tool in post process section of the used CFD code, that allows to measure the value of a given parameter in a specified point of the fluid domain, the O_2 residual in the geometrical center of each capsule.

The detected values are shown in Table 3.

Table 3: O_2 residual in capsules' center for current configuration

O_2 Residual in Capsules' Center		
Capsule	**N_2 Concentration**	**O_2 Residual**
Capsule 1	90.66 %	1.96 %
Capsule 2	83.51 %	3.46 %
Capsule 3	83.59 %	3.45 %
Capsule 4	90.88 %	1.92 %
Mean O_2 Residual		2.70 %

As can be noticed from the previous Table, in each capsule O_2 residual is higher than the target value of 1% and the mean O_2 residual is equal to 2.70%. It is interesting to note also that the two capsules located in the center position of the conveyor belt (indicated with Capsule 2 and Capsule 3) reach a lower N_2 concentration and consequently show a higher O_2 residual. Figure 5 shows the O_2 concentration inside Capsule 2.

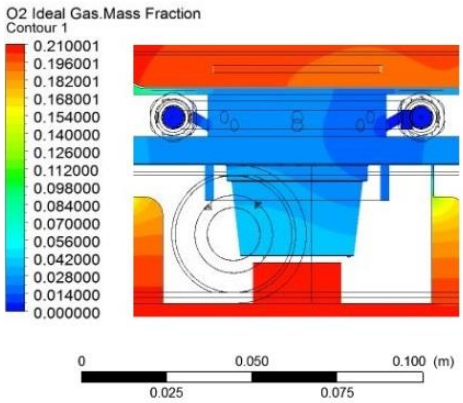

Figure 5: O_2 mass fraction inside one of central capsules

Streamlines have been analyzed too. In fact they represent the preferred trajectories of gas particles therefore their visualization could be useful to identify any N_2 leakage points. Figure 6 provides an illustration of the fluid streamlines within the domain.

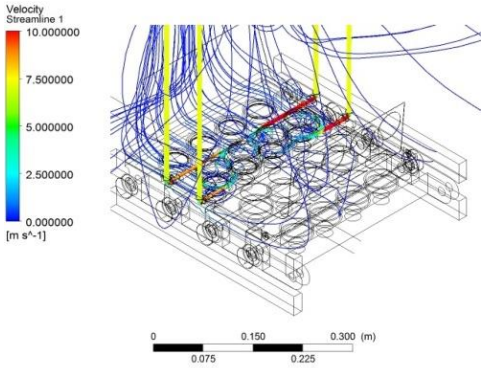

Figure 6: streamlines within the domain

It was not found any particular point of leakage, with the exception of the connecting zone between the sealing station and the tunnel, where there is the N_2 flushing with previously mentioned. This zone was however not considered like a real leakage point since the gas flowing out from here is not lost but goes inside the tunnel and thus contributes anyhow to the effectiveness of the packaging process.

Other analyzed results (respectively shown in Figure 7 and Figure 8) are the absolute pressure and the velocity distribution inside the groove for N_2 distribution, in order to observe the conditions which lead to the O_2 residuals indicated in Table 1.

In particular it has been noticed that the pressure distribution inside the groove is not perfectly homogeneous and that low velocities especially near the holes which address N_2 in the capsules. This may be the cause of the higher O_2 residual detected in the central capsules.

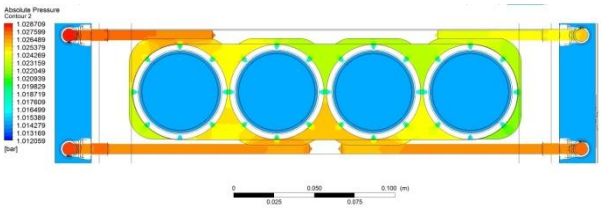

Figure 7: absolute pressure inside groove for N_2 distribution (original case)

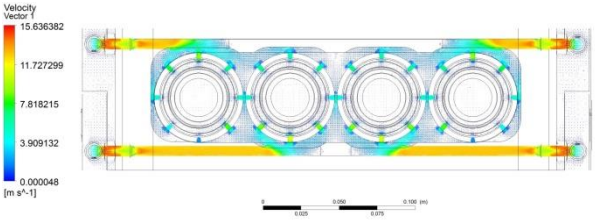

Figure 8: velocity vectors inside groove for N_2 distribution (original case)

3.2. Experimental phase validation

The CFD model has been validated with an experimental phase, which has been performed on the described packaging machine.

The followed experimental procedure is the one described in paragraph 2.3. Table 4 shows tests' results.

Table 4: experimental validation results

Experimental Tests Results				
Test no.	**Capsule**	**O_2 Residual [%]**	**N2 Flow-Rate [l/min]**	**Pressure [bar]**
1	1	2.1	80	2.5
	2	3.4		
	3	3.6		
	4	1.9		
2	1	1.8	80	2.5
	2	4.0		
	3	3.7		
	4	2.0		
3	1	2.1	80	2.5
	2	3.5		
	3	3.7		
	4	2.0		

The experimental validation phase showed good agreement between CFD model and the real case.

3.3. Design of a new N_2 distribution system

Considering the results obtained with the first CFD simulation and during the model validation phase a new N_2 distribution system has been developed. In particular, the main variation is in the shape of the groove realized within the plate. A section of the new plate is shown in Figure 9.

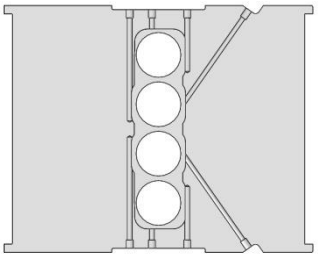

Figure 9: new plate section

As can be noticed from the previous picture the introduced changes have resulted in an increase in the number of N_2 inlet points (from 4 to 8).

After obtaining a new fluid domain a CFD simulation of the modified case has been set up. For the mesh generation the settings described in paragraph 2.2.1 have been adopted, while boundary and initial conditions are the same of the ones shown in Table 1, except for the Inlets. In fact, as previously explained, with the new plate eight Inlets are present thus on each one of them a Volumetric Flow-Rate of 10 l/min, and a Temperature of 25°C have been fixed, in order to keep the total flow rate constant.

3.4. CFD simulation of the new case

The results obtained for O_2 residual with the new plate are shown in Table 5.

Table 5: O_2 residual in capsules' center for new configuration

O_2 Residual in Capsules' Center				
Capsule	**N_2 Concentration**	**O_2 Residual**	**Increase in N_2 Conc.**	**Decrease in O_2 Residual**
Capsule 1	96.44 %	0.75 %	6.4 %	- 61.7 %
Capsule 2	97.34 %	0.56 %	16.6 %	- 83.8 %
Capsule 3	97.42 %	0.55 %	16.5 %	- 84.1 %
Capsule 4	96.25 %	0.78 %	5.6 %	- 59.4 %
Mean O_2 Residual		0.66 %		
Mean Increase in N_2 Conc.			11.28 %	
Mean Decrease in O_2 Residual				- 72.25 %

As can be noticed from previous Table, the introduced changes allow to reach the target goal of an O_2 residual lower than 1% by mass. In particular the new configuration shows a mean decrease in O_2 residual of - 72.25 %, allowing to reach a mean O2 residual of 0.66% (max residual 0.78 %). Furthermore, with this configuration the most disadvantaged capsules are no longer the ones in central position but are Capsule 1 and Capsule 4.

Also in this case, absolute pressure and velocity distribution inside the groove realized within the plate have been analyzed (respectively Figure 10 and Figure 11).

In particular it has been noticed a more homogeneous pressure distribution, with values closer to atmospheric pressure and higher velocity values in correspondence of some of the injection holes (maximum velocity of about 16 m/s).

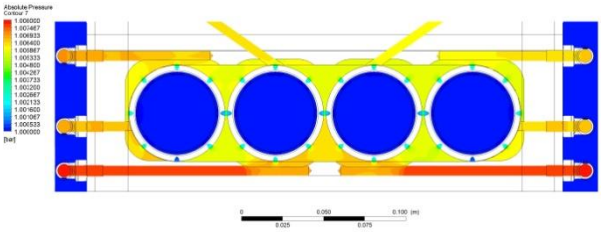

Figure 10: absolute pressure distribution inside groove for N_2 distribution (modified case)

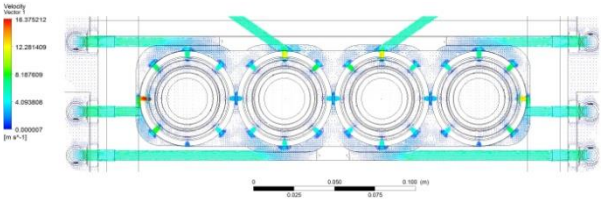

Figure 11: velocity vectors inside groove for N_2 distribution (modified case)

Clearly, maintaining the total flow-rate constant but increasing the number of inlets, N_2 velocity inside the distribution pipes is lower than in the original case,

and also this fact can be noticed comparing Figure 9 and Figure 11.

3.5. Experimental phase results

As previously stated, experimental tests have been executed also on the new configuration of the packaging machine, in order to validate the CFD model.

The followed experimental procedure has been described in paragraph 2.3. Table 6 shows tests' results.

Table 6: experimental phase results

Experimental Tests Results				
Test no.	**Capsule**	**O_2 Residual [%]**	**N2 Flow-Rate [l/min]**	**Pressure [bar]**
1	1	0.5	80	1.8
	2	0.4		
	3	0.4		
	4	0.4		
2	1	1.80	80	2.1
	2	0.7		
	3	0.7		
	4	1.0		
3	1	0.6	80	2.5
	2	0.6		
	3	0.6		
	4	0.7		

The experimental tests, especially test no. 3, show a good correspondence between CFD modeling and experimental phase.

3.6. Other CFD simulations

The CFD simulations with the other type of capsules have been performed only in steady state mode.

The O_2 residual results are presented in Table 7 for the model "A Modo Mio" and in Table 8 for the Nespresso-Like capsule.

Table 7: O_2 residual in "A Modo Mio" capsules' center

O_2 Residual in Capsules' Center		
Capsule	**N_2 Concentration**	**O_2 Residual**
Capsule 1	96.55 %	0.73 %
Capsule 2	97.63 %	0.49 %
Capsule 3	96.94 %	0.64 %
Capsule 4	96.65 %	0.71 %
Mean O_2 Residual		0.643 %

Table 8: O2 residual in capsules' center for Nespresso-Like capsules

O_2 Residual in Capsules' Center		
Capsule	**N_2 Concentration**	**O_2 Residual**
Capsule 1	94.15 %	1.22 %
Capsule 2	95.08 %	1.03 %
Capsule 3	95.27 %	0.98 %
Capsule 4	95.06 %	1.04 %
Mean O_2 Residual		1.068 %

In Figure 12 is compared the O_2 mass fraction inside the container for this two kind of capsules.

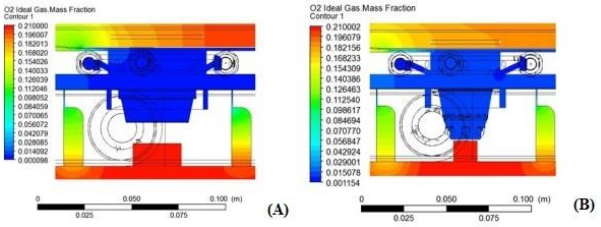

Figure 12: O_2 mass fraction inside one of central capsules for the model "A Modo Mio" (A) and the Nespresso-Like capsule (B)

4. CONCLUSIONS

Modified atmosphere packaging of coffee in capsule is increasingly used because producers need to preserve as long as possible final product quality. In particular it is increasingly felt the need to obtain a O_2 residual in the head space of containers equal to or less than 1% by mass. Thus, the aim of this work was to optimize, by means of CFD analysis, the geometrical shape of some components in the sealing station of a coffee packaging machine, in order to achieve the desired O_2 residual with an equal or lower inert gas (N_2 in this case) consumption. In particular, it has been modified a groove realized within a stainless steel plate which composes the sealing station of the machine and that is used for N_2 distribution. To avoid the need to consider the effectiveness of the coffee degassing process capsules were considered empty. The model of the capsule used in the simulation is "Blue", produced by Lavazza.

The original configuration of the packaging machine was first simulated, using the plate currently installed, showing how this design could not allow to reach an O_2 residual lower than 1% for each capsule. In particular a mean residual of 2.70 % was detected for the simulation.

The CFD model has been validated with an experimental phase, executed on the packaging machine with the old plate installed on it. The tests showed a good correspondence between simulations and experimental data.

Subsequently, it has been simulated the new configuration of the packaging line, with the modified

plate installed. This analysis showed how the new plate can allow to reach the prefixed goal: in fact, a mean O_2 residual of 0.66 % has been detected for the simulation, which means that the introduced changes have led to a mean decrease in unwanted gas residuals of - 72.25 %. Thus it is confirmed that the new sealing station is more effective in reaching a low level of O_2 residual than the previous one.

Other two simulations have been performed in order to analyze if the introduced changes were effective also with other capsules models which can be processed by the machine object of this study. The analyzed capsules in this case were the model "A Modo Mio", made by Lavazza, and a Nespresso-Like capsule. In the first case a mean O_2 residual of 0.643% has been obtained, while in the second case the mean O_2 residual was equal to 1.068%.

These new simulations also have highlighted a correlation between the capsule shape and the level of O_2 residual that can be reached. In particular it has been noticed that higher is the capsule height, harder is to reach a low level of O_2 residual and that smaller is the capsule diameter, harder is to reach a low residual.

Future researches could be addressed to improve the CFD simulation process and make the analysis more accurate, adding a moving mesh, in order to take account of the motion of the conveyor belt.

REFERENCES

ANSYS CFX-solver modeling guide, release 14.0. ANSYS, Inc. Southpointe 275 Technology Drive, 2011.

ANSYS CFX-solver theory guide, release 14.0. ANSYS, Inc. Southpointe 275 Technology Drive, 2011.

Bottani E., Rizzo R., Vignali G., 2008. Numerical Simulation of Turbulent Air Flows in Aseptic Clean Rooms. Recent Advances in Modeling and Simulation. pp. 633-650.

Carrieri G., De Bonis M.V., Ruocco G., 2012. Modeling and experimental validation of mass transfer from carbonated beverages in polyethylene terephtalate bottles. Journal of Food Engineering 108:570-578.

Delele M.A., Vostermans B., Creemers P., Tsige A.A., Tijskens E., Schenk A., Opara U.L., Nicolaï B.M., Verboven P., 2012. CFD model development and validation of a thermonebulisation fungicide fogging system for postharvest storage of fruit. Journal of Food Engineering 108:59-68.

De Bonis M.V., Cefola M., Pace B., Ruocco G., 2013. Mass and heat transfer modeling of bio-substrates during packaging. Heat and Mass Transfer 49 (6):799-808.

Ferrua M.J., Singh R.P., 2009. Modeling the forced-air cooling process of fresh strawberry packages, Part I: Numerical model. International Journal of Refrigeration:335-348.

Floros J.D, 1990. Controlled and modified atmospheres in food packaging and storage. Chemical Engineering Progress 86, Issue 6:25-32.

AUTHORS BIOGRAPHY

Simone SPANU is a scholarship holder at Interdepartmental Center CIPACK of the University of Parma. In Match 2014 he has achieved a master degree in Mechanical Engineering for the Food Industry at the same university. His main fields of research concern food process modelling and simulation, with a particular focus on the CFD simulation for the advanced design of food and beverage processing plants.

Giuseppe VIGNALI is an Associate Professor at University of Parma. He graduated in 2004 in Mechanical Engineering at the University of Parma. In 2009, he received his PhD in Industrial Engineering at the same university, related to the analysis and optimization of food processes. Since August 2007, he worked as a Lecturer at the Department of Industrial Engineering of the University of Parma. His research activities concern food processing and packaging issues and safety/security of industrial plant. Results of his studies related to the above topics have been published in more than 60 scientific papers, some of which appear both in national and international journals, as well in national and international conferences.

DYNAMIC FREIGHT FLOW MODELLING FOR RISK EVALUATION IN FOOD SUPPLY

Andreas Balster[(a)], Hanno Friedrich[(b)]

[(a),(b)] Technische Universität Darmstadt, Institute for Traffic and Transport, 64287, Darmstadt, Germany

[(a)]balster@verkehr.tu-darmstadt.de, [(b)]friedrich@verkehr.tu-darmstadt.de

ABSTRACT

The research presented in the paper defines a new dynamic model of food supply. The model includes 51 food categories including four different temperature ranges. It differentiates between the different actors in a supply chain: food producers, food retailers, wholesalers, logistics service providers, and the consumer. It works on an aggregate level of 402 regions within Germany as well as the most important trading nations. In the model, inventories for every food category, every group of actors, and every region are recorded in a single data cube. This data cube is recalculated incrementally every day, considering the production, relocation of food products, and consumption. Gravity models calibrated with data of the Federal Transport Plan generate the aggregate commodity flows between the regions. A detailed sectorial input output model for food is calculated for the year 2012 based on data from public authorities, food-related associations, and professional data providers.

Keywords: risk evaluation, simulation, German food supply, freight transport modelling

1. INTRODUCTION

This paper introduces a new concept of modelling dynamic commodity flows in supply networks. Where supply relations exist, commodities flow between locations from production via processing and distribution to the points of sale. These commodity flows are modelled for all supply relations of all companies of one specific sector on a national level. The dynamic aspect of the commodity flows is realized by modelling changeable relations between the different locations as well as by modelling the chronological sequence of production and transportation.

The modelling of dynamic commodity flows is necessary for the risk assessment of supply networks because in supply networks processing depends on the availability of preliminary products. If a supplying location fails or a connection gets disrupted, the affected actors in the supply network have to react in order to keep their production running. For example, commodity flows have to be rerouted, new connections have to be established, or safety stocks have to be used. The better a supply network can react to disruptions the more agile it is, lowering the risk of a supply shortfall. The measurement of risk and agility is of growing importance because increasingly widespread supply networks are prone to specific kinds of risks. In addition, principles like lean, where amongst others safety stocks are reduced, are intensifying this need.

The concept of modelling dynamic commodity flows presented in this paper has the ability to meet this claim by mapping the agile supply network and its evasive reactions to disruptions on a detailed level. In the following sections, the concept is explained with a test case and first results are shown. The food supply sector in Germany is chosen as the test case. It is one of the most important sectors because it is the foundation for the life of the population. Since food supply shortfalls could endanger the lives of many people, risks have to be identified correctly and possible reactions have to be planed accordingly.

2. METHODOLOGY

The model consists of four tiers representing the supply chain: agricultural production, processing, warehousing, and consumption. It covers the German land area divided into 402 NUTS3-regions. In these 402 regions the most important stakeholders are aggregated. These are food producers, food retailers and wholesalers as well as logistics service providers. For the tiers agricultural production and processing, the relevant supplying regions are considered as well. The foods are categorised into 51 groups including four different temperature ranges, which represent the majority of the German food supply network from agricultural raw products like crops or raw milk to consumable foods like bread and pastries or cheese.

Since production, processing, warehousing, and consumption of food products are not taking place in the very same regions, the food products have to be transported between the regions while passing all four tiers. Transport within the tiers processing and warehousing is possible too, in case some foods are processed more than one time or the supply chain of a retailer has a hierarchic warehouse structure. The decision which region is supplying which region will be modelled with a gravity model for each food category.

In the model, inventories for every food category, every group of actors, and every region are recorded in a single data cube. This data cube is recalculated incrementally every day, considering the production, relocation of food products, and consumption (see Figures 1 and 2).

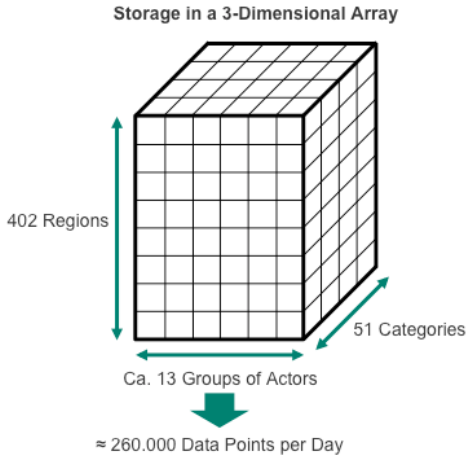

Figure 1: Dimensions of the Data Cube

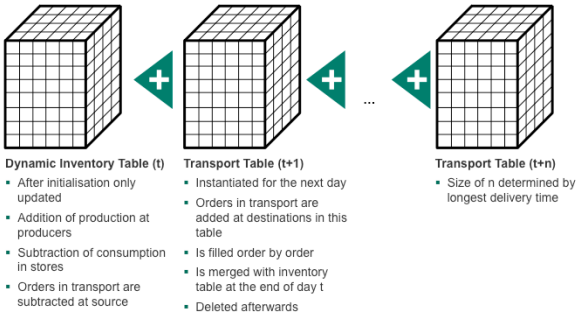

Figure 2: Interactions of Data Cubes for Inventories and Transports

The required data is collected for the year 2012 from the Federal Statistical Office, the Federal Ministry of Food and Agriculture, the Federal Ministry of Transport and Digital Infrastructure, food-related associations, and professional data providers. The gathered data and modelled processes are verified by interviews with experts from the production, logistics, and retailing sector. A model with more recent data will be possible, but it is important to consider only data from the same time period to get a consistent overall picture. Lots of data could be collected for the years 2013 and 2014, but especially national accounts are updating slowly and are still only available for 2012.

3. FINDINGS

So far, the data sources have been consolidated and aggregated to match 51 food categories. For each category the amount of metric tons produced, imported, and exported has been determined on a national level. In addition, the usage of the resulting amounts for consumption, other food products and other productions has been identified. The result is a detailed input-output-table for the German food sector.

In a second step, the consumption and production has been split from the national level to the 402 regions. While the consumption has been split up relative to the distribution of population, production has been split up by data from the Federal Ministry of Food and Agriculture as well as employment data.

Using the detailed regional production data and the results of the gravity model as well as an optimal interaction distribution the two average distances from the Federal Transport Plan for agricultural products and processed products could be detailed to all 51 food categories.

Combining all this with the data concerning the dates of harvest, processing and consumption, the level of stocks over time are calculated allowing statements regarding times of minimal stock and necessary minimum stock levels.

4. RESEARCH LIMITATIONS

The amount of data used in the model is a problem for different reasons. The gathering of data is complex and time consuming. Other issues are restrictions due to excessive time necessary for computing such big data, making model generation and visualisation with software tools difficult.

5. PRACTICAL IMPLICATIONS

The dynamic simulation of supply networks of single companies should be interesting for all supply chain managers. The dynamic simulation of a whole sector offers new insights to companies as a kind of market analysis. The main application of such dynamic sector model will be the national emergency preparedness. In this case, the public authorities will use the model to identify weaknesses in the food supply and take measures to improve the security and reliability of the food supply in Germany.

This is done using different scenarios, which can be integrated into the normal scenario of 2012. This enables predictions about stock levels in regions affected by disruptions. In addition, different measures taken by public authorities could be tested for their effects on stock levels and freight transport demand.

6. ORIGINALITY

A model is proposed, which uses system dynamics and operations research methods to show commodity flows in multi-level supply networks dynamically developing over time. It improves market and risk analyses and makes the assessment of agile networks possible.

FINITE ELEMENT ANALYSIS INVESTIGATION OF RESPONSE OF PUMPKIN TISSUE UNDER UNIAXIAL LOADING

Maryam Shirmohammadi[a*], Prasad KDV Yarlagadda[b]

[a*]University of South Australia, Adelaide, Australia
[b] Queensland University of Technology, Brisbane, Australia

[a]maryam.shirmohammadi@unisa.edu.au
[b]y.prasad@qut.edu.au

ABSTRACT

Finite element analysis (FEA) models of uniaxial loading of pumpkin peel and flesh tissues were developed and validated using experimental results. The tensile model was developed for both linear elastic and plastic material models, the compression model was develop d only with the plastic material model. The outcomes of force versus time curves obtained from FEA models followed similar pattern to the experimental curves however the curve resulted with linear elastic material properties had a higher difference with the experimental curves. The values of predicted forces were determined and compared with the experimental curve. An error indicator was introduced and computed for each case and compared. Additionally Root Mean Square Error (RMSE) values were also calculated for each model and compared. The results of modelling were used to develop material model for peel and flesh tissues in FEA modelling of mechanical peeling of tough skinned vegetables.

Keywords: mechanical properties, tensile, compression, Finite Element Model, peel and flesh tissues, Root Mean Square Error, error indicator.

1. INTRODUCTION

Reducing the volume of loss and waste in post harvesting and processing stages of agricultural products can increase food availability globally (Hodges, Buzby et al. 2011). Applying Finite Element methods and software in modelling industrial operations is a new trend among researchers, particularly in the food and beverage industry. Researchers focus on determining and optimising the best possible conditions and highest quality of products considering conditional variables, mainly application of these methods in analysing stress versus strain for food materials under external loading, as it is usually difficult to use common experimental methods (Li, Li et al. 2013). Additionally, computer based models are capable of predicting the outputs of operations even before manufacturing the equipment (Schaldach, Berger et al. 2000). Considering the advantages of these methods and software, there are some limitations which need to be well thought-out. Material modelling, boundary conditions, dimensions and geometric aspects are some of these crucial parameters. Additionally, regarding the complexity of industrial operations, it is necessary to simplify the models in order to reduce the computation time and error. The response of agricultural crops and food materials differs in terms of damage on different sections and magnitude of load; specifically under large deformations the rate of loss can be high due to the nature of tissue. This paper details the research carried out in development of FE models of the mechanical loading process of pumpkin peel and flesh samples utilizing Finite Element Method (FEM). Tensile and compression tests are two common methods of evaluating mechanical response of food materials under loading. In order to select an appropriate material model, results of compression and tensile tests (Shirmohammadi, Yarlagadda et al. 2011, Shirmohammadi 2013, Shirmohammadi, Yarlagadda et al. 2013, Shirmohammadi and Yarlagadda 2014) were used to develop FE model. The model development was designed to present accurately the mechanical response of peel and flesh samples. The model has been constructed to create a numerically stable and efficient representation of tough skinned vegetable response under large deformation. The model was developed using the LS DYNA v971 (2001) program which is utilized in large deformation static and dynamic behaviours of materials (Hallquist 2006).

1.1. Response of material

Response of structure under loading is an important aspect in modelling and simulation of any engineering system. This response can be classified as linear or non-linear, which is highly related to the type of structure and operations that have been modelled. Linear response is defined as a direct relationship between stress and strain values (Kilcast 2004), which is normally limited to a very low rate of load for a short period of time related to the softness of material. In a real world operation the response to the loading process is usually non-linear. In the case of agricultural and food materials, the linear response of materials is limited only to the small deformation condition, while the raise in the deformation value leads to non-linear behaviours of materials (Lu and Puri 1991, Lu and Puri 1992, Lu and Chen 1998). Although an elastic portion is usually considered as response of material to simplified mechanical loading tests, even this portion is restricted to the deformation condition, value of yield stress and the limit of elasticity. In this study the material behaviour is considered to be nonlinear and the failure criterion was used to develop FE models. The bio-yield and rupture points of samples obtained from

experimental results were considered as effective parameters in modelling procedure.

1.2. Material Model Evaluation Using Experimental Results

Agricultural and food material behaviours under external loading can be complex as these materials are naturally soft and there are various parameters affecting their response. For example, the level of moisture content, variety and ripening stage are some of these influential parameters. FE modelling of their response in mechanical operations is a challenge. The important aspect is selecting an appropriate material model which exhibits similar properties of materials in both elastic and plastic regions. LS DYNA package is used in this project to develop the model; in terms of material modelling the main concerns were the accuracy of the FE model behaviour under loading in comparison with the experimental results. Stress versus strain and force versus deformation were the parameters to compare the results of modelling with the empirical outcomes. In order to evaluate the material response to the external loading, two compression and tensile models were developed and the results of simulations were validated using the experimental tests results. A piecewise model with the capability of inputting elastic and plastic section details has been chosen to create the material model. The bio-yield stress was used as a point in which the failure starts in the tissue structure, and the details of plastic section of stress strain curve were entered as the guide for plastic changes in material. Piecewise-linear plasticity formulation (MAT_24) is one of the available material types in the LS DYNA package which classifies material response to elastic and plastic sections. In the elastic zone, material's modulus of elasticity (E) is the main parameter and the limit of elasticity is defined by Yield stress. The other option available is to define 8 points after yielding as effective plastic stress and effective plastic strain values, to define the actual stress versus strain curve in plastic region. After yielding the tangent modulus of material is required for the material model. However when the stress versus strain curves is input as the effective plastic stress and strain data, defining the values of tangent modulus were not required (2001).

Failure phenomenon was another essential parameter to be defined and considered. This failure breaks the cell walls and creates elastic and inelastic deformations in agricultural crops such as apple, which have been defined as bio yield point by Mohsenin (Mohsenin 1986). For the harder materials such as kernels this phenomenon creates cracks that can be visible or invisible on the surface of grain, in meat however it has been defined as the tearing and separating that happens in the connected parts of tissues (Mohsenin 1986). For agricultural materials the failure is directly related to the cell wall resistance to the applied load. Plastic deformation basically is known as a state of failure in material structure (Fischer-Cripps 2000) which can happen due to various changes on structure of tissue such as cleavage, slip and bruise (Holt and Schoorl 1983). There are different failure criteria depending on the type of material and external loading. In this study the Yielding stress (Von Mises Criterion) has been considered as the main factor of causing failure in the material. In this failure condition mainly deviatoric stress creates the changes rather than the hydrostatic stress (Fischer-Cripps 2000). Based on experimental results the Von Mises failure criterion is more accurate than the Tresca failure criterion (Leckie and Dal Bello 2009).

2. MATERIAL MODEL

Experimental results (Shirmohammadi 2013, Shirmohammadi, Yarlagadda et al. 2013) were used to develop and validate the FE model using both elastic and plastic properties of tissue. The Picewise_Linear Plasticity model uses the Cowper Symonds model with the following formulation for scaling the strain rate (2001):

$$\sigma_y\left(\varepsilon_{eff}^p, \dot{\varepsilon}_{eff}^p\right) = \sigma_y^s\left(\varepsilon_{eff}^p\right) + SINGY.\left(\frac{\dot{\varepsilon}_{eff}^p}{C}\right)^{1/p} \quad \text{Equation 1}$$

Equation 1 is used in dynamic case where the $SINGY > 0$, however for static problems when the $SINGY = 0$ the model will apply the following solution:

$$\sigma_y\left(\varepsilon_{eff}^p, \dot{\varepsilon}_{eff}^p\right) = \sigma_y^s\left(\varepsilon_{eff}^p\right)\left[1 + \left(\frac{\dot{\varepsilon}_{eff}^p}{C}\right)^{1/p}\right] \quad \text{Equation 2}$$

In Equation 2, the $SINGY$ is the Yield stress, ε_{eff}^p and $\dot{\varepsilon}_{eff}^p$ are effective strain and strain rates, and $\sigma_y^s\left(\varepsilon_{eff}^p\right)$ is the static stress. Nonlinearity and large strains happening in small stress condition in mechanical loadings of food materials (Mohsenin 1986), and the possibility of applying both elastic and plastic behaviours of tissue with failure criteria at the bio-yield point was the reason of selecting material MAT_24 for FE model.

2.1. Model development

Compression and tensile models were developed based on the size and dimensions of the samples in experimental tests (Maryam Shirmohammadi, 2013). The following assumptions were considered:

The compression loading process happens with the constant rate of 20 mm/min.

Tensile samples were dog bone-shaped with a narrow section in the middle. The length of samples was 40 mm with a width of 10 mm.

Shell element was selected for the tensile model and the thickness of samples was 3 mm according the experimental dimensions of samples.

The material is assumed to be homogenous and moisture content assumed to be constant.

According the unit consistency in LS DYNA the system of units: tonnes, mm, s, N, Mpa and N.m (2013) was selected for all the models.
The flesh and peel samples had different heights according to the experimental specimen dimensions.
Material properties were obtained from the empirical results.
Both flesh and peel models were developed using solid element and triangular mesh.
A cylindrical model of flesh and peel samples with diameter of 40 mm were developed for compression test. The height of peel and flesh samples were 5 mm and 34.44 mm respectively. The values of stress versus strain curve were input for the material model. The elastic modulus was considered to be the slope of stress-strain curve. Poisson's ratio value for flesh samples also was obtained from experimental tests (Shirmohammadi 2013, Shirmohammadi, Yarlagadda et al. 2013). Poisson's ratio value for flesh considered 0.43, for peel samples however the Poisson's ratio was considered as the the value determined for unpeeled samples (0.33) (Shirmohammadi and Yarlagadda 2014). A set of nodes was defined on the bottom surface of the model and fixed support was applied at this area limiting the transactional and rotational movement in X, Y and Z directions. The compressive movement also modelled as a displacement-time as applied on a set of nodes on the top side of samples which moved in a negative direction of Z axis. The termination was applied as the time that the compressive loading experiment has been stopped. A Prescribed_Motion_Set was applied for a set of nodes that was defined on top surface of the samples with the displacement in Z direction and the load curve obtained from experimental tests. The termination time for all models was considered to be the termination time of experimental tests with the time step of 0.1 s.
Dog bone-shaped samples with length of 40 mm, width of 10 and thickness of 3 mm were modelled (Shirmohammadi 2013, Shirmohammadi, Yarlagadda et al. 2013). The tests were performed on flesh and peel samples of Jap pumpkin previously as a part of PhD study (Shirmohammadi 2013, Shirmohammadi, Yarlagadda et al. 2013) under deformation rate of 20 mm/min using an INSTRON universal testing machine. A fully integrated element type was applied for the FE model, which is commonly used for plasticity problems in LS DYNA software (Hallquist 2006). A displacement was applied on a set of nodes defined on one side of the model; a fixed boundary condition was applied on this set. Prescribed_Motion_Set was applied on a set of nodes defined on the free side of the model. The motion assumed to be a displacement in X direction and the detail of elongation versus time was obtained from experiments. Stress versus strain curve has been calculated using the results of the force-extension curve obtained from experimental tests from literature (Shirmohammadi 2013, Shirmohammadi, Yarlagadda et al. 2013).

True stress and true strain values were used in the modelling (Pruitt and Chakravartula 2012):

$$\sigma_t = \sigma(1+e) \qquad \text{Equation 3}$$

$$\varepsilon_t = \ln(1+e) \qquad \text{Equation 4}$$

In Equation 3 and Equation 4, $\sigma_t, \varepsilon_t, \sigma$ and e are true stress, true strain, engineering stress and engineering strain respectively. Termination time was obtained from experimental testing and the time step was 0.1s. The model was saved as a Key file and sent to LS DYNA solver, the post-processing step was completed afterward using the results of simulation.

3. RESULTS AND DISCUSSION

Finite element models with a non-linear elasto-plastic material type for pumpkin tissues were developed assuming that material is isotropic and homogenous. Models were created and simulated based on the following performance criteria: the FE models of compression and tensile loadings are numerically compatible with the experimental and constitutive results, and the material model selected for each model should accurately represent the mechanical behaviours of tough skinned vegetables under loading. The performance criteria were employed to facilitate developing an accurate FE model for each part. Results of FE models were compared with the results of experimental compression and tensile tests (Shirmohammadi 2013, Shirmohammadi, Yarlagadda et al. 2013), an error indicator values were defined based on the following description:

$$e_{force} = \frac{|F_{exp} - F_{FEA}|}{|F_{exp}|} \times 100 \qquad \text{Equation 5}$$

In Equation 5, e_{force}, F_{exp} and F_{FEA} are error indicators for the force predicted, experimental force value and FEA predicted force value. For each FEA set of results, the individual differences between experimental values and values predicted by model, an error percentage was determined.

3.1. Development and Validation of Finite Element Model of Tensile Test

The tensile model was developed for two different material behaviours including linear elastic and plastic material response. As existing FE modelling studies in literature mainly used linear elastic material model for development and validation of their models (Wu and Pitts 1999, Hernandez and Belles 2005, Lewis, Yoxall et al. 2008, Sadrnia, Rajabipour et al. 2008, Li, Li et al. 2013), it was decided to create and validate a tensile model in order to be able to compare the results with available literature. Afterward, models of tensile and compression tests were developed using plastic material model.
The displacement versus time curve was applied up to the elastic limit for the loading and as is mentioned before, the stress versus strain relationship assumed to be linear with the slope equal to elastic modulus value. The density, elastic modulus and Poisson's ratio of

tissues were determined from experimental study (Table 1) (Shirmohammadi and Yarlagadda 2014).

Table 1: Mechanical properties of samples input for the tensile model.

	Density(ton/mm^3)	Elastic Modulus (Mpa)	Bio-Yield Stress (Mpa)	Poisson's Ratio
Peel	0.903×10^{-9}	25.02	1.5	0.33
Flesh	0.934×10^{-9}	7.63	0.58	0.434

The models were solved and the outcomes of force versus time were determined as shown in Fig. 1. The maximum stress happened in the narrow middle section of the samples, which is the section where rupturing happened in experimental tensile tests as well. This was expected as the cross sectional area is smaller than the sides of sample, and as a result the value of stress will be higher on the middle section in comparison with the sides. Maximum tensile load reached 22.8 N, which was close to the experimental value 20.21 N for peel samples. The results of force in flesh samples were 7.4 N while the experimental value was 7.8 N. The difference between errors for the predicted value from the FE model and the actual experimental values were calculated as error percentage values and the percentage of error versus time curves was determined for both samples as is shown in Fig. 1(b).

Table 2: RMSE and maximum load predicted by FE model using linear elastic material properties.

Linear Elastic Material		RMSE	Maximum Force (N)
FEA	Peel	1.06	22.8
	Flesh	0.39	7.87
EXP	Peel	-	20.21
	Flesh	-	7.47

The Root Mean Square Error (RMSE) values also were determined to compare the accuracy of the FE models, the RMSE values for peel and flesh samples were 1.03 Mpa and 0.36 Mpa respectively. These RMSE values show the difference between the FE predicted value with the actual values observed in experimental tests. The ratio of individual differences over the experimental values for force was also determined as error indicator (see Equation 1) for sets of data obtained from FE and experimental results.

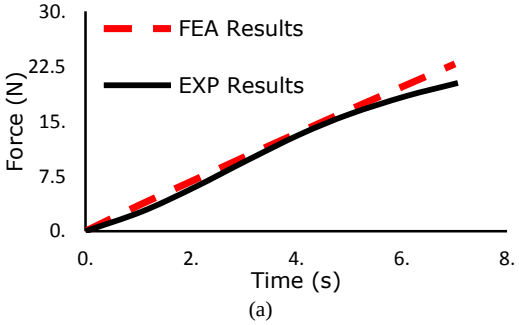

(a)

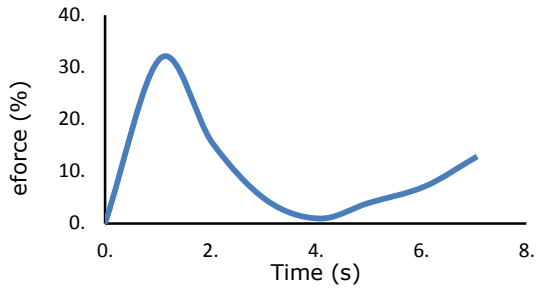

(b)

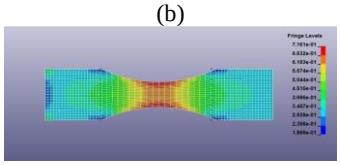

(c)

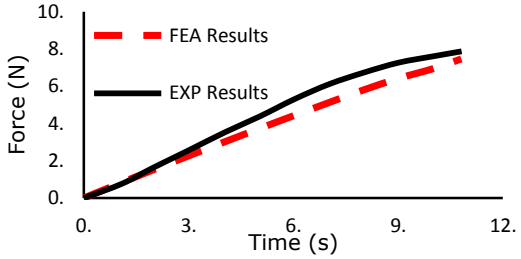

(d)

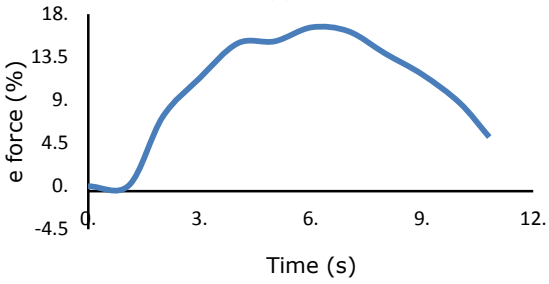

(e)

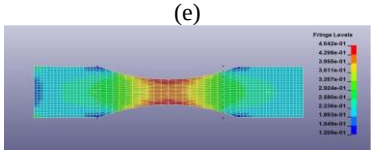

(f)

Fig. 1: Tensile force versus time for peel samples (a), error percentage between predicted and experimental values (b) and (c) the stress distribution resulted from FE model, (d), (e), (f) results of flesh model..

Values of error shown in Fig. 1(b) showed that the maximum difference between predicted and experimental value happened where the experimental curve bends, while the FE results is a linear line regarding the material type selected. Maximum error value was 31% for peel samples. The results of stress for flesh samples with elastic material properties showed the maximum error near the force peak value which was 16% (Fig. 1(b)).

The comparison between FE and experimental work shows a better agreement for smaller deformation; similarly it is reported by Dintwa et al. (Dintwa, Jancsók et al. 2011) for tomato under compressive loading. Where the results of the FE model showed a very close result under smaller deformation (less than 0.2 mm), the error values for flesh samples were much

lower than the error percentage for peel samples, according to the shape of experimental curve. For flesh samples, under smaller deformation the difference between predicted values was lower while for peel samples, smaller errors appeared under larger deformation (see Table 2 and Fig. 1). In comparison between peel and flesh results also there was a better correlation between experimental and FE results for flesh samples; the percentage of error and RMSE were lower. This indicates the development of permanent plastic deformations are starting to occur and the stress versus strain relationship is changing to a nonlinear. As is mentioned before regarding the curved shape of peel samples, the first section of peel results was less linear than the flesh samples, which were flatter than peel samples. The modulus of elasticity, density, Poisson's ratio, bio yield stress, and the true stress versus strain curve were input as material properties (see Table 1**)** for material properties to develop a PieceWise_Linear_Plasticity model. This material model is a failure-based material type which requires the details of yielding point and the effective plastic stress versus strain curves. The curves in Fig. 2 feature a force versus time curve resulted from FE modelling; the differences between experimental values and predicted values with FE in two different cases have also been presented. Root Mean Squared Error also was calculated for the obtained results and shown in Table 2 and Table 4. The RMSE was also 0.44 Mpa which is lower than the values determined for FEA with the experimental input model (1.36 Mpa). For the first two seconds of the loading, the FEA model results followed a close pattern with the experimental curve Fig. 2(a) and the maximum predicted values of force was higher than the experimental results.

The results of FE models for flesh samples have been presented in Fig. 2. The maximum force predicted by the FE model was 8.53 N and the RMSE was 0.18 Mpa and error indicator factor for peel samples showed the maximum error of 18.5%.

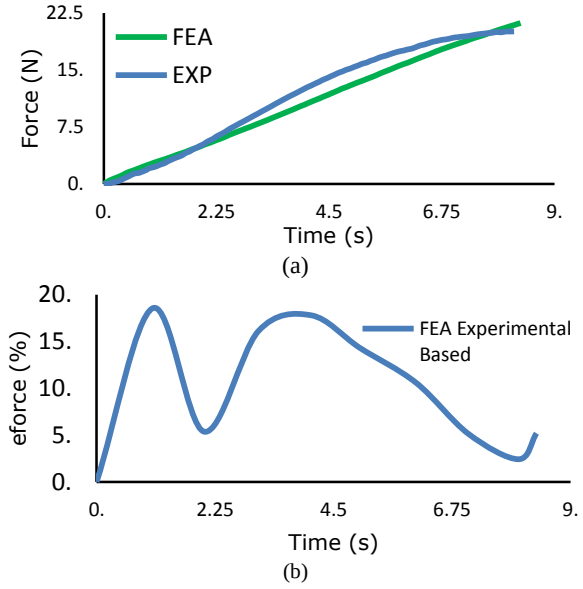

Fig. 2: Results of FE model with experimental input properties, and percentage of error for peel samples under tensile loading.

The comparison between peel results showed that both predicted maximum load values for peel samples were higher than the experimental values. From the error point of view however, maximum error for FEA model of flesh sample was over 35%, which happened in under 2 seconds of test (see Fig. 3(a)).

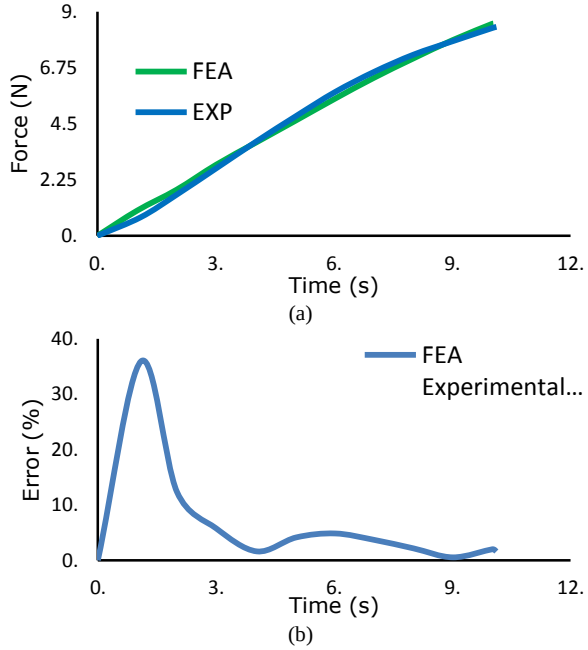

Fig. 3: Results of FE model with experimental and constitutive input properties,and the error percentage for flesh samples under tensile loading.

3.2. Development and Validation of Finite Element Model of Compression Test

The FE model of compressive loading consisted of two parts, including the compression test of flesh and peel samples. Model geometry was developed based on experimental sample size (Shirmohammadi 2013). Poisson's ratio value for flesh samples was calculated using the results of experiments from literature, for the peel samples Poisson's ratio assumed to be 0.33 equal to the value calculated for unpeeled samples under uniaxial compression (Shirmohammadi 2013, Shirmohammadi, Yarlagadda et al. 2013).

The results of experimental tests were used to develop stress versus strain curves for both samples (Fig. 4). Bio-yield point was defined for the samples as a point where the compressive force value decreases or stays unchanged with the increase in deformation value and elastic modulus was defined as the slope of curve in that limit (see Table 3**)** for material properties of tissue).

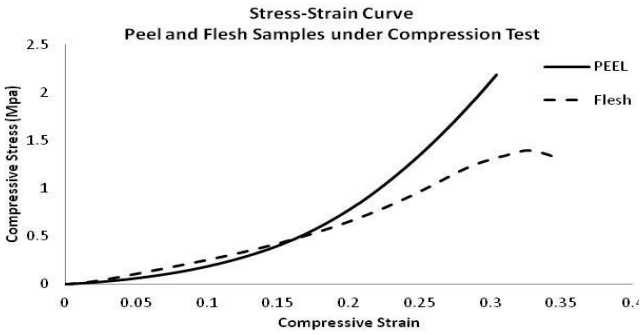

Fig. 4: Stress versus strain for peel and flesh samples obtained from experimental study under compressive loading.

Force versus time results have been presented in Fig. 5, the first curve (a) in Fig. 5 shows the results of FE modelling test for peel samples. The input data was obtained from experimental results and included the density, elastic modulus, Bio-Yield stress and the effective plastic stress versus strain curve. Regarding the failure criterion, the effective stress and effective strain were required in order to consider the material behaviours after yielding happens where failure in materials is assumed to occur.

Table 3: Material properties were defined for peel and flesh samples under compressive loading obtained from experimental study.

Material	Density (ton/mm^3)	Elastic Modulus (Mpa)	Bio-Yield Stress (Mpa)	Poisson's ratio
Peel	0.903×10^{-9}	2.59	2.18	0.33
Flesh	0.934×10^{-9}	4.19	1.39	0.434

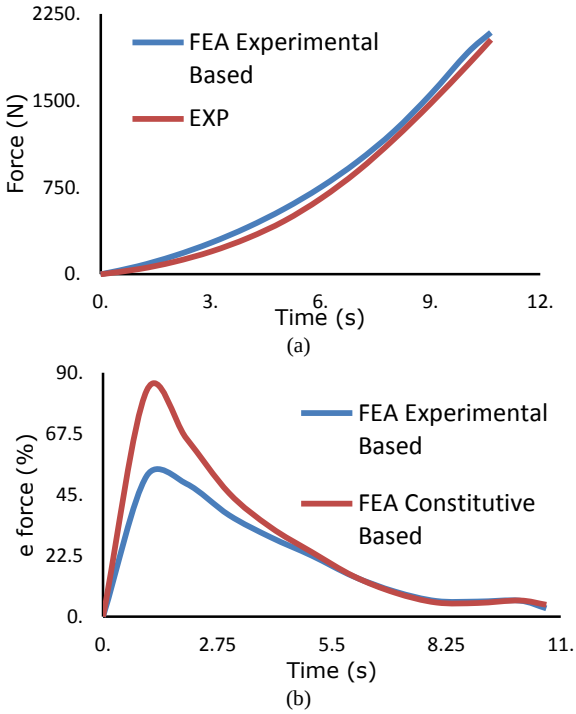

Fig. 5: Force versus time curve resulted from FE model, and comparison with experimental results for peel samples.

Fig. 5 (b) represents error indicator for predicted values for force in comparison with experimental values for FEA. As it has been shown, the errors were higher for the first 2 seconds of test while the error values dropped gradually after a peak and reached minimum after 8 seconds. Despite the difference between percentages of error during the model running time, FE curve results had a similar pattern in comparison with experimental curve. The Root Mean Squared Error (RMSE) value for experimental based FEA was 16.77 Mpa. The values for peel samples were 76.8 Mpa for FEA.

Table 4: Comparison between FEA and experimental results and RMSE values for tensile ad compression tests.

Tensile	RMSE		Maximum Tensile Load (N)	
	Peel	Flesh	Peel	Flesh
FEA	1.36	0.18	21.19	8.53
Experimental	-	-	20.14	8.39
Compression	**RMSE**		**Maximum Compressive Load (N)**	
	Peel	Flesh	Peel	Flesh
FEA	76.98	16.77	2088.81	1073.68
Experimental	-	-	2026.658	1176.19

As is presented in Fig. 6, the error calculated for experimental based FE model is higher for the first 20 seconds of compression loading test, while the error percentages are lower after 20s. The error indicator had a peak for both peel and flesh samples in the first 2 seconds of the test with 42%, while the error value in peel results was much higher than the flesh. This high rate of error was due to the curve shape of force versus time diagram (see Fig. 5(b)). The FEA results also showed a stress distribution from the top to the bottom where the force is applied on top of the cylindrical samples (Fig. 6 (d)); the same pattern was observed for peel samples. This phenomenon was similar to what happened in experiments; damage was observed as crushed layer of tissue on the side of samples where load was applied was higher and the deformation was clear.

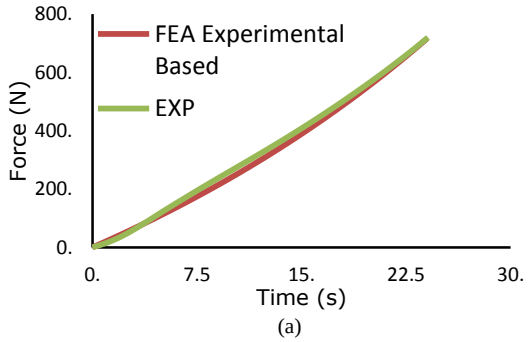

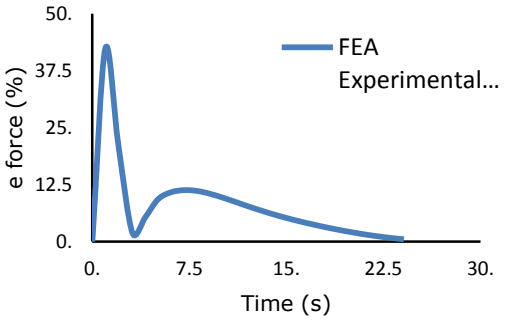

(b)

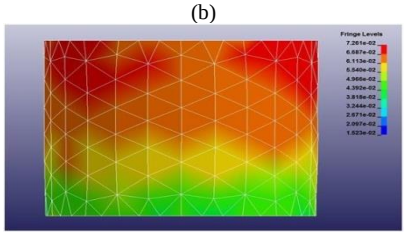

(c)

Fig. 6: Force versus time curve resulted from FE model and comparison with experimental and constitutive results for flesh sample.
(a) Results of FEA with experimental input, (b) the error percentages for FE model with experimental and constitutive based input, (c) the FEA stress distribution results.

The RMS Error for compression model was lower for flesh samples in both experimental and constitutive input cases (Table 4**)** Maximum predicted force values were higher than the experimental values for peel samples for both FE models, while the flesh results were both lower than the experimental values.

4. CONCLUSION

The predicted values for force in the tensile model with linear elastic material properties were 22.8 N and 7.4 N where the experimental data was 20.21 N and 7.8 N for peel and flesh respectively. In general, the outcomes of FE model followed a linear line as expected regarding the type of material was chosen. For the tensile model with piecewise material model where the plastic deformation of tissue was considered, maximum load was predicted 21.19 N and 8.35 N while the experimental values were 20.14 N and 8.39 N for peel and flesh respectively. As mentioned in the previous sections, the force-deformation curve for food and agricultural materials are usually different from other engineering materials. The curve resulted from FE model was similar to the experimental curve in terms of pattern on force versus time curve. Obviously, the Picewise_linear Plasticity model illustrated better outcomes however the models were developed for one deformation rate according to the experimental condition while further studies on rate of deformation can provide a clearer details of tissue behaviour.

In compression model the maximum compressive load was determined by FE model 2088 N and 1073 N for peel and flesh respectively while the experimental values were 2026 N and 1176 N for peel and flesh respectively. The maximum stress in both tensile and compression models occur on the expected region were the highest deformation and rupturing on the tissue surface.

This study was one of the few attempts on modelling actual behaviours using FEA approach, however it is recommended to apply this method for other types of tissues where mechanical properties of material plays an important role in reducing volume of unwanted deformation on tissue during post harvesting and processing operations.

REFERENCES

(2001). LD-DYNA Keyword User's Manual. California, Livemore Software Technology Corporation.

(2013). LS-DYNA Support, LSTC Inc and DYNAmore GmbH.

Dintwa, E., P. Jancsók, H. Mebatsion, B. Verlinden, P. Verboven, C. Wang, C. Thomas, E. Tijskens, H. Ramon and B. Nicolaï (2011). "A finite element model for mechanical deformation of single tomato suspension cells." Journal of Food Engineering **103**(3): 265-272.

Fischer-Cripps, A. C. (2000). Introduction to contact mechanics, Springer Verlag.

Hallquist, J. O. (2006). "LS-DYNA theory manual." Livermore Software Technology Corporation **3**.

Hernandez, L. F. and P. M. Belles (2005). "A 3-D finite element analysis of sunflower (Helianthus annuus L>) fruit. Biomechanical approach for the improvement of its hullability." Journal Of Food Engineering: 861-869.

Hodges, R. J., J. C. Buzby and B. Bennett (2011). "Postharvest losses and waste in developed and less developed countries: opportunities to improve resource use." The Journal of Agricultural Science **149**(S1): 37-45.

Holt, J. and D. Schoorl (1983). "Fracture in potatoes and apples." Journal of Materials Science **18**(7): 2017-2028.

Kilcast, D. (2004). Texture in Food volume2: solid foods.

Leckie, F. A. and D. J. Dal Bello (2009). Strength and stiffness of engineering systems, Springer.

Lewis, R., A. Yoxall, M. Marshall and L. Canty (2008). "Characterising pressure and bruising in apple fruit." Wear **264**(1-2): 37-46.

Li, Z., P. Li, H. Yang and J. Liu (2013). "Internal mechanical damage prediction in tomato compression using multiscale finite element models." Journal of Food Engineering.

Lu, R. and Y. R. Chen (1998). "Characterization of nonlinear elastic properties of beef products under large deformation." Transactions of the ASAE **41**(1): 163-171.

Lu, R. and V. Puri (1991). "Characterization of nonlinear creep behavior of two food products." Journal of Rheology **35**: 1209.

Lu, R. and V. Puri (1992). "Characterization of nonlinear behavior of apple flesh under stress relaxation." Journal of Rheology **36**: 303.

Mohsenin, N. (1986). Physical properties of plant and animal materials: structure, physical characteristics, and mechanical properties, Routledge.

Pruitt, L. A. and A. M. Chakravartula (2012). "Mechanics of biomaterials: Fundamental principles for implant design." MRS Bulletin **37**(07): 698-698.

Sadrnia, H., A. Rajabipour, A. Jafari, A. Javadi, Y. Mostofi, J. Kafashan, E. Dintwa and J. De Baerdemaeker (2008). "Internal bruising prediction in watermelon compression using nonlinear models." Journal of Food Engineering **86**(2): 272-280.

Schaldach, G., L. Berger, I. Razilov and H. Berndt (2000). "Computer simulation for fundamental studies and optimisation of ICP spray chambers." ISAS (Institute of Spectrochemistry and Applied Spectroscopy) Current Research Reports, Berlin, Germany.

Shirmohammadi, M. (2013). Process Modelling and Simulation of Tissue Damage during Mechanical Peeling of Pumpkin as Tough Skinned Vegetable. Brisbane, Queensland University of Technology**:** 301.

Shirmohammadi, M. and P. K. Yarlagadda (2014). Determination of Poisson's Ratio and Young's Modulus of Pumpkin Tissue, Queensland University of Technology.

Shirmohammadi, M., P. K. D. V. Yarlagadda, Y. Gu, P. Gudimetla and V. Kosse (2013). "Tensile Properties of Pumpkin Peel and Flesh Tissue, A Review of Current Testing Methods." Transactions of the ASAE **56**(4): 1521-1527.

Shirmohammadi, M., P. K. D. V. Yarlagadda, P. Gudimetla and V. Kosse (2011). "Mechanical Behaviours of Pumpkin Peel under Compression Test." Journal of Advanced Materials Research **337**: 3-9.

Wu, N. and M. J. Pitts (1999). "Development and validation of a fruit element model of an apple fruit cell." Post harvesting Biology Technology **16**: 1-8.

BREAKAGE MATRIX COMPARISON OF GRANULATED FOOD PRODUCTS FOR PREDICTION OF ATTRITION DURING LEAN-PHASE PNEUMATIC CONVEYING

B.A. Kotzur[(a)], M.S.A. Bradley[(b)], R.J. Berry[(c)], R.J. Farnish[(d)]

[(a),(b),(c),(d)]The Wolfson Centre for Bulk Solids Handling Technology, University of Greenwich, United Kingdom

[(a)]B.A.Kotzur@greenwich.ac.uk, [(b)] M.S.A.Bradley@greenwich.ac.uk, [(c)] R.J.Berry@greenwich.ac.uk, [(d)]R.J.Farnish@greenwich.ac.uk

EXTENDED ABSTRACT

1. INTRODUCTION

Pneumatic conveying is widely used in the production and handling processes of many food products. These food products can take the form of powders or flake type bulk materials, including items such as tea leaves, granulated sugar, flour, and flavorings. The main advantages of using pneumatic conveying to transport materials throughout a process include the maintenance of product hygiene, and the potential for flexibility in pipework routing in comparison to mechanical conveying. However, the fulfilment of the many benefits of pneumatic conveying can only be realised if the system is correctly configured and operated optimally. In instances where this is not the case, a common repercussion, is bulk material attrition due to excessive impact forces exerted on the particles as they pass through the system, and encounter changes in direction at bends. The final result can often be the generation of excess quantities of degraded particle size fractions – often in the form of fines or dust. The presence of these smaller particle sizes can have significant implications for the reliability of subsequent process operations or customer perception.

1.1. Motivation

The research presented in this document will provide a comparative breakage analysis of two types of food products, one crystalline in structure, and the other non-crystalline. This information may then be used to predict with a greater degree of confidence, the magnitude of anticipated attrition when pneumatically conveying particulate materials.

1.2. Lean Phase Pneumatic Conveying

There are three main modes of pneumatic conveying:

1. Dense-phase.
2. Lean-phase.
3. Pulse/dune flow.

Mode 1 describes conveying conditions when the entire cross-section of the pipe is occupied by particles at relatively low velocity (approximately 2-8 m/s). Mode 2 describes conveying conditions when the particles are fully suspended in the air flow under high velocity conditions (greater than approximately 12 m/s). Mode 3 describes transient conveying conditions between Modes 1 and 2, and describes the flow of ‘dunes’ of material progressing through the pipeline.

This study will consider lean phase pneumatic conveying effects specifically, as the combination of high velocity and low particle concentration yields the most likely conditions to induce an increased level of particle attrition.

1.3. Repercussions of excess fines content

The term ‘fines’ in this research shall refer to the d_{10} content of the virgin cumulative size distribution. Should the material within this size range make up too large a proportion of the overall mass, adverse material handling and performance issues can occur. These types of issues are extensive, and include:

- Unreliable discharge from hoppers,
- Dust generation, leading to explosion or health hazards,
- Segregation of mixtures,
- Excess dust in commercial products leading to customer complaints,
- Error in volumetric dosing operations due to variations in bulk density.

The occurrence of such issues typically results in additional time and financial costs to the producers of the product. These costs are consumed in amending the configuration or operating conditions of the existing process, or in reformulating the nature of the material handled.

1.4. Advantages of predictive analysis

This research seeks to provide an improved tool that can be applied to identify risk within processes. The approach will use predictive analysis of the product through empirical testing. Particle impact conditions can be carefully controlled within a centrifugal accelerator attrition tester, to provide comparative data

for qualitative analysis. Then, based on a comparison with products previously handled, insight into the breakage behavior may be attained and its subsequent attrition behavior estimated.
A selection of advantages that predictive analysis would yield include:

- Reduced requirement for post-installation troubleshooting,
- Enhanced understanding of the operating parameters that cause an unacceptable degree of attrition,
- Heightened stakeholder awareness of the nature of the material, with regard to particle attrition.

2. LITERATURE

There has been significant research conducted into lean phase pneumatic conveying, with respect to the erosion of pipeline bends. A number of models exist which seek to predict the level of erosion through modelling and empirical testing (Burnett 1996; Deng 2005; Macchini 2013; Sato 1995). As an issue that is closely related to erosion, there is presently a lack of research focusing solely on modelling of attrition of bulk material particles during lean phase pneumatic conveying.
Kalman (2000) conducted an extensive programme of pneumatic conveying tests, exploring the effect of a wide number of parameters on the attrition of various bulk materials. The equipment used in this study has the potential to cause particle attrition, and this has been addressed in the manuscript. The output of the research is limited to general relationships and recommendations in limiting the degree of particle attrition caused by a pneumatic conveying system.
Bridle (2000) performed an in-depth study of particle attrition through the testing and comparison of results between two testing facilities: a single bend test apparatus, and an industrial scale apparatus. The drawbacks of this study were that only three bulk materials were considered: granulated sugar, basmati rice, and malted barley. In addition to this, the testing programme did not consider the attrition behavior of narrow size fractions, nor could the test be performed in a conventional laboratory due to floor space requirements.
Chapelle P (2004) demonstrated a method for taking measurements from a bench top tester and scaling them up to predict the particle attrition behavior in an industrial-scale pneumatic conveying system. While this work lays the foundation for obtaining a scale-up procedure from a bench top scale, the range of variables for this form of testing were not fully explored, omitting the effect of solids loading ratio and impact angle. Additionally, a 5 gram sample was used, making the data exceedingly sensitive to variation in sample size distribution.
van Laarhoven, (2012) developed a new attrition tester of a scale suitable for placement on a laboratory desk. This tester contained the test sample within an oscillating box, where the particles would impact against the walls, causing attrition. Impact velocities estimated to be in the order of 1-5 m/s were attained. The significantly larger impact velocities observed in pneumatic conveying systems (up to 40 m/s) were simulated through increasing the number of impacts in the tester. The study was also limited to two granular materials, and tested a wide sample size distribution.

3. METHOD

Section 3 will describe the methods used to acquire the results in this course of research.

3.1. Materials

Two materials were selected for this course of research: golden breadcrumbs, and cooking salt. The former has a non-crystalline structure, and the latter exhibits a crystalline structure. Additionally, each material has a significantly different size distribution, with respect to the mean and range of particle sizes.

3.2. Statistically Representative Sampling

Due to the generally highly variable nature of bulk materials, it is essential that the testing be conducted using statistically representative samples obtained from the master batch. Should this prerequisite be neglected, subsequent tests could be conducted using samples with significant variation in size distribution or mixture composition. Therefore, statistical subdivision was conducted through the use of two apparatuses: a spinning riffler and riffle boxes.

3.2.1. Spinning Riffler

This piece of equipment is used for statistically subdividing samples of up to 40 litres in volume and is depicted in Figure 1.

Figure 1: Spinning Riffler

A mass-flow hopper is positioned above a vibratory feeder, which in turn dispenses the bulk material master sample into eight sub-samples on a rotating carousel. The amplitude of the vibratory feeder can be varied to

control the bulk material dispensary rate. This method produces eight statistically representative samples from a master sample.

3.2.2. Riffle Boxes

Riffle boxes are used for statistical subdivision of sample sizes up to approximately 500 millilitres. Figure 2 depicts the riffle boxes used for this programme of research.

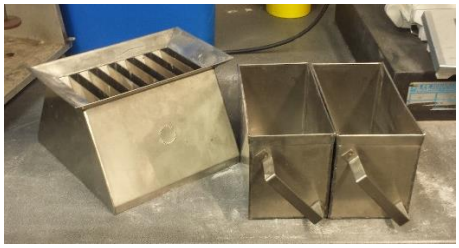

Figure 2: Riffle Boxes

Material is poured into the top of the separating section, which contains a series of slots, alternating between two receiving vessels underneath. This method produces two statistically representative samples from a master sample.

3.3. Particle Size Measurement

In order to determine the virgin size distribution of the sample and the post-test size distribution, a stack of mechanical sieves was used. These were cleaned in an ultrasonic bath prior to use in order to remove any contaminants.

The sieve size progression chosen for this course of research followed a $\sqrt{2}$ progression increase in aperture size. Due to the interest in the smaller size fractions generated, as detailed in the introduction, the sieve progression will begin at the smallest size of 45 µm. This will enable closer inspection of the material residing within small size fractions generated as a result of the degradation testing.

The bulk material sample was loaded into the top of the sieve stack, after which the stack was placed on a vibrating plate, depicted in Figure 3. The subsequent sieving was performed for 15 minutes.

Once sieving was complete, a set of electronic scales was used to determine the mass retained on each sieve to the nearest 0.01 g.

3.4. Attrition Test

The attrition testing was performed on a centrifugal accelerator style attrition tester, depicted in Figure 3.

Figure 3: Centrifugal Attrition Tester

The sample material is inserted into the upper mass-flow hopper of the apparatus. It is then fed into the tester below via an increasing-capacity screw. The rate of screw rotation was kept constant throughout the course of the testing, and consistency in material delivery rate was stable. The function of the screw feeder is to ensure that the volumetric flow rate of material into the attrition test is controlled – a trait that is not closely controlled in many forms of attrition testing.

The material fed from the screw feeder then enters the center of a rotating spindle, and accelerated outwards through a series of radial tubes. The accelerated particles then impact with a target array at a known angle of impact.

The post-test sample is collected at the base of the impact chamber, and taken for size analysis.

3.4.1. Sample Preparation

To obtain the required sample size for each test, the master sample was riffled down to a suitable size for separation via mechanical sieving. In the knowledge that each material batch fed into the sieving unit is statistically representative of the master sample, the size fraction retained on each sieve may also be treated as statistically representative samples. Therefore, samples of known size range with upper and lower bounds may be prepared for testing in the centrifugal accelerator attrition tester.

4. RESULTS

The results for this course of research consist of the initial virgin size distribution, the resultant size distributions when a statistically representative sample is degraded under known conditions, and the resultant size distribution when a known size fraction of material is degraded under known conditions.

It should be noted that the value of '0 µm' for the sieve size represents the material retained in the pan at the base of the sieve stack.

4.1. Virgin Size Distribution

The initial analysis undertaken was to determine the virgin size distribution of the 16 kg master sample for

golden breadcrumbs and salt, presented in Figure 4 and Figure 5 respectively.

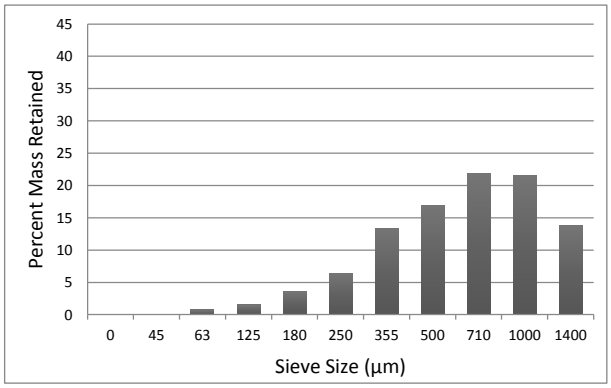

Figure 4: Virgin Size Distribution of Golden Breadcrumbs

No particles used for testing were retained on a 2000 µm sieve – the next sieve in the √2 progression.
Though inspection of the size distribution of golden breadcrumbs, the three size fractions representing the largest proportions of material by mass were chosen to undergo narrow size fraction degradation tests. These size fractions consist of the material retained on 500, 710 and 1000 µm sieves. These fractions represent approximately 58% of the total sample distribution by mass.

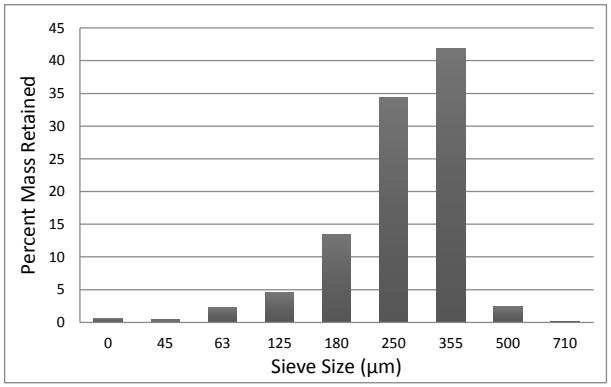

Figure 5: Virgin Size Distribution of Salt

No particles used for testing were retained on a 1000 µm sieve – the next sieve in the √2 progression.
Through inspection of the size distribution of salt, two size fractions, 250 and 355 µm, were chosen for narrow size fraction degradation testing. These fractions represent approximately 75% of the total sample distribution by mass.

4.2. Size Distribution Post-Breakage

This section presents the results of the degradation tests performed with the full virgin size distribution as the input material. Three velocities were tested: 15, 25 and 35 m/s. The results for the golden breadcrumbs are presented in Figure 6, and the results for the salt are presented in Figure 7.

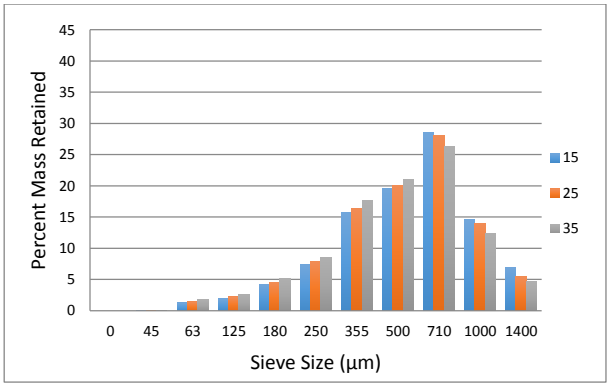

Figure 6: Results of Full Size Distribution Tests under Three Impact Velocities (measured in m/s) for Golden Breadcrumbs

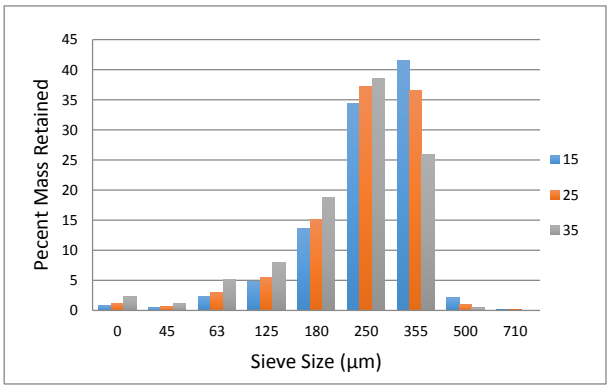

Figure 7: Results of full size distribution tests under Three impact velocities (measured in m/s) for salt

4.3. Narrow-Fraction Size Distribution Post-Breakage

This section presents the results of degradation tests of narrow size fractions across three impact velocities: 15, 25, and 35 m/s. Figures 8, 9 and 10 present the results for golden breadcrumbs, and Figures 11 and 12 present the results for salt, all at impact velocities of 15, 25 and 35 m/s.

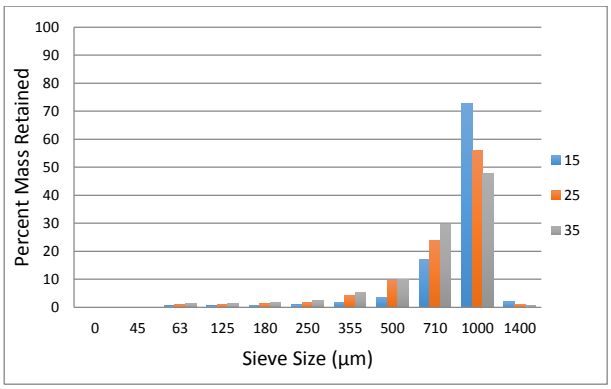

Figure 8: Results of 1000-1400 µm size fraction tests under three impact velocities (measured in m/s) for golden breadcrumbs

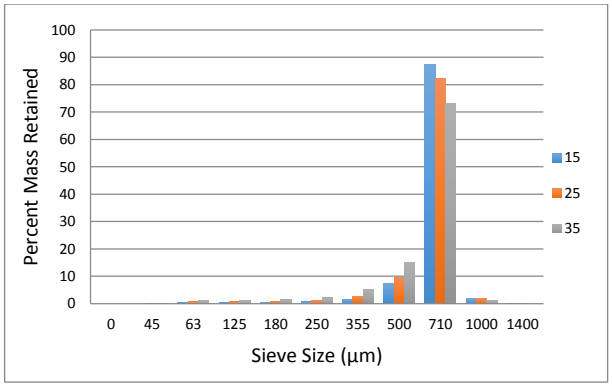

Figure 9: Results of 710-1000 µm Size Fraction Tests under Three Impact Velocities (measured in m/s) for Golden Breadcrumbs

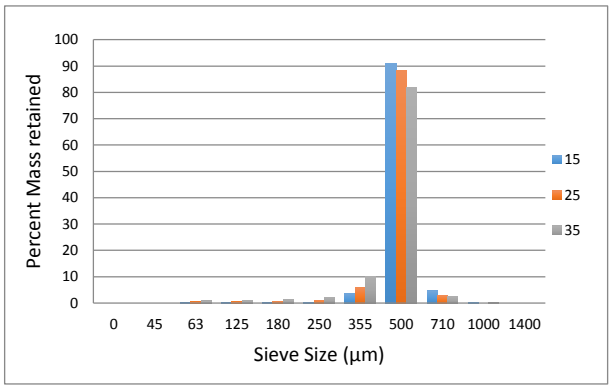

Figure 10: Results of 500-710 µm Size Fraction Tests under Three Impact Velocities (measured in m/s) for Golden Breadcrumbs

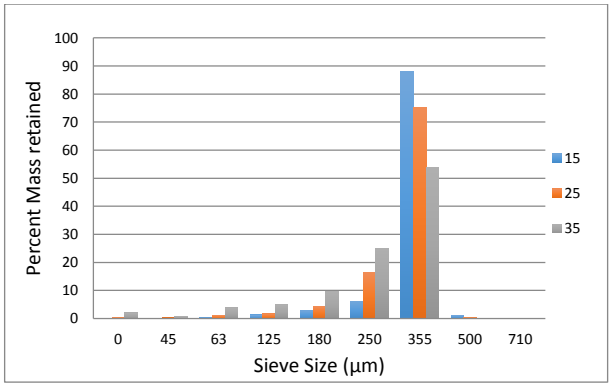

Figure 11: Results of 355-500 µm Size Fraction Tests under Three Impact Velocities (measured in m/s) for Salt

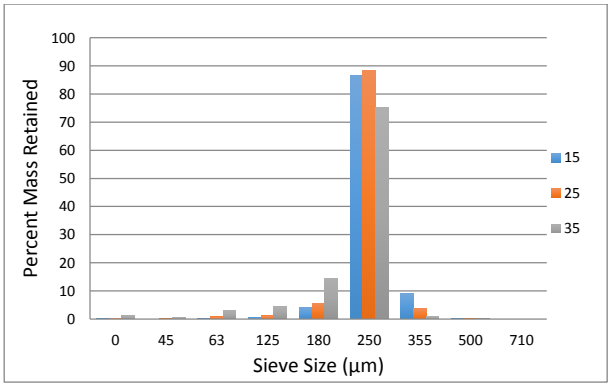

Figure 12: Results of 250-355 µm Size Fraction Tests under Three Impact Velocities (measured in m/s) for Salt

5. DISCUSSION

This section will present the analysis of the results, looking at each of the materials and their representative size fractions in turn.

5.1. Virgin Size Distributions

There are considerable differences observable between the virgin size distributions of the subject materials in this research. Firstly, the golden breadcrumbs exhibit a wider size distribution, where considerable sample mass is clearly spread across seven size fractions from 180 to 1400 µm. Additionally, smaller size fractions are represented with smaller mass percentages. In comparison, the salt exhibited a much narrower overall size distribution, with 75% of the sample by mass residing in two size fractions – on the 250 and 355 µm sieves.

5.2. Full Size Distribution Tests

Observations of the full size distribution tests display behavior typical of attrition tests for most common materials. In the larger size fractions, more mass is retained for low impact velocities in comparison to the high impact velocities. This indicates that more of the larger particles in a sample break under high impact energies. Additionally, it is evident that less mass is retained in the smaller size fractions at low impact velocities in comparison to the higher impact velocities. As expected, an increased number of smaller particles are generated at higher impact velocities.

Figure 13 shows the percentage gain or loss in material for golden breadcrumbs in each size fraction, based on the virgin size distribution for each of the three impact velocities considered.

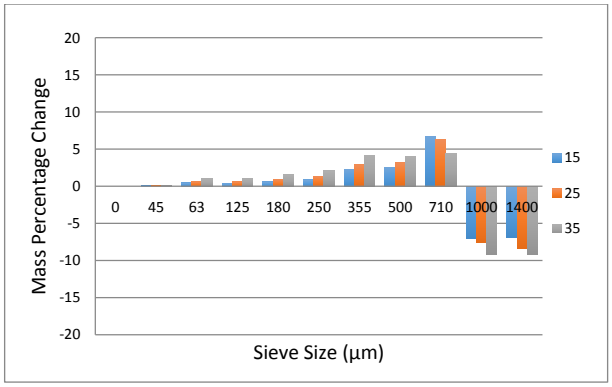

Figure 13: Mass Percentage Change of Golden Breadcrumbs under Impact Velocities (measured in m/s)

The only size fraction that does not follow the expected trend with regards to impact velocity, is the 710 µm sieve. Rather than gaining more material as the impact velocity increases, the reverse is true. This may indicate that this particular size fraction loses more material through particle breakage, than it gains from particle breakage of larger size fractions, namely the 1000 and 1400 µm fractions. By increasing the impact velocity, and hence the impact energy, this behavior is emphasized. Figure 14 presents the results of the same analysis for salt.

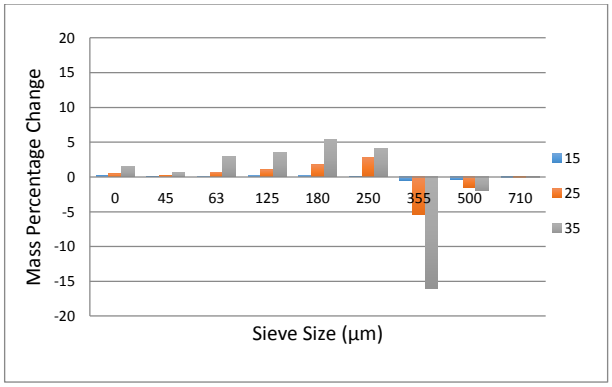

Figure 14: Mass Percentage Change of Salt under Impact Velocities (measured in m/s)

It is evident from the minimal migration of material across the size fractions at 15 m/s, that the impact energy is not sufficient to cause a significant amount of degradation. However, it can be concluded that at 25 and 35 m/s, the impact energy is sufficient to generate smaller particles from the larger size fractions. In particular, large changes are observed at 35 m/s, where a significant proportion of particles undergo size changes.

5.3. Narrow Size Fraction Tests

General observations of the narrow size fraction attrition tests clearly show that larger particles are more susceptible to breakage in comparison to smaller particles for the materials studied. Additionally, the narrow size fractions display similar behavior to that observed in the full size distribution tests, where more particles are broken at higher impact velocities.

Figures 15, 16 and 17 show the percentage change in the size distribution for narrow size fractions of 1000-1400, 710-1000, and 500-710 µm for golden breadcrumbs respectively.

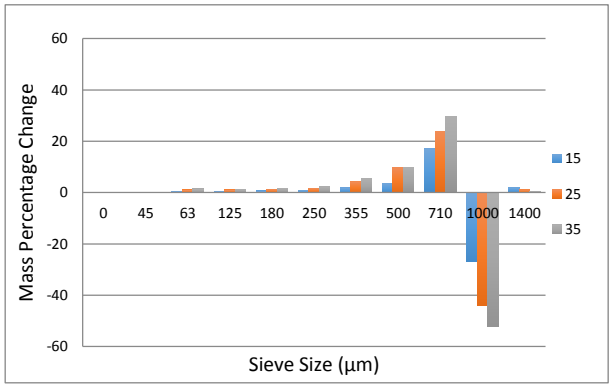

Figure 15: Mass Percentage Change of Golden Breadcrumbs under Impact Velocities (measured in m/s) for the Size Fraction 1000-1400 µm

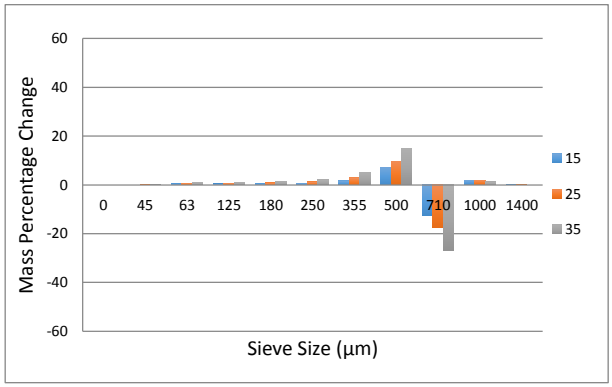

Figure 16: Mass Percentage Change of Golden Breadcrumbs under Impact Velocities (measured in m/s) for the Size Fraction 710-1000 µm

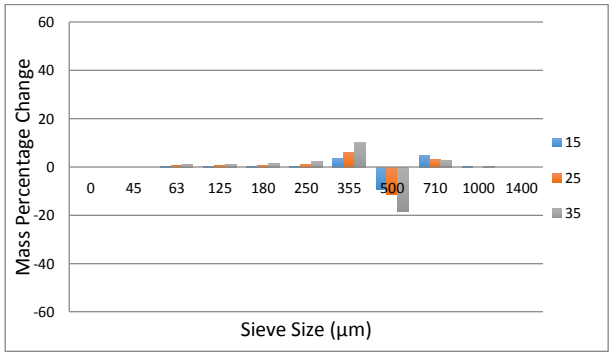

Figure 17: Mass Percentage Change of Golden Breadcrumbs under Impact Velocities (measured in m/s) for the Size Fraction 500-710 µm

This analysis shows some mass retained on sieves larger than the size fraction under scrutiny. This is due to the irregular shape of the particles, which have diameters dependent on the orientation of the particle with respect to the sieve mesh.

In comparing the analysis of three adjacent size fractions for golden breadcrumbs, particle sizes greater than 1000 µm in diameter break to a considerably greater degree than either of those retained on 500 or 710 µm sieves. This suggests that once particles reach 1000 µm in diameter, the particle material does not have enough internal strength to withstand the momentum transfer of the impact. However, with the reduced diameter of the 710 and 500 µm particles, the mass is sufficiently small to maintain the structure of more particles post-impact.
Figures 18 and 19 show the mass percentage change analysis of the 355-500 and 250-355 µm size fractions for salt respectively.

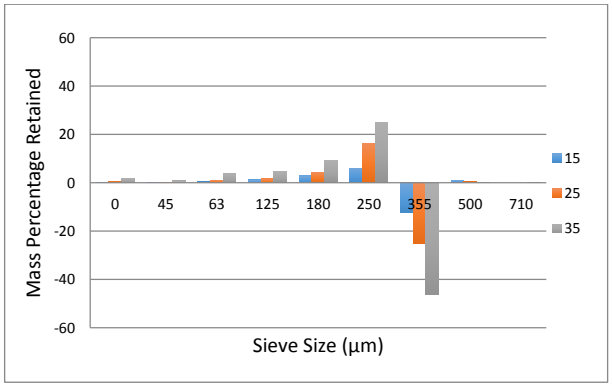

Figure 18: Mass Percentage Change of Salt under Impact Velocities (measured in m/s) for the Size Fraction 355-500 µm

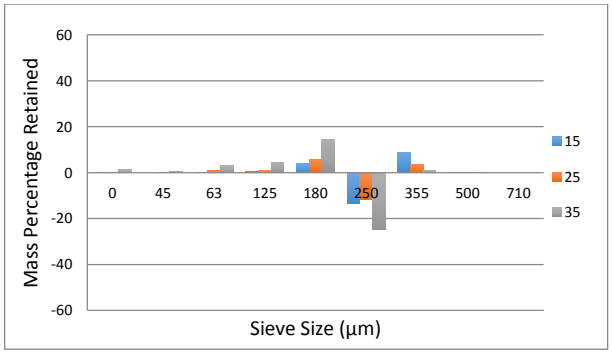

Figure 19: Mass Percentage Change of Salt under Impact Velocities (measured in m/s) for the Size Fraction 250-355 µm

Even though the size fractions considered for salt are smaller than those considered for golden breadcrumbs, the magnitude of breakage occurring is comparable under some impact velocities. For example, the amount of material lost for salt in the 355 µm size fraction tested at 35 m/s, is of the same order of magnitude as that lost for golden breadcrumbs in the 1000 µm size fraction at 35 m/s. While there is little relationship between the two materials with respect to particle size, this demonstrates the influence of the material with regard to the particle strength.

5.4. Particle Breakage Relationships

The full size distribution of a sample material post-breakage should be composed of breakage of each size fraction if a logical progression is followed. Therefore, the breakage of the narrow size fractions will be used to construct a predictive size distribution for the full distribution of material at each of the breakage velocities. The simulated size distributions will calculated from three components:

1. The percent mass of the virgin size distribution,
2. The amount of material lost in each of the size fractions tested for their breakage characteristics,
3. The amount of material contributed to each size fraction from the breakage tests address in Component 2.

This approach will make the following assumptions/limitations:

- Material collected on sieves greater than the diameter of size fractions of interest in the narrow size fraction post-breakage measurements will be omitted and treated as an error in the experimental method,
- Material in the virgin size distribution greater in diameter than that considered in narrow size fraction testing will be omitted from the results displayed, however will still be accounted for in overall sample size to calculate percentage masses of subsequent size fractions,
- Material in size fractions smaller than those tested under the narrow size fraction tests will be treated as stationary (undergo no breakage in the simulation),
- Only a limited number of size fractions will be considered in the testing regime, as addressed in Section 4.3.

The generalized equation used to calculate the simulated percentage mass retained on the sieve for a given size fraction is given in Equation 1.

$$m_{frac,sim} = m_{frac,vir} + \sum_{Frac} \left(\frac{p_{frac}}{100} \times m_{tot,sim} \right) \quad (1)$$

Where:

- $m_{frac,sim}$ is the simulated mass retained in a simulated breakage,
- $m_{frac,vir}$ is the mass retained for a given fraction in the material virgin size distribution,
- $m_{tot,sim}$ is the total sample mass of material input into the simulated breakage and is composed of the full size distribution,
- p_{frac} is the percentage change in mass of each fraction as a function of the sample mass.

Figures 20, 21 and 22 compare the experimental results (denoted by FSD) and the simulated results (denoted by SIM) for golden breadcrumbs at impact velocities of 15, 25, and 35 m/s respectively.

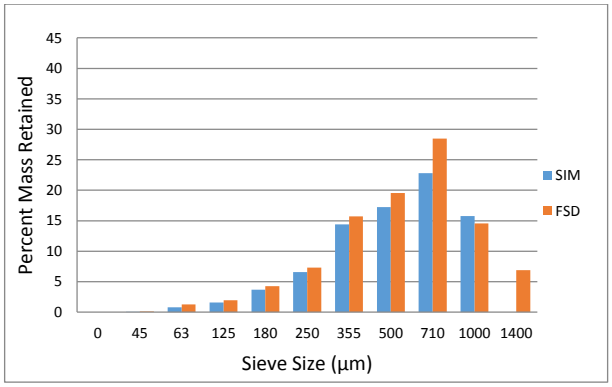

Figure 20: Simulated and Experimental Post-Test Golden Breadcrumb Size Distributions at 15 m/s Impact Velocity

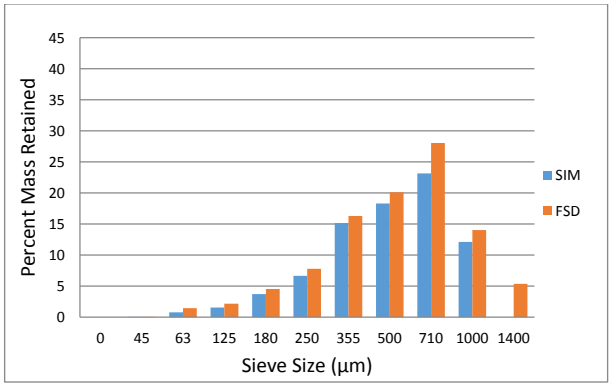

Figure 21: Simulated and Experimental Post-Test Golden Breadcrumb Size Distributions at 25 m/s Impact Velocity

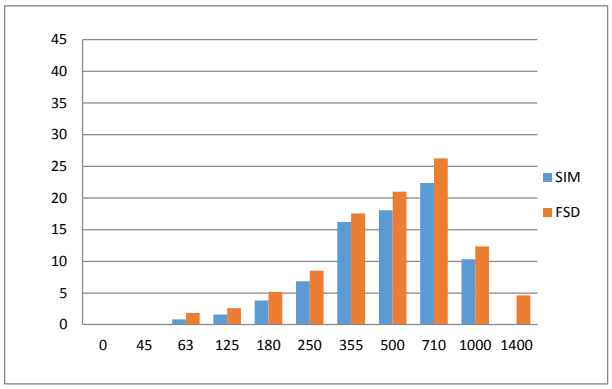

Figure 22: Simulated and Experimental Post-Test Golden Breadcrumb Size Distributions at 35 m/s Impact Velocity

Considering the assumptions made in the simulation method, the predictions made fit reasonably well with the full size distribution breakage results. The most notable differences that can be observed lie primarily in the larger size fractions, namely 710 and 1000 µm. This observation is expected, as the 1400 µm size fraction was not considered in the narrow size fraction breakage analysis. It would be logically sound to state that this size fraction would contribute to the 710 and 1000 µm fractions, increasing agreement between the simulated and experimental values.

With regard to the smaller size fractions, the simulation underestimates the magnitude consistently. This may be explained by the simulation failing to account for the movement of all size fractions below those for which results are presented. It is expected that all fractions will break to some degree, thus contributing to the stated error.

By taking into consideration both of the aforementioned statements, the accuracy of the simulated predictions could be increased.

Figures 23, 24 and 25 compare the experimental results (denoted by FSD) and the simulated results (denoted by SIM) for salt, at impact velocities of 15, 25, and 35 m/s respectively.

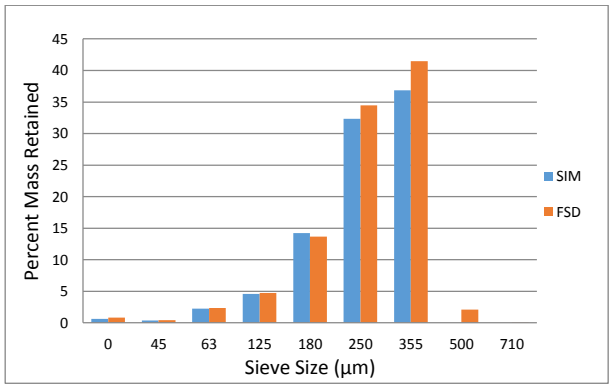

Figure 23: Simulated and Experimental Post-Test Salt Size Distributions at 15 m/s Impact Velocity

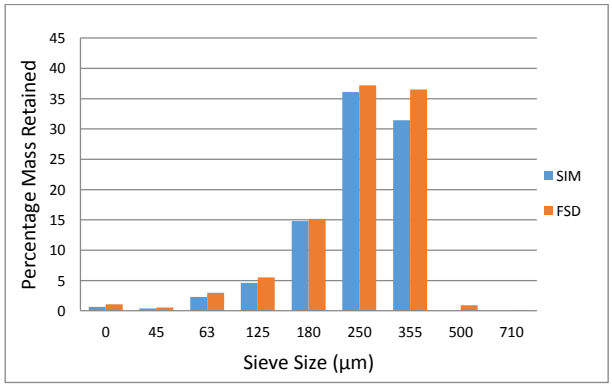

Figure 24: Simulated and Experimental Post-Test Salt Size Distributions at 25 m/s Impact Velocity

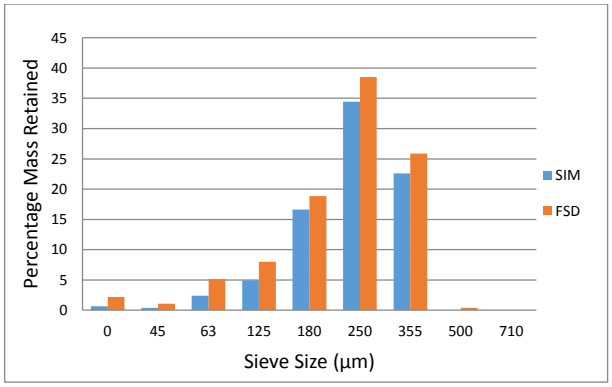

Figure 25: Simulated and Experimental Post-Test Salt Size Distributions at 35 m/s Impact Velocity

As with the golden breadcrumbs, a good agreement between the simulated and experimental results for salt is achieved. Almost all size fractions are under-predicted once again, and as with the golden breadcrumbs, the logical explanations for this behavior lie with the omission of larger size fractions than what underwent testing, in addition to the migration of smaller size fractions.

6. CONCLUSIONS

Research into the breakage characteristics of two granulated food products, one crystalline in structure and the other non-crystalline, has been performed. The virgin size distributions were determined, and then the resulting size distributions were tested under three impact velocities: 15, 25 and 35 m/s. Subsequently, three size fractions for golden breadcrumbs and two size fractions for salt were tested under the same conditions as the full size distributions. The results of the latter tests were used to simulate the conditions of the full size distribution breakage characteristics.

The simulated results found good agreement across each of the two materials and the three impact velocities considered. The discrepancies between the experimental and simulated results have been attributed to a combination of omitting the larger size fractions not considered in the testing, and neglecting the migration of the smaller size fractions down the material size distribution. Both discrepancies may be addressed with further testing.

7. FUTURE DIRECTION

The future direction of this work falls primarily into two categories: enhancing the predictive capabilities of this method of analysis, and to enhance understanding of how this analysis may be used in the design and/or optimization process.

Enhancing the predictive capabilities of this method includes looking more holistically at the size distribution and testing the breakage characteristics of every available size fraction. From this, increasing the accuracy of the final size distribution prediction should be achievable.

The application of this analysis would involve obtaining a greater understanding of the process in question, subsequently followed by identifying the undesirable material qualities that result from excess attrition. Determining the ratio of size fractions that exhibit these undesirable qualities will then enable quantification of the process conditions to be avoided.

ACKNOWLEDGEMENTS

The author would like to express gratitude for the valuable input of others in this programme of research. In particular, Mr Jonathon Larkin for his technical advice, and Mrs Caroline Chapman for her administrative assistance. Without their support, this work would not be possible.

REFERENCES

Bridle I., 2000. The analysis of particle degradation in pneumatic conveyors utilizing a pilot-sized test facility. Thesis (PhD). University of Greenwich.

Burnett A.J., 1996. The use of laboratory erosion tests for the prediction of wear in pneumatic conveying bends. Thesis (PhD). University of Greenwich.

Chapelle P., Abou-Chakra H., Christakis N., Patel M., Abu-Nahar A., Tüzün U., Cross M., 2004. Computational model for prediction of particle degradation during dilute-phase pneumatic conveying: the use of a laboratory-scale degradation tester for the determination of degradation propensity. Advanced Powder Technology, 15 (1), 13-29.

Deng T., Li J., Chaudhry A.R., Patel M., Hutchings I., Bradley M.S.A., 2005. Comparison between weight loss of bends in a pneumatic conveyor and erosion rate obtained in a centrifugal erosion tester for the same materials. Wear, 258, 402-411.

Kalman H., 2000. Attrition of powders and granules at various bends during pneumatic conveying. Powder Technology, 112, 244-250.

Macchini R., Bradley M.S.A., Deng T., 2013. Influence of particle size, density, particle concentration on bend erosive wear in pneumatic conveyors. Wear, 303, 21-29.

Sato S., Shimizu A., Yokomine T., 1995. Numerical prediction of erosion for suspension flow duct. Wear, 186-187, 203-209.

van Laarhoven B., Schaafsma S.H., Meesters G.M.H., 2012. Towards a desktop attrition tester; validation with dilute phase pneumatic conveying. Chemical Engineering Science, 73, 321-328.

AUTHOR'S BIOGRAPHY

Benjamin Kotzur commenced his PhD research at The Wolfson Centre for Bulk Solids Handling Technology, at the University of Greenwich, in May 2014. Having grown up in a family business designing bulk solids storage and handling facilities, he completed his Bachelor of Engineering (Scholars) (Honors) at the University of Wollongong, Australia, with a focus on modelling of bulk materials in dynamic systems. He specialises in the measurement and prediction of particle attrition during lean phase pneumatic conveying, however, he retains a keen interest in all bulk solids handling processes, across a vast range of industrial and academic spheres.

OPTIMIZATION OF TRANSPORTATION DECISIONS UNDER EXCLUSIONARY SIDE CONSTRAINTS IN FOOD SUPPLY CHAIN

Marcin Anholcer[(a)], Arkadiusz Kawa[(b)]

[(a),(b)]Poznań University of Economics,
al. Niepodległości 10, 61-875 Poznań, Poland

[(a)]m.anholcer@ue.poznan.pl, [(b)]arkadiusz.kawa@ue.poznan.pl

ABSTRACT

The main objective of this paper is to develop an effective model of planning food supplies, when exclusionary constraints are present. In order to achieve this objective, we performed two stages of research, each of which had its own partial goals. The first part of the research aims for identification of the types of the exclusionary constraints that exist in the real world. The objective of the second stage is to develop mathematical models of transportation problems that include the exclusionary constraints existing in reality.

Keywords: optimization of transportation, exclusionary constraints, food supply chain

1. INTRODUCTION

A supply chain is a network of organizations working together in different processes and activities in order to bring products and services to the market, with the purpose of satisfying customers' demands (Ahumada and Villalobos 2009). In the case of a food supply chain, as any other supply chain, it is an integrated process where raw materials are acquired, converted into products and then delivered to the consumer; speaking colloquially, it flows from the plant to the plate. The chain is linked with the feed forward flow of materials and the feedback flow of information (Jiang 2009). Tijskens et al. (2001) conclude that the main fact that differentiates food supply chains form other supply chains is a continuous change in quality from the time the raw materials leave the grower to the time the food reaches the consumer.

The topic of the food supply chain is very popular among scientists. This is evidenced by a wide range of research and publications. They concern general problems in food supply chains (Vorst 2000), but there are also investigations which tackle specific problems, such as safety and security issues in the fresh good supply chain (Bruzzone, Longo, Massei, Nicoletti and Agresta 2014), optimization of the fresh food supply chain (Rong, Akkerman and Grunow 2011), evaluating the effectiveness of different policies in managing frozen goods supply chain, (Bruzzone, Massei and Poggi 2007), sustainability and efficiency of logistics in the integrated food district (Bottani, Rizzi and Vignali 2014), traceability (De Cindio, Longo, Mirabelli and Pizzuti 2011a) and track & trace system (De Cindio, Longo, Mirabelli and Pizzuti 2011b) for a food supply chain.

According to Mardsen, Banks and Bristow (2000), creation, operation and evolution of food supply chains are key dimension in the new patterns of rural development now emerging.

The food supply chain is also an interesting subject for institutions which create some rules and best practices for business. In 2010 the European Commission (EC) introduced The High Level Forum for a Better Functioning Food Supply Chain, which ensures the follow up of the recommendations of the High Level Group on the Competitiveness of the Agro-Food Industry (ec.europa.eu 2015). According to EC, the food supply chain consists of three important issues – agriculture, the food processing industry and the distribution system. Those three sectors together account for more than 5% of the European added value and 7% of employment. It is worth to emphasize that the food supply chain has direct consequences for all European citizens, because food represents 16% of the European household expenditures (Commission of the European Communities 2009).

A characteristic thing of the food supply chain is a large variety of entities: farmers, food processors, traders, wholesalers, distributors, logistics companies and retailers. Among these, there are also very large companies and small and medium-sized enterprises which are simultaneously competitors, suppliers or customers. In this industry, companies increasingly cooperate in order to optimize the supply chain. This is reflected most often as: joint commercialization agreements, tying and bundling, joint purchasing agreements (buying alliances) and the increasing use of private labels (Commission of the European Communities 2009).

A lot of challenges are related with food supply chains. One of them is price pressure which forces supply chain leaders into constant efforts to decrease product prices, even when the competitive strategy is primarily focused on such characteristics as quality or delivery time. Globalization and internationalization of enterprises have also contributed to the fact that a large number of

European and American companies produce or commission production in the Asian market (Anholcer and Kawa 2012). According to the McKinsey consultancy, by 2020, production of approximately 80% of goods will take place in a country different from the one where it will be consumed. It will cause huge changes in the movement and consumption of goods (Balou 2007).

What is closely connected with the flow of goods among the entities of the food supply network is transport, which is considered to be one of the most important elements of a logistic system and requires careful planning and control. Lack of planning, ineffective decision making, and poor visibility in transportation can cause companies to overpay, miss delivery targets, and loose valuable business. Transportation costs can be a significant part of a company's overall logistics spending (Murray 2014). According to various estimates, transportation constitutes one-third of the logistics costs (Tseng et al. 2005). Moreover, transportation is the largest end-use contributor toward global warming in many developed countries. Transportation has a significant impact on the food sector because it often involves long-distance shipments, most frequently by road (Wakeland, Cholette and Venkat 2012). Pirog et al. (2001) notice that nearly half of all fruit sold in the US is imported, and that produce grown in North America travels an average of 2.000 km from the source to the point of sale. All the costs are transferred to the customer who needs to pay more for the goods. That is why cutting transportation costs is the major target for companies.

There is a number of transportation strategies that can be applied by management to help improve performance (Murray 2014). One of them is logistics outsourcing. Companies commonly use outside resources, particularly in transport. Logistics service providers often handle loads that come from many different customers. These are products having different physical and chemical properties. They also show different susceptibility to transport, which causes some problems. That is why in many cases it is necessary to impose some exclusionary constraints on the transportation process. In particular, it can be the case when some types of goods cannot be transported by the same mean of transport (like alive animals and frozen fruits and vegetables). Another situation where such constraints have to be imposed is when some suppliers do not want their products to be delivered to the same customer (e.g. because of some reasons concerning the marketing strategy of the company). However, as we can see below, it is not easy to find effective methods of dealing with such types of constraints.

For these reasons the main objective of this paper is to develop an effective model of planning food supplies, when the exclusionary constraints are present.

2. EXCLUSIONARY CONSTRAINTS

For the purpose of this paper we have performed two stages of research. In the first stage empirical research was conducted with the use of secondary and primary sources. On the basis of the secondary sources (scientific papers, industry materials, market reports), we identified exclusionary constraints that were subjected to primary research. Next, we conducted the primary empirical research based on qualitative research in the form of FGI (Focus Group Interview). The main objective of this research was to diagnose the types of exclusions emerging in transport. In July 2015 we conducted FGIs in three cities in Poland using questionnaires with managers from transport and distribution companies. The sample size was three groups, each of which consisted of 5-7 persons.

In order to ensure comparability, the studies in the three cities proceeded along the same scenario. A moderator supervised the procedure, and was also responsible for making all participants contribute to the discussion as equally as possible and, if necessary, for stopping those who excessively tried to impose their views on the other group members. The interviews took place in professional focus rooms, making the experiment comfortable. They took approximately one and a half hours, the procedure was recorded (audio and video).

On the basis of those focus group interviews, the following exclusionary constraints that occur in shipment were determined:

- Sensitivity to duration of transport.
- Sensitivity to carriage temperature.
- Sensitivity to air humidity.
- Sensitivity to effects of light.
- Sensitivity to absorption of odors.
- Chemical composition of the product.
- Perishable goods.
- Dangerous goods.
- Animals.
- Competitive products.
- Exclusive transport agreement.

The majority of the above agree with the exclusionary constraints presented in the literature.

In the second stage, based on the determined exclusionary constraints existing in reality, we developed mathematical models of the transportation problems.

3. TRANSPORTATION PROBLEM MODEL

The transportation (and, more generally, network) problems with linear side constraints were considered e.g. in (Glover et al. 1978; Klingman anf Russel 1975; Thompson and Setbi 1986). It seems that the transportation problem with exclusionary constraints (TPESC), which are in turn nonlinear, appeared for the first time in (Cao 1992). The author considered an ordinary transportation problem with additional condition that for each supplier there are some pairs of destinations that cannot be served at the same time, i.e.:

$$x_{ij} x_{ik} = 0 \tag{1}$$

for certain triples (i, j, k), where i is number of a supplier and $i \neq j$ are numbers of destinations. The author provided a branch and bound method to solve this problem. In (Cao and Uebe 1995) the same problem was solved with tabu search. In (Sun 2002), Sun proposed two branch and bound methods to solve the 0-1 mixed integer formulation of the discussed problem. Goossens and Spieksma in (Goossens and Spieksma 2009) studied the computational complexity of the TPESC, proving that it is NP-hard and becomes solvable in pseudo-polynomial time when the number of supply nodes is fixed. They also studied the TPESC with identical exclusionary sets. Recently, Vancroonenburga et al. (2014) studied the so-called red-blue transportation problem, being a special case of the TPESC, where suppliers are assigned to one of two disjoint sets, and each customer is supposed to obtain the deliveries only from the suppliers from one of these sets.

Of course all the above problems have very specific form, as the transportation network in each case has the form of bipartite graph. This is usually not the case in the real-life problems. Another issue is that the authors rather arbitrarily assumed the type of possible exclusions, at least they did not refer to any real-life data.

Also other types of networks were studied. Darmann et al. in (2011) consider the Minimum Spanning Tree Problem, the Maximum Matching Problem and the Shortest Path Problem with binary disjunctive constraints. Pferschy and Schauer in (2013) studied, among others, the Maximum Flow Problem with additional exclusionary constraints, where the exclusions were not restricted to the arcs starting in one vertex. As one can easily see, the last mentioned problems, although involving various types of possible networks, do not focus on the optimization of the transportation process. In some sense, this was the goal of Zhang et al. (2011), who considered the Minimum Spanning Tree Problem with exclusionary constraints and of Öncan et al. (2013), who considered the Minimum Cost Perfect Matching Problem with exclusionary constraints. In both cases, however, the transportation network has so simple structure, that it is far away of the reality.

To summarize, no one so far has considered the minimization of the transportation costs in the networks (especially in food supply chain), which structure is close to the real-life networks and exclusionary constraints are present. Only some attempts were made in the last years to investigate simple models. In consequence no one has studied the methods of solution of problems similar to the real-life problems. From this point of view, the model presented below has pioneering nature.

Let us start with the structure of a typical logistic food supply chain. If we consider a single product, such a chain has the structure of layered network, as presented on Fig.1. Between the layers all the connections are possible, however, in practice, only few of them are in use (it follows from the properties of the solutions of network problems and consistent with the common sense).

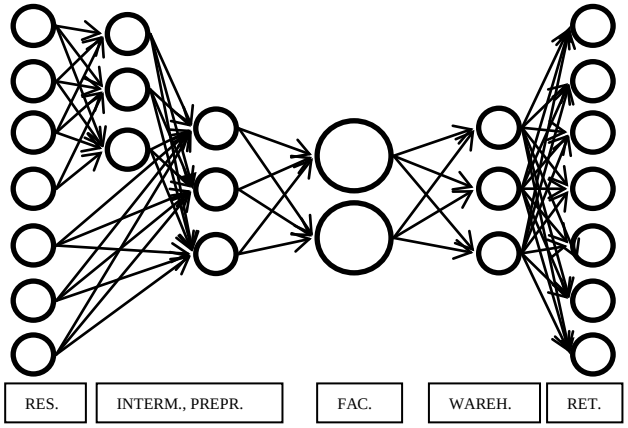

Figure 1: Scheme of food supply chain

What is important, there are many suppliers of the resources, then there are some intermediaries and factories pre-processing the resources and very few (sometimes even one) factories producing the final product. Then the chain starts to be wider again – there are usually more warehouses/logistic centers than factories and much more retailers/ final customers. If we divide the chain into two parts, one can easily see that the part before the main factories can be a little bit complicated (some resources are delivered to the first layer of factories, some of them to the second layer, sometimes the same resource may be necessary in various layers), which sometimes may even cause the network loose the layer structure. What is more important for us – the chains of various products are usually disjoint in this stage. According to the performed research, the problems with exclusions more likely appear in the second part of the chain. Even if the exclusionary constraints rarely touch the products leaving one factory, they start to be important on the level of warehouses/logistic centers, where various products are combined. It is a direct consequence of the fact that the logistic chains of many products intersect at this stage. In the remainder of this section we will thus focus on the second part of the chain.

As we already observed, it can be assumed that the transportation network on this stage consists of the layers and the transportation is possible only between two neighboring ones. We number the layers with consecutive integers and denote the number of a layer with l, $l = 1, 2, \ldots, L$ (where L denotes the total number of layers). The number of agents in layer l (factories, centers, warehouses, shops etc.) will be denoted by $n(l)$ and the index of chosen agent by $i(l)$. The total number of goods to be transported is G, and the index of a good will be denoted by g. The amount of good g accessible at any node of the network in the considered period will be denoted by $a(l, i(l), g)$ – this numbers are positive for all the layers except the last one, where the negative

values correspond with the demand (all those numbers are parameters in the presented model, but can be treated as variables if one considers a dynamic version, see the section "Conclusions and future work"). We assume that the links between nodes are not capacitated (e.g., it is always possible to send more trucks in order to transport all goods). The capacities of the nodes are denoted by $u(l, i(l))$ (they are defined only for the inner nodes, i.e. the nodes in all the layers except the first and last ones). The volume of a unit of good g is $v(g)$. The unit costs of transferring good through respective node (e.g. the production costs, storage costs etc.) will be denoted by $d(l, i(l), g)$. The unit cost of transportation of good g between agent $i(l)$ from layer l and agent $i(l + 1)$ from layer $l + 1$ will be denoted by $c(l, i(l), i(l + 1), g)$.
The variables will correspond with the flows of goods between the nodes/agents and to the amounts of good transferred through the respective nodes. In particular, the amount of good g transported between agent $i(l)$ from layer l and agent $i(l + 1)$ in layer $l + 1$ will be denoted by $x(l, i(l), i(l + 1), g)$. The total amount of good g transferred through node $i(l)$ in layer l will be denoted by $y(l, i(l), g)$.
Since we are interested in the minimization of the cost, the objective function (to be minimized) has the form:

$$f(x) = \sum_{g=1}^{G}\sum_{l=1}^{L-1}\sum_{i(l)=1}^{n(l)}\sum_{i(l+1)=1}^{n(l+1)} c(l,i(l),i(l+1),g)x(l,i(l),i(l+1),g) + \sum_{g=1}^{G}\sum_{l=1}^{L}\sum_{i(l)=1}^{n(l)} d(l,i(l),g)y(l,i(l),g) \quad (2)$$

The capacity constraints have the form:

$$\sum_{g=1}^{G} v(g)y(l,i(l),g) \le u(l,i(l)), \quad l = 2,...,L-1, i(l) = 1,...,n(l) \quad (3)$$

$$x(l,i(l),i(l+1),g) \ge 0, \quad l = 1,...,L, i(l) = 1,...,n(l), \quad i(l+1) = 1,...,n(l+1), g = 1,...,G \quad (4)$$

The mass balance constraints are:

$$\sum_{i(2)=1}^{n(2)} x(1,i(1),i(2),g) \le a(1,i(1),g), \quad i(1) = 1,...,n(1), g = 1,...,G \quad (5)$$

$$\sum_{i(l-1)=1}^{n(l-1)} x(l-1,i(l-1),i(l),g) + a(1,i(1),g) = y(l,i(l),g), \quad l = 2,...,L-1, i(l) = 1,...,n(1), g = 1,...,G \quad (6)$$

$$\sum_{i(l+1)=1}^{n(l+1)} x(l+1,i(l),i(l+1),g) \le y(l,i(l),g), \quad l = 2,...,L-1, i(l) = 1,...,n(1), g = 1,...,G \quad (7)$$

$$\sum_{i(L-1)=1}^{n(L-1)} x(L-1,i(L-1),i(L),g) \ge -a(L,i(L),g), \quad i(L) = 1,...,n(L), g = 1,...,G \quad (8)$$

Finally, we need to include the exclusionary constraints. As mentioned before, sometimes two goods cannot be transported together because of their properties. Assume that good g_1 and g_2 cannot be included in the same transport. Then the constraints could take the form:

$$x(l,i(l),i(l+1),g_1)x(l,i(l),i(l+1),g_2) = 0, \quad l = 1,...,L-1, i(l) = 1,...,n(l), i(l+1) = 1,...,n(l+1) \quad (9)$$

This is a nonlinear constraint. However, we can preserve the linearity of the model by introducing sufficiently large number M (for example equal to the maximum capacity of a node in the supply chain) and binary variables $\alpha(g_1, g_2, l, i(l), i(l+1))$ (equal to 1 if the good g_1 can be transported and g_2 cannot, and 0 otherwise). Then for each l, $i(l)$ and $i(l + 1)$, the constraint (9) can be written in an equivalent form (note that we need to use two constraints here instead of one):

$$x(l,i(l),i(l+1),g_1) \le \alpha(g_1,g_2,l,i(l),i(l+1))M \quad (10)$$

$$x(l,i(l),i(l+1),g_2) \le (1-\alpha(g_1,g_2,l,i(l),i(l+1)))M \quad (11)$$

Another kind of exclusion can take place if two goods cannot be transferred simultaneously through chosen nodes. In such case the constraint, for defined l and $i(l)$, would be as follows:

$$y(l,i(l),g_1)y(l,i(l),g_2) = 0 \quad (12)$$

Again we can use a similar transformation as in the case of constraints (9), by using respectively defined variables $\beta(g_1, g_2, l, i(l))$:

$$y(l,l(i),g_1) \le \beta(g_1,g_2,l,i(l))M \quad (13)$$

$$y(l,l(i),g_2) \le (1-\beta(g_1,g_2,l,i(l)))M \quad (14)$$

4. CONSLUSIONS AND FUTURE WORK

The exclusionary constraints are defined for goods – e.g. if some pair of good cannot be transported together, the constraint looks same for all the combinations of nodes. This together with the possibility of involving the binary variables suggests that the problem can be solved by a branch-and-bound method. It is well-known, however, that such methods work in a polynomial time, which is not acceptable when taking

into account the number of the binary variables even in small instances of the problem. Thus usage of some heuristics or metaheuristics could be useful. The design of various solutions methods for the problem described above will be our main interest in the nearest future.

What is worth mentioning, the above model is quite simple. At least four modifications could be introduced and will be analyzed in the future. The first one is introduction of time to the model, i.e. changing the static model described in this article into a dynamic one. The second modification is the generalization to the supply chains where transportation is possible also between two non-neighboring layers (or, in other words, the network is no more a layered network). Third possible modification is considering the fixed charge costs. The fourth one – considering the model where the costs are nonlinear (in particular piecewise linear). Also in the case of these four modifications the development of effective solution methods will be one of our interests.

ACKNOWLEDGMENTS

The paper was written with financial support from the National Center of Science (Narodowe Centrum Nauki) – the grant of the no. DEC-2014/13/B/HS4/01552.

REFERENCES

Ahumada O., Villalobos J. R., 2009. Application of planning models in the agri-food supply chain: A review. European Journal of Operational Research,196(1), 1-20.

Anholcer M., Kawa A., 2012. Optimization of Supply Chain via Reduction of Complaints Ratio". In: Jezic G., Kusek M., Ngoc-Thanh Nguyen N.-T., Robert J., Howlett R.J., Lakhmi C., Jain L.C. (eds.): "Agent and Multi-Agent Systems. Technologies and Applications". Lecture Notes in Computer Science, 2012, Volume 7327/2012.

Balou R.H., 2007. The evolution and future of logistics and supply chain management, "European Business Review", vol. 19, no. 4.

Bottani E., Rizzi, A. and Vignali G. 2014. Improving logistics efficiency of industrial districts: a framework and case study in the food sector. International Journal of Logistics Research and Applications, (ahead-of-print), 1-22.

Bruzzone A.G., Massei M. and Poggi S., 2007. Simulation based analysis on different logistics solutions for fresh food supply chain. In Proceedings of the 2007 spring simulation multiconference-Volume 3 (pp. 84-89). Society for Computer Simulation International.

Bruzzone A.G., Longo F., Massei M., Nicoletti L. and Agresta M., 2014. Safety and security in fresh good supply chain, "International Journal of Food Engineering", 10 (4), pp. 545-556.

Cao B., 1992. Transportation problem with nonlinear side constraints a branch andbound approach. Mathematical Methods of Operations Research (ZOR) 36, 185–197.

Cao B., Uebe G., 1995. Solving transportation problems with nonlinear side constraints with tabu search. Computers and Operations Research 22, 593–603.

Commission of the European Communities, 2009. A better functioning food supply chain in Europe, Communication from the Commission to the European Parliament, the Council, the European economic and social committee and the committee of the regions, Brussels, 28.10.2009, COM, 591 final.

Darmann A., Pferschy U., Schauer J., Woeginger GJ., 2011. Paths, trees and matchings under disjunctive constraints. Discrete Appl Math 159 (16):1726–1735.

De Cindio B., Longo F., Mirabelli G., Pizzuti T., 2011a. Modelling a Traceability System for a Food Supply Chain: Standards,Technologies and Software Tools. In: Proceedings of the 10th International Conference on Modeling and Applied Simulation. p. 488-494, ISBN: 978-88-903724-5-2, Rome, SEPTEMBER 12-14 2011.

De Cindio B., Longo F., Mirabelli G., Pizzuti T., 2011b. Tracking and tracing in the food industry: Opportunity and competitiveness advantage analysis. Industrie alimentari, vol. 50, p. 7-19.

Glover F., Karney D., Klingman D., and Russel R., 1978. Solving singly constrained transshipment problems, Transportation Science 12, 277–297.

Goossens D., and Spieksma F.C.R., 2009. The transportation problem with exclusionary side constraints. 4OR, A Quarterly Journal of Operations Research, 7, 51–60.

http://ec.europa.eu/agriculture/markets-and-prices/food-supply-chain/index_en.htm (accessed 14 July 2015).

Jiang Y., Zhao L. and Sun S.A., 2009. Resilient Strategy for Meat-food Supply Chain Network Design, 2009 IEEE International Conference on Industrial Engineering and Engineering Management.

Klingman D., Russel R., 1975. Solving constrained transportation problems. Operations Research 23:91 – 106.

Marsden T., Banks, J. and Bristow G., 2000. Food supply chain approaches: exploring their role in rural development. Sociologia ruralis, *40*(4), 424-438.

Murray M. (2014), Reducing Transportation Costs, http://logistics.about.com/od/forsmallbusinesses/a/Reducing-Transportation-Costs.htm (accessed 14 July 2015).

Öncan T., Zhang R. and Punnen A.P., 2013. The minimum cost perfect matching problem with conflict pair constraints, Computers and Operations Research, Volume 40, Issue 4, April 2013, Pages 920–930.

Pferschy U., Schauer J., 2013. The maximum flow problem with disjunctive constraints. Journal of Combinatorial Optimization, 26, 109–119.

Pirog R., Pelt T.V., Enshayan K. and Cook E., 2001. Food, fuel, and Freeways: An Iowa perspective on how far food travels, fuel usage, and greenhouse gas emissions. Ames, Iowa: Leopold Center for Sustainable Agriculture.

Rong A., Akkerman R., Grunow M., 2011. An optimization approach for managing fresh food quality throughout the supply chain. International Journal of Production Economics, 131(1), 421-429.

Sun M., 2002. The transportation problem with exclusionary side constraints and two branch-and-bound algorithms. European Journal of Operational Research,140, 629–647.

Thompson G.L., Setbi A.P., 1986. Solution of constrained generalized transportation problems using the pivot and probe algorithm. Computer and Operational Research 13:1- 9.

Tijskens L.M.M., Koster A.C., Jonker J.M.E., 2001. Concepts of chain management and chain optimization, Food Process Modeling, Woodhead Publishing Ltd., Cambridge, UK.

Tseng Y., Yue W.L. and Taylor M.A.P., 2005. The role of transportation in logistics chain. Proceedings of the Eastern Asia Society for Transportation Studies, Vol. 5, 1657–1672.

Vancroonenburga W., Della Croce F., Goossensd D., Spieksmae F.C.R., 2014. The Red–Blue transportation problem, European Journal of Operational Research 237, 814–823.

Vorst, V. D. J., 2000. Effective food supply chains; generating, modelling and evaluating supply chain scenarios, PhD Thesis.

Wakeland W., Cholette S., and Venkat K., 2012. Food transportation issues and reducing carbon footprint. In Green Technologies in Food Production and Processing (pp. 211-236). Springer US.

Zhang R., Kabadi S.N. and Punnen A.P., 2011. The minimum spanning tree problem with conflict constraints and its variations. Discrete Optimization 8(2):191–205.

AUTHORS BIOGRAPHY

Dr. **Marcin Anholcer** is assistant professor at the Department of Operations Research. He got PhD in economics (2006) and mathematics (2011). His scientific interests are related to graph theory and network optimization.

Dr. **Arkadiusz Kawa** is assistant professor at the Department of Logistics and Transport. He got PhD in economics (2009). His scientific interests are related to logistics, supply chain management and business network.

EFFECT OF FOAMING AGENT, FOAM STABILIZER AND WHIPPING TIME ON DRYING PROCESS OF TOMATO PASTE UNDER DIFFERENT DRYING EQUIPMENT

A.M. Olaniyan[a], J.A. Adeoti[b], M.O. Sunmonu[c]

[(a)]Department of Agricultural and Bioresources Engineering, Faculty of Engineering, Federal University Oye Ekiti, P.M.B. 373, Oye Ekiti 371101, Ekiti State, Nigeria

[(b),(c)]Department of Agricultural and Biosystems Engineering, Faculty of Engineering and Technology, University of Ilorin, P.M.B. 1515, Ilorin 240003, Kwara State, Nigeria

[(a)]amolan397@hotmail.com; adesoji.olaniyan@fuoye.edu.ng

ABSTRACT

Laboratory experiments were conducted to determine the effect of foaming agent (egg white, EW), foam stabilizer (carboxyl methyl cellulose, CMC) and whipping time on drying rate and quality of tomato (*Lycopersicon esculentus)* paste dried under air oven, microwave oven and mechanical dryer. A 4^3 factorial experiment in Randomized Complete Block Design (RCBD) was used to study the effect four levels each of foaming agent (5, 10, 15 and 20% EW), foam stabilizer (0.15, 0.30, 0.45 and 0.60% CMC) and whipping time (3, 5, 7 and 9 min) on drying rate and quality of foam-mat dried tomato powder in the three drying equipment. Each trial was performed in triplicates making a total number of 576 samples that were individually tested and measured. 25 g sample of the paste were dried to a moisture content of 7.60 % (wb) for 8 h in mechanical dryer and oven dryer at temperatures of 55 ^{0}C and 50 ^{0}C respectively and 10 min in microwave oven at 540W. Data obtained from the experiments were statistically analyzed using the analysis of variance (ANNOVA) while the Duncan's Multiple Range Test was used to compare the means. Results showed that drying rate increased with increase in foaming agent, foam stabilizer and whipping with minimum values of 9.21 g/h obtained in mechanical dryer, 9.31 g/h in air oven, and 8.05 g/h in microwave oven. Increase in foaming agent, foam stabilizer and whipping time did not cause any adverse effect on vitamin C, ash, protein, fat, carbohydrate, crude fibre contents of the samples. Samples reached a stable moisture content of 7.60 % (wb) in less than 8 h in mechanical dryer and air and less than 10 min in microwave oven. The results of the study showed that egg white, CMC and whipping time influenced the drying rate and quality of foam-mat dried tomato powder.

Keywords: foaming agent, foam-mat drying, foam stabilizer, drying rate, equipment, tomato

1. INTRODUCTION

Tomato (*Lycopersicon esculentus*) is the second most important vegetable in many regions of the world with the production in Nigeria being more than doubled in the last ten years. In 2001 alone, the production was 879,000 metric tonnes (FAO 2002) and these were largely consumed in the fresh state. Large quantities are processed into soups, juices, sauces, puree, paste and canned products. Transportation of tomatoes over long distance, hauls in lorries or trucks or in basket subject the tomatoes to vibration and bruising, hence cause loss of nutrient due to enzymatic actions.

Daily intake of tomatoes provides the body some nutrients such as carotene, vitamin, lycopene which lower the risk of cancer and cardiovascular diseases as recommended by the American Cancer Society (Block, Patterson, and Subar 1992). Tomatoes also have antioxidant components that are medically useful in the area of cataracts, bone metabolism and asthma. About 90 % of the developing nations' (such as Nigeria) food supply are wasted owing to postharvest deterioration each year. Tomato production is seasonal and it is a highly perishable commodity in its natural state after harvest. Thus processing it to a form that can be easily preserved is crucial to minimizing wastage and spoilage during

the production season and ensuring that maximum nutritional values of the fruit are retained. Literature and past researches (Sachin, Janghan, and Mujumdar 2011) have shown that drying is one of the best methods of preserving fruits, vegetable and foods.

Various methods of drying fruits, vegetables and food exist; such methods include open sun drying, controlled solar drying, hot-air drying, freeze drying, vacuum drying and more. Idah, Obajemihi, Adeboye, and Olaniyan (2014) studied the assessment of osmotic dehydration-assisted drying of tomato at different drying temperatures under a hot-air dryer. They reported that the osmotic dehydration pretreatments had great influence on the drying kinetics and quality of tomato. The drying characteristic of banana chips and physicochemical changes during drying process were investigated by Itang (2010a, 2010b). Result of the study revealed that a drying temperature and microwave energy of 55 ^{0}C and 2.5 W/g respectively were the most suitable drying parameters while the biggest physicochemical changes were found at the primary drying stage. Olaniyan and Omoleyomi (2013) investigated the drying process of Okra (*Abelmoschus caillei*) under different conditions using a hot-air dryer. Result showed that an optimum drying rate could be achieved by subjecting okra to osmotic dehydration pretreatment prior to drying.

According to Jangan, Law, and Mujumdar (2011), the four major considerations in drying food, vegetables and fruits are speed of operation, energy efficiency, cost of operation and quality of dried products. It is essential that any food drying process should carefully establish these parameters as objective functions. This present study was conducted to investigate some of these parameters in drying tomato paste to tomato powder under different drying equipment: air oven, microwave oven and mechanical dryer. Therefore, the objectives of the study were: (i) to develop mathematical models to estimate the effects of foaming agent (egg white, EW), foam stabilizer (carboxyl methyl cellulose, CMC) and whipping time on drying rate and quality of tomato paste dried under air oven, microwave oven and mechanical dryer; and (ii) to optimize the drying process for maximum drying rate and quality of dried product. It is expected that this will elucidate the problems of drying and enable the establishment of process parameters for optimal drying of tomato paste to tomato powder.

2. MATERIALS AND METHODS

2.1. Experimental Equipment

The following equipment and apparatus were used for the study: (i) a mechanical dryer designed and fabricated by Omodara, Olaniyan, and Oyewole (2011) as shown in Figure 1; (ii) a microwave oven (Model: HTMO- 2890EG); (iii) an air oven (Model: MINO/50-10G039, Genlab Engineers); (iv) an electronic weighing balance; (v) a stainless steel knife; (vi) desiccators; and (vii) a blender (Model: HR-2815).

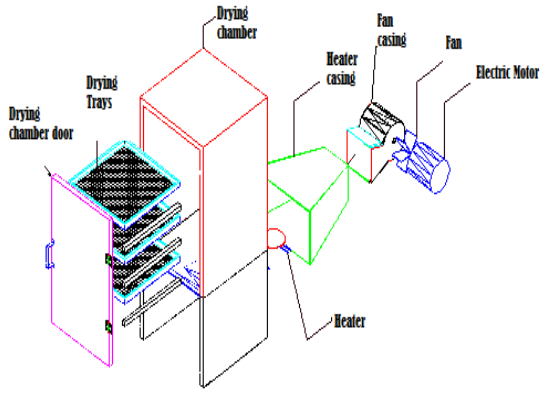

Figure 1: Exploded View of the Mechanical Dryer showing the Component Parts

2.2. Experimental Design

A 4^3 factorial experiment in a randomized complete block design was used in this study. The factors taken into consideration included 3 levels each of foaming agent, foam stabilizer, and whipping time. The range of foaming agent considered was 5, 10, 15 and 20 % EW; foam stabilizer was 0.15, 0.30, 0.45 and 0.60 % CMC while the whipping time was 3, 5, 7. and 9 min. Every trial was carried out in triplicate in the three drying equipment (mechanical dryer, air oven and microwave oven), making total of 576 samples that were individually tested and measured.

2.3. Experimental Procedure

The experiment was carried out in the Department of Chemical Engineering Laboratory, University of Ilorin. The average room temperature was 30 ^{0}C throughout the period of experimentation. Enough quantities of fresh and ripe tomatoes were bought from a local market in Ilorin metropolis. The tomatoes were graded to ensure uniformity of samples to be used for experimentation.

2.3.1. Sample Preparation

The graded tomatoes were washed in clean water, sliced and deseeded with the use of the stainless steel knife on a stainless steel tray and then blended to form tomato concentrate. 100 ml of the concentrate was measured and foamed with 5, 10, 15 and 20 % EW and 0.15, 0.30, 0.45 and 0.60 % CMC. The mixture was then foamed for 3, 5, 7 and 9 min whipping time with the aid of the blender to form a ready-for-drying foamed mixture.

2.3.2. Drying Procedure

The air oven and mechanical dryer were set at temperatures 50 ^{0}C and 55 ^{0}C respectively while the microwave oven was set at power of 540W. 25g of foamed samples prepared as described earlier were spread evenly on the labelled laboratory dishes at a foam thickness of between 2-3 mm and carefully placed inside each of the drying equipment for drying as shown in Figures 2, 3 and 4 below. The weights of the samples were taken every one hour and the drying operation continued until there was no more changes in the weight of the samples. The experiment was performed in triplicate in all the three drying equipment.

Figure 2: Samples in the Mechanical Dryer during Drying

Figure 3: Sample in the Air Oven during Drying

Figure 4: Samples in the Microwave Oven during Drying

2.4. Output Parameters

2.4.1. Drying Kinetics

In this study, drying rate is the amount of moisture removed from product per unit time during a drying operation. It was determined by the equation used by Olaniyan and Omoleyomi (2013) which is expressed below as:

$$R=\left(\frac{dM}{dt}\right)=\frac{m_i-m_f}{t} \quad (1)$$

where; R is the drying rate in g/h; dM is change in mass of okra in g; dt change in time in h; t is the total time of drying in h; m_i and m_f are the initial and final mass of okra samples respectively in g.

2.4.2. Quality of Dried Product

Proximate analysis of the dried samples were carried out to determined their crude protein, crude fat,

vitamin C, ash content, carbohydrate, crude fibre and moisture contents using the standard procedures (AOAC 1990). These together with colour evaluation were used as quality determining criteria in this study.

2.5. Experimental Analysis

Using the SPSS (16.0) computer software package, model equations were developed by employing essential regression analysis. The model equations were used to predict the drying rate and quality of dried product based on foaming agent, foam stabilizer and whipping time. Furthermore, the drying process was optimized for maximum drying rate and maximum post-drying quality considered in the study.

3. RESULTS AND DISCUSSION

3.1. Development of Model Equations

The model was based on a three-factor essential regression model and the factors were foaming agent, foam stabilizer and whipping time. From the regression analysis, the following regression models (Equations 2 – 9) were obtained for drying rate, vitamin C content, ash content, fat content, crude fibre content, carbohydrate content, protein content and moisture content respectively.

3.1.1. Drying Process in Mechanical Dryer

The model developed for the drying process of tomato paste in the mechanical dryer is described by the equations below:

$$Y_{ddr} = 10.96 - 0.232\alpha - 5.619\beta + 0.01177\alpha^2 + 1.508\alpha\beta \quad ; R^2 = 0.89 \qquad (2)$$

$$Y_{dvc} \quad -0.453\gamma + 1.575\alpha\beta - 0.00232\alpha^2{}_2 \quad ; R^2 = 0.91 \qquad (3)$$

$$Y_{das} \quad -0.04316\alpha\beta + 0.000861\alpha\gamma + 0.08476\beta\gamma - {}_2 \quad ; R^2 = 0.85 \qquad (4)$$

$$Y_{dfa} = 1.637 - 0.113\gamma - 0.000976\alpha^2 - 0.06560\alpha\beta + 0.00651\alpha\gamma + 0 \quad ; R^2 = 0.81 \qquad (5)$$

$$Y_{dcf} = 3.323 - 0.00547\gamma - 0.127\alpha\beta + 0.995\beta^2 = 0.00431\alpha^2\beta \quad ; R^2 = 0.85 \qquad (6)$$

$$Y_{dca} = 4.170 + 0.000591\alpha^2\gamma - 0.001\alpha^2\gamma + 0.000297\alpha\beta\gamma \,, \quad R^2 = 0.90 \qquad (7)$$

$$Y_{dpr} = 0.547 - 0.03686\alpha - 0.08069\gamma + 0.00284\alpha\beta^2 + 0.02757\alpha\beta + 0 \quad R^2 = 0.91 \qquad (8)$$

$$Y_{dmc} = 87.83 - 0.00381\alpha^2 + 0.252\alpha\beta - 4.071\beta^2 + 0.000539\alpha^2\gamma - 0.0 \quad , R^2 = 0.88 \qquad (9)$$

where Y_{ddr}, Y_{dvc}, Y_{das}, Y_{dfa}, Y_{dcf}, Y_{dca}, Y_{dpr} and Y_{dmc} are drying rate, vitamin C content, ash content, fat content, crude fibre content, carbohydrate content, protein content and moisture content respectively and **α**, β and γ are foaming agent, foam stabilizer and whipping time respectively.

3.1.2. Drying Process in Air Oven

The model developed for the drying process of tomato paste in the air oven is described by the equations below:

$$Y_{adr} = = 7.693 + 24.22\beta - 1.159\alpha\beta + 0.07100\alpha\gamma - 23.53\beta^2 \quad -2.352\ \beta\ 43.36 - 8.527\ \beta \quad ; \quad R = 0.80 \qquad (10)$$

$$Y_{avc} = = 39.17 + 1.112\alpha\beta + 0.03877\alpha\gamma - 14.64\beta^2 - 0.05078\alpha^2\beta \quad +1.124\ 1.252 \quad ; R = 0.90 \qquad (11)$$

$$Y_{aas} = 1.235+0.0778\,\alpha-0.00204\,\alpha\gamma-0.00260\,\alpha^2\,\beta+0.0\ ;\ R^2 = 0.89 \quad (12)$$

$$Y_{afa} = 1.524-0.106\,\gamma+0.01515\,\gamma^2-0.0001\,\alpha^2\,\gamma+0.146\ ;\ R^2 = 0.83 \quad (13)$$

$$Y_{acf} = 3.953-0.05952\,\alpha-0.07786\,\gamma-2.237\,\beta^2+0.308\ ;\ R^2 = 0.89 \quad (14)$$

$$Y_{aca} = 4.302+1.593\,\beta-0.08763\,\gamma-0.353\,\alpha\,\beta+0.01306\ ;\ R^2 = 0.91 \quad (15)$$

$$Y_{apr} = 1.843+0.04380\,\alpha+3.393\,\beta-0.288\,\alpha\,\beta-4.824\,\beta^2\ ,\ R^2 = 0.85 \quad (16)$$

$$Y_{amc} = 88.46-12.20\,\beta+0.852\,\alpha\,\beta-0.02793\,\alpha\,\gamma+10.68\,\beta^2\ ;\ R^2 = 0.81 \quad (17)$$

where Y_{adr}, Y_{avc}, Y_{aas}, Y_{afa}, Y_{acf}, Y_{aca}, Y_{apr} and Y_{amc} are drying rate, vitamin C content, ash content, fat content, crude fibre content, carbohydrate content, protein content and moisture content respectively and **α**, β and γ are foaming agent, foam stabilizer and whipping time respectively.

3.1.3. Drying Process in Microwave Oven

The model developed for the drying process of tomato paste in the microwave oven is described by the equations below:

$$Y_{mdr} = 4.383+0.559\,\alpha+2.424\,\alpha^2-0.01861\,\alpha^2-0.155\,\alpha\ ;\ R^2 = 0.85 \quad (18)$$

$$Y_{mvc} = 41.33-0.315\,\alpha+9.552\,\beta+0.122\,\alpha\,\gamma-3.292\,\beta\gamma-0.00849\,\alpha\,\gamma\ ,\ R^2 = 0.90 \quad (19)$$

$$Y_{mas} = 1.248+0.01769\,\alpha-0.392\,\beta-0.000995\,\alpha^2+0.718\,\beta^2+0.0003\ ;\ R^2 = 0.91 \quad (20)$$

$$Y_{mfa} = 1.336-0.07280\,\alpha+0.155\,\gamma+0.00308\,\alpha^2+0.109\,\alpha\,\beta-0.196\,\beta\ ;\ R^2 = 0.88 \quad (21)$$

$$Y_{mcf} = 3.715-4.013\,\beta+0.00132\,\alpha^2-0.01627\,\alpha\,\beta+3.715\,\beta^2+0.768\ ;\ R^2 = 0.85 \quad (22)$$

$$Y_{mca} = 4.257-0.00335\,\gamma^2+0.00220\,\alpha^2\,\beta-0.113\,\alpha\,B^2+0.00869\,\beta\,\gamma^2\ ;\ R = 0.90 \quad (23)$$

$$Y_{mpr} = 2.206+0.000121\,\alpha^2+0.00200\,\gamma^2+0.00346\,\alpha\,\beta\gamma-0.000164\,\alpha\ ;\ R^2 = 0.91 \quad (24)$$

$$Y_{mmc} = 86.51+8.292\,\beta-0.00201\,\alpha^2+0.02645\,\alpha\,\gamma-9.302\,\beta^2-1.364\ R^2 = 0.88 \quad (25)$$

where Y_{mdr}, Y_{mvc}, Y_{mas}, Y_{mfa}, Y_{mcf}, Y_{mca}, Y_{mpr} and Y_{mmc} are drying rate, vitamin C content, ash content, fat content, crude fibre content, carbohydrate content, protein content and moisture content respectively and **α**, β and γ are foaming agent, foam stabilizer and whipping time respectively.

3.2. Model Validation

The measured (observed) outputs of drying rate and post-drying quality attributes of tomato paste were compared with the predicted values from the developed models. The two sets of data were plotted on the same graph to see how favourably compared the two of the curves are and the plots are shown in Figures 5, 6 and 7. From the figure, it is obvious that little or no difference could be noticed in the trend of the paired curves generated. This shows that all the predicted values compared favourably with the observed values. Therefore, the models reliably predicted the drying characteristics of tomato paste very well in terms of these output parameters.

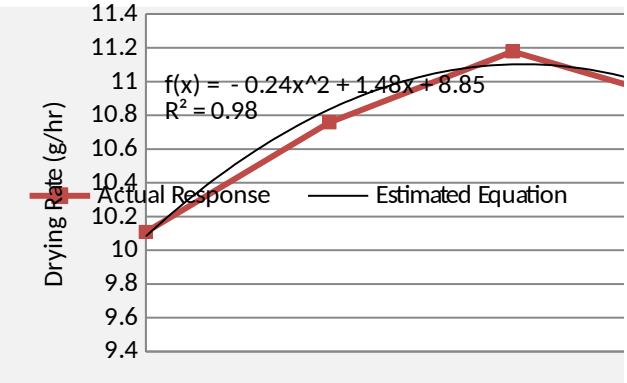

Figure 5: Effect of Foaming Agent on Drying Rate using Mechanical Dryer

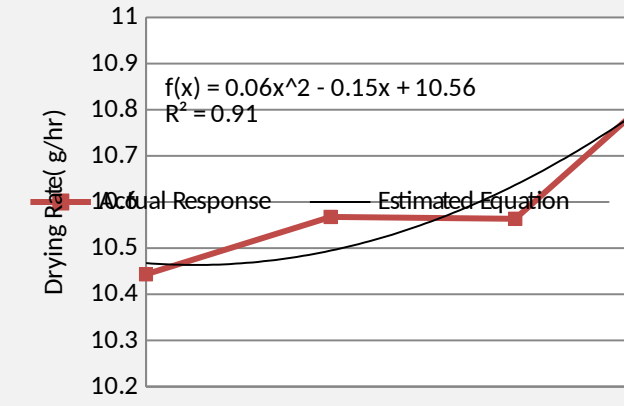

Figure 6: Effect of Foaming Agent on Drying Rate using Air Oven

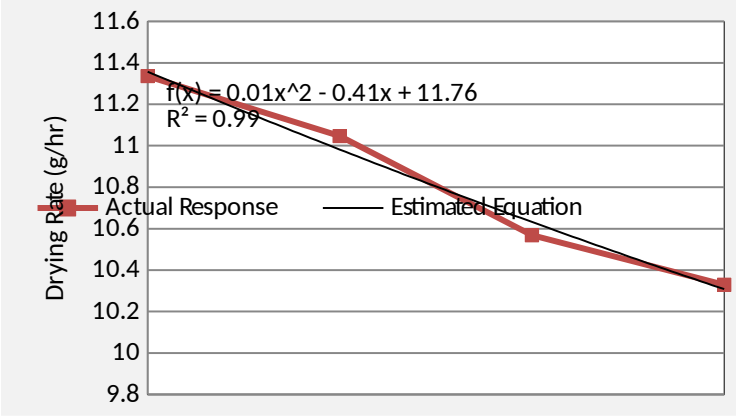

Figure 7: Effect of Foaming Agent on Drying Rate using Microwave Oven

3.3. Process Optimization

The optimum values of the process variables (foaming agent, foam stabilizer and whipping time) and optimized value of process outputs (drying rate and post-drying qualities) are presented in Table 2. The table shows that in order to maximize drying rate of tomato paste in the mechanical dryer, foaming agent, foam stabilizer and whipping time of 14.0 %EW, 0.48 %CMC and 9 min respectively must be combined to give the optimum drying rate of 11.36 g/h. For ash content, a combination 20 %EW foaming agent, 0.6 %CMC foam stabilizer and whipping time of 9 min resulted to the optimum value of 1.3 %.

An optimum value of 43.4 % was obtained for vitamin C at a foaming agent of 8.78 %EW, foam stabilizer of 0.6 %CMC and whipping time of 9 min. The crude fat content of tomato paste has 1.39 % as its optimum value and this corresponds to a combination of 5 %EW foaming agent, 0.15 %CMC foam stabilizer and 3 min whipping time. A foaming agent of 5 %EW, foam stabilizer of 0.15 %CMC and whipping time of 3 min should be selected to give the optimum crude fibre of 3.25 %.

Carbohydrate requires a foaming agent of 20 %EW, foam stabilizer of 0.6 %CMC and whipping time of 3 min to give the optimum value of 4.3 %. An optimum value of 2.5 % was obtained for protein at a foaming agent of 20 %EW, foam stabilizer of 0.15 %CMC and whipping time of 3 min. Ash content of dried tomato powder has 1.18 % as its minimum value and this

corresponds to a combination of 20 %EW foaming agent, 0.3 %CMC foam stabilizer and 3 min whipping time.

Table 2: Optimized Values of Process Parameters and Process Outputs

Drying Equipment	Output Parameters	Foaming Agent (%EW)	Foam Stabilizer (%CMC)	Whipping Time (min)	Optimized Value	Nature of Solution
Mechanical Dryer	Drying Rate (g/h)	14.0	0.48	9	11.36	Maximized
		5	0.15	3	10.16	Minimized
	Vitamin C (%)	58.78	0.6	9	43.4	Maximized
		20	0.15	6	40.9	Minimized
	Ash (%)	20	0.6	9	1.3	Maximized
		20	0.3	3	1.18	Minimized
	Fat (%)	5	0.15	3	1.39	Maximized
		13.2	0.6	6.7	1.25	Minimized
	Crude Fibre (%)	5	0.15	3	3.25	Maximized
		14.79	0.47	9	3.0	Minimized
	Carbohydrate (%)	20	0.6	3	4.3	Maximized
		20	0.15	9	4.0	Minimized
	Protein (%)	20	0.15	3	2.5	Maximized
		9.29	0.15	5.87	2.2	Minimized
Air Oven	Moisture Content (%)	20	0.15	9	8.8	Maximized
		20	0.15	3	8.7	Minimized
	Drying Rate (g/h)	20	0.15	6.7	11.57	Maximized
		5	0.6	6.5	9.56	Minimized
	Vitamin C (%)	15.6	0.3	3	42.7	Maximized
		5	0.5	3	39.9	Minimized
	Ash (%)	12	0.6	3	1.3	Maximized
		20	0.4	3.8	1.2	Minimized
	Fat (%)	5	0.6	3	1.39	Maximized
		20	0.4	6.5	1.18	Minimized
	Crude Fibre (%)	5	0.2	3	3.5	Maximized
		17	0.5	9	3.0	Minimized
	Carbohydrate (%)	20	0.15	6.4	4.2	Maximized
		20	0.3	3	3.8	Minimized
	Protein (%)	20	0.15	3	2.4	Maximized
		20	0.3	9	2.2	Minimized
	Moisture Content (%)	20	0.3	3	8.9	Maximized
		5	0.4	9	8.7	Minimized
Microwave Oven	Drying Rate (g/h)	5	0.15	6.26	12.05	Maximized
		13	0.6	3	9.59	Minimized
	Vitamin C	20	0.15	7.3	43.5	Maximized

Drying Equipment	Output Parameters	Foaming Agent (%EW)	Foam Stabilizer (%CMC)	Whipping Time (min)	Optimized Value	Nature of Solution
	(%)	5	0.6	6.5	41	Minimized
	Ash (%)	11.1	0.15	9	1.3	Maximized
		20	0.6	3	1.2	Minimized
	Fat (%)	5	0.15	5.4	1.4	Maximized
		14.5	0.15	3	1.2	Minimized
	Crude Fibre (%)	5	0.16	9	3.5	Maximized
		7.4	0.6	9	2.9	Minimized
	Carbohydrate (%)	20	0.2	3	4.3	Maximized
		15.5	0.6	3	3.95	Minimized
	Protein (%)	20	0.6	9	2.3	Maximized
		5	0.15	3	2.2	Minimized
	Moisture Content (%)	12.9	0.6	6.4	8.8	Maximized
		5	0.15	3.2	8.7	Minimized

EW= Egg white, CMC= Carboxyl Methyl Cellulose, WT= Whipping Time

3.4. Practical Application

Preservation of tomato and quality retention could be best achieved if it is processed to a powdery form immediately after harvest. The process involves drying tomato paste to a powdery form with a shelf-stable moisture content. Since tomato is a food product, pretreatment methods, drying conditions and other process parameters should be carefully controlled in order not to destroy or denature the sensory characteristics such as flavor, aroma and other quality attributes. The result of this research provides useful information for process monitoring, control and observation during the drying of tomato. The model can be used for optimizing the efficiency of commercial food drying process and the performance of commercial food dryers. An important aspect of the research is the microwave drying process which is a new technology for dehydrating fruits, vegetables and food without damaging their nutritive and sensory values. Therefore, a food drying process based on the result of this research would ensure a high process efficiency and appreciable retention of product quality.

4. CONCLUSION

The empirical models developed to relate the drying rate and post-drying qualities of tomato paste to foaming agent, foam stabilizer and whipping time were found to have described the dying characteristics of tomato very well and sufficiently predicted output parameters. Therefore these models can be applied for industrial drying of tomato under different process pretreatments and different drying conditions. Further analysis of the models by optimization showed that an optimum drying rate of 11.36 g/h could be achieved using a mechanical dryer if tomato paste is pretreated with foaming agent, foam stabilizer and whipping time of 14.0 %EW, 0.48 %CMC and 9 min respectively. The vitamins C content of the tomato powder could be maximized to an optimum value of 43.4 % if foaming agent, foam stabilizer and whipping time of 8.78 %EW, 0.6 %CMC and 9 min were used to pretreat tomato paste and then dried in the mechanical dryer. In the same development, tomato powder of water an optimum ash content of 1.3 % could be obtained with a foaming agent of 20 %EW, foam stabilizer of 0.6 %CMC and whipping time of 9 min. It could be inferred from this study that the drying process of tomato paste could be optimized under different pretreatments and drying conditions. Further studies should be carried out on the factors that affect the storability of tomato powder for long-time storage and preservation.

ACKNOWLEDGEMENT

The authors wish to appreciate the efforts of the Head, Department of Chemical Engineering, University of Ilorin, for providing a conducive environment throughout the period of experimentation.

REFERENCES

AOAC 1990. Official Methods of Analysis, (ed), Washington D.C.: Association of Official Analytical Chemists.

Block G., Patterson B., and Subar A., 1992. Fruits, Vegetables and Cancer Prevention. A Review of the Epidemiological Evidence, Nutrition and Cancer, 18: 1- 29.

FAO 2002. World Crop Production Statistics, 1st ed., Rome: Food and Agriculture Organisation of United Nations Statistical Database Online Service.

Idah P.A., Obajemihi O.I., Adeboye O.A., and Olaniyan A.M. 2014. Assessment of Osmotic Pre-drying Treatments on Drying Rates of Fresh Tomato Fruits. Nigerian Journal of Technological Development, 11 (1): 22-26.

Jangan S.V., Law C.L., and Mujumdar A.S., 2011. Drying of Foods, Vegetables and Fruits, Vol. III. Available Online at http:/www.mujumdar.net178.net/ and http:/serve.me.nus.edu.sg/arun/

Olaniyan A.M., and Omoleyomi, B.D. 2013. Characteristics of Okra under Different Process Pretreatments and Different Drying Conditions. Journal of Food Processing and Technology 4 (6): 2-6.

Omodara M.O., Olaniyan A.M., and Oyewole S. N. 2011. Drying of African Catfish (*Clarias garipinus*), 1st ed., Deutschland: LAP Lambert Academic Publishing.

BIOGRAPHY OF THE AUTHORS

1. Dr. Adesoji Matthew Olaniyan graduated with B.Eng, M.Eng and PhD in Agricultural Engineering from University of Ilorin, Nigeria in 1991, 1998 and 2006 respectively. Since 1998, he has been working on techniques, processes and equipment for processing agricultural and bioresources materials to food, fibre and industrial raw materials. Dr. Olaniyan's principal area of research is on Bioproduct Processing and Food Process Engineering, where he has carried out a number of projects and published a number of papers in local and international journals. He joined the service of the University of Ilorin in 1998 as an Assistant Lecturer in the Department of Agricultural and Biosystems Engineering and rose to the position of a Senior Lecturer in 2009. Currently, he is an Associate Professor at the Department of Agricultural and Bio-resources Engineering, Federal University Oye-Ekiti, Nigeria. Dr. Olaniyan has bagged several awards including the Award for the Best Paper (2007) in the Journal of Food Science and Technology, Mysore, India; Chinese Government Sponsorship (2008) for International Training Programme in Protected Agriculture at International Exchange Centre, Yangling, China; Netherlands Fellowship Programme (2009) for International Training Programme in Milk Processing at Practical Training Centre, Onkerk, the Netherlands; and Postdoctoral Fellowship (2011) of the Academy of Sciences of Developing Countries.

2. Dr. Musliu Olushola Sunmonu graduated with B.Eng, M.Eng and PhD in Agricultural Engineering from Federal University of Technology, Mina, Nigeria in 2000, 2006 and 2014 respectively. Since 2008, he has been working on postharvest processing and storage of agricultural products. Dr. Sunmonu's principal area of research is on postharvest storage and packaging, where he has carried out a number of projects and published a number of papers in local and international journals. He joined the service of the University of Ilorin in 2008 as an Assistant Lecturer in the Department of Agricultural and Biosystems Engineering and rose to the position of Lecturer I in 2013. Dr. Sunmonu has received some awards including the Netherlands Fellowship Programme (2010) for International Training in Milk Processing at Practical Training Centre, Onkerk, the Netherlands.

LIFE CYCLE ASSESSMENT OF A NEW FEED PRODUCTION OBTAINED BY WASTED FLOUR FOOD COLLECTED FROM THE DISTRIBUTION AND RETAIL PHASES

David Mosna[(a)], Giuseppe Vignali[(b)]

[(a)]CIPACK Interdepartmental Center, University of Parma, Parco Area delle Scienze 181/A, 43124 Parma (Italy)
[(b)]Department of Industrial Engineering, University of Parma, Parco Area delle Scienze 181/A, 43124 Parma (Italy)

[(a)]davidmosna@hotmail.it [(b)] giuseppe.vignali@unipr.it

ABSTRACT

Every year in Emilia Romagna more than 10000 tons of food are wasted during the retail and distribution phase. Landfill is nowadays the most adopted end of life, but working on a specific sorting system it would be possible to separate food from packaging and recover both of them in the most preferable way. In this case, Food Waste could be valorized by means of different technologies, such as anaerobic digestion, composting, and animal feed production. In this study the environmental performance of two Food Waste valorization scenarios using the Life Cycle Assessment (LCA) methodology has been analyzed. For both scenarios the Floor Food Products Fraction, like bread, pasta and biscuits, was valorized to produce animal feed. The environmental impacts of these new scenarios were compared with the impacts caused by the traditional feed production. The new scenarios lead to benefit for all the considered impact categories.

Keywords: Food waste, LCA, Waste valorization, Environmental impacts.

1. INTRODUCTION

Vermeulen et al., (2012) estimated that food production is responsible for up to 29% of the anthropogenic greenhouse gases emissions. One of the major problems related to food production is the waste generated throughout the Food Value Chain. In 2011, the Food and Agriculture Organization of the United Nations (FAO) determined that one third of the global production of food for human consumption is lost or passed out as waste, corresponding to approximately 1.3 billion tons each year (Gustavsson et al., 2011; FAO 2013a; FAO 2013b).Three main definitions of Food Waste (FW) can be found in literature. Firstly, the Food and Agriculture Organization (FAO) defines FW as wholesome edible material intended for human consumption, arising at any point in the food supply chain that is instead discarded, lost, degraded or consumed by pests (FAO 1981). Stuart (2009) adds to the FAO's definition, by stating that FW should also include edible material that is intentionally fed to animals or is a by-product of food processing diverted away from the human food chain. Finally, Smil (2004) suggests that FW covers the definitions above, but adds over-nutrition, the gap between the energy value of consumed food per capita and the energy value of food needed per capita.

Throughout the Food Value Chain, food is wasted in different stages, namely during production, food processing, distribution, and use. Several causes of this wastage exist (European Commission 2015), and they can be mainly attributed to:

- *Production*: overproduction, product and packaging damage from farmers and food processing;
- *Retail*: inefficient stock management, marketing strategies that lead to overbuying (e.g. 2 for 1, buy 1 get one for free), and aesthetic issues;
- *Catering*: the meal sizes and the difficulty to anticipate the number of clients;
- *Households*: lack of awareness towards food wastage, lack of shopping planning, misconception regarding the "best before" and "use by" date labels, and absence of knowledge/innovation to reuse and cook with the leftovers; and
- In general throughout the entire food value chain due to inappropriate storage and packaging methods.

The main reasons for food waste generated during distribution are examined in the literature, including inappropriate packaging, poor handling and transportation, failures on forecasting and storage (Kantor et al., 1997).

The management of FW should follow certain policies based on the 3R's concept, i.e., reduce, reuse, and recycle (Memon 2010; Sakai et al., 2011). In the European context, the Waste Framework Directive 2008/98/EC proposes the following waste management hierarchy: prevention, preparing for re-use, recycling, other recovery (e.g. energy recovery), and disposal (European Commission 2008). As illustrated in Figure 1, the best option is "prevention", and at the bottom of the inverted pyramid, the least favorable option is "disposal".

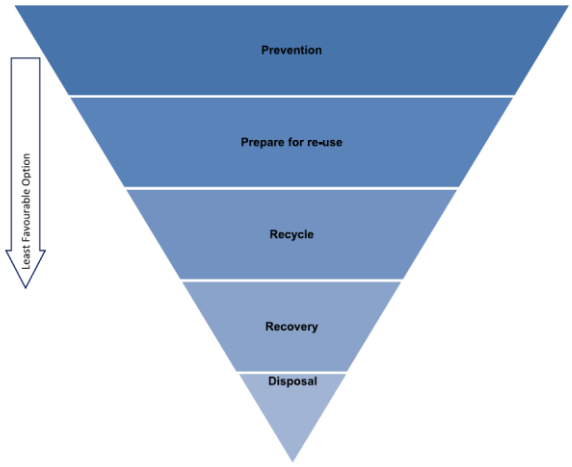

Figure 1: The waste hierarchy. (Source: European parliament council 2008)

Several studies evaluating the environmental performance of different FW management options can be found in literature. Lundie and Peters (2005) compared several FW disposal options, and showed that codisposal at landfill made a greater contribution than aerobic composting or central composting. Also Mendes et al., (2003) confirmed that the landfilling of biodegradable waste is generally the worst strategy from an environmental point of view. In addition, Güereca et al., (2006) reported that a composting based system had less impact on global warming than an incineration based system in the biowaste treatment of Barcelona, Spain. According to Khoo et al., (2009), using the FW for aerobic composting system is more environmentally sustainable than incinerators, but less compared to the anaerobic digestion process, due mainly to CO_2 and NH_3 emissions. Also in a study made in USA, anaerobic digestion had the best environmental results (Levis and Barlaz 2011). In the same study the authors showed than composting and landfill disposal with energy recovery presented lower environmental impacts than landfill disposal. Cherubini et al., (2009) showed that landfill systems is the worst alternative; the study also show that a sorting plant coupled with electricity and biogas production is the best option for waste management. Also from the study on municipal solid waste disposal by Eriksson et al. (2005) and Hong et al. (2006), landfill had more impact on global warming than incineration.

A few studies evaluated the use of FW to produce animal feed. According to Kim and Kim (2010) and Lee et al., (2007) using FW for feed production presented lower environmental impact than landfill disposal. Vandermeersch et al., (2014) showed than FW can be valorized through animal feed production, reducing the environmental impact mainly due to the avoided products from traditional supply chain.

The objective of this study was to evaluate which FW valorization scenarios could bring more environmental benefit. The environmental performance was evaluated by means of LCA method.

The remainder of the paper is organized as follows. LCA methodology has been explained considering all the phases according to ISO 14044. Environmental impact assessment has been performed considering the current scenario (disposal in landfill), comparing it with the new ones and evaluating the production impacts of existing feeds in comparison with those partly originated by FW. A sensitivity analysis has been then performed showing how changes could influence the results. Finally, conclusion section is reported in order to resume the main results of this work.

2. LIFE CYCLE ASSESSMENT METHODOLOGY AND DATA

The LCA methodology was applied according to the principles and requirements provided standards. LCA consists of four main steps of analysis: goal and scope definition; inventory analysis; impact assessment; and interpretation (ISO 14044, 2006). The SimaPro 8.0.5 LCA software was used in this assessment.

2.1. Goal and scope definition

The purpose of this work is to evaluate and compare the environmental impacts of 2 FW valorization scenarios by identifying the inputs and outputs for both option and their impacts.

2.1.1. Functional unit

The functional unit provides a reference unit for which the inventory data are normalized (ISO 14040, 2006). The concept of the functional unit is key in LCA, as it facilitates the comparison of alternative products and services (ISO 14044, 2006). The functional unit of this study is 1 kg of animal feed product with 10% of FFPF. In scenario 1 we had compared the production of 1 kg corn feed with a new feed where 10% of corn was replaced with the same quantity of FFPF (Table 1). Instead in scenario 2 we compared the production of 1 kg animal feed (Table 1) with a new animal feed production where 10% of each ingredients was replaced with the same quantity of FFPF.

Table 1: Recipe for 1 kg of animal feed in 2 scenarios

Recipe for 1kg of animal feed					
Input scenario 1	Traditional animal feed	Animal feed with FFPF	Input scenario 2	Traditional animal feed	Animal feed with FFPF
Corn grains	100%	90%	Wheat grains	91.0%	81.9%
FFPF	0%	10%	Soybeans	5.0%	4.5%
			Tallow	4.0%	3.6%
			FFPF	0.0%	10.0%

We have chosen to replace only the 10%, in weight, with FFPF in the animal feed according to Prandini et al., (2007). In this study they have demonstrated that by replacing 10% of corn with the same amount of FFPF, no differences were shown for weight losses at different phases of seasoning and for the chemical analysis of seasoned hams.

2.2. System boundaries and assumptions

In order to quantify the impact of the product analyzed, system boundaries need to be determined. The case study involves the food product wasted during the retail and distribution field, located in Emilia Romagna (northern Italy). The annual generation of FW was estimated at 14,600 tons in 2013. In this study were analyzed only the FFPF, corresponding to 19% of FW (Lipinski et al., 2013).

The generation of FW happens in several supermarkets spread out through Emilia Romagna. This FW is composed by food products that were no sold to consumers, i.e., products exceeded the expiration date stated on the package, deteriorated, or that no longer seemed to be edible (Lipinski et al., 2013, HLPE 2014; BCFN 2012). Nowadays this products are disposed of in landfills (Figure 2A and Table 1).

Table 2: Summary of disposal n landfill

Current Scenario

Input	Unit	Quantity
Transport, freight, lorry 3.5-7.5 metric ton, EURO4	km	80
Landfill of biodegradable waste EU 27	ton	1

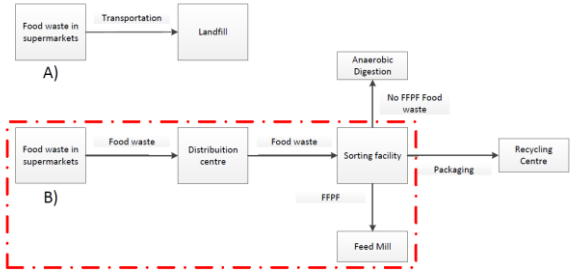

Figure 2: Graphical scheme of the A) disposal in landfill and B) new valorization scenarios

Instead in the new proposed scenarios the FW will be transported to a Distribution center and every 4 days. It will be transported from the distribution center to a centralized retort center, where a mechanical sorting will be performed, separating the organic fraction from packaging. The FFPF will be transported to a Feed mill where will be used to produce animal Feed. The other fraction of FW will be recovered in the most preferable rate such as through Anaerobic digestion (Vandermeersch et al., 2014). The sorted packaging materials will be then sent to specific recycling centres. The system boundaries can be visualized in Figure 2B, and included only the FFPF fraction.

2.3. Inventory analysis and data collection

The life cycle inventory analysis quantifies the resources use, energy use, and environmental releases associated with the system being evaluated (ISO 14040 2006). Ecoinvent Database 3.1 is used for secondary data by considering data related to the Italian situation (Ecoinvent 2015).

In this paragraph we have defined the incoming and avoided phases regarding the new scenarios (Figure3 and Figure 4). The considered incoming stages are: 1) Generation of FW; 2) Transportation of FW to distribution centre; 3) Storage in distribution centre; 4) Transportation of FW to Sorting facility; 5) Sorting of FW; 6) Transportation of FFPF to feed mill; 7) Feed production. While the avoided phases are: 8) Transportation of FW to the landfill, 9) Disposal product in landfill and 10) The produce of corn grain (Scenario 1) wheat grains, soybeans and tallow (Scenario 2), and 11) the relative transport.

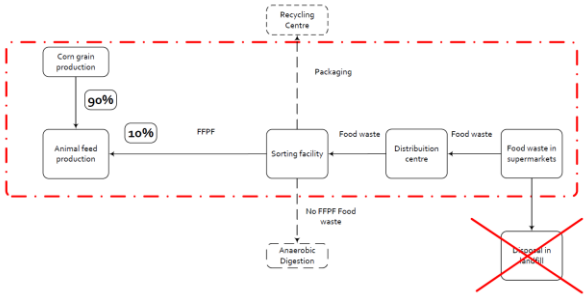

Figure 3: Graphical scheme of the scenario 1

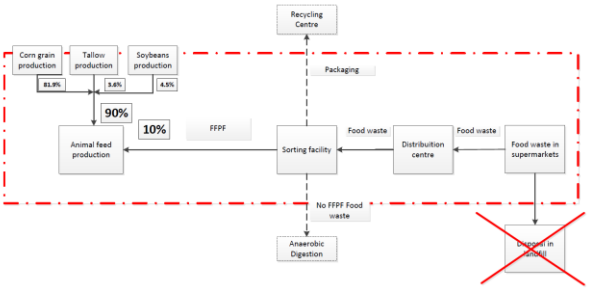

Figure 4: Graphical scheme of the scenario 2

Within the system boundary, the following assumptions and limitations are applied:

- The data from the transports was obtained based on the average distance traveled;
- Mass based allocation was used in order to account the share between FFPF, organic mass and packaging into the FW
- The average Italian electricity mix is used in this study.
- In this study, data from Italy were used when available. In case of unavailable data, relevant background data from Europe or Switzerland were used.
- Regarding the cut-off criteria applied, less than 1% of the energy and mass flows of the inputs and outputs was excluded from this analysis.

2.4. Methods of impact assessment

The data collected in the inventory analysis are the basis for the impact assessment phase whose aim is to evaluate the potential environmental impact of the system (ISO 14040 2006) caused by effluent emissions,

releases into the environment and resources consumption. The impact analysis was carried out using the ReCiPe method. The hierarchic perspective has been selected in this work, as it is considered to be the most balanced of the three proposed by the method (Egalitarian, Individualist and Hierarchist). Impact values were calculated at midpoint level for 18 impact categories, i.e. (i) climate change, (ii) ozone depletion, (iii) terrestrial acidification, (iv) freshwater eutrophication, (v) marine eutrophication, (vi) human toxicity, (vii) photochemical oxidant formation, (viii) particulate matter formation, (ix) terrestrial ecotoxicity, (x) freshwater ecotoxicity, (xi) marine ecotoxicity, (xii) Ionising radiation, (xiii) agricultural land occupation, (xiv) urban land occupation, (xv) natural land occupation, (xvi) water depletion, (xvii) metal depletion and (xiii) fossil depletion.

3. LIFE CYCLE IMPACT ASSESSMENT

3.1. Current scenario: disposal in landfill

The results for the current scenario are reported in Table 2, while Figure 5 shows the relative contribution of each processing input.

Table 3: Characterization results for the overall impact of the disposal in landfill scenario.

Impact category	Unit	Total	Transport	Disposal in Landfill
Climate change	kg $CO_{2\ eq}$	1.45E+06	2.89E+04	1.42E+06
Ozone depletion	kg CFC-11 eq	1.33E-02	5.05E-03	8.22E-03
Terrestrial acidification	kg $SO_{2\ eq}$	9.71E+02	1.11E+02	8.60E+02
Freshwater eutrophication	kg $P_{\ eq}$	1.27E+03	5.91E-01	1.27E+03
Marine eutrophication	kg $N_{\ eq}$	1.18E+03	4.75E+00	1.18E+03
Human toxicity	kg 1,4-DB eq	6.00E+03	4.22E+03	1.78E+03
Photochemical oxidant formation	kg NMVOC	1.50E+03	1.38E+02	1.36E+03
Particulate matter formation	kg PM10 eq	1.36E+03	5.03E+01	1.31E+03
Terrestrial ecotoxicity	kg 1,4-DB eq	9.45E+00	7.97E+00	1.48E+00
Freshwater ecotoxicity	kg 1,4-DB eq	3.32E+01	1.70E+01	1.62E+01
Marine ecotoxicity	kg 1,4-DB eq	9.14E+01	6.73E+01	2.41E+01
Ionising radiation	kBq U235 eq	1.18E+04	1.82E+03	9.95E+03
Agricultural land occupation	m^{2a}	4.32E+02	4.32E+02	0.00E+00
Urban land occupation	m^{2a}	9.71E+02	9.71E+02	0.00E+00
Natural land transformation	m^2	1.01E+01	1.01E+01	0.00E+00
Water depletion	m^3	5.85E+02	-1.42E+01	6.00E+02
Metal depletion	kg Fe eq	5.34E+03	1.67E+03	3.67E+03
Fossil depletion	kg oil eq	7.21E+04	1.01E+04	6.20E+04

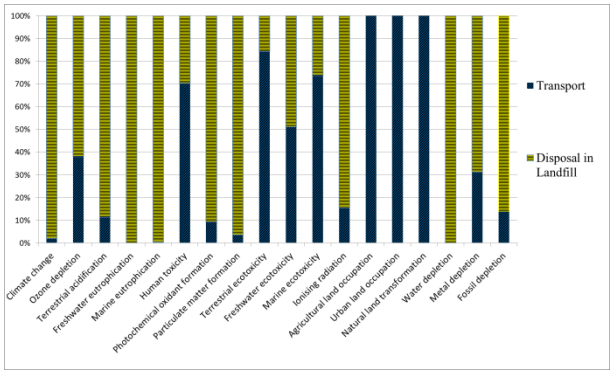

Figure 5: Relative contribution of different phases to the overall impacts for disposal in landfill

As can be seen from the total environmental impact divided according to stages (Table 1), disposal in landfill is the most important contributor to most impact categories; while, the transportation of FFPF to the landfill contributes mostly in 6 categories: Human toxicity, Terrestrial ecotoxicity, Marine ecotoxicity, Agricultural land occupation, Urban land occupation and Natural land transformation.

3.2. Scenario 1

In this case we compared the production of 1 kg corn feed with a new animal feed production where 10% of corn was replaced with the same quantity of FFPF. The results for 18 midpoint indicators can be seen in Table 4 and Figure 6.

Table 4: Characterization results for the scenario 1.

Impact category	Unit	Mais 100%	Mais 90% ; FFPF 10%	Avoided impact
Climate change	kg $CO_{2\ eq}$	5.86E-01	4.39E-01	1.47E-01
Ozone depletion	kg CFC-11 eq	3.51E-08	3.13E-08	3.73E-09
Terrestrial acidification	kg $SO_{2\ eq}$	7.06E-03	5.70E-03	1.36E-03
Freshwater eutrophication	kg $P_{\ eq}$	8.44E-05	2.24E-05	6.20E-05
Marine eutrophication	kg $N_{\ eq}$	9.36E-03	7.45E-03	1.91E-03
Human toxicity	kg 1,4-DB eq	6.69E-02	5.66E-02	1.03E-02
Photochemical oxidant formation	kg NMVOC	1.87E-03	1.54E-03	3.35E-04
Particulate matter formation	kg PM10 eq	1.50E-03	1.19E-03	3.12E-04
Terrestrial ecotoxicity	kg 1,4-DB eq	3.68E-03	2.95E-03	7.31E-04
Freshwater ecotoxicity	kg 1,4-DB eq	2.97E-03	2.39E-03	5.80E-04
Marine ecotoxicity	kg 1,4-DB eq	8.53E-04	7.30E-04	1.23E-04
Ionising radiation	kBq U235 eq	1.36E-02	1.18E-02	1.85E-03
Agricultural land occupation	m^{2a}	1.35E+00	1.08E+00	2.70E-01
Urban land occupation	m^{2a}	2.45E-02	2.02E-02	4.31E-03
Natural land transformation	m^2	6.53E-05	5.87E-05	6.60E-06
Water depletion	m^3	1.71E-02	1.37E-02	3.41E-03
Metal depletion	kg Fe eq	2.69E-02	2.30E-02	3.98E-03
Fossil depletion	kg oil eq	9.89E-02	8.42E-02	1.47E-02

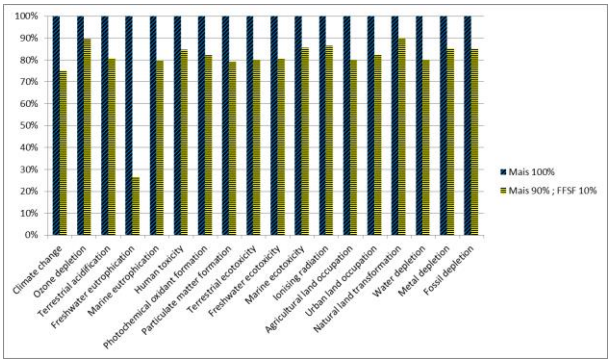

Figure 6: Results of the LCA for the Scenario 1

The new scenario showed better results in each impact categories analyzed; in almost all the categories the impact were resulted less than 10-20%, while for the Freshwater eutrophication the impact was resulted less than 73 %, mainly due to the avoided disposal in landfill of FFPF. For the other categories, the main reason for these results are the same; by valorizing the FFPF with feed production, avoids partly the production

of animal feed from corn, avoiding the environmental impact that are directly related to agriculture activities, such as land occupation. The Relative contribution of each processing input for the new scenario can be seen in Appendix A.

3.3. Scenario 2

In scenario 2 we compared the production of 1 kg animal feed (Table 1) with a new animal feed where 10% of each ingredients was replaced with the same quantity of FFPF. The results for 18 midpoint indicators can be seen in Table 4 and Figure 7.

Table 5: Characterization results for the scenario 2

Impact category	Unit	0% FFPF	10% FFPF	Benefit
Climate change	kg $CO_{2\ eq}$	6.04E-01	4.54E-01	1.51E-01
Ozone depletion	kg CFC-11 $_{eq}$	5.30E-08	4.57E-08	7.32E-09
Terrestrial acidification	kg SO2 $_{eq}$	6.32E-03	5.11E-03	1.21E-03
Freshwater eutrophication	kg P $_{eq}$	1.05E-04	3.87E-05	6.61E-05
Marine eutrophication	kg N $_{eq}$	1.11E-02	8.88E-03	2.27E-03
Human toxicity	kg 1,4-DB $_{eq}$	9.31E-02	7.75E-02	1.55E-02
Photochemical oxidant formation	kg NMVOC	2.23E-03	1.83E-03	4.07E-04
Particulate matter formation	kg PM10 $_{eq}$	1.48E-03	1.17E-03	3.07E-04
Terrestrial ecotoxicity	kg 1,4-DB $_{eq}$	4.96E-03	3.97E-03	9.87E-04
Freshwater ecotoxicity	kg 1,4-DB $_{eq}$	2.38E-03	1.91E-03	4.63E-04
Marine ecotoxicity	kg 1,4-DB $_{eq}$	7.86E-04	6.77E-04	1.10E-04
Ionising radiation	kBq U235 $_{eq}$	1.81E-02	1.54E-02	2.75E-03
Agricultural land occupation	m^{2a}	1.40E+00	1.12E+00	2.79E-01
Urban land occupation	m^{2a}	1.40E-02	1.18E-02	2.22E-03
Natural land transformation	m^2	9.47E-05	8.22E-05	1.25E-05
Water depletion	m^3	3.26E-02	2.61E-02	6.51E-03
Metal depletion	kg Fe $_{eq}$	4.01E-02	3.35E-02	6.62E-03
Fossil depletion	kg oil $_{eq}$	1.11E-01	9.35E-02	1.70E-02

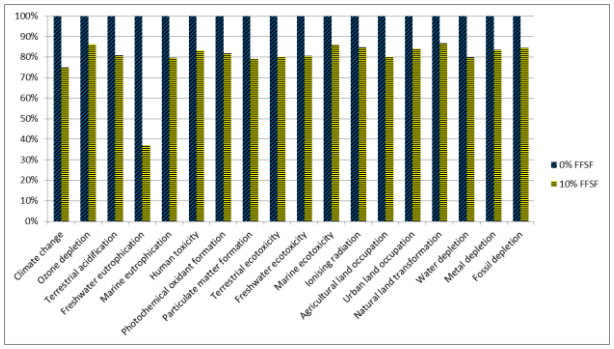

Figure 7: Results of the LCA for the Scenario 2

Also this scenario showed better results in each impact categories analyzed; in almost all the categories the impact were resulted less than 14-25%, while for the Freshwater eutrophication the impact was resulted less than 63%. The reasons are the same as already discussed in the previous sections.
The Relative contribution of each processing input for the new scenario can be seen in Appendix B.

3.4. Comparison between Scenario 1 and scenario 2

In this paragraph we compared the environmental benefits (avoided impacts thanks to using FFPF in the animal feed) between scenario 1 and 2 (Figure 8).

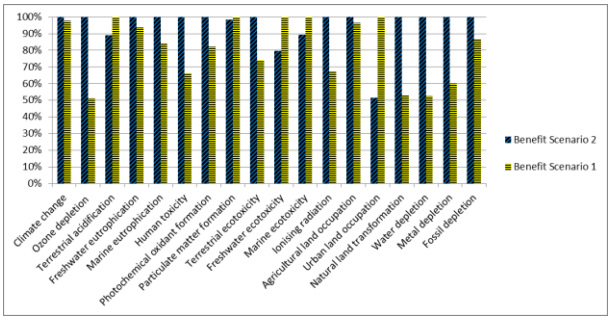

Figure 8: Comparison results between 2 scenarios

Scenario 2 showed better results in 13 categories (Climate change, Ozone depletion, Freshwater eutrophication, Marine eutrophication, Human toxicity, Photochemical oxidant formation, Particulate matter formation, Terrestrial ecotoxicity, Ionising radiation and Natural land transformation), while scenario 1 had better results in 5 categories (Terrestrial acidification, Freshwater ecotoxicity, Marine ecotoxicity, Agricultural land occupation and Urban land occupation).
Summarizing scenario 2 can bring more environmental gains than scenario 1 because the FFPF is valorized for producing Animal feed containing soybeans and wheat grain that they have most environmental impactful than producing corn grain (Figure 9).

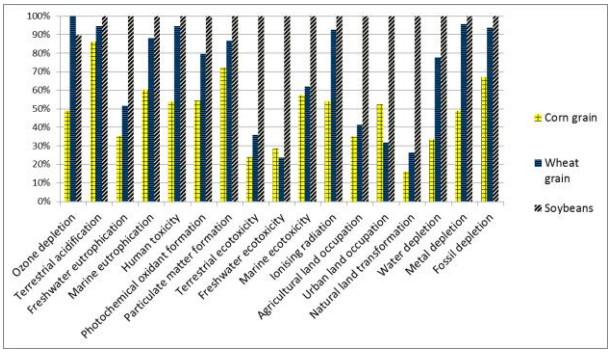

Figure 9: Total impact of vegetable productions

Table 6: Comparison results between 2 scenarios

Impact category	Unit	Benefit Scenario 2	Benefit Scenario 1
Climate change	kg $CO_{2\ eq}$	1.51E-01	1.47E-01
Ozone depletion	kg CFC-11 $_{eq}$	7.32E-09	3.73E-09
Terrestrial acidification	kg $SO_{2\ eq}$	1.21E-03	1.36E-03
Freshwater eutrophication	kg P $_{eq}$	6.61E-05	6.20E-05
Marine eutrophication	kg N $_{eq}$	2.27E-03	1.91E-03
Human toxicity	kg 1,4-DB $_{eq}$	1.55E-02	1.03E-02
Photochemical oxidant formation	kg NMVOC	4.07E-04	3.35E-04
Particulate matter formation	kg PM10 $_{eq}$	3.07E-04	3.12E-04
Terrestrial ecotoxicity	kg 1,4-DB $_{eq}$	9.87E-04	7.31E-04
Freshwater ecotoxicity	kg 1,4-DB $_{eq}$	4.63E-04	5.80E-04
Marine ecotoxicity	kg 1,4-DB $_{eq}$	1.10E-04	1.23E-04
Ionising radiation	kBq U235 $_{eq}$	2.75E-03	1.85E-03
Agricultural land occupation	m^{2a}	2.79E-01	2.70E-01
Urban land occupation	m^{2a}	2.22E-03	4.31E-03
Natural land transformation	m^2	1.25E-05	6.60E-06
Water depletion	m^3	6.51E-03	3.41E-03
Metal depletion	kg Fe $_{eq}$	6.62E-03	3.98E-03
Fossil depletion	kg oil $_{eq}$	1.70E-02	1.47E-02

Table 6 shows the comparison of the avoided environmental impact of the two scenarios; considering the whole use of the FFPF (2774 ton) to produce Animal feed (2774,000 ton).

4. SENSITIVITY ANALYSIS

Sensitivity analysis is a systematic procedure for estimating the effects of the choices made regarding methods and data on the outcome of a study (ISO 14040, 2006). A sensitivity assessment was performed to evaluate the environmental performance when the transport phase (Transportation of FW to distribution center, transportation of FW to Sorting facility; and transportation of FFPS to feed mill) varies. We assume that no variations occur in the other processing phases when changing the transport phase. This sensitivity analysis considers different distances; in particular they were increased by 2-3-4-5-10 times to see the influence on the whole process.

Table 7: Summary of transport phase

Transport Phase

Phase	Means of transport	Unit	Quantity
Transportation of FW to distribution centre	Lorry 3.5-7.5 metric ton, EURO4	km	250
Transportation of FW to Sorting facility	Lorry 16-32 metric ton, EURO4	km	80
Transportation of FFSF to feed mill	Lorry 3.5-7.5 metric ton, EURO4	km	40

The results of the sensitivity analysis show that the variation in the transport phase (Table 7) has a limited influence on the environmental impacts (Figure 10 and Figure 11). In fact, increasing by 3 times the transport phase in scenario 1, only in 2 categories (Ozone depletion and Ionising radiation) the impact of the new scenario is higher the impact of the scenario where animal feed is produced only with corn. Instead in scenario 2 solely increasing by 4 times the transport phase, the new scenario showed a higher impact in one unique category (Natural land occupation) compared to the original scenario (Table 4).

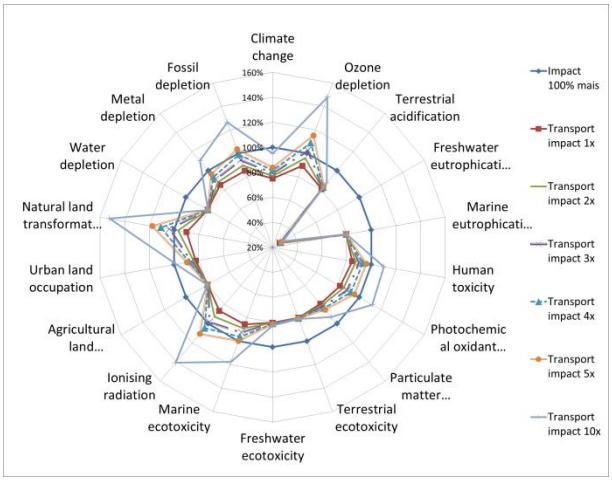

Figure 10: Graphical results of the sensitivity analysis for the variation in transport phase, scenario 1

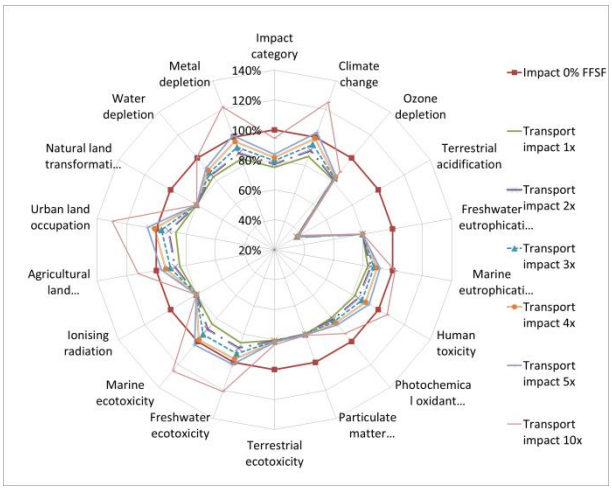

Figure 11: Graphical results of the sensitivity analysis for the variation in transport phase, scenario 2

5. CONCLUSIONS

The purpose of this work is to evaluate and compare the environmental impacts of 2 FW valorization scenarios by identifying the inputs and outputs for both option and their impacts. Both scenarios ensure a reduction of the environmental impact in all categories considered as compared to the current scenario (landfill). The LCA study showed than scenario 2 can bring more environmental gains than scenario 1 (in particular in 13 categories such as Climate change, Ozone depletion, Freshwater eutrophication and Terrestrial ecotoxicity).The results showed that about 4E+6 kg CO_2-eq. of greenhouse gases would be avoided valorizing the FFPS through both scenarios This study prove clearly that the method

of manufacturing feed from FW for animals can be an environment friendlier method than landfilling.

Further studies could investigate the environmental performance of other FW treatment scenarios, for instance, separating the meat and fish fractions of FW for pet food production.

REFERENCES

BCFN, 2012. Food Waste: Causes, Impacts and Proposals; Barilla Center for Food and Nutrition: Parma, Italy.

Cherubini F., Bargigli S., Ulgiati S., 2009. Life cycle assessment (LCA) of waste management strategies: Landfilling, sorting plant and incineration Energy 34 2116–2123.

Ecoinvent, 2015. Ecoinvent data v2.2. Ecoinvent reports No1-25. Dübendorf: Swiss Centre for Life Cycle Inventories.

Eriksson O., Carlsson R. M., Frostell B., Bjorklund A., Assefa G., Sundqvist J. O., 2005. Municipal solid waste management from a systems perspective. J Clean Prod 13, 241–52.

European Commission, 2008. Directive (2008/98/EC) of the European parliament and of the council of 19 November 2008 on waste and repealing certain Directives. Strasbourg: Official Journal of the European Union; 2008, L312/222008.

European Commission 2015. "Causes of Food Waste." http://ec.europa.eu/food/food/sustainability/causes_en.htm. [access 02/2015]

European Parliament Council, 2008. Directive 2008/1/EC of the European Parliament and of the Council of 15 January 2008 Concerning Integrated Pollution Prevention and Control. Brussels.

FAO, 1981. Food Loss Prevention in Perishable Crops. Rome: Food and FAO Agricultural Service Bulletin, no. 43, FAO Statistics Division.

FAO, 2013a. Food Wastage Footprint Impacts on Natural Resources. FAO. http://www.fao.org/docrep/018/i3347e/i3347e.pdf. [access May 2015]

FAO, 2013b. Food Waste Footprints FAO. http://www.fao.org/fileadmin/templates/nr/sustainability_pathways/docs/Factsheet_FOODWASTAGE.pdf. [access May 2015]

Güereca L. P., Gassó S., Baldasano J. M., Guerrero P. J., 2006. Life cycle assessment of two biowaste management systems for Barcelona, Spain. Resour Conserv Recy 49(1), 32–48.

Gustavsson J., Cederberg C., Sonesson U., Otterdijk R., and Meybeck A.. 2011. Global Food Losses and Food Waste. Rome: FAO.

Kantor L. S., Lipton K., Manchester A., Oliveria V., 1997. Estimating and addressing America's food losses. Food Rev. 20(1): 2–12.

Khoo A., Hsien H., Teik Z. L., Reginald B. H. T., 2009. Food waste conversion options in Singapore: Environmental impacts based on an LCA perspective Science of The Total Environment. 408 (6),1367–1373.

Kim M. H., Kim J. W., 2010. Comparison through a LCA evaluation analysis of food waste disposal options from the perspective of global warming and resource recovery Science of the Total Environment 408, 3998–4006.

HLPE, 2014. Food losses and waste in the context of sustainable food systems. A report by the High Level Panel of Experts on Food Security and Nutrition of the Committee on World Food Security, Rome 2014.

Hong R. J., Wang G. F., Guo R. Z., Cheng X., Liu Q., Zhang P. J. , Qian G. R., 2006. Life cycle assessment of BMT-based integrated municipal solid waste management: case study in Pudong, China. Resour Conserv Recy. 49(2), 129–46.

ISO 14040, 2006. Environmental Management – Life Cycle Assessment. Principles and Framework. International Organisation for Standardisation, Geneva, Switzerland.

ISO 14044, 2006. Environmental Management – Life Cycle Assessment. Requirements and Guidelines. International Organisation for Standardisation, Geneva, Switzerland.

Lee S. H., Choi K. I., Osako M., Dong J. I., 2007. Evaluation of environmental burdens caused by changes of food waste management systems in Seoul, Korea. Science of the Total Environment 387, 42–53.

Levis J. W., Barlaz M. A., 2011. What is the most environmentally beneficial way to treat commercial food waste? Environ Sci Technol. 45, 7438–44.

Lipinski B., Hanson C., Lomax J., Kitinoja L., Waite R., Searchinger T., 2013. Reducing Food Loss and Waste. Working Paper, Installment 2 of Creating a Sustainable Food Future. Washington, DC: World Resources.

Lundie S., Peters M. G., 2005. Life cycle assessment of food waste management options. J Clean Prod 13, 275–86.

Memon M., 2010. Integrated solid waste management based on the 3R approach. J Mater Cycles Waste Manage12, 30–40.

Mendesa M. R., Aramaki T., Hanakic K., 2003. Assessment of the environmental impact of management measures for the biodegradable

fraction of municipal solid waste in Sao Paulo City. Waste Management 23 403–409.

Ohlsson T., 2014. Sustainability and Food Production. In: Motarjemi Y and Lelieveld H, eds. Food Safety Management, . San Diego: Academic Press, 1085-1097.

Prandini A., Morlacchini M., Cerioli C., Piva G., 2007. Derivati della lavorazione di prodotti da forno nella razione di suini pesanti. Suinicoltura 5, 81-86.

Sakai S., Yoshida H., Hirai Y., Asari M., Takigami H., Takahashi S., 2011. International comparative study of 3R and waste management policy developments. J Mater Cycles Waste Manage 13, 86–102.

Smil V., 2004. Improving efficiency and reducing waste in our food system. Environ. Sci. 1, 17-26.

Stuart T., 2009. Waste. Uncovering the Global Food Scandal. Penguin, London. Sustainable Restaurant Association. Too Good to Waste. Restaurant Food Waste Survey Report, London.

Vandermeersch T., Alvarenga R.A.F., Ragaert P., Dewulf J., 2014. Environmental sustainability assessment of food waste valorization options. Resources, Conservation and Recycling 87. 57–64.

Vermeulen, S. J., Campbell B. M. J., Ingram J. S. I., 2012. Climate Change and Food Systems. Annual Review of Environment and Resources 37, 195-222.

AUTHORS BIOGRAPHY

David MOSNA is scholarship holder at Interdepartmental Center CIPACK of the University of Parma. In October 2014 he has achieved a master degree in Mechanical Engineering for the Food Industry at the same university. His main fields of research concern LCA on food products, packaging systems and industrial applications in general.

Giuseppe VIGNALI is Associate Professor at University of Parma. He graduated in 2004 in Mechanical Engineering at the University of Parma. In 2009, he received his PhD in Industrial Engineering at the same university, related to the analysis and optimization of food processes. Since August 2007, he worked as a Lecturer at the Department of Industrial Engineering of the University of Parma. His research activities concern food processing and packaging issues and safety/security of industrial plant. Results of his studies related to the above topics have been published in more than 60 scientific papers, some of which appear both in national and international journals, as well in national and international conferences.

APPENDIX

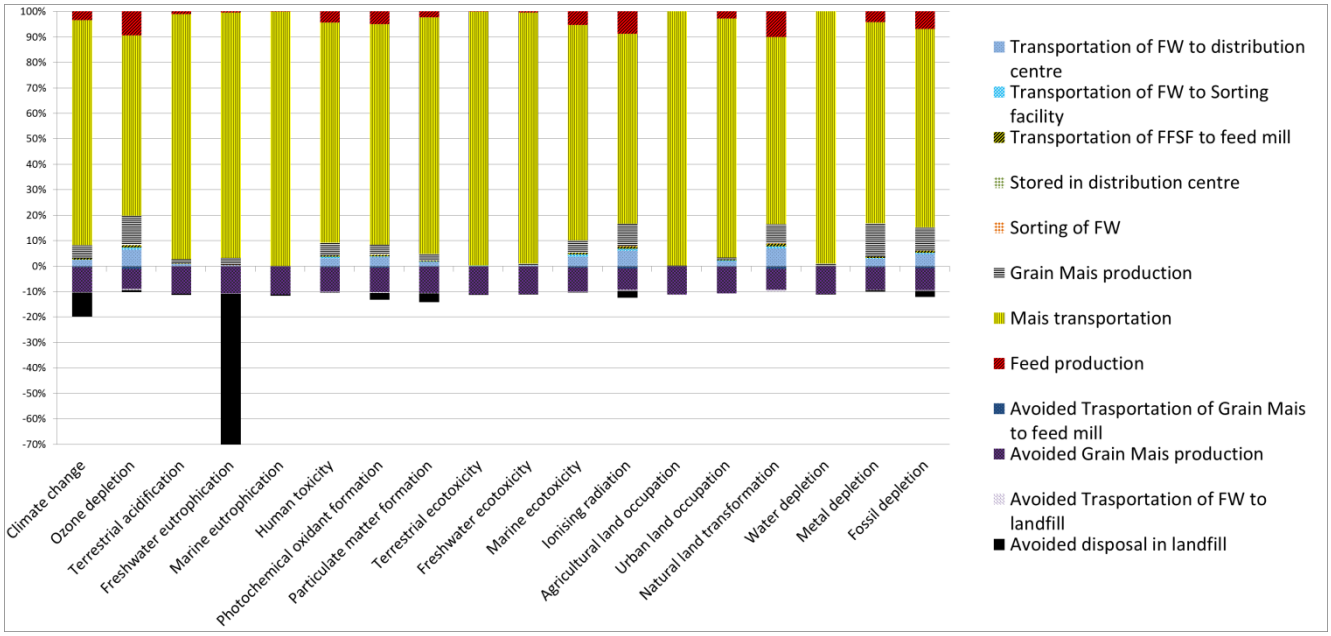

Appendix A: Relative contribution of different phases to the overall impacts for scenario 1

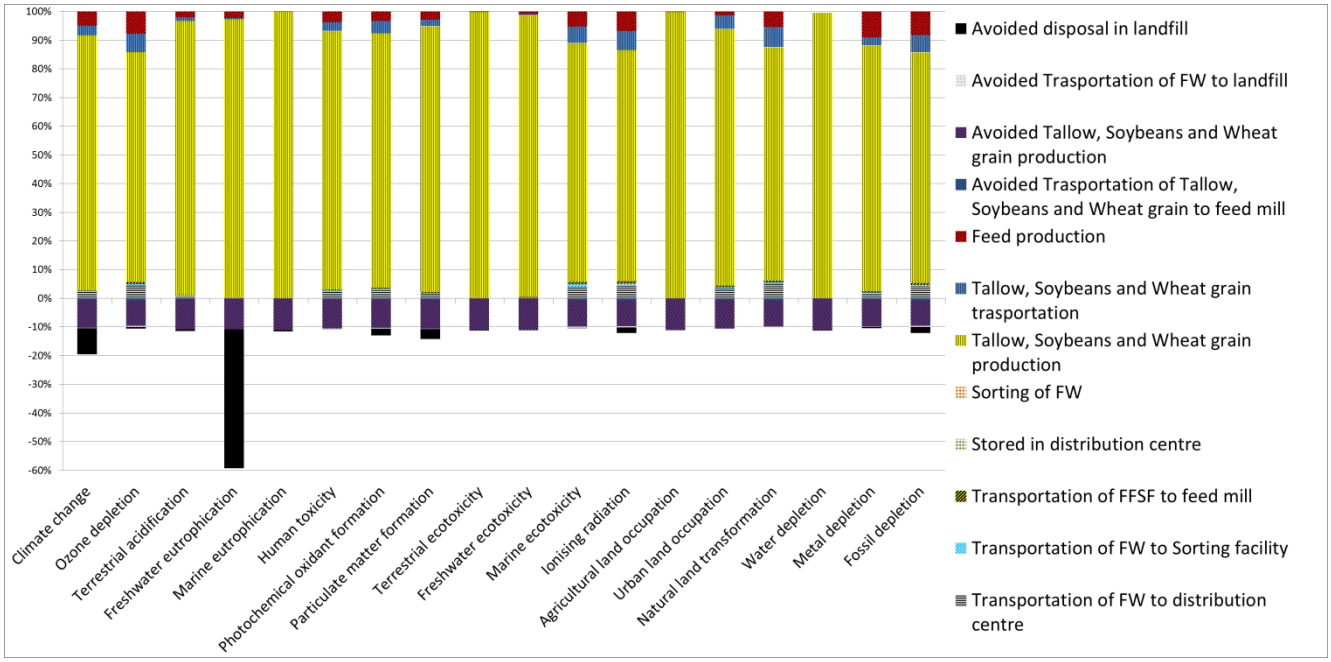

Appendix B: Relative contribution of different phases to the overall impacts for scenario 2

DEVELOPMENT OF A SMALL SCALE MACHINE FOR ROASTING SHEA KERNEL PRIOR TO SHEA BUTTER EXTRACTION

A.M. Olaniyan[(a)], A.O. Yusuf[(b)], O.F. Osadipe[(c)]

[(a)]Department of Agricultural and Bioresources Engineering, Faculty of Engineering, Federal University Oye Ekiti, P.M.B. 373, Oye Ekiti 371101, Ekiti State, Nigeria
[(b),(c)]Department of Agricultural and Biosystems Engineering, Faculty of Engineering and Technology, University of Ilorin, P.M.B. 1515, Ilorin 240003, Kwara State, Nigeria

[(a)]amolan397@hotmail.com

ABSTRACT
Shea kernel roasting prior to shea butter extraction is done to prepare the kernel in a good condition for the extraction of the fat (shea butter). Besides, roasting reduces the viscosity of oil to be extracted, ruptures the oil cells, adjusts the moisture content of the kernel to the optimum level for oil extraction and destroys or deactivates enzymes which inhibit the release of oil from the kernel. All these facilitate the extraction process. A small scale machine for roasting shea kernels prior to shea butter extraction was designed, constructed and tested The machine consists of a hopper, top cover, roasting chamber, chamber support, an auger or screw conveyor, temperature-controlled heating device, a discharge outlet, a 2 hp electric motor and a speed-reduction gear box. The machine derives its power from the electric motor through a gear reduction box to the shaft of the screw conveyor. Shea kernel is fed through the hopper into the roasting chamber and then conveyed to the discharge end after being roasted. Heat is supplied to the kernel inside the roasting chamber form two 750 W ring-type heaters placed at both ends of the chamber. The roasting temperature is regulated by a thermostat connected to the electric heaters. The machine has a capacity of 20 kg/h and the production cost was USD100. Test results revealed weight losses of 12.1, 27.6, 31.8 and 32.8 % in the kernels at roasting temperatures of 50, 70, 90 and 110 ^{0}C respectively. The kernels were of uniform deep-brown colour with clear film of oil on the surface after roasting indicating that they experienced uniform roasting.

Keywords: development, roasting machine, roasting temperature, shea butter, shea kernel

1. INTRODUCTION

Oilseed materials with high protein content are usually roasted before pressing in order to coagulate the protein and free the oil for extraction. Shea kernel (SK) roasting prior to shea butter (SB) extraction is a common practice among SB processors in the Nigerian rural communities because it facilitates oil extraction process. Besides, roasting reduces the viscosity of oil to be extracted, rupture the oil cells, adjusts the moisture content of the kernel to the optimum level for oil extraction and destroys or deactivates enzymes which inhibit the release of oil from the kernel. SB is the fat content of SK which is used in food, soap, cosmetics, pharmaceutical, medical and engineering industries for the production of cooking oils, toilet soaps, pomade, drugs, ointments and metal cutting fluids respectively. The residual cake from which the oil is extracted – shea cake (SC) – can be an excellent ingredient for livestock feed production and a substitute for cocoa butter in the chocolate and confectionary industries. These products, in Nigeria, have high potential for export and as foreign exchange earners.

Olopade and Akinoso (2004) designed and fabricated 2 kg capacity roaster for roasting cassia sieberiana seeds. Visual observation while testing the roaster revealed that physical changes on the seeds were time dependent; 200 ^{0}C roasting temperature and 15 min roasting time gave the best samples of cassia sieberiana during the testing. Mahama, Mburidiba, Mensah, and Seidu (2004) developed a machine for roasting crushed SK in Northern Ghana. The roaster consists of an enclosed cylindrical drum with a lid welded to the opening to prevent the material from falling out during operation. Inside the drum are agitators which transfer the material into different positions in order to prevent burning, mixes the material in the drum for uniform roasting and sweeps the roasted materials properly in the drum in order to receive fresh one. However, the machine is very slow in operation and operates with much heat loss and too much heat to body contact with possibility of fire disaster during roasting (Mahama, Mburidiba, Mensah, and Seidu 2004).

Akinoso, Asiru, and Awoliyi (2004) developed a 300 kg/h manual cashew nut roasting machine which uses charcoal as a source of heat energy. Performance evaluation showed that the roaster could roast 15 kg of raw cashew nut having a moisture content of 12 %

wet basis for 3 minutes using 130 ^{0}C as a roasting temperature. Davids (2003) stated that roasting machines basically operate at temperatures between 240-275 ^{0}C for a period of time ranging from 3 to 30 minutes. Raemy and Lambelet (1982) explained that coffee roasting process is initially endothermic (absorbing heat) but becomes exothermic (giving off heat) at a temperature of about 175 ^{0}C. It implies that, at this temperature, the beans are heating themselves; thus, roaster design engineers should know that roaster's heat source should be adjustable and controllable. Basically, there are two common types of roasting machines which include drum roasters and hot-air roasters (Anonymous, 2012). Others that are less common include packed bed roasters, tangential roasters and centrifugal roasters (Anonymous, 2012). In hot air coffee roasters, heated air is forced through a perforated plate under the coffee beans with a force sufficient enough to lift the beans while tumbling and circulation of the beans within the fluidized bed aid the process of heat transfer to the beans (Anonymous, 2012).

In the traditional method of SB extraction, SK is roasted over fire for a certain period of time using some local devices. One of such devices is made of a perforated clay pot inside which the kernels are placed and then heated from the bottom using firewood. Another one consists of an empty drum with a perforated bottom while the kernels are fired underneath using firewood. This traditional method is crude, tedious, labour intensive, has no provision for ergonomic factors and also exposes the operators to excessive smoking and heat radiation. SB extracted from SK treated using this method has been found to be poor quality. A SB processor in the rural communities needs a SK roasting device that can easily be operated, used and maintained. Therefore, the objectives of this work are to design, construct and test a simple small scale machine for roasting SK prior to SB extraction in the rural communities. Such a machine would remove the hazards involved in the traditional roasting of SK and eventually improve the efficiency of SB extraction.

2. THE MACHINE

3.1. Description and Working Principles

The roaster consists of a hopper, top cover, roasting chamber, chamber support, an auger or screw conveyor, temperature-controlled heating device, a discharge outlet, a 2 hp electric motor and a speed-reduction gear box. The machine derives its power from the electric motor through a gear reduction box to the shaft of the screw conveyor. SK is fed through the hopper into the roasting chamber and then conveyed to the discharged end after being roasted. Heat is supplied to the kernel inside the roasting chamber form two 750 W ring-type heaters placed at both ends of the chamber. The roasting temperature is regulated by a thermostat connected to the electric heaters. The isometric view of the machine is shown in Figure 1.

3.2. Design Considerations

Design considerations included machine capacity of 20 kg/h; roasting chamber adequately insulated to prevent heat loss during roasting operation; a speed-reduction mechanism to step down the motor to the desired shaft speed; temperature-control device to regulate the roasting temperature; a screw auger to serve the dual purposes of conveying and stirring the kernels in the roasting chamber thereby preventing burning of the kernels; roasting chamber designed to accommodate the required quantity of SK; roasting chamber designed to ensure maximum contact of individual kernel with the heat output in order to increase efficiency and reduce heating time; and a strong main frame to serve as structural support for the machine.

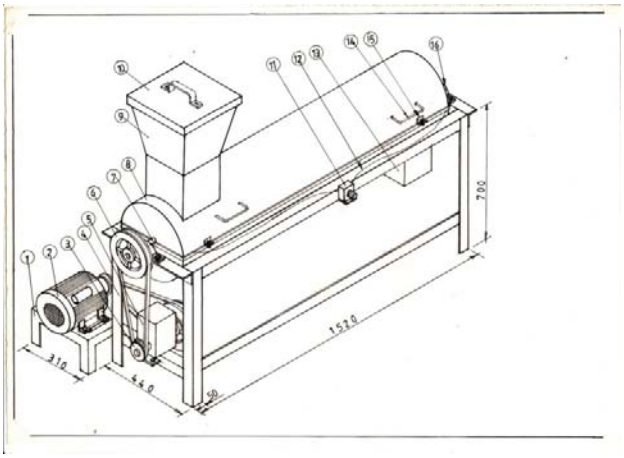

Figure 1: Isometric View of the Roasting Machine: 1-Electric motor stand, 2-Electric motor, 3-Speed reduction pulley, 4-Machine stand, 5-Speed reduction box, Machine pulley, 7-Conveyor shaft, 8-Roasting drum, 9-Feeding hopper, 10-Hopper lid, 11-Thermostat, 12-Thermocouple wire, 13-Kernel outlet, 14-Drum handle, 15-Drum flange, 16-Bearing housing

2.3. Design Theorems

2.3.1 Transmission Shaft

The main shaft that makes the screw conveyor in the roasting chamber is subjected to bending moment and shear stress during rotation. The permissible diameter of the shaft, according to American Society of Mechanical Engineers (ASME) Code was determined as:

$$d^3 = \frac{16}{\delta_o \pi}\sqrt{M^2 + T^2} \quad (1)$$

where d is the permissible shaft diameter in m, M is the bending moment in Nm, T is the maximum torque in Nm, δ_o is the yield stress in N/m^2 and π is a constant. With M = 13.13 Nm, T = 60 Nm, and δ_o = 72 x 10^6 N/m^2, hence d = 15.11mm. Therefore, a solid mild steel rod of diameter of 20 mm was used for the transmission shaft.

2.3.2. Auger Capacity

The theoretical capacity of the auger was calculated from the equation developed Onwualu, Akubuo, and Ahneku (2006) as:

$$Q = 60\,x\frac{\pi}{4}(D^2 - d^2)\,pN\phi \quad (2)$$

where Q is the theoretical capacity in m^3/h, D is the screw diameter in m, d is the shaft diameter in m, p is the screw pitch in m, N is the shaft speed in rpm and ϕ is the filling factor. Substituting D = 30 cm, d = 20 mm, p = 30 cm, N = 30 rpm and ϕ =.8, hence, Q = 30.401 m^3/h.

2.3.3. Power Requirement

The power required to rotate the auger was determined using an adapted form of Onwualu, Akubuo, and Ahneku (2006)'s equation as:

$$P = \frac{QL\rho gF}{3600} \quad (3)$$

where P is the power required in W, L is the length of the conveyor in m, ρ is the density of shea kernel in kg/m^3, g is the acceleration due to gravity in m/s^2 and F is the material factor. Substituting Q = 30.401 m^3/h, L = 150 cm, ρ = 754.18 kg/m^3, g = 9.81 m/s^2 and F = 0.4 into Equation 2.3 and taking into consideration the speed-reduction ratio of 15:1, hence, P = 562.298 W. To give allowance to power used in driving the pulley and other losses, the rated power was 570 W. The power of the electric motor to drive the system was estimated as:

$$P_m = \frac{P}{\eta} \quad (4)$$

where P_m is the power of electric motor in W and η is the efficiency of the motor in decimal. Given that η = 0.8, therefore, P_m = 712.5 W or 0.96 hp. The machine can be driven by a 1 hp electric motor. However, a 2 hp single-phase electric motor was selected.

2.3.4. Operating Capacity

The operating capacity of the machine was calculated from the energy equations used by Akinoso, Asiru, and Awoliyi (2004) and Olopade and Akinoso (2004) as:

$$Q_o = mc\theta \quad (5)$$

and

$$t = \frac{Q_o}{P_h} \quad (6)$$

where Q_c is the quantity of heat required in kJ, m is the mass of shea kernel in kg, c is the specific heat capacity of shea kernel in kJ/kg ^{0}C, θ is the change in temperature in ^{0}C, t is the roasting time in s and P_h is the rated power of the heaters in kW. With m = 7 kg, c = 1.507 kJ/kg ^{0}C, θ = 120 ^{0}C and P_h = 1.5 kW substituted into Equation 2.4, hence, Q_c = 1265.88 kJ and t = 14.07 min. Therefore, the machine can roast 7 kg of SK in about 15 min.

3. MATERIALS SELECTION AND CONSTRUCTION

The feeding hopper was fabricated from a standard length of 1.5 mm thick metal sheet. Four pieces of dimension 300 x 450 mm were cut from the metal sheet to make the four sides of the hopper. A 50 mm length was cut from both sides of the width to a height 200 mm to form a base of dimension 200 x 200 mm for the hopper. The four pieces of metal sheet were welded together to form the required shape of the feeding hopper. The roasting chamber is essentially a double wall cylindrical container made from mild steel sheet of 1.5 mm and 1.2 mm for the outer and inner walls respectively. The outer cylinder was of dimension 1000 x 1500 mm while the inner one was 950 x 14500 mm and the clearance was filled with insulation materials. The metal sheet was cut by a treadle-operated guillotine while a rolling machine was used to fold the sheet into a cylindrical shape.

The main frame was fabricated using a 40 x 40 mm angle iron. The procedures involved measurement with steel tape, marking out with scriber and cutting using power hacksaw. After cutting each component to the required dimensions, they were welded together to serve as support and stand for the roasting chamber and prime mover thereby enhancing the stability of the whole machine. The screw conveyor (auger) was made from a mild steel shaft (Φ 20 mm) on which a 1.2 mm metal sheet was welded spirally to form a screw. The turning and facing of the shaft

were carried out on the lathe. The specification of construction materials is shown in Table1. Fabrication was carried out at the Central Engineering Workshop, University of Ilorin. Figures 2 and 3 show the exploded and orthographic front views of the roasting machine respectively.

Table 1: Materials of Construction of the Shea Kernel Roasting Machine and their Specifications

Material of Construction	Specifications	Quantity
Metal sheet	1.5 mm thickness, standard size	1
Metal sheet	1.2 mm thickness, standard size	1
Mild steel rod	Φ 25 mm, $\frac{1}{2}$ standard size	1
Angle iron	40 X 40 mm, standard length	3
Electric heater	750 W	2
TDC*	0-150 ^{0}C	1
Electric wire	3 m length	1
Welding electrode	Gauge 12	18
Electric plug	15 A	2
Bolts and nuts	M12	10
Bolts and nuts	M13	10
V - belt	A 42, 12.5 X 1125 mm	1
V - belt	A 35, 12.5 X 925 mm	1
Insulating materials	25 kg	1

*TDC: Temperature Control Device

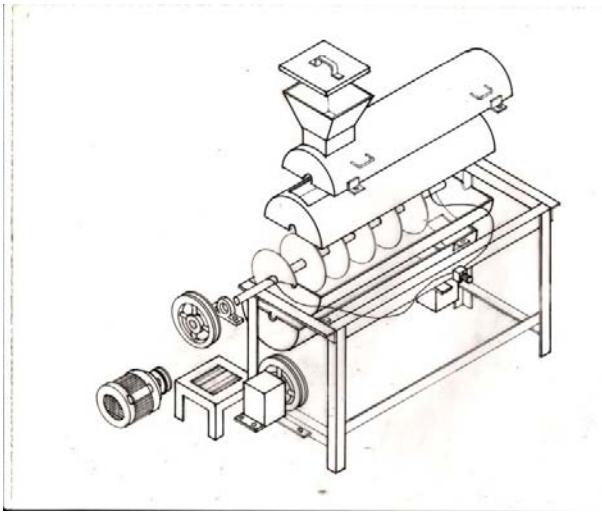

Figure 2: Exploded View of the Roasting Machine

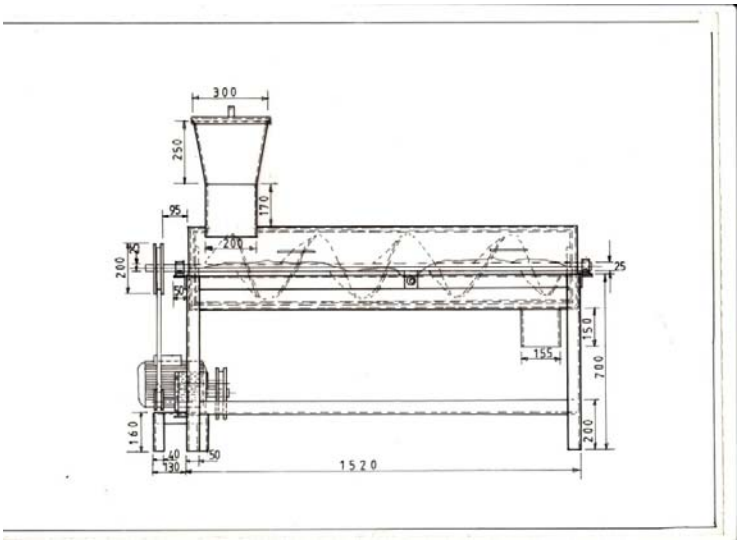

Figure 3: Front View of the Roasting Machine

4. MATERIALS AND METHODS USED FOR PERFORMANCE EVALUATION

In order to test for the performance of the machine, 2 bags (100 kg) of shea nuts (SN) were obtained from a produce merchant in Ilorin. The nuts were cracked, winnowed, dried, packaged in moisture-proof bags and stored in the laboratory at room conditions. The moisture content of the kernels was determined according to Adeeko and Ajibola (1989). After the assembly of the machine, the heater was switched on and the roasting chamber was allowed to attain a desired temperature (50 ^{0}C) using the thermostat. The machine was then set into operation and a known quantity of SK was introduced through the hopper. The rotary motion of the auger (screw conveyor) provided stirring and tumbling of the kernels in the roasting chamber. In this way, burning was prevented while even roasting of the kernels was ensured. The kernels were discharged after 20 min of roasting and reweighed. Weight loss, W_{LS} in %, was then determined as follows:

$$W_{LS} = \frac{100\left(W_{BR} - W_{AR}\right)}{W_{BR}}\% \qquad (7)$$

where W_{BR} and W_{AR} are weight before roasting and weight after roasting respectively in g. The same procedure was repeated for 70, 90 and 110 ^{0}C with each test being replicated thrice. Samples of SK roasted by the machine were processed by two screw

press expellers and a model cage press for SB extraction. Oil yield, extraction efficiency and process loss were determined from standard formulae (Adeeko and Ajibola 1989; Olaniyan and Oje 2007) as follows:

$$O_Y = \frac{100 W_{OE}}{W_{US}} \% \quad (8)$$

$$E_E = \frac{100 W_{OE}}{x W_{US}} \% \quad (9)$$

$$P_L = \frac{100\{W_{US} - (W_{OE} + W_{RC})\}}{W_{US}} \% \quad (10)$$

where O_Y, E_E and P_L are oil yield, extraction efficiency and process loss respectively in %; W_{OE}, W_{RC} and W_{US} are weights of oil extracted, residual cake and shea kernel sample respectively in g and x is the oil content of shea kernel in decimal. Each trial was carried out in triplicates.

5. RESULTS AND DISCUSSION OF PERFORMANCE EVALUATION

The results of weight loss in kernel after roasting and that of the extraction experiments are shown in Tables 2 and 3 respectively. The average percentage weight loss increased from 12.1 % to 32.8 % when the roasting temperature was increased from 50 ^{0}C to 110 ^{0}C. From visual observation, it was revealed that the kernels were of uniform deep-brown colour with clear film of oil on the surface after roasting indicating that the kernels experienced uniform roasting. During roasting operation, the flavour and aroma peculiar with roasting of SK were perceived. As shown in Table 3, the roasted SK gave appreciable yield of SB and high extraction efficiency during extraction experiments with a model ram press and the screw expellers. Process losses were very small using the three oil extraction equipment. These results showed that the SK roaster performed efficiently and effectively with a high degree of satisfaction.

Table 2: Results of Investigation of Weight Loss of the Roasted Shea Kernels*

Roasting Temperature (^{0}C)	Weight Loss (%)
50	12.1
70	27.6
90	31.8
110	32.8

* Each value is the mean of triplicates ± standard deviation

Table 3: Results of Investigation of Shea Butter Extraction from the Roasted Shea Kernels*

Measured Parameters	20 kg/h Screw Press Expeller	250 kg/h Screw Press Expeller	Model Cage Press
Oil Yield (%)	28.6	40.56	35.1
Extraction Efficiency (%)	47.6	67.6	58.5
Process Loss (%)	18.9	5.0	2.8

* Each value is the mean of triplicates ± standard deviation

6. CONCLUSION

A small scale machine for roasting SK prior to SB extraction was designed, constructed and tested. The construction materials were readily available locally and at affordable costs. With a production cost of USD100, the machine has an output capacity of 20 kg/h and was operated by a 2 hp single-phase electric motor. While testing the machine, the flavour and aroma peculiar with roasting of SK were perceived. Visual observation revealed that the kernels were of uniform deep-brown colour with clear film of oil on the surface after roasting indicating that the kernels experienced uniform roasting.

REFERENCES

Olopade A.A., Akinoso R., 2004. Design of a Rotary Roaster for Cassia Seberiana Seeds. Proceedings of the 5th International Conference and 26th Annual General Meeting of the Nigerian Institution of Agricultural Engineers, 26, 322-325.

Mahama A.A., Mburidiba S., Mensah E., and Seidu M., 2004. Developing the Shea Butter Bean Roaster used in Northern Ghana. Proceedings of the 2nd International Conference of the West African Society of Agricultural Engineering, 85-91.

Akinoso R., Asiru W.B., and Awoliyi O.O., 2004. Design, Development and Performance Evaluation of a Manual Cashew Nut Hot Oil Roasting Machine. Nigerian Food Journal, 22, 183-188.

Davids K., 2003. Home Coffee Roasting: Romance and Revival, 2nd ed., London: St. Martins Griffin.

Raemy A., Lambelet P.A., 1982. Calorimetric Study of Self-Heating in Coffee and Chicory. International Journal of Food Science and Technology, 17 (4), 451-460.

Anonymous, 2012. Coffee Roasting. In Wikipedia: The Free Encyclopedia (Ed.). Wikipedia Foundation, Inc., http://en.wikipedia.org/wiki/Coffee.roasting, 24/05/2012.

Onwualu A.P., Akubuo C.O., Ahneku I.E., 2006. Fundamentals of Engineering in Agriculture, 1st ed., Enugu: Immaculate Publications Limited.

Adeeko K.A., Ajibola O.O., 1989. Processing Factors Affecting Yield and Quality of Mechanically Expressed Groundnut Oil. Journal of Agricultural Engineering Research, 5: 31- 43.

Olaniyan A.M., Oje K., 2007. Development of Mechanical Expression Rig for Dry Extraction of Shea Butter from Shea Kernel. Journal of Food Science and Technology, 44 (5): 465-470.

NOMENCLATURE

c	Specific heat capacity	kJ/kg ^{0}C
d	Shaft diameter	m
D	Screw Diameter	m
E_E	Extraction efficiency	%
F	Filling factor	-
g	Acceleration due to gravity	m/s^2
L	Length of conveyor	m
M	Mass	kg
N	Rotational speed	rpm
N_1	Rated speed of electric motor	rpm
N_2	Speed of the shaft	rpm
O_Y	Oil yield	%
P	Power	W
p	Screw pitch	m
P_m	Power of electric motor	W
P_h	Rated power of the heater	W
P_L	Process loss	%
Q	Auger capacity	m^3/h
Q_o	Operating capacity	kJ
T	Torque	N/m^2
t	Roasting time	s
W_{AR}	Weight after roasting	kg
W_{BR}	Weight before roasting	kg
W_{US}	Weight of shea kernel sample	kg
W_{OE}	Weight of oil extracted	kg
W_{LS}	Weight loss	%
W_{RC}	Weight of residual cake	kg
δ_o	Yield stress	N/m^2
ρ	Density	kg/m^3
θ	Change in temperature	^{0}C
ϕ	Filling factor	-
η	Efficiency	%

BIOGRAPHY OF THE MAIN AUTHOR

Dr. Adesoji Matthew Olaniyan graduated with B.Eng, M.Eng and PhD in Agricultural Engineering from University of Ilorin, Nigeria in 1991, 1998 and 2006 respectively. Since 1998, he has been working on techniques, processes and equipment for processing agricultural and bioresources materials to food, fibre and industrial raw materials. Dr. Olaniyan's principal area of research is on Bioproduct Processing and Food Process Engineering, where he has carried out a number of projects and published a number of papers in local and international journals. He joined the service of the University of Ilorin in 1998 as an Assistant Lecturer in the Department of Agricultural and Biosystems Engineering and rose to the position of a Senior Lecturer in 2009. Currently, he is an Associate Professor at the Department of Agricultural and Bio-resources Engineering, Federal University Oye-Ekiti, Nigeria. Dr. Olaniyan has bagged several awards including the Award for the Best Paper (2007) in the Journal of Food Science and Technology, Mysore, India; Chinese Government Sponsorship (2008) for International Training Programme in Protected Agriculture at International Exchange Centre, Yangling, China; Netherlands Fellowship Programme (2009) for International Training programme in Milk Processing at Practical Training Centre, Onkerk, the Netherlands; and Postdoctoral Fellowship (2011) of the Academy of Sciences of Developing Countries.

ANALYSIS, SIMULATION AND OPTIMIZATION OF THE MILKING PROCESS IN A COWSHED FOR THE PRODUCTION OF PARMIGIANO REGGIANO

Mattia Armenzoni[(a)], Eleonora Bottani[(b)], Roberto Montanari[(c)], Marta Rinaldi[(d)], Sergio Amedeo Gallo[(e)]

[(a), (b), (c), (d)] Department of Industrial Engineering – University of Parma, Viale delle Scienze 181/A, 43124 Parma (Italy)
(e) Department of Engineering Enzo Ferrari, DIEF (ex DIMeC), University of Modena and Reggio Emilia (Italy)

[(a)]mattia.armenzoni@unipr.it, [(b)]eleonora.bottani@unipr.it, [(c)]roberto.montanari@unipr.it, [(d)]marta.rinaldi@unipr.it, [(e)]sgallo@unimore.it

ABSTRACT
The aim of this study is to optimize the current milking process of a cowshed, which provides milk for the production of Parmigiano Reggiano cheese. The ultimate goal of the analysis is to reduce the time required for milking operations, thus optimizing the whole management of the farm processes. The analysis described is based on a real case study, referring to a farm located near Parma (Italy). To optimize the milking process, a discrete-event simulation model was designed under Simul8™ professional platform. The model reproduces the main processes of the cowshed, and in particular, the movements of the animals inside the cowshed, during milking. Real data were collected to allow the reproduction of the milking process. Exploiting again the simulation model, two new configurations of the cowshed layout were designed and tested, and their performance, in terms of the total time required for milking, was compared to the current one, showing interesting savings.

Keywords: simulation; animal behavior; milking process; Parmigiano Reggiano production.

1. INTRODUCTION

In Europe, the dairy sector is one of the most important sectors within the food industry. The production of milk intended for the dairy industry is estimated around 159 million tons per year in 2013 (European Commission, 2015). The main cheese producers of Europe are Germany, France, the United Kingdom, Poland, the Netherlands and Italy, which together account for almost 70% of the EU production (European Commission, 2015). Parmigiano Reggiano is a typical Italian hard cheese, known among the most typical products of the Italian food industry (Bellesia et al., 2003) and as one of the oldest cheeses in Europe, dating back to the 13th-14th century (Zannoni, 2010).
The production of Parmigiano Reggiano is located mainly in the North of Italy, in a limited geographic area, to comply with the protected designation of origin of the product (Zannoni, 2010). A specific consortium (i.e., *Consorzio del Parmigiano Reggiano*) collects the small and medium sized cheese factories and cooperatives that operates in the production of Parmigiano Reggiano. In 2013, the main figures of the Parmigiano Reggiano production sector were as follows: over 15.6 million tons of milk processed per year, which led to the production of more than 2.9 million wheels of cheese in 2013. The production of Parmigiano Reggiano cheese employs approx. 88% of the total production of cow's milk of Italy. The breeders operating in the Parmigiano Reggiano production chain are more than 3,100, with approx. 340 active dairy companies (Regione Emilia-Romagna, 2014). Approx. 33% of the production is exported outside Italy.
Parmigiano Reggiano is produced using raw, semi-skimmed milk, which can not in any way be subjected to chemical treatment nor been addicted with any substance. A specific set of rules, indeed, regulates the production of Parmigiano Reggiano cheese, to comply with the quality standards and protected designation of origin of the product (Consorzio del Parmigiano-Reggiano, 2011). Among others, this set of rules defines the feed for cows, the milk, the milking process and the manufacturing process of the cheese.
In this paper, we focus on the milking process for a cowshed that produces milk for the manufacturing of Parmigiano-Reggiano cheese. The farm analyzed is located in the area of Parma (Italy). The objective of the analysis was, overall, to improve the current milking process carried out at the farm, in terms of the total time, thus enhancing the productivity of the whole process. The analysis was supported by an *ad hoc* discrete-event simulation model, developed under Simul8™ professional platform. The remainder of the paper is organized as follows: section 2 provides an overview of the farm analyzed and describes the current (AS IS) milking process. Section 3 describes the data collection related to the AS IS scenario. Section 4 details the simulation model used to reproduce the milking process of the farm. Section 5 describes two alternative (TO BE) configurations that were designed to improve the AS IS milking process, as well as their analysis by means of the simulation tool. Section 6 summarizes the main findings of the study, the related implications and limitations, and indicates possible future research activities.

2. THE CONTEXT AND THE "AS IS" MILKING PROCESS

The farm analyzed owns 171 cows, and carries out two milking operations per day, one in the early morning and one in the afternoon. Milking processes are carried out in an appropriate room (milking room), where up to 16 cows can be handled simultaneously. Milking operations usually take approx. 3 hours, which is lower than the maximum allowed time of 4 hours, according to the requirements of Consorzio del Parmigiano-Reggiano, (2011). Currently, the milking process employs two people per work shift, resulting, overall, in 4 people involved in the milking activities. A scheme of the cowshed is proposed in Figure 1.

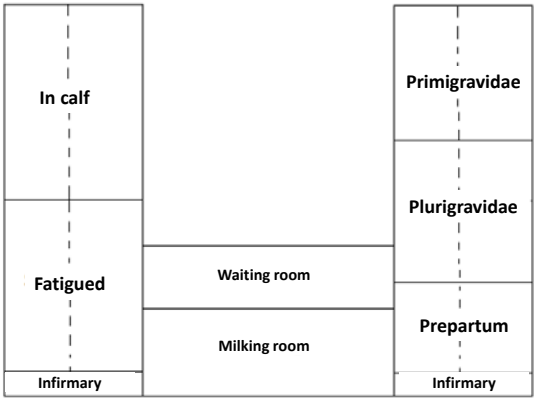

Figure 1: scheme of the cowshed and animals' groups

The milking process requires the cows to move from their positions in the cowshed (where they are located for most of the day) to the waiting room and then to the milking room. The waiting room is directly linked to the cowshed, so that the cows can easily reach it. One group of animals is moved at a time. Indeed, the cows can be classified in different groups, called 1-fatigued, 2-in calf, 3-primigravidae; 4-plurigravidae. The first group to be milked is that of fatigued cows, which consists of 48 animals. This group includes the oldest cows, which do not have a high production of milk and that require, under some circumstances, more time to complete the milking process. The second group to be milked is that of the in calf cows, which consists of 48 animals. Their milk production may not be so high, although the time required for milking is, in general, shorter. The third group is the smallest one (24 animals) and includes cows that, up to that moment, had only one pregnancy. The last group includes 51 animals, which, up to that moment, had more than one pregnancy. The last two groups of cows provide, in general, the highest quantity of milk, although the production may vary significantly during the year. Indeed, the daily production of the plant can slightly vary, reflecting the variation in the production of milk by cows across the year, due, in turn, to breed, season, or other management factors (e.g., nutrition or frequency of milking) (Jialina et al., 1998). In addition, the status of an animal can also change in time: for instance, a cow belonging to group 3 (primigravidae) could become a member of group 4 (plurigravidae) after some time. Sometimes, cows can be moved to the farm infirmary, because of health problems. The milk produced by these animals should not be used for the production of Parmigiano Reggiano for a given time period, because of the possible presence of antibiotics.

The whole amount of milk produced by the milking process is moved to a tank, where it is stored at 18°C, and subsequently moved to the cheese manufacturing company.

3. DATA COLLECTION

On the basis of the analysis of the current milking process, the aim of the work done in this paper was to look for alternatives configurations of that process, at the same time keeping the layout of the cowshed unchanged. As mentioned, the analysis was supported by a discrete-event simulation model, whose construction required some preliminary data, primarily related to the time required to move the animals in the cowshed. Those data were collected through direct measurements. It was found that the time required to move the animals ranges from three minutes for the groups closer to the milking room (i.e., plurigravidae and fatigued) to four minutes for the groups more distant (primigravidae and in calf). This time was considered as adequate, in the light of the number of animals to move. The time required for milking operations was also recorded. The milking process has a defined structure, including:

- Preparation phase, including washing of the breast and of the immediate surrounding areas, and subsequent accurate drying, made with paper, which is then trashed;
- Attachment phase, where the employee checks the health status of the breast and sticks the teats of the milking to the cows' nipples. From this moment on, the data for the milk production, time and cow identity are recorded in the database of the farm;
- Detachment phase, which is the opposite of the attachment phase. This is an automatic step;
- Post-dipping phase, which is carried out with an appropriate detergent used on the cows' nipples.

The data related to the milking process were collected exploiting both the farm's information system and direct measurements. Specifically, the data related to 9 days (18 milking processes) were extracted from the farm's database. This set of records included the following pieces of information: (1) animal number, (2) group number; (3) milk production; (4) milking start time; (5) milking end time; (6) milking duration. During the period of measurement, the farm's database recorded 48 fatigued cows, 48 in calf, 24 primigravidae and 51 plurigravidae.

The analysis of the data recorded showed that, on average, a cow produced 10.24 l of milk per day in the analyzed period. At the same time, however, the production is quite variable (see Figure 2).

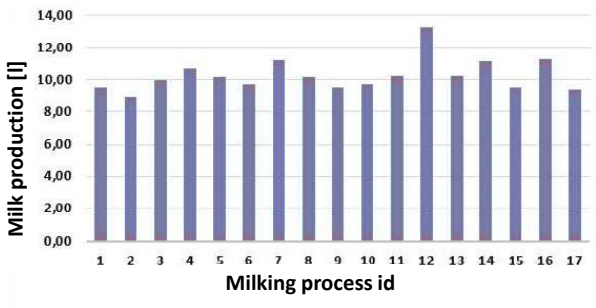

Figure 2: milk production [l]

With respect to the time required for milking, the data elaborated from the farm's information system led to the results reported in Figure 3.

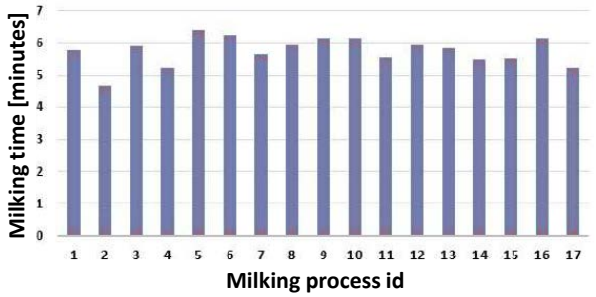

Figure 3: time required for milking.

Moreover, for 10 days (20 milking processes), direct measurements were made at the farm. During these measurements, the time required to complete the following activities on the animals was recorded:

- Cows' movement from their position to the waiting room;
- Exit of the cows from the milking room and return in their positions.

Also, some measurements were carried out to assess the time required to the employees to complete some specific activities, such as:

- Preparation Phase
- Attachment phase
- Detachment phase.

The time required for milking was not measured because it could be directly derived from the data recorded in the farm's database.
Finally, the detailed movements of the cows in the cowshed during milking were analyzed. As mentioned, the milking room is equipped with two sets of milking machines, each one able to handle 8 cows, resulting in 16 animals handles simultaneously. As an example, let us consider the first group of cows to be handled (i.e., group 1-fatigued); their initial movement inside the cowshed is described in Figure 4.

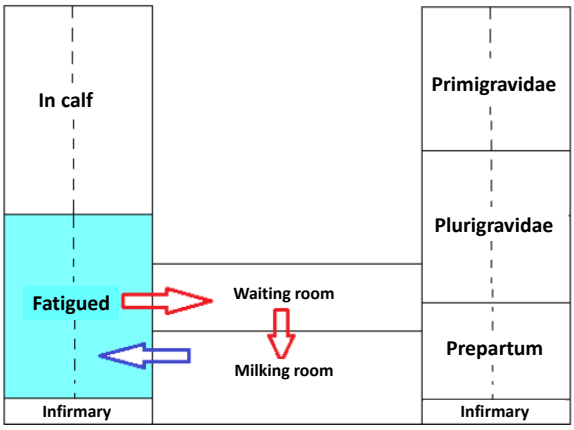

Figure 4: example of cows' movements in the cowshed.

Once the milking process of group 1 starts, the cows should be moved back to their positions, while group 2 of cows should be moved to the milking room, as shown in Figure 5.

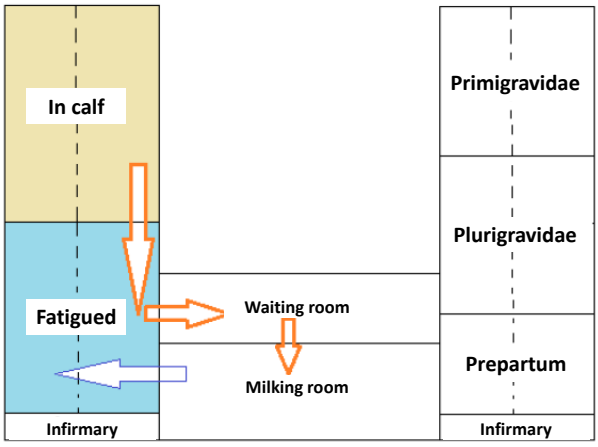

Figure 5: example of cows' movements in the cowshed.

Similarly, the movements of group 3 and 4 of cows were analyzed.

4. THE MODEL

The "AS IS" status of the milking process was reproduced in a simulation model, developed *ad hoc* exploiting the commercial software Simul8™ (Visual Thinking International Ltd). Simul8™ uses dynamic discrete simulation and is commonly exploited to simulate systems that involve processing of discrete entities at discrete times. Examples of those systems are production, manufacturing, logistic or service provision systems. As output, it generates statistics of performance parameters and metrics of the production system examined (Concannon et al., 2007).
The scheme of the model is proposed in Figure 6.

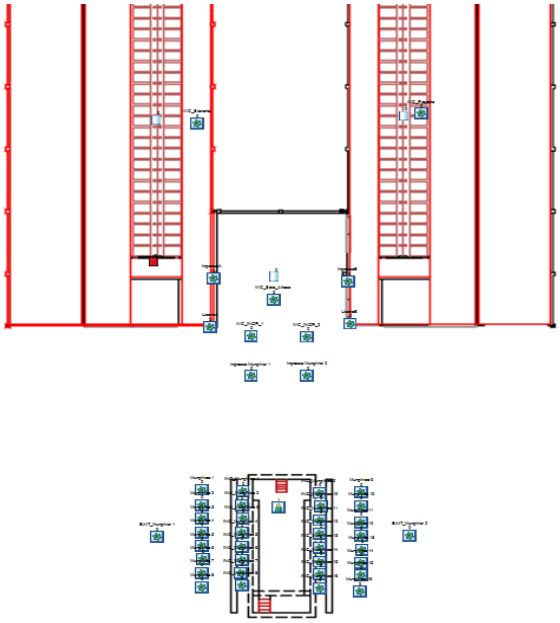

Figure 6: scheme of the Simul8™ model – AS IS scenario.

The model makes use of the input data described in section 3. Appropriate logics were embodied in the model to reproduce the behavior of the cows in the cowshed (cf. Figures 4 and 5), as well as the random order by which the cows move to the waiting room and milking room. Overall, the model includes 61 variables and 13 labels and takes the input data from 16 excel files.

To validate the model, we compared the results returned, in terms of the total time required for the milking process, with those measured during the data collection phase. In the real process, the total time required for milking varies from 2 hours 40 minutes to 3 hours. The results obtained through simulation reproduce the real scenario quite well, as can be seen from the frequency distribution in Figure 7.

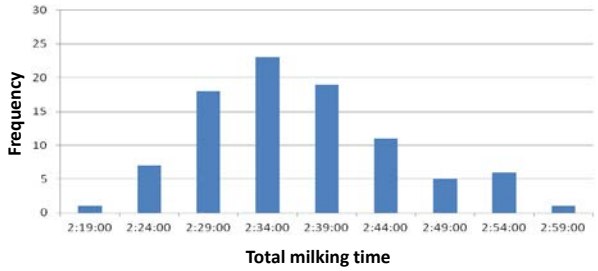

Figure 7: simulated results for the milking time - AS IS scenario.

The model was used to derive some further outcomes, such as the total amount of milk produced and the total production of milk per animal (cf. Figures 8 and 9). In can be seen from these figures that the model estimate the milk production per cow to range from approx. 11 to approx. 12 liters/cow, which is in line with the data collected from the real process. Therefore, the model could be considered as validated.

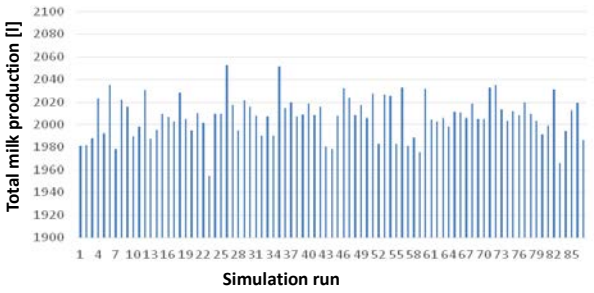

Figure 8: simulated results for the total milk production – AS IS scenario.

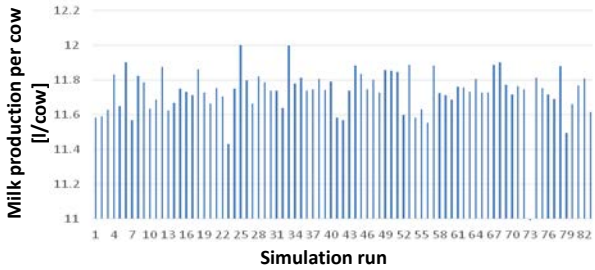

Figure 9: simulated results for the total milk production per cow – AS IS scenario.

5. TO BE CONFIGURATIONS

5.1. Definition of the TO BE scenarios

Once validated, the simulation model was used to examine two alternative configurations for the milking process, resulting in as many TO BE scenarios.

1. The first configuration examined considers a milking room with the same structure as that of the AS IS scenario. The equipment installed in the milking room, however, has a higher capacity, allowing to handle 24 cows (instead of 16) simultaneously. To simulate this TO BE configuration, some adjustments were made to the original simulation model, as well as to some of the input data. From a practical perspective, such a configuration would also require a slight reorganization of the space available in the milking room, to be implemented. Nonetheless, it is reasonable to expect that increasing the production capacity of the milking room will result in a decrease in the time required to complete the milking activities, resulting in a more efficient process.
2. The second TO BE configuration considered requires the complete reorganization of the cowshed layout, with the milking room and waiting room located in a different position compared to the AS IS scenario. A scheme of this TO BE configuration is proposed in Figure 10. The new positions of the milking room and waiting room would be useful, in particular, to

facilitate the movement of in calf and primigravidae cows, compared to the original structure of the cowshed. The second TO BE scenario would obviously modify the movements of the cows in the cowshed. Therefore, the model logics were slightly changed to reproduce the new cow movements. It is also hypothesized that 24 cows can be handled simultaneously in this configuration.

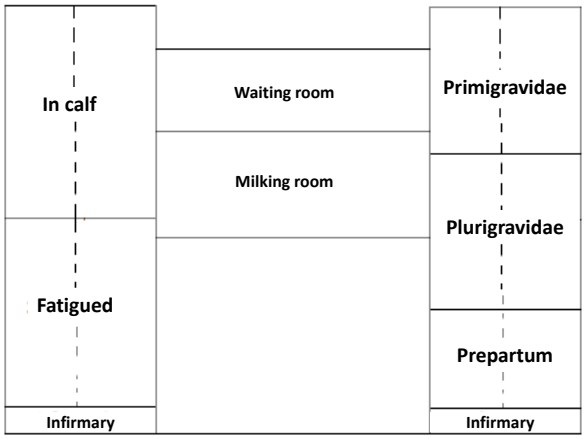

Figure 10: scheme of the second TO BE configuration.

5.2. Results for the first TO BE scenario

Simulating this TO BE configuration required some changes in the input data of the model (MS Excel™ files). For instance, the time required for preparation, washing, attachment and detachment were recalculated, considering the presence of 24 cows instead of 16 in the milking room. Conversely, data related to the behavior of the cows (e.g., the time for their movement or the waiting rime) or those related to the milking process (e.g., the milking time and milk production) were not changed. With respect to the simulation model, simulating this TO BE scenario required adding 4 work centers in the milking process, to take into account the increased number of cows that can be handled simultaneously. The new model is proposed in Figure 11. Specific logics were defined for these new work centers. The relevant results obtained for the first TO BE configuration (with 300 simulation runs) are reported in Figure 12.

It can be seen from Figure 12 that, with this new configuration, the milking time decreases (overall) by approx. 20 minutes, equally shared among the different groups of cows (i.e., 5 minutes per group, on average). By saving 20 minutes in the milking process, employees can be allocated to different activities for a total of approx. 20x2x2=80 minutes per day.

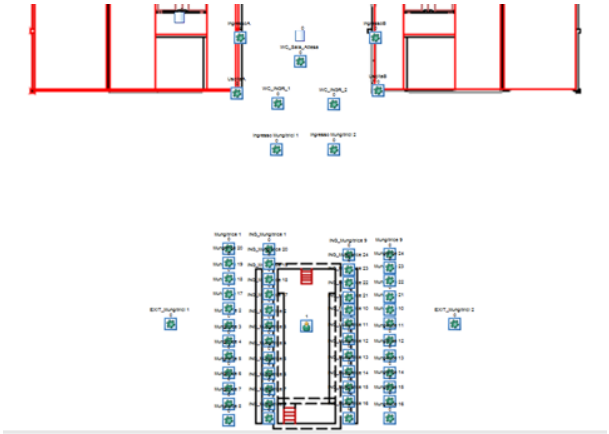

Figure 11: scheme of the Simul8™ model – TO BE scenario #1.

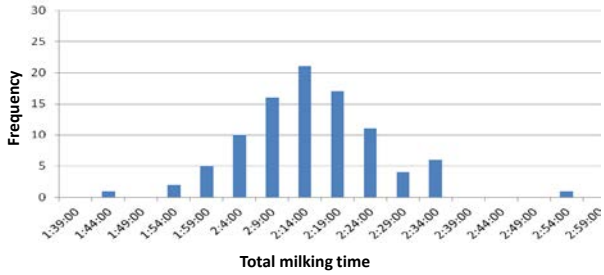

Figure 12: simulated results for the total milking time – TO BE scenario #1.

5.3. Results for the second TO BE scenario

Simulating the second TO BE configuration required some modifications to the input data, in terms of the time required to the cows to enter the milking room and the waiting room, as well as to go back to their locations in the cowshed. These data were recalculated based on the modified distances to be covered in the new configuration. Conversely, the simulation model was not changed in its structure.

The relevant results obtained for the second TO BE configuration (with 300 simulation runs) are reported in Figure 13.

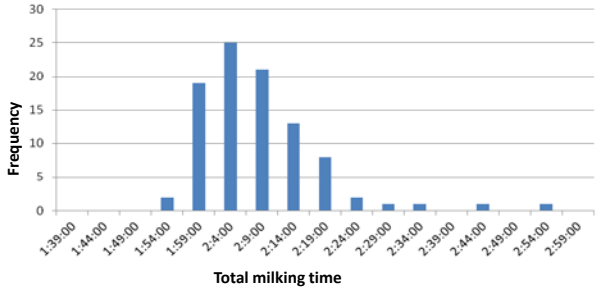

Figure 13: simulated results for the total milking time – TO BE scenario #2.

As can be seen from Figure 13, with this new configuration the time required for milking reduces to approx. 2 hours (between 2 hours 5 minutes to 2 hours 10 minutes), resulting in a significant saving compared to the original scenario. Only some simulation runs

returned a milking time close to 3 hours. Approx. 20,000 liters of milk are produced at every milking process, with an average production of 11.7 liters of milk per cow. As per the previous scenario, by saving approx. 30 minutes per milking process, employees could be allocated to different activities for a total of 30x2x2=120 minutes per day.

6. CONCLUSIONS

The aim of this study was to optimize the current milking process of a cowshed, which provides milk for the production of Parmigiano Reggiano cheese. The ultimate goal of the analysis was to reduce the time required for milking operations, thus optimizing the whole management of the farm processes.

To reach this aim, an *ad hoc* simulation model was developed to reproduce the milking process at the cowshed. The discrete-event simulation model was designed under Simul8™ professional platform. The main processes of the cowshed, and in particular, the behavior of the animals (e.g., their movements, waiting time and so on), were reproduced in the model, grounding on real data collected at the cowshed.

In line with the fact that the animals' behavior can significantly vary in time, the data collected were found to be characterized by high variance. Nonetheless, the simulation model allowed to estimate the time required for milking with a good approximation. Then, exploiting again the simulation model, two alternative configurations of the cowshed layout were tested and the related performance, in terms of the total time required for milking, was compared to the current one.

Both the new configurations of the milking process show interesting savings, in terms of the total time required for milking, compared to the current scenario. The first solution, in particular, allows saving approx. twenty minutes, compared to the AS IS scenario, allowing milking operations to be completed in approx. two hour and a quarter. As for the second configuration, the time saving is even greater, due to the greater proximity of all four groups of cows to the waiting room. On average, the groups most isolated, today, employ four minutes to reach the milking room. The final time saving is approx. half an hour compared to the initial situation.

From the practical perspective, both solutions could be considered for implementation by the company analyzed, although the first one is easier to be implemented, because it does not require modifications to the cowshed layout.

From the scientific point of view, this paper shows that simulation can be used also to reproduce very stochastic situations, such as the behavior of animals, with a good approximation, thus providing useful findings to the cowshed owners.

Among the limitations of the present study, it should be mentioned that the two TO BE scenarios examined does not cover all possible alternative configurations for the milking process examined. Other TO BE scenarios could be designed considering, for instance, modifications to the equipment used for milking. Therefore, future research could be directed toward the development of additional TO BE scenarios. Another point is that, as recalled earlier in the paper, the production of milk can significantly vary during the year (Jialina et al., 1998). In this work, the data collection phase was carried out at the beginning of the summer, reflecting the period where the milk production is lower. Repeating the analysis in a different period of the year could be useful to confirm the validity of the model, as well as to assess the sensitivity of the results as a function of the milk production.

REFERENCES

Bellesia, F., Pinetti, A., Pagnoni, U. M., Rinaldi, R., Zucchi, C., Caglioti, L., & Palyi, G., 2003. Volatile components of Grana Parmigiano-Reggiano type hard cheese. *Food Chemistry*, 83, 55-61. DOI: 10.1016/S0308-8146(03)00037-2.

Concannon, K., Elder, M., Hindle, K., Tremble, J. and Tse, S. (2007). *Simulation Modelling with Simul8™* (ISBN: 0973428503). Visual Thinking International. Available online at: www.simtech.hu/_data/VFS_6084183539ff1c826da47589a021838c.pdf.

Consorzio del Parmigiano Reggiano, 2011. *Disciplinare di produzione del formaggio Parmigiano Reggiano* (in Italian). Available online at https://www.politicheagricole.it/flex/files/e/0/4/D.c8955158b36b0dff6455/Disciplinare_parmigiano_reggiano.pdf.

European Commission, 2015. *Milk and milk products*. Available online at http://ec.europa.eu/agriculture/milk/index_en.htm.

Jialina, B., Mingqianga, W., Zhonglina, L., & Cheswortha, J.M., 1998. The milking performance of dual-purpose crossbred yaks. *Animal Science*, 66(2), 471-473. DOI: 10.1017/S1357729800009632.

Regione Emilia-Romagna, 2014. La filiera del Parmigiano Reggiano - Latte, produzione, mercato. Available online at http://www.regione.emilia-romagna.it/urp/allegati/SpecAgric_Giugno_2014Web.pdf (in Italian).

Zannoni, M., 2010. Evolution of the sensory characteristics of Parmigiano-Reggiano cheese to the present day. Food Quality and Preference, 21, 901-5.DOI: 10.1016/j.foodqual.2010.01.004.

AUTHORS BIOGRAPHY

Marta RINALDI is research fellow of the University of Parma. She graduated (with distinction) in Industrial Engineering and Management in 2011, and got her Ph.D. in Industrial Engineering in 2015, both at the University of Parma. She currently works on discrete event simulation and its application to industrial plants, logistics, supply chain management, supply chain

modelling and simulation, inventory management, manufacturing systems and business processes. She is author (or co-author) of more than 10 papers published in international journals.

Eleonora BOTTANI is Associate professor of Industrial Logistics at the Department of Industrial Engineering of the University of Parma. She graduated (with distinction) in Industrial Engineering and Management in 2002, and got her PhD in Industrial Engineering in 2006, both at the University of Parma. Her research interests are in the field of logistics and supply chain management. She is author (or co-author) of approx. 120 scientific papers, referee for more than 60 international scientific journals, editorial board member of five scientific journals, an Associate Editor for one of those journals, and editor-in-chief of a scientific journal.

Mattia ARMENZONI is currently research fellow at the Department of Industrial Engineering, University of Parma. He graduated in Mechanical Engineering for the Food Industry in 2010, with a thesis related to the proper design of static dryers for pasta through the use of simulation tools. His research interests refer to the fields of industrial engineering (with a specific attention to the food sector), process analysis, product analysis, production facilities, process simulation and modeling. He published some papers related to these topics both in international journals and international conference proceedings.

Roberto MONTANARI is Full professor of Mechanical Plants at the University of Parma. He graduated (with distinction) in 1999 in Mechanical Engineering at the University of Parma. His research activities mainly concern equipment maintenance, power plants, food plants, logistics, supply chain management, supply chain modelling and simulation, inventory management. He has published his research in approx. 70 papers, which appear in qualified international journals and conferences. He acts as a referee for several scientific journals, is editorial board member of 2 international scientific journals and editor of a scientific journal.

Sergio Amedeo GALLO graduated (with distinction) in Mechanical Engineering at the University of Naples "Federico II" and got a Ph.D. in Industrial Plants and Technology at the same University. As an adjunct professor at the University of Modena and Reggio Emilia, he carried out numerous teaching activities, with a significant production of materials and exercises. His research interests refer to several topics in the field of plant engineering, logistics, industrial production, occupational safety. He is the author of numerous scientific publications and supervisor of several theses.

OPERATING STRATEGIES TO MINIMISE THE METHANOL CONTENT IN DISTILLATES OBTAINED IN ALEMBICS

Luna R. [a], Pérez-Correa J.R [a], López F. [b], Fernández-Fernández M. [c]

[a]Department of Chemical and Bioprocess Engineering, Pontificia Universidad Católica de Chile, Vicuña Mackenna 4860, Macul, Santiago, Chile.
[b]Department d'Enginyeria Química, Universitat Rovira I Virgili, Av. Països Catalans 26, 43007, Tarragona, Spain.
[d]Department of Industrial Technology, Universidad de Talca, Camino a Los Niches km 1, 3340000, Curicó, Chile.

[a] rlluna@uc.cl, [a] perez@ing.puc.cl, [b] francisco.lopez@urv.cat, [c] mafernandez@utalca.cl

ABSTRACT

The aromatic composition of fruit distillates not only depends on the raw material, but also on the distillation system and its operating conditions. One of the several compounds recovered during distillation is methanol, which is toxic for human consumption. In this paper, a multi-objective optimal control problem is formulated to minimise methanol's recovery and maximise ethanol's recovery in a batch distillation system, by adapting the heating trajectory. The dynamic optimisation problem is solved using orthogonal collocation on finite elements. Compared with a standard operation policy, the optimal heating trajectory reduced the methanol concentration in the distillate by 50%, without significantly affecting the ethanol recovery.

Keywords: aroma distillation, methanol, multi-objective optimisation, spirits.

1. INTRODUCTION

Distilled alcoholic beverages are produced worldwide from a wide variety of fruits and cereals, for example, Whisky (UK, Ireland), Cachaça (Brazil), Tequila (Mexico), Cognac/Brandy (France, Spain) and Pisco (Peru, Chile), to name a few. In the case of Pisco, the fermented juice is made from Muscat grapes containing 94-98% v/v of a mixture of water and ethanol, where the rest is comprised of hundreds of volatile compounds (Thorngate 1998; Voilley & Lubbers 1998). These minority volatile compounds are called congeners and essentially define the quality of the fruit distillates. The preparation of many of these distillates goes throw several stages, and distillation is the most relevant in the final composition of the spirit. For distillation, Charentais copper alembics are the most frequently used in small scale production facilities. This system is operated in batch mode, recovering three cuts, head, heart and tail, where the heart cut gives rise to the final product. Although the operation of this alembic is relatively simple, its operation is exposed to many disturbances that generate variability in the composition of the final product.

Nowadays, consumers are more demanding, asking for new products that are safe and aromatically distinctive. Therefore, the distillate should be rich in positive aromas as well as free from off-flavours and toxic compounds. Moreover, these products should keep their quality from year to year.

In this study, we focus on minimising the methanol content of the distillates, which is recovered in the three cuts. Methanol is slowly metabolized in the human body, producing formaldehyde and formic acid which are extremely toxic in high concentrations. Excessive intake of methanol generates various ailments such as fatigue, thirst, headache, stomach pains, nausea, vomiting, sensitivity to light and noise, lack of concentration and attention, tremors, excessive sweating and hypertension (Swift & Davidson 1998). Hence, in many countries, methanol content in alcoholic beverages is regulated. In Chile, methanol concentration must be less than 1.5 g/L of absolute alcohol (L.a.a).

Mathematical models have been developed for exploring new operating strategies in food and chemical processes, in order to obtain reproducible products with a predefined composition. Several phenomenological models have been presented in the literature for wine batch distillation, for example, in plate rectification columns (Osorio et al., 2004), packed rectification columns (Carvallo et al., 2011) and alembics (Scanavini et al 2010; Scanavini et al., 2012; Sacher et al., 2013). In addition, several numerical techniques have been applied to design dynamic optimization strategies for batch distillation. These techniques approach the design

as an optimal control problem, where the goal is to optimise a specific performance index (minimum time, maximum distillate, maximum quality or maximum profit) by searching for the best control path. For example, for a plate column batch distillation system, Osorio et al. (2005) solved the optimal control problem finding the trajectory of the cooling flow rate in the partial condenser. The objectives were to maximise the terpene recovery and minimise the fatty acid recovery in a Muscat wine distillate. The process model was very complex, with many differential and implicit algebraic equations; therefore, the formulation solution of a full optimisation problem is extremely difficult. To simplify the numerical solution of the optimisation problem, the cooling flow rate was established as a predefined smooth function of time, derived from previous experiences. The optimisation resulted in the parameters of the predefined function that maximised a multi-objective cost function. The optimal strategy obtained was validated in lab scale experiments. De Lucca et al. (2013) explored various operating policies, with a simulator of a packed bed column, to minimise the methanol content in the distillate. They used the same predefined function with adjustable parameters of Osorio et al. (2005) to find an optimal cooling flow rate trajectory. In these studies, the predefined function restricted the cooling flow rates to a sub-optimal solution space.

In this paper, a full optimal control problem is formulated and solved for a Charentais alembic distillation. The aim is to minimise the methanol recovery and maximise the ethanol recovery in the distillate in a fixed operation time, by manipulating the heating power trajectory. A ternary version of a previous alembic model (Sacher et al., 2013) was used in the optimisation.

2. MATERIALS AND METHODS

2.1. Distillation system

The distillation system is an automatic controlled Charentais copper alembic (Figure 1) which has the following features and elements:

- 4.8 L capacity
- Total condenser
- Three Pt100 sensors to measure the temperature in the boiler, partial condenser and surroundings
- Electrical resistance inside the kettle (1200 W)
- A Programmable Logic Controller (PLC) receives data from the temperature sensors and sends the control signal to the electrical resistance in the boiler.

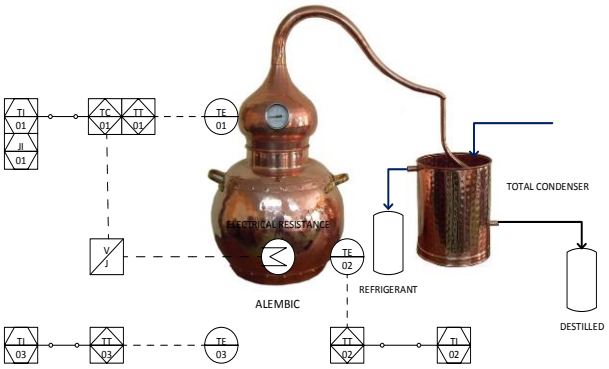

Figure 1: P&ID of the distillation system.

2.2. Experimental conditions

The Muscat wine was approximated as a synthetic ternary mixture of 13% v/v of ethanol and 1.5 g/L.a.a. of methanol (Osorio et al. 2004). The alembic was initially loaded with 1.8 L, and the ambient temperature was constant at 24 ºC.

2.3. Modelling

To simplify, the liquid-vapour (L/V) equilibrium was considered to be a non-ideal "quasi binary" mixture of ethanol/water plus a congener (Sacher et al., 2013). The model includes mass and energy balances for the two equilibrium stages, the boiler and the partial condenser. The congeners' L/V equilibrium depends on ethanol concentration only, due to the assumption of "quasi binary" mixture. Activity coefficients were calculated using the UNIFAC group contribution method.

The mathematical model used in this paper is a simplified version of Sacher et al. (2013), which only considers a mixture of water, methanol and ethanol.

Mass (total, ethanol, methanol) and energy balances in the boiler,

$$\frac{d(M_B)}{dt} = L - V_B \tag{1}$$

$$\frac{d(M_B \cdot x_B^e)}{dt} = L \cdot x_L^e - V_B \cdot y_B^e \tag{2}$$

$$\frac{d(M_B \cdot x_B^m)}{dt} = L \cdot x_L^m - V_B \cdot y_B^m \tag{3}$$

$$\frac{d(M_B \cdot u_B)}{dt} = L \cdot h_L - V_B \cdot H_B + \dot{Q}_B \tag{4}$$

Mass (total, ethanol, methanol) and energy balances in the partial condenser (negligible liquid holdup),

$$V_B - L - V_D = 0 \tag{5}$$

$$V_B \cdot y_B^e - L \cdot x_L^e - V_D \cdot y_D^e = 0 \tag{6}$$

$$V_B \cdot y_B^m - L \cdot x_L^m - V_D \cdot y_D^m = 0 \tag{7}$$

$$V_B \cdot H_B - L \cdot h_L - V_D \cdot H_D - \dot{Q}_C = 0 \tag{8}$$

Thermodynamic equilibrium ethanol-water

The mole fraction of ethanol vapour (y_B^e, y_D^e), equilibrium temperatures and enthalpies ($H_{B,D}, h_L$) are calculated from empirical correlations (Sacher et al., 2013). These equations depend on the ethanol mole fraction in the liquid phase (x_B^e, x_L^e) only.

Thermodynamic equilibrium relationships for methanol,

$$y_D^m = K_C^m \cdot x_L^m \tag{9}$$

$$y_B^m = K_B^m \cdot x_B^m \tag{10}$$

$$K_{B,C}^m(x_B^e, x_L^e) = \frac{y_{B,D}^m}{x_{B,L}^m} = \frac{P_m(x_B^e, x_L^e) \cdot \gamma_m(x_B^e, x_L^e)}{P} \tag{11}$$

The activity coefficient for methanol γ_m is estimated using the UNIFAC contribution groups method. Given the assumption of a quasi-binary mixture, the activity coefficient only depends on the ethanol concentration since an infinite dilution of methanol in a mixture of water-ethanol is assumed.

Heat transfer model

$$\dot{Q}_B = \dot{Q}_{cal} - U \cdot A \cdot (T_B - T_{amb}) \tag{12}$$

$$\dot{Q}_C = U \cdot A \cdot (T_C - T_{amb}) \tag{13}$$

where $\dot{Q}_{cal}$ and T_{amb} are input variables corresponding to the control variable and disturbance of the system, respectively. This model has only one empirical parameter, $U \cdot A$, which can be easily fitted with data normally available in commercial distillation facilities (Pérez-Correa et al., 2013).

Simulation

To simulate the model, a reordering of equations is convenient. The distillate molar flow rate is obtained from mass and energy balances in the partial condenser (Eqs. 5, 6 and 8).

$$V_D = \frac{\dot{Q}_C}{(H_B - H_D) + \frac{(y_B^e - y_D^e)}{(x_L^e - y_D^e)} \cdot (H_D - h_L)} - \frac{-\dot{Q}_C}{(h_L - H_D) + \frac{(x_L^e - y_D^e)}{(y_B^e - y_D^e)} \cdot (H_D - H_B)} \tag{14}$$

To calculate the volume of distillate, an empirical correlation which calculates the density of the mixture from ethanol composition is used (Neuburg & Perez-Correa 1994),

$$\rho_L = \frac{x_D^e \cdot PM_E + (1 - x_D^e) \cdot PM_W}{\phi \cdot x_D^e + (1 - x_D^e) \cdot PM_W / \rho_W} \tag{15}$$

$$\phi = f(x_D^e, T_D) \tag{16}$$

Finally to calculate the composition of ethanol in the partial condenser, a rearrangement of the energy balance (Eq. 4) from mass balances in the boiler (Eqs. 1 and 2) is required,

$$\left(L(x_L^e - x_B^e) - V_B(y_B^e - x_B^e)\right)\left(\frac{\partial h_B}{\partial x_B} + \frac{\partial h_B}{\partial T_B}\frac{dT_B}{dx_B}\right) = L(h_L - h_B) - V_B(H_B - h_B) + \dot{Q}_B \tag{17}$$

This equation is an implicit function that depends on the value of x_L^e. This equation was solved in the AMPL code (see appendix) as a constraint in the optimisation problem.

2.4. Optimisation

The multi-objective weighted cost function considers methanol (main objective of this study) and ethanol recoveries in the distillate. The weight defines the priority in the respective distillation. Then, the objective function is,

$$\min_u J(u) = \alpha Rec_{met}(tf) - (1 - \alpha) Rec_{et}(tf) \tag{18}$$

$$0 \leq \alpha \leq 1 \tag{19}$$

where the recoveries are,

$$Rec_k = \frac{\int_{t0}^{tf}(D(t) \cdot x_k(t))dt}{M_0 \cdot x_k(t0)} \tag{20}$$

α is the adjustable weight, Rec_k is the recovery of compound k (met = methanol, et = ethanol), $D(t)$ is the molar flow rate of distillate, x_k is the mole fraction of compound k, M_0 is the initial mass, and finally, t_0 and t_f are the initial and final distillation times respectively.

A common practice in the fruit distillates industry is to use the cooling rate in the partial condenser to control the reflux rate. In the alembic used in this study, the reflux rate is given by natural condensation and is not directly controllable. Hence, we manipulated the heating power in the alembic boiler instead. The optimisation process must find an optimal heating power path that minimises methanol recovery and maximises ethanol recovery in the distillate. We applied the simultaneous simulation-optimisation method (direct transcription), using orthogonal collocation on finite elements (Biegler, 2010), which has been shown to be useful in tackling large scale optimisation problems. Only one cut was considered in computing the cost function (Eq. 18), corresponding to the heart/tail cut that was set at 2 h. Additional optimisation constraints are: (i) the heating power varies between 0 and 1100 W; (ii) the minimum distillate flow rate is 2 mL/min.

The optimal control problem in its discrete form can be expressed as:

$$\min_u J(u) \tag{21}$$

subject to

$$\forall\, i = 1 \ldots ne, j = 1 \ldots ncp$$

$$x_{i,j} = x_{i-1} + h_i \sum_{j=1}^{ncp} \Omega_j(\tau_j) \cdot \frac{dx}{dt_{i,j}} \tag{22}$$

$$g(x_{i,j}, y_{i,j}, u_{i,j}, \theta) = 0 \tag{23}$$

$$u_L \leq u_{i,j} \leq u_U \tag{24}$$

$$x_L \leq x_{i,j} \leq x_U \tag{25}$$

$$\theta_L \leq \theta \leq \theta_U \tag{26}$$

$$\frac{dx}{dt_{i,j}} = f(x_{i,j}, y_{i,j}, u_{i,j}, \theta) \tag{27}$$

where ne is the number of finite elements, ncp is the number of collocation points, x are differential state variables, y are algebraic state variables, u are control variables and θ are model parameters. Equation 22 corresponds to the discrete approximation of the differential state variables. h_i corresponds to the length of the finite element, which is given by the total process time divided by the number of finite elements; τ represents the normalised time in the finite element. Finally Ω are the interpolation polynomial functions in each finite element. In this study, we used 3 Radau collocation points (Biegler, 2010). The optimisation problem was coded in AMPL and solved using IPOPT (Biegler, 2010). Figure 2 shows the flowchart of the simultaneous simulation-optimisation method, using the orthogonal collocation on finite elements strategy used in this work.

3. RESULTS AND DISCUSSION

The optimisation was solved in a Samsung Intel core i7 laptop using the student version of AMPL. Therefore, we considered only 5 finite elements, since the maximum number of variables and constraints allowed were 300. We also tried using the NEOS web interface, but the optimisation problem did not converge with any solver available.

Different values of the weight α were tried, but the solver only found solutions for $0.5 \leq \alpha \leq 1$. For values below 0.5 the cost function took high negative values, resulting in a degenerated optimization problem; hence, some constraints were not met. Table 1 shows the cost function (J), the distillate alcohol grade (GA_d), the relative methanol concentration in the distillate (Met_d), the ethanol recovery (Rec_{et}) and the methanol recovery (Rec_{met}) for different values of α.

Table 1: Optimization results for different values of α.

α	J (-)	GA_d (%)	Met_d (g/L.a.a)	Rec_{et} (%)	Rec_{met} (%)
0.5	-8,1	46.0	1.37	64.8	48.7
0.6	1,8	52.4	1.16	59.8	42.9
0.72	31	78.5	0.75	58.3	41.2
0.8	22	52.4	1.16	59.8	42.9
0.9	31	78.5	0.75	58.3	41.2
1	41	53.5	1.09	58.3	41.0

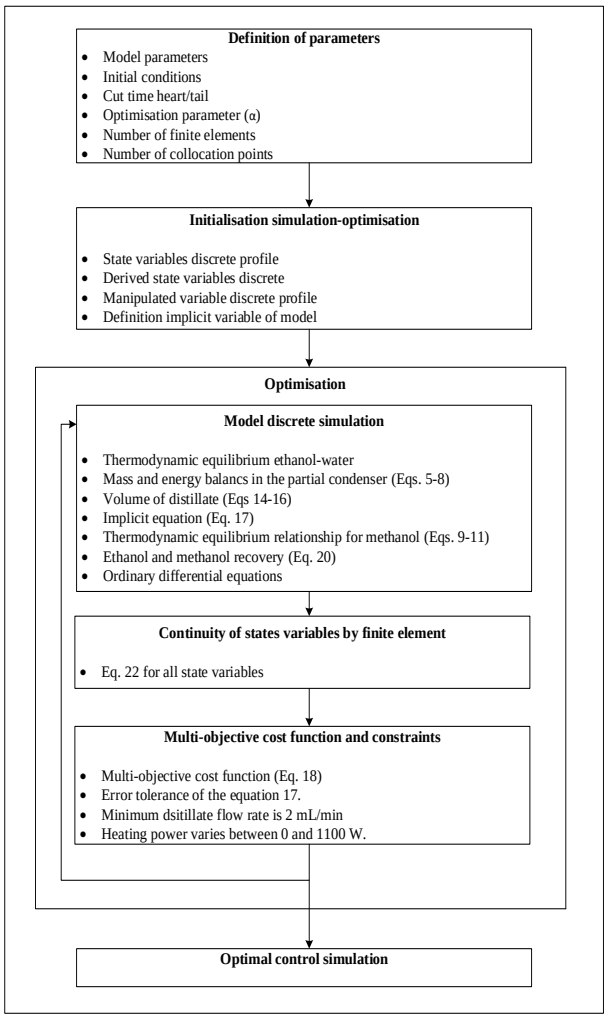

Figure 2: Flowchart of the simultaneous simulation-optimisation method.

It is important to highlight that for values of α = 0.75 and 0.9, a very low relative concentration of methanol in the distillate was obtained. These optimal trajectories reduce the relative concentration of methanol by 50% compared with the initial wine. In previous research (Luna et al., 2014) relative concentration of methanol were reduced by only 29%. In turn, for α = 0.5, the highest methanol recovery was obtained. We observed that lower methanol relative concentrations were obtained when the distillates were more concentrated in ethanol and less total volume was recovered.

Figure 3 shows optimum trajectories of the heating power for the extreme cases (α = 0.5 and α = 0.9). To obtain a distillate with a low concentration of methanol (α = 0.9), a high heating power is required at the beginning of the distillation and a low heating power at the end. In turn, if a low heating power is applied at the beginning and a high heating power at the end (α = 0.5), a distillate with high methanol concentration will be obtained.

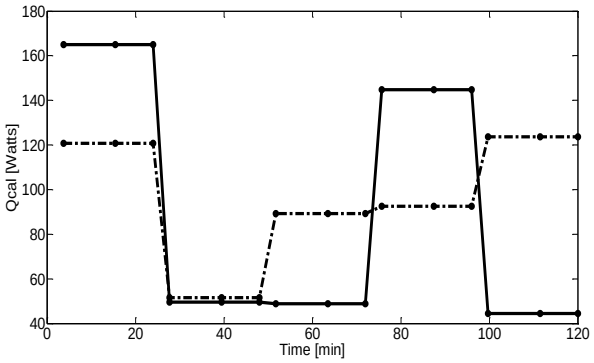

Figure 3: Heating power vs. time.
Dashed line: α = 0.5; Solid line: α = 0.9.

4. CONCLUSIONS AND FUTURE WORK

This is the first study that apply a direct transcription method to minimise methanol content in Charentais alembic spirit distillations. Our results indicate that by properly managing the heating power in the boiler, significant reductions in the distillate methanol concentrations can be achieved. We have previously applied several operating strategies, and never achieved such low methanol concentrations as shown in this work. We expect that by testing more robust cost-functions, improving the method for solving the implicit algebraic constraint, and using more finite elements, we will be able to attain smoother heating power trajectories and even lower methanol concentrations.

Future work consider experimental validation, addition of more congeners in the distillation model, develop more complex cost-functions, and including cut times as decision variables.

Results shown here are general, therefore these can be applied to reduce methanol content in any fruit distillate obtained in alembics of any size.

APPENDIX

AMPL Code

This program minimises the concentration of methanol (Cmet) and maximises recovery of ethanol (ETR) for the batch distillation process in a copper Charentais, with a fixed operating time (tf) and less than or equal final concentration of 1.5 g methanol/L.a.a. To achieve this goal, heating power (Qcal) was handled during distillation with a constant room temperature. The model was published in its first version in Sacher et al. 2013.

First version: Ricardo Luna 14/01/2015.
Process parameters or constants
param UAb := 0.3196778; # Coefficient and heat transfer area of the boiler
param UAc := 0.3333333; # Coefficient and heat transfer area of the condenser

```
param Tamb  := 24+273.15; # Room temperature [k]
param MWe   := 46.07;     # Ethanol Molecular weight
param MWw   := 18.0153;     # Water Molecular weight
param MWmet := 32.04;  # Methanol Molecular weight
param rhow  := 1;                  # Water density [g/mL]
param time  := 7200;                  # Final time [hours]
param alpha := 1;     # Weight of function multi-purpose
# Initial conditions for differential variables
param x1_init := 91.789;       # Boiler initial moles (Mb)
param x2_init := 0.0437;    # Ethanol molar fraction in boiler (xb)
param x3_init := 0;           # Distilled initial volume (V)
param x4_init := 0;           # Moles of distilled ethanol (M_etd)
param x5_init := 0.000116; # Methanol molar fraction in bolier (xb_met)
param x6_init := 0;         # Moles of distilled methanol (M_metd)
param t_init  := 0;                  # Initial time (seg)
# Indexes, number of placement points and number of finite elements
param nfe >= 1 integer;
param ncp >= 1 integer;
let nfe       := 5;                  # Finite element numbers
let ncp       := 3;               # number of placement points
set fe := 1..nfe;                  # Finite element index
set cp := 1..ncp;                  # placement points index
param h{fe} := (time/nfe);  # length of a finite element
# Matrix of Radau placement coefficient (implicit Runge-Kutta)
param a{cp,cp};
let a[1,1] :=  0.19681547722366;let a[1,2] := 0.39442431473909;
let a[1,3] :=  0.37640306270047;let a[2,1] := -0.06553542585020;
let a[2,2] :=  0.29207341166523;let a[2,3] := 0.51248582618842;
let a[3,1] :=  0.02377097434822;let a[3,2] := -0.04154875212600;
let a[3,3] :=  0.11111111111111;
# Discrete profiles of state variables and time
var x1 {fe,cp}  >= 0 := x1_init ;
var x2 {fe,cp}  >= 0, <=1, := x2_init ;
var x3 {fe,cp}  >= 0 := x3_init ;
var x4 {fe,cp}  >= 0 := x4_init ;
var x5 {fe,cp}  >= 0, <=1, := x5_init ;
var x6 {fe,cp}  >= 0 := x6_init ;
var t  {fe,cp}  >= 0 := t_init  ;
# Discrete derivative of state variables and time
var x1dot {fe,cp}  ;
var x2dot {fe,cp}  ;
var x3dot {fe,cp}  ;
var x4dot {fe,cp}  ;
var x5dot {fe,cp}  ;
var x6dot {fe,cp}  ;
var tdot  {fe,cp}  ;
# Discrete profiles of control variables
var Qcal  {fe}  >= 0, <= 1000, := 300;          # Watt
# Declaration of implicit variable of the model
var xL {fe,cp} >=0, <=1, := 1.1*x2_init;     # Reflux liquid mole fraction L
# Constitutive equations (explicit algebraic)
# Liquid/vapor equilibrium in the boiler
# Steam mole fraction in boiler
var yb {i in fe,j in cp} = -59.6868501+-89.4037240*x2[i,j]+-39.8552042*x2[i,j]^1.5+81.47664393*exp(x2[i,j])-21.7897938*exp(-x2[i,j]);
# Boiler temperature
var Tb {i in fe,j in cp} =  273.15+(-0.02214517+-0.05785120*x2[i,j]^1.5+0.032146591*exp(x2[i,j]))^-1;
# Liquid enthalpy [J/gmol]
var hb {i in fe,j in cp} = (55.678*x2[i,j]+75.425)*Tb[i,j]-15208.44*x2[i,j]-20602.34;
# Gas enthalpy [J/gmol]
var Hb {i in fe,j in cp} = 36172.03-2919.83*yb[i,j]+(31.461-11.976*yb[i,j])*Tb[i,j]+(4.063*10^-4+0.0734*yb[i,j])*Tb[i,j]^2;
# dhb/dxb partial derivative
var dhbdxb {i in fe,j in cp} = 55.678*Tb[i,j]-15208.44;
# dhb/Tb partial derivative
var dhbdTb {i in fe,j in cp} = 55.678*x2[i,j]+75.425;
# dTbdxb partial derivative
var dTbdxb {i in fe,j in cp} = -(1.5*-0.05785120*x2[i,j]^0.5+0.032146591*exp(x2[i,j]))/(-0.02214517+-0.05785120*x2[i,j]^1.5+0.032146591*exp(x2[i,j]))^2;
# Total derivative
var DhbDxb {i in fe,j in cp} = dhbdxb[i,j]+dhbdTb[i,j]*dTbdxb[i,j];
# Liquid/vapor equilibrium in condenser
# Steam mole fraction in boiler
var yD {i in fe,j in cp} = -59.6868501+-89.4037240*xL[i,j]+-39.8552042*xL[i,j]^1.5+81.47664393*exp(xL[i,j])-21.7897938*exp(-xL[i,j]);
# Condenser temperature
var Tc {i in fe,j in cp} = 273.15+(-0.02214517+-0.05785120*(xL[i,j]^(1.5))+0.032146591*exp(xL[i,j]))^-1;
# Liquid enthalpy [J/gmol]
var hL {i in fe,j in cp} = (55.678*xL[i,j]+75.425)*Tc[i,j]-15208.44*xL[i,j]-20602.34;
# Gas enthalpy [J/gmol]
var Hd {i in fe,j in cp} = 36172.03-2919.83*yD[i,j]+(31.461-11.976*yD[i,j])*Tc[i,j]+(4.063*10^-4+0.0734*yD[i,j])*Tc[i,j]^2;
# Stationary mass balances in the condenser
# Molar flow of vapor ascending
var Vb {i in fe,j in cp} = UAc*(Tc[i,j]-Tamb)/((Hb[i,j]-Hd[i,j])+(yb[i,j]-yD[i,j])/(xL[i,j]-yD[i,j])*(Hd[i,j]-hL[i,j]));
# Molar flow of liquid reflux
```

```
var L {i in fe,j in cp} = -UAc*(Tc[i,j]-Tamb)/((hL[i,j]-Hd[i,j])+(xL[i,j]-yD[i,j])/(yb[i,j]-yD[i,j])*(Hd[i,j]-Hb[i,j]));
# Molar flow of distillate
var D {i in fe,j in cp} = Vb[i,j]-L[i,j];
# Calculation of volumetric flow of distillate
# Molecular weight of the mixture
var MWm {i in fe,j in cp} = MWe*yD[i,j]+(1-yD[i,j])*MWw;
# Apparent molal volume for mixing [m3/kmol]
var oa {i in fe,j in cp} = 5.1214e-2+6.549e-3*yD[i,j]+7.406e-5*(Tc[i,j]-273.15);
# Mixture density [g/mL]
var rhom {i in fe,j in cp} = MWm[i,j]/(oa[i,j]*1000*yD[i,j]+(1-yD[i,j])*(MWw/rhow));
# Distillate volume [mL]
var Vd {i in fe,j in cp} = D[i,j]*MWm[i,j]*(1/rhom[i,j]);
var tiempo {i in fe,j in cp} = t[i,j]/60;
var Flujo {i in fe,j in cp} = x3[i,j]/tiempo[i,j];
# Implicit algebraic constitutive equation
# Left side of the equation
var g1 {i in fe,j in cp} = (L[i,j]*(xL[i,j]-x2[i,j])-Vb[i,j]*(yb[i,j]-x2[i,j]))*(DhbDxb[i,j]);
# Right side of the equation
var g2 {i in fe,j in cp} = L[i,j]*(hL[i,j]-hb[i,j])-Vb[i,j]*(Hb[i,j]-hb[i,j])+(Qcal[i]-UAb*(Tb[i,j]-Tamb));
# Error definition of the equation
var e {i in fe,j in cp} = (g1[i,j]-g2[i,j])^2;
# Calculation of properties and methanol balances
var Kmetanolb {i in fe,j in cp} = -407274.016707888*x2[i,j]^5+137084.909351167*x2[i,j]^4-19714.4353078579*x2[i,j]^3+1757.07481156027*x2[i,j]^2-125.445056947666*x2[i,j]+7.99009392867259;
var Kmetanolc {i in fe,j in cp} = -407274.016707888*xL[i,j]^5+137084.909351167*xL[i,j]^4-19714.4353078579*xL[i,j]^3+1757.07481156027*xL[i,j]^2-125.445056947666*xL[i,j]+7.99009392867259;
# Mole fraction of methanol vapor in the boiler
var ybmet {i in fe,j in cp} = Kmetanolb[i,j]*x5[i,j]*x5_init; # Multiply by x5_init to return to the original value # Liquid mole fraction in the gooseneck
var xLmet {i in fe,j in cp} = (Vb[i,j]*ybmet[i,j])/(L[i,j]+D[i,j]*Kmetanolc[i,j]);
# Vapor mole fraction in the gooseneck
var yDmet {i in fe,j in cp} = xLmet[i,j]*Kmetanolc[i,j];
# Alcoholic strength
var GLb {i in fe,j in cp} = -38.950116015168470*x2[i,j]^6+231.0609445800233*x2[i,j]^5-548.2530421230588*x2[i,j]^4+704.8795688586179*x2[i,j]^3-570.0321285089950*x2[i,j]^2+321.3122048471700*x2[i,j]+0.001131244289002;
var GLd {i in fe,j in cp} = -38.950116015168470*yD[i,j]^6+231.0609445800233*yD[i,j]^5-548.2530421230588*yD[i,j]^4+704.8795688586179*yD[i,j]^3-570.0321285089950*yD[i,j]^2+321.3122048471700*yD[i,j]+0.001131244289002;
# Methanol concentration [gmethanol/L.a.a]
var Cmet {i in fe ,j in cp} = x6[i,j]*MWmet*1000/((x3[i,j]*(GLd[i,j]/100))+0.00000001);
#  Ethanol recovery [%]
var Etr {i in fe,j in cp} = x4[i,j]*100/(x1_init*x2_init);
#  Methanol recovery [%]
var Mtr {i in fe,j in cp} = x6[i,j]*100/(x1_init*x5_init);
# Differential equations
# Moles balance in the kettle
odex1{i in fe,j in cp}: x1dot[i,j] = L[i,j]-Vb[i,j];
# Ethanol balance in the kettle
odex2{i in fe,j in cp}: x2dot[i,j] = 1/x1[i,j]*(L[i,j]*(xL[i,j]-x2[i,j])-Vb[i,j]*(yb[i,j]-x2[i,j]));
# Distillate volume in time
odex3{i in fe,j in cp}: x3dot[i,j] = Vd[i,j];
# Moles of distilled ethanol in time
odex4{i in fe,j in cp}: x4dot[i,j] = D[i,j]*yD[i,j];
# Methanol balance in the kettle
# Normalized equation to x5_init (to avoid tolerance error)
odex5{i in fe,j in cp}: x5dot[i,j] = (1/x1[i,j]*(L[i,j]*(xLmet[i,j]-x5[i,j]*x5_init)-Vb[i,j]*(ybmet[i,j]-x5[i,j]*x5_init)))*(1/x5_init);
# Moles of distilled methanol in time
odex6{i in fe,j in cp}: x6dot[i,j] = (D[i,j]*yDmet[i,j]);
# Operating time
odet{i in fe,j in cp}: tdot[i,j] = 1;
# Declaration of real variable (denormalization of x5)
var X5 {i in fe,j in cp} = x5[i,j]*x5_init;
# Continuity of the states through finite element and its definition in the placement points for finite element i=2, nfe
# Moles in the kettle
fecolx1{i in fe diff{1},j in cp}: x1[i,j] = x1[i-1,ncp]
  +h[i]*sum{k in cp} a[k,j]*x1dot[i,k];
# Ethanol fraction in the kettle
fecolx2{i in fe diff{1},j in cp}: x2[i,j] = x2[i-1,ncp]
  +h[i]*sum{k in cp} a[k,j]*x2dot[i,k];
# Distillate volume
fecolx3{i in fe diff{1},j in cp}: x3[i,j] = x3[i-1,ncp]
  +h[i]*sum{k in cp} a[k,j]*x3dot[i,k];
# Moles of distilled ethanol
fecolx4{i in fe diff{1},j in cp}: x4[i,j] = x4[i-1,ncp]
  +h[i]*sum{k in cp} a[k,j]*x4dot[i,k];
# Methanol in the kettle
fecolx5{i in fe diff{1},j in cp}: x5[i,j] = x5[i-1,ncp]
  +h[i]*sum{k in cp} a[k,j]*x5dot[i,k];
# Moles of distilled methanol
fecolx6{i in fe diff{1},j in cp}: x6[i,j] = x6[i-1,ncp]
  +h[i]*sum{k in cp} a[k,j]*x6dot[i,k];
# tiempo
fecolt{i in fe diff{1},j in cp}: t[i,j] = t[i-1,ncp]
  +h[i]*sum{k in cp} a[k,j]*tdot[i,k];
```

```
# Continuity of the states through finite element and its definition in the placement points for the first finite element
# Moles in the kettle
fecolx10{i in 1..1,j in cp}: x1[i,j] = x1_init
  +h[i]*sum{k in cp} a[k,j]*x1dot[i,k];
# Ethanol fraction in the kettle
fecolx20{i in 1..1,j in cp}: x2[i,j] = x2_init
  +h[i]*sum{k in cp} a[k,j]*x2dot[i,k];
# Distillate volume
fecolx30{i in 1..1,j in cp}: x3[i,j] = x3_init
  +h[i]*sum{k in cp} a[k,j]*x3dot[i,k];
# Moles of distilled ethanol
fecolx40{i in 1..1,j in cp}: x4[i,j] = x4_init
  +h[i]*sum{k in cp} a[k,j]*x4dot[i,k];
# Methanol in the kettle
fecolx50{i in 1..1,j in cp}: x5[i,j] = x5_init/x5_init
  +h[i]*sum{k in cp} a[k,j]*x5dot[i,k];
# Moles of distilled methanol
fecolx60{i in 1..1,j in cp}: x6[i,j] = x6_init
  +h[i]*sum{k in cp} a[k,j]*x6dot[i,k];
# Time
fecolt0{i in 1..1,j in cp}: t[i,j] = t_init
  +h[i]*sum{k in cp} a[k,j]*tdot[i,k];
# Objetives
var J1  = alpha*Mtr[nfe,ncp];
var J2  = (1-alpha)*Etr[nfe,ncp];
var Jt  = J1+J2;
# Objetive Function
Minimize fcosto: alpha*Mtr[nfe,ncp]-(1-alpha)*Etr[nfe,ncp];
# Constraints
subject to r1 {i in 1..nfe,j in 1..ncp} : e[i,j]<=0.0000001; # Error tolerance in the implicit equation
subject to r2                  : Etr[nfe,ncp] <=100;
subject to r3                  : Mtr[nfe,ncp] <=100;
subject to r4 {i in 1..nfe,j in 1..ncp}  : Flujo[i,j]>=2;
subject to r5                  : Mtr[nfe,ncp] >=0;
subject to r6                  : Etr[nfe,ncp] >=0;
```

REFERENCES

Biegler, L.T., 2010. Nonlinear Programming Concepts, Algorithms, and Applications to Chemical Processes T. Liebling, ed., Pittsburgh, Pennsylvania.

Carvallo, J. et al., 2011. Modelling methanol recovery in wine distillation stills with packing columns. Food Control, 22(8), pp.1322–1332.

De Lucca, F. et al., 2013. Operation Strategies to Minimize Methanol Recovery in Batch Distillation of Hydroalcoholic Mixtures. International Journal of Food Engineering, 9(3), pp.259–265.

Luna, R. et al., 2014. Operating strategies to reduce the methanol content in distillates obtained in alembics. Worldwide Distilled Spirits Conference, Glasgow.

Neuburg, H.J. & Pérez-Correa, j. R., 1994. Dynamic and steady state modelling of a pilot binary tray distillation column. Latin American Applied Research, 24(1), pp.1–15.

Osorio, D. et al., 2004. Rigorous dynamic modeling and simulation of wine distillations. Food Control, 15(7), pp.515–521.

Osorio, D. et al., 2005. Wine distillates: practical operating recipe formulation for stills. Journal of agricultural and food chemistry, 53(16), pp.6326–31.

Pérez-Correa J. R. et al., 2013. Impacto de las condiciones de operación de un alambique Charentais en las curvas de recuperación de destilado. XII Congreso de los Grupos de Investigación Enológica (Gienol). Madrid.

Sacher, J. et al., 2013. Dynamic modeling and simulation of an alembic pear wine distillation. Food and Bioproducts Processing, 91(4), pp.447–456.

Scanavini, H.F. et al., 2010. Cachaça production in a lab-scale alembic: Modeling and computational simulation. Journal of Food Process Engineering, 33(2010), pp.226–252.

Scanavini, H.F. a, Ceriani, R. & Meirelles, J., 2012. Cachaça distillation investigated on the basis of model systems. Brazilian Journal of Chemical Engineering, 29(02), pp.429–440.

Swift, R. & Davidson, D., 1998. Alcohol hangover, mechanisms and mediatirs. Alcohol Health and Research World, 22(1), pp.54–60.

Thorngate, J.H., 1998. Yeast Strain and Wine Flavor: Nature or Nurture? In A. L. Waterhouse & S. E. Ebeler, eds. Chemistry of Wine Flavor. Washington D. C: ACS Symposium Series, pp. 66–80.

Voilley, A. & Lubbers, S., 1998. Flavor-Matrix interactions in wine. In A. L. Waterhouse & S. E. Ebeler, eds. Chemistry of Wine Flavor. Washington D. C: ACS Symposium Series, pp. 217–229.

AUTHORS BIOGRAPHY

Ricardo Luna Hernández obtained his Chemical Engineering degree at Universidad Tecnológica Metropolitana de Chile (2013). His thesis focused on the development of automatic control system for batch distillation processes, to be used in wine distillation to obtain reproducible fruit distillates with aromatic characteristics. Currently, he is a PhD student at Pontificia Universidad Católica de Chile.

José R. Pérez-Correa received his M.Eng. degree at Universidad de Chile (1982) and his Ph.D. at Imperial College – London (1987), both in Chemical Engineering. Since 2011, he is a full Professor at the Chemical and Bioprocess Engineering Department of the Pontificia Universidad Católica de Chile. His research interests are dynamic modelling, automatic control, process and biological systems engineering and natural products.

Francisco López-Bonillo obtained a Chemistry degree from Universitat de Barcelona (UB) in 1981 and a PhD degree in Chemical Sciences also in the UB in 1988. Since 2009 he is a full Professor at the Departament d'Enginyeria Química, Facultat d'Enologia of the Universitat Rovira I Virgili (URV) in Tarragona (Spain). His research interests are wine technology and spirits distillation.

Mario Alberto Fernández-Fernández received his E.Eng. degree from the Universidad Nacional de San Juan, Argentina (1986); Master of Science (1998) and PhD (2001) from Universidad de Chile. Currently, he is a full Professor at the Industrial Technologies Department of the Universidad de Talca, Chile. His research interests are automatic process control, instrumentation and mechatronics.

STUDY AND OPTIMISATION OF A CO_2 SPARGER FOR CARBONATED BEVERAGES AND BEER BY MEANS OF CFD MODELLING

Massimiliano Rinaldi[(a)], Matteo Cordioli[(b)], Davide Barbanti[(c)], Marco Dall'Aglio[(d)]

[(a), (b), (c)] Department of Food Science, University of Parma, Viale delle Scienze 47/A, 43124 Parma – Italy
[(d)] Valfor srl, Via Achille Grandi, 1, 43045 Fornovo di Taro PR – Italy

[(a)]massimiliano.rinaldi@unipr.it, [(b)]matteo.cordioli@studenti.unipr.it, [(c)]davide.barbanti@unipr.it (d) sales@valfor.it

ABSTRACT
In the present work, two different geometries of spargers for beverage carbonation were modelled by means of CFD technique. The first geometry presented a radial inlet of liquid food while the second one a tangential one. Calculation allowed to identify the best solution and mathematical results were confirmed by experimental tests with both water and apple juice. CFD resulted a very useful technique for in-silico designing not only for simple parts of plants but also for very complicated ones such as carbon dioxide spargers in which gas and liquid ix together.

Keywords: carbonated beverage, computational fluid dynamic, dense phase carbon dioxide,

1. INTRODUCTION

The consumption of soft drinks in their various forms has taken place for many centuries in order to meet the body's fundamental requirement for hydration. The discovery of the means of artificially carbonating water by dissolution of CO2 under pressure is attributed to Dr Joseph Priestley in the late 1760s, though there were many other workers active in this field at the same time which probably deserve equal credit.
Production of carbonated drinks was traditionally carried out by means of adding concentrated syrup to the bottle and then topping up with carbonated water. A considerable improvement in speed was achieved in 1937, when the Mojonnier Brothers Corporation of Chicago introduced a continuous blending/cooling/carbonating system (Steen and Ashurst, 2008).
In general, two basic methods for carbonating a drink are possible: the injection and dispersion of carbon dioxide into the liquid to be carbonated, and the fine spraying of the product into a carbon dioxide atmosphere. However, in-line carbonation methods are being used increasingly. These either sparge carbon dioxide into the liquid or inject the liquid into a gas stream. When the gas is sparged into the liquid this allows small bubbles of gas to be formed which can be easily absorbed by the liquid. The higher the pressure the smaller the gas bubbles formed at the sparger and the greater the gas bubbles surface area available for the gas to be absorbed by the liquid. In addition, also design of both the spargers and the housing of the sparger play an important role in optimal dissolution of gas into liquid. For this reason the aim of this work was to study and optimize different designs of CO2 sparger for water or soft drink carbonation by means of CFD modelling.

2. MATERIALS AND METHODS

Two sparger geometries were studied and modelled by means of computational fluid dynamics technique.
The modelled sparger geometries were firstly drawn by means of SolidWorks 2013 and then 3D simulated by means of ANSYS 14 software with Boussinesq's approximation that uses a constant density for both fluids but considers gravity acceleration as a function of expansiveness and temperature of fluids. Sparger for carbonation presented a diameter of 64 mm and an height of 203 mm. the two geometries are reported in figure 1.

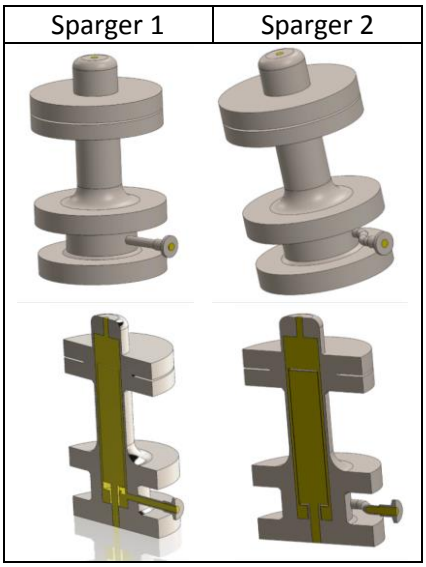

Figure 1: Radial (Sparger 1) and tangential (Sparger 2) sparger geometries

Flow rate of the food liquid was set at 16 L/h while carbon dioxide at 5.6 L/h. The incoming fluid was considered water while carbon dioxide was considered as the gas. Properties of fluids are reported in the following Table 1:

Table 1: Properties of modelled fluids

	CO_2	Water
Molar mass [kgmol^{-1}]	44.01	18.02
Density [kgm^{-3}]	1.977	997
Dynamic viscosity [mWm^{-1}K^{-1}]	0. 0149	0.8899
Thermal expansivity [K^{-1}]	0.00366	0.000257

After modelling, water carbonation was experimentally tested on a pilot plant developed by Valfor srl and located in University of Parma laboratories. The pilot plant presented a total volume of about 2 L and a flow rate varying from 10 to 40 L/h. The equipment could work up to 200 bar and presented several water baths to have constant temperature both of carbon dioxide and product to be carbonated.
The carbonation evaluation was performed by means of image analysis: on the pipeline of the pilot three inspection units as reported in Figure 2 made of transparent polycarbonate were added. By means of a camera images of carbonated water were obtained and dimensions of gas bubbles were measured.

Figure 2: Inspection unit for bubble measurement

3. RESULTS AND DISCUSSIONS

As shown in Figure 3, tangential connection (Sparger 2) seemed to give a better mixing of gas and liquid at the

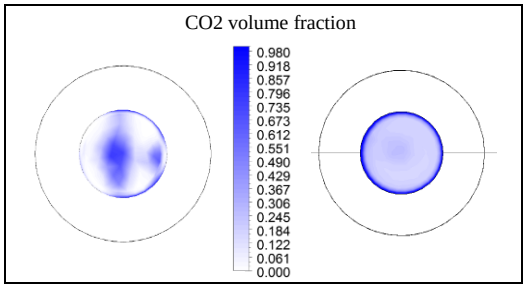

Figure 3: CO2 volume fraction distribution in the outlet section

On the contrary, in Sparger 1, fluid streamlines were present with less homogenous dispersion at the outlet of the sparger.
In Figure 4, sections of both spargers are reported: as previously observed Sparger 1 presented streamlines with a less homogeneous mixing efficacy.

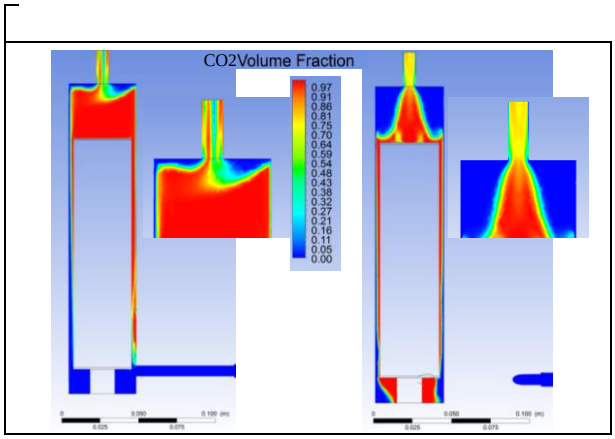

Figure 4: Radial (Sparger 1) and tangential (Sparger 2) sparger geometries results of modelling

As it's possible to see the housing for the sparger was the same while the angle of the inlet flux changed. The gas entered from the basis in the central channel and the liquid food from the lateral connection. Thus, mixing results depended only on fluid flow and relative movements between liquid and CO2
In order to quantify mixing efficacy, CO2 volume on the radius of the outlet of the sparger was calculated and reported in Figure 5

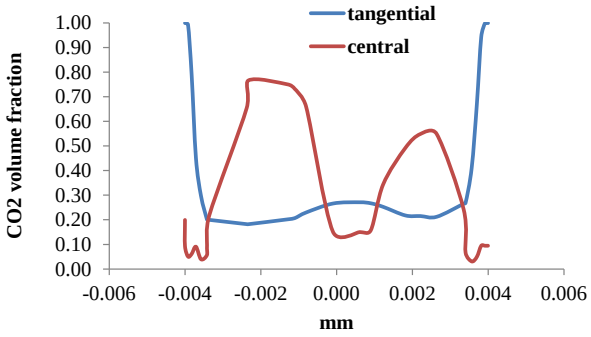

Figure 5: CO2 volume fraction distribution in the outlet section

Data confirmed what previously observed: Sparger 2 gave a more homogenous distribution but unfortunately gave also a lower mean CO2 volume fraction with a worse mixing effect. In Sparger 2 a great part of gas exited near the wall of the pipe without an actual dissolution into the liquid.
Picture of inspection element (Figure 6) confirmed the presence of gas bubble near the wall in Sparger 2 that were not mixed with liquid

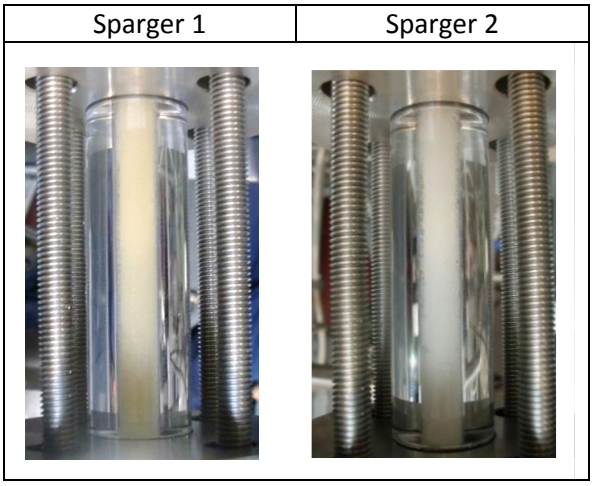

Figure 6: Bubbles inside the inspection unit

Also from experimental tests Sparger 1 gave better results with a better mixing between water and CO_2 and a more stable carbonated water, as consequence. Thus tangential inlet was not the best solution even if the liquid generated itself turbulence inside the housing and prevented fluid streamlines formation. Probably, turbulence inside the Sparger 2 and the spiral flux on the filter limited the spilling of CO2.

4. CONCLUSIONS

In conclusion, this work demonstrated the effectiveness of mathematical model to predict fluid mixing also in complex systems and the usefulness of these models for designing and optimizing also gas sparging systems for the beverage industry.

REFERENCES

Steen D. and Ashurst P.R., 2006. Carbonated soft drinks: formulation and manufacture. Oxford: Blackwell Publishing Ltd.

AUTHORS BIOGRAPHY

Massimiliano Rinaldi

Food Technologist with a narrow field of experience in food process modelling both regarding heat and mass transfer. Dr. Rinaldi has more than 10 years of experience in this topic and more than 40 scientific publications. He is currently Adjunct Professor in University of Parma in the Department of Food Science – Food Technology Area.

Matteo Cordioli

PhD student at University of Parma in the Department of Food Science – Food Technology Area. The main topic of his work is food process modelling by means of Computational Fluid Dynamics (CFD) techniques.

Davide Barbanti

Food Technologist with a narrow field of experience in food processing in particular fruit and vegetable products. Prof. Barbanti has more than 20 years of experience in this topic and more than 50 scientific publications. He is currently Associate Professor in University of Parma in the Department of Food Science – Food Technology Area.

Marco Dall'Aglio

Mechanical Engineer with more than 20 years of experience and CEO of Valfor srl, a company operating for more than 30 years in the agro-food sector, designing machinery and equipment for the production of tomato puree, canned fruit, processed vegetables, processed fish, pasta and condiments.

ANALYSIS OF THE ENERGETIC AND EXERGETIC EFFICIENCY OF THE ELECTROHYDRODYNAMIC DRYING PROCESS

M. Havet [(a)], E. Bardy [(b)], S. Manaï [(c)], M. Hamdi [(d)], O. Rouaud [(e)]

[(a),(c),(d),(e)] LUNAM Université, ONIRIS, UMR 6144 GEPEA, CS 82225, 44322 Nantes Cedex 3, France
[(b)] Department of Mechanical Engineering, Grove City College, 100 Campus Drive, Grove City, PA 16127, USA

[(a)]michel.havet@oniris-nantes.fr, [(b)]ERBardy@GCC.EDU, [(c)]sabrine.manai@oniris-nantes.fr
[(d)]merouane.hamdi@oniris-nantes.fr, [(c)]olivier.rouaud@oniris-nantes.fr

ABSTRACT

Drying is an energy intensive unit operation encountered in many industrial sectors, especially in the food industry. Still over 85% of industrial dryers are convective type. Electrohydrodynamic convective drying (EHD drying) is a novel drying method used to enhance forced convection drying by using electrodes to create an electrostatic field and generate an electric wind. This latter may alter the boundary layer and enhance the heat and mass transfer. In this study, experiments were performed to analyze the drying kinetics during EHD and forced convection (FC) drying experiments. Transient energy and exergy efficiencies expressions were discussed, proposed and computed for each experiment. With airflow of 0.3 m/s in the case of EHD configurations, similar drying rates than FC at 1.0 - 2.0 m/s can be achieved. Moreover, it leaded to greater energy efficiency (x5) and it was confirmed, using exergy efficiency concept, that EHD better used energy than FC.

Keywords: ElectroHydroDynamic, Drying, Convection, Energy, Exergy

1. INTRODUCTION

Drying is an energy intensive unit operation encountered in many industrial sectors, especially in the food industry. It offers many benefits including: extended shelf-life, reduced packaging, storage, handling and transportation costs. Several developed countries have reported that between 12 – 20% of their national industrial energy consumption is due to thermal dehydration operations (Mujumdar, 2014). Still, over 85% of industrial dryers are convective type with hot air or combustion gases as the heat transfer medium (Moses and Norton and Alagusundaram and Tiwari, 2014). Several innovations have been developed to improve product quality and energy efficiency. Forced convective drying (FC drying) uses high air velocity which leads to high energy consumption. One innovative approach to reducing this energy consumption is through ElectroHydroDynamic drying (EHD drying). The main principle behind EHD drying is to generate a corona discharge by one or more electrodes placed in an air stream in order to disrupt the primary airflow. The ionic air stream significantly alters the boundary layer, and intensifies convective heat transfer between the air and the drying product for low primary airflow velocities. Recent work focus on the influence of operating parameters on energy consumption (Ould Ahmedou and Rouaud and Havet, 2009, Bai and Hu and Li, 2011). Some studies have investigated the EHD drying effect on specific food products (Taghian Dinani and Havet, 2015) and pointed out its interest.

An effective drying process should account for the sustainability issue (Amantea and Fortes and Martins and Ferreira, 2011). Combining energy and exergy analysis is powerful for modeling and optimizing food drying. In a pioneering work, the usefulness of exergy analysis in the thermodynamic assessment of drying processes was demonstrated (Dincer and Sahin, 2004). Based on this approach, an expression for exergetic efficiency was adapted to EHD Drying (Bardy and Hamdi and Havet and Rouaud, 2015). In this work, both energy and exergy analysis are performed on a EHD drying process and the influence of operating parameters is discussed.

2. EXPERIMENTAL PROCEDURE

2.1. Experimental set-up

The set-up (Figure 1) consisted of a rectangular airflow channel (15 cm x 19 cm x 200 cm) used to perform drying experiments by means of forced convection with and without an electrostatic field (i.e. EHD and FC drying).

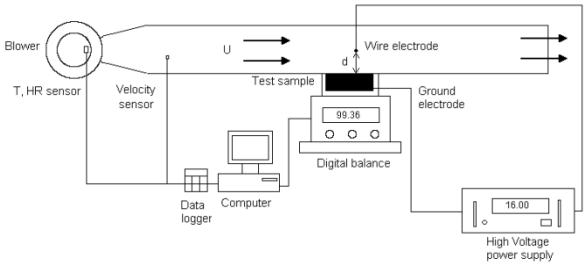

Figure 1: Experimental set-up

The mass loss was measured during drying using a weight scale (Radwag, PS600, Germany). The channel was connected to an air handling unit (ML180, Munters, France) used to control the psychrometric conditions, and the flow rate of the air entering the channel. The averaged temperature and relative humidity at the inlet of the airflow channel were T_i=28.9±0.5 °C and RH_i=16.8±0.7%. A wire-electrode(s) (diameter = 150 µm) suspended above the test specimen was connected to a high voltage generator (GLHT2260R2, Sefelec, France) in order to produce an electrostatic field. Details on this set-up and the methods are available (Bardy and Hamdi and Havet and Rouaud, 2015). From a preliminary experimental work on convective heat transfer enhancement (Hamdi 2014), a total of three different wire-electrode configurations were used for EHD drying in this study:

- 1 wire-electrode aligned perpendicular to airflow (Perp.),
- 1 wire-electrode aligned parallel to airflow (Paral. 1),
- 2 wire-electrodes arranged parallel to each other and aligned parallel to airflow (Paral. 2).

For each configuration, an applied voltage V=16 kV and an airflow velocity of 0.3 m/s were considered. The evolution of the electric current I was recorded over the drying experience. The wire-electrodes were placed according to the positions that resulted in the greatest increase in heat transfer (Hamdi 2014). Table 1 shows the exact arrangement of each configuration. For Forced Convection cases (FC drying), the airflow velocity were 1 and 2 m.s^{-1}.

Table 1: Dimensional placement of wire-electrodes for EHD drying experiments

Electrode arrangement	Perpendi - cular	Parallel	Parallel
Number of electrodes	1	1	2
Gap between electrode and surface (cm)	6	4	4

For this study, methylcellulose gel was chosen to be used as a test specimen because its thermophysical properties are close to those of meat it and can be controlled to a specific moisture content. Dimensions of test specimens were 15 x 15 x 1 cm and the moisture content was fixed at 80% (i.e. moisture content on dry basis: X_{db}= 4 kg w/kg dm). Average test specimen mass was 231.33 g ± 8.82 g.

2.2. Drying kinetics

The evolution of mass of the product m_p over time was used to compute the moisture content on dry basis over time as well as the drying kinetics (1) and (2).

$$X_{db}(t) = \frac{m_p(t)}{m_{dc}} - 1 \quad (1)$$

$$\frac{dX_{db}}{dt}(t) = \frac{X_{db}(t_i) - X_{db}(t_{i-1})}{t_i - t_{i-1}} \quad (2)$$

3. ENERGY AND EXERGY EFFICIENCIES

As the moisture in the the drying product is assumed to be in a saturated liquid water state at the drying product temperature (i.e. product temperature, T_p), the liquid water is then evaporated to a saturated vapor state at the temperature of the air at the inlet of the airflow channel (T_i). It is further assumed that $T_p = T_i$. Mass, energy and exergy balances for the system (Figure2) were performed by Hamdi (2014).

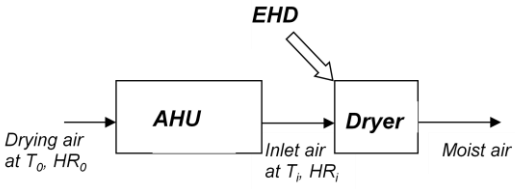

Figure 2: Sketch of Air Handling Unit and Dryer

3.1. Energy efficiency

Since the previous assumption, the energy use rate to evaporate moisture from the drying product is trivial (3). When computing energy efficiency, large differences may occur due to the dependence with the type of process used for conditioning the air. To avoid this effect, some author (Kudra 2012) calculated the energy performance by considering the energy used to heat/dry the air. It is possible to calculate this specific energy consumption by the difference between the enthalpy available in the drying air and a reference state (Amantea and Fortes and Martins and Ferreira, 2011). Nevertheless, this approach overestimates the energy efficiency because it completely makes abstraction of technology constraints. We propose in this study to calculate a realistic energy for the AHU based on the minimal energy required to deliver air from the standard conditions (T_0, RH_0, ω_0) to the measured inlet conditions in the dryer (T_i, RH_i, ω_i). We theoretically calculate that air should be dehumidified from the standard conditions (T_0, ω_0) to an intermediate stage (T_0, ω_i) and then heated to the inlet conditions (T_i, ω_i). The energy required to treat the drying air is then broken in two terms (4). This method minimizes the energy consumption in the Air Handling Unit because the dehumidification would require a higher cooling power. Using the energy use rate to evaporate moisture (3), the energy supplied by the AHU (4) and the energy supplied by the EHD sytem (5) we calculated a transient energetic efficiency (6).

$$\dot{Q}_{vap} = \dot{m}_w L_v \quad (3)$$

$$\dot{Q}_{air} = \dot{m}_{da} |h_{interm} - h_0| + \dot{m}_{da} (h_i - h_{interm}) \quad (4)$$

$$with\ h = h_{da} + \omega h_v$$

$$\dot{Q}_{EHD} = VI \quad (5)$$

$$\dot{\eta}_{en}(t) = \frac{\dot{Q}_{vap}}{\dot{Q}_{air}+\dot{Q}_{EHD}} \quad (6)$$

3.2. Exergy efficiency

An expression for exergetic efficiency as a function of time (i.e., transient exergetic efficiency) was defined as the ratio of the exergy use rate to evaporate moisture from the drying product ($\dot{\psi}_{use}$) over the exergy supply rate ($\dot{\psi}_{supply}$) as shown in equation (7). The exergy use rate to evaporate moisture from the drying product ($\dot{\psi}_{use}$) is shown in equation (8). The exergy supply rate due to the air (the state difference between the air at the inlet of the drying tunnel and the dead state ($\dot{\psi}_{air}$), is shown in equation (9). It is broken down into three components: thermal, mechanical and chemical. Contrary to the definition of the energy supply rate for air, this definition is shared by the energy community. The exergy supply due to the EHD effect ($\dot{\psi}_{EHD}$) is shown in equation (10).

$$\dot{\eta}_{ex}(t) = \frac{\dot{\psi}_{use}}{\dot{\psi}_{air}+\dot{\psi}_{EHD}} \quad (7)$$

$$\dot{\psi}_{use} = \left(1 - \frac{T_0}{T_p}\right)\dot{Q}_{vap} \quad (8)$$

$$\dot{\psi}_{air} = \dot{m}_{air}\left[\begin{array}{c}\left(C_{p,a} + \omega_i C_{p,v}\right)\left(T_i - T_0 - T_0 \ln\left(\frac{T_i}{T_0}\right)\right) \\ +T_0\left(R_a + \omega_i R_v\right)\ln\left(\frac{P_i}{P_0}\right) \\ +T_0\left\{\begin{array}{c}\left(R_a + \omega_{in} R_v\right)\ln\left(\frac{1+1.6078\omega_0}{1+1.6078\omega_i}\right) \\ +1.6078\omega_i R_a \ln\left(\frac{\omega_i}{\omega_0}\right)\end{array}\right\}\end{array}\right] \quad (9)$$

$$\dot{\psi}_{EHD} = VI \quad (10)$$

For each case, the dead state was assumed to be T_0 = 20 ºC, P_0 = 101.3 kPa, and RH_0 = 50% (standard conditions as stated by ISO 5011). It should be noticed that the overall energetic and exergetic efficiencies, can be determined by integrating equations (3) to (10).

4. RESULTS AND DISCUSSION

4.1. Drying kinetics

Figure 3 presents the variation of the moisture content X_{db} of the drying product as a function of time. As expected, the moisture content decreased over time for each experiment. It can be seen that the EHD cases are between the FC drying at 1 m/s and the FC drying at 2 m/s. This latter provides the greatest decrease. For the EHD cases, one wire-electrode parallel to airflow had a greater moisture loss over time than other cases and a moisture loss equivalent to that of FC at 2.0 m/s. It corresponds to the best case also found by Hamdi (2014) who look at the convective heat transfer enhancement. It is noted that the moisture content of all cases would converge if drying continued towards the point of equilibrium moisture content.

It is also interesting to compare the drying kinetics using the evolution of the drying rate (2) according to the moisture content (figure 3). This type of representation is known as Krischer curve. From the initial moisture content to a value of 3.5 g w/g dm, there was a fluctuation in drying rate with an initial decrease in drying rate followed by an increase. The drying rate then decreased steadily for the remainder of the experiment. FC at 2.0 m/s resulted in the greatest initial fluctuation in drying rate. This initial decrease and then increase was also present for EHD cases although not as pronounced. This initial decrease of the drying rate is attributed to the formation of a thin crust during the gel preparation. The water diffusion across this layer is reduced. The increase is more conventional, it corresponds to a thermal effect. As the product was colder than air, the surface temperature increased to the air wet-bulb temperature and provokes an enhancement of diffusion phenomena. The maximum values of the drying rate correspond to the period when the heat transfer by convection is used to evaporate water at the surface. As drying continues, moisture, entrapped within the product, diffuses towards the surface. This diffusion effect becomes more significant as time progresses and causes the drying rate to decrease. As previously, one can distinguish that the one wire-electrode parallel to airflow is equivalent to that of FC at 2.0 m/s and quite higher than other cases. A deeper analysis of drying phenomena may be performed by measuring shrinkage phenomena and quality attributes. Nevertheless, at this stage, it is important to consider that similar drying were obtained by convection with an airflow velocity at 0.3 m/s assisted by EHD and by forced convection at 2 m/s. The benefit of EHD drying should be discussed from an energetic point of view.

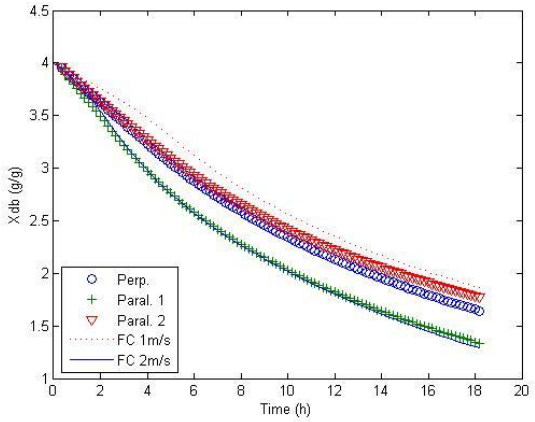

Figure 3: Moisture content as a function of time for each EHD and 2 FC drying cases

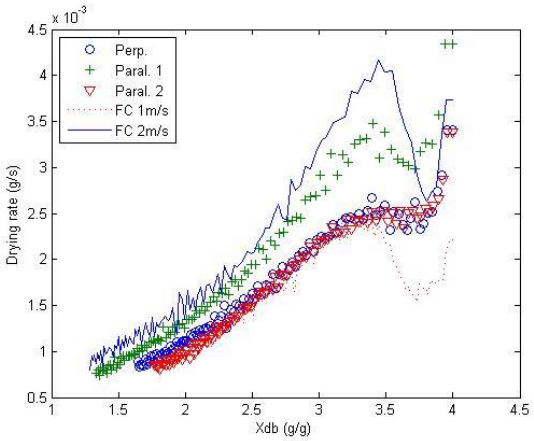

Figure 4: Drying rate as a function of Moisture Content for each EHD and 2 FC drying cases

4.2. Energy and exergy efficiencies

The evolution of the energetic efficiency during the time is depicted on figure 5. It should be firstly mentioned that the maximum energy efficiency is only close to 5%. This value could be considered as extremely low compared to results from literature (Amantea and Fortes and Martins and Ferreira, 2011, Kudra 2012, Hamdi 2014). It is firstly merely due to the definition of the energy supply for air treatment. Considering another definition would increase the energy efficiency but it would not affect the comparison of each case. Moreover, the surface of the specimen was relatively small (15 x 15 cm) compared to the airflow rate and the specific humidity of air did not evolve a lot inside the channel.

It clearly appears that FC cases have very low energy efficiencies compared to EHD case. EHD is 4 to 5 times more efficient. This great difference is due to airflow rate because the velocity is only 0.3 m/s in EHD case whereas it is up to 2 m/s for FC drying. In the first hours, we observe fluctuations due to the evolution of the drying rates but after 5 hours drying, all EHD cases reach similar values of energy efficiency. This values decrease from 3 to 1 % during the drying time.

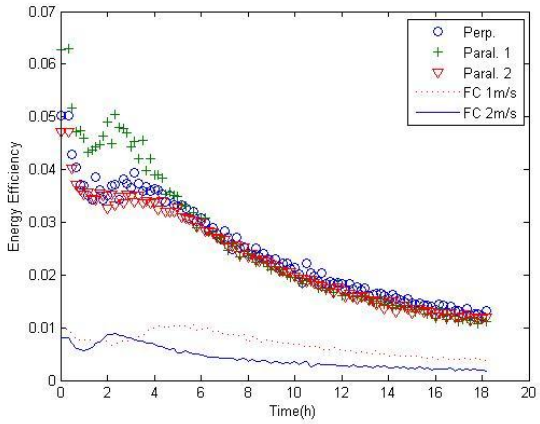

Figure 5: Energetic efficiency as a function of time for each EHD and 2 FC drying cases

The evolution of the exergetic efficiency during the time is depicted on figure 6. It is amazing to see that the values are quite similar to that of energy efficiency. They are in a classical order of magnitude found in literature with values lower than 10% (Dincer and Sahin 2004, Amantea and Fortes and Martins and Ferreira, 2011). The differences in exergetic efficiency between the EHD and FC cases can be attributed to the airflow velocity since the psychrometric inlet conditions of the primary airflow were held constant. The same dead state conditions were assumed for all experimental runs. It is noted that variations in the dead state assumption would lead to variations in computed exergetic efficiencies, but only in scale. For FC cases, exergetic efficiencies are still extremely low and increasing the air velocity reduces the efficiency. It is due to water diffusion that becomes the dominant mode and increasing convection is not relevant at all.

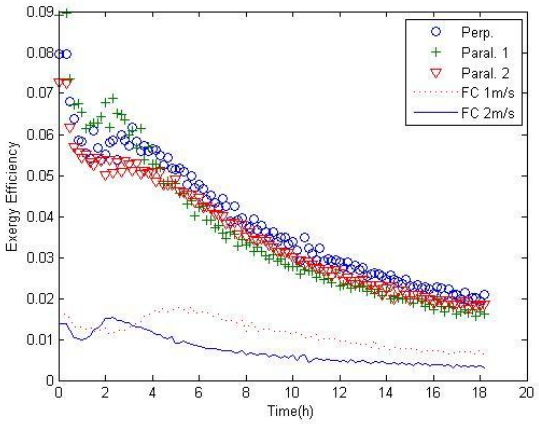

Figure 6: Exergetic efficiency as a function of time for each EHD and FC drying case

5. CONCLUSION

Expressions for the transient energetic and exergetic efficiencies of EHD drying were presented. The energy efficiency considered a minimum energy required to deliver air. The exergy efficiency took into account the power consumed by the EHD effect. The drying experiments indicated, that in the case of the EHD configurations, the same drying rate for FC at 1.0 - 2.0 m/s can be achieved with an airflow of only 0.3 m/s, leading to greater energy and exergy efficiencies. It should also be mentioned that these promising results could possibly be optimized by working with a higher applied voltage. This is a major finding that will also contribute to the design of low energy consumption process for air conditioning.

All EHD drying configurations had significantly higher energetic and exergetic efficiencies than FC drying, especially at the beginning of the drying. The higher exergetic efficiencies were due to the lower airflow velocity associated with EHD drying.

ACKNOWLEDGMENTS
This research was supported by the Pays de Loire program (PERLE2).

REFERENCES
Amantea R., Fortes M., Martins J., Ferreira W., 2013. Numerical Simulation Techniques for Optimizing Thermodynamic Efficiencies of Cereal grain Dryers. Drying Technology. 31:672–683.

Bai Y., Hu Y., Li X., 2011. Influence of Operating Parameters on Energy Consumption of Electrohydrodynamic Drying. International Journal of Applied Electromagnetics and Mechanics. 35:57–65.

Bardy E., Hamdi M., Havet M., Rouaud O., 2015. Transient Exergetic Efficiency and Moisture Loss Analysis of Forced Convection Drying With and Without Electrohydrodynamic Enhancement. Energy. http://dx.doi.org/10.1016/j.energy.2015.06.017

Dincer I., Sahin A., 2004. A New Model for Thermodynamic Analysis of a Drying Process. International Journal of Heat and Mass Transfer. 47:645–652.

Hamdi M., 2014. Etudes thermiques et dynamiques de l'intensification des transferts par vent ionique - Application au procédé de séchage. PhD Thesis, University of Nantes.

Kudra T., 2012. Energy Performance of Convective Dryers. Drying Technology. 30:1190–1198.

Moses J., Norton T., Alagusundaram K., Tiwari B., 2014. Novel Drying Techniques for the Food Industry. Food Engineering Reviews. 6:43–55.

Mujumdar A., 2014. Perspectives on International Drying Symposium Series - Past, Present and Future Prospects. Proceedings of the 19th International Drying Symposium, 24-27 august 2014, Lyon, France.

Ould Ahmedou S., Rouaud O., Havet M., 2009. Assessment of the Electrohydrodynamic Drying Process. Food and Bioprocess Technology. 2:240–247.

Taghian Dinani S., Havet M., 2015. The Influence of Voltage and Air Flow Velocity of Combined Convective-Electrohydrodynamic Drying System on the Kinetics and Energy Consumption of Mushroom Slices. Journal of Cleaner Production. 95:203-211.

AUTHORS BIOGRAPHY

Michel Havet received the PhD degree in Fluid Mechanics and Thermal Engineering at the University of Poitiers in 1995. He works since this date at ONIRIS, a public institute of higher education and research affiliated to the French Ministry of Agriculture. He is professor since 2008 and is currently assistant Director of the Joint Unit Research GEPEA 'Laboratoire Génie des Procédés Environnement Agroalimentaire', (UMR GEPEA 6144) and Head of the Research team 'Energy Engineering' in this laboratory. His main research interests concerns the enhancement of heat and mass transfer in convective food processes. He already supervised 8 PhD students and is actually supervising 2 PhD students. He wrote more than 50 scientific articles and 5 book chapters. He previously collaborated to 3 European projects. He is member of national scientific association and of the commission C2 'Food science & engineering' of the International Institute of Refrigeration since 2012.

Erik Bardy is a professor of Mechanical Engineering at Grove City College located in Western Pennsylvania. E. Bardy received his Bachelor of Science, Master of Science and Ph.D. from the State University of New York at Buffalo. He received his PhD in Mechanical Engineering, in 2006. A portion if his graduate studies was completed at Poly'Tech Lille. His current research interest lies in electrohydrodynamic drying and International Education.

Sabrine Manaï received her Master of Food Engineering from 'Ecole Supérieure des Industries Alimentaires de Tunis', Tunisia, in 2014 and she prepares a Master of Food Science at University of Montpellier, France, in 2015.

Merouane Hamdi received his PhD in Fluid Mechanics and Thermal Science from the University of Nantes, France, in 2014. He previously received his Master of Science in Energy and sustainability from University of Boumerdes, Algeria, and Ecole des Mines de Nantes, France. He performed experiments and numerical modeling in thermal and fluid mechanics. His main objective concerns the reduction of energy consumption in food processes with specific applications in electrohydrodynamics and in microwave.

Olivier Rouaud received his PhD in Fluid Mechanics and Thermal Science from the University of Nantes, France, in 2002. During his PhD he was interested in the airflow inside clean rooms and in the behaviour of dynamic barriers such as plane air jets. Since September 2004 he is an assistant professor at ONIRIS and a member of the CNRS laboratory GEPEA (Génie des Procédés Environnement Agroalimentaire). His work deals with the heat and mass transfer phenomena and he carries out experiments and numerical modeling for heat treatments such as convective air drying, food freezing, microwave heating, ohmic heating and electrohydrodynamics (EHD) drying among others. He was the co-supervisor of more than 15 Master's theses and 6 PhD theses (2 currently). He is the co-author of more than 20 peer-reviewed papers and was also involved in several national and international research projects relating to heat and mass transfer in food engineering.

OPTIMIZATION OF HYDRATION PROCESS OF DATE PALM FRUITS FROM EXPERIMENTAL AND NUMERICAL APPROACHES

A. Lakoud[(a)], S. Curet[(b)], M. Hassouna[(c)]

[(a),(c)]Ecole Supérieure des Industries Alimentaires de Tunis, 58 Alain Savary,1003 Tunis El Khadra, Tunisie
[(b)]L'UNAM Université, ONIRIS, CNRS, GEPEA, UMR 6144, site de la Géraudière, Nantes, F-44322, France

[(a)]lakoudatef@yahoo.fr, [(c)]Mnasser.Hassouna@isbb.rnu.tn
[(b)]sebastien.curet@oniris-nantes.fr

ABSTRACT
This study focuses on the hydration process of dates from experimental and numerical investigations. Dry Tunisian Deglet Nour dates were hydrated at a laboratory scale by using saturated air. A theoretical model based on a finite element scheme was developed to describe mass transfer phenomena that occur during the hydration process. This model considers the real shape of dates with a 2D axisymmetric analysis. Both moisture diffusivity and convective mass transfer coefficient of dates were estimated by using an optimization algorithm based on a least square approach from experimental and numerical average moisture contents. Overall, the experimental moisture contents as a function of hydration time were found in good agreement with the simulated values for various operating conditions. Such a methodology can now be used as a predictive tool to simulate the hydration of dates in order to improve the quality of final product and reducing processing time.

Keywords: Dates hydration, modeling, moisture diffusivity, convective mass transfer coefficient

1. INTRODUCTION

In Tunisia, date palm (Pheoenix dactylifera L.), especially the Deglet Nour Cultivar, constitutes an important food and financial source. The chemical composition, in particular moisture content, of Deglet Nour date palm fruits can vary depending on agronomic practices, climatic conditions as well as ripening stage (El Arem et al. 2010). During last years, there has been an increase in the proportion of dry dates in annual crops. These dry dates are processed in the industry in order to obtain fruits similar to those labeled as Extra category dates. Hydration represents the key unit operation of this process. Therefore, the control of this operation is of paramount importance especially when excessive times of hydration could reduce the shelf stability of dates and induce a waste of energy whereas insufficient hydration durations lead to non acceptable final product quality.

2. MATERIAL AND METHODS

2.1. Raw material

Deglet Nour dates were harvested in 2014 and stored at 4°C and 65% of relative humidity.

2.2. Experimental procedure

Hydration experiments were conducted at laboratory scale approaching industrial conditions by placing dates in a closed environment at atmospheric pressure and where air reaches relative humidity of 100% and inner temperatures between 50 and 65°C. To achieve this, a metallic enclosure was filled with water and heated with a temperature controlled hot plate. Dates were placed in the head space of the enclosure without any contact with the water. The level of heating was set in such a way that temperatures of surrounding air medium, which are recorded by thermocouples placed near the dates, remain in the range of desired temperatures during each experiment. The experimental system designed is presented in Figure 1. Average moisture contents of dates flesh were measured at regular intervals during hydration by a method modified from Singh et al. (2013) which consists of drying 3 g of dates in an oven at 105°C for at least 18h.

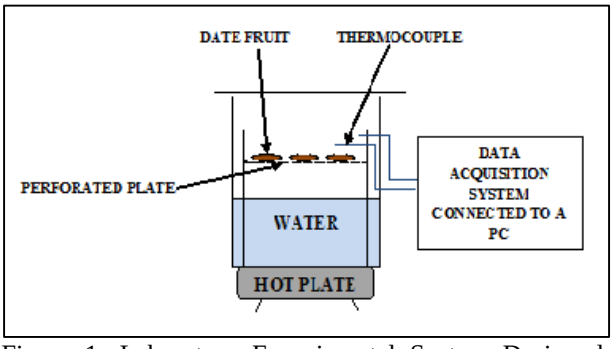

Figure 1: Laboratory Experimental System Designed for Dates Hydration

2.3. Modeling of hydration

Prior to modeling, monitoring of the temperatures within the dates flesh for the range of hydration times used for undertaking experiments showed that the

temperature can be considered as homogenous. Therefore a theoretical model based on a finite element scheme was developed to describe only mass transfer phenomena during the hydration operation based on Fick's law according to Eq.(1).

$$\frac{\partial C}{\partial t} = \nabla.(D\nabla C) \quad (1)$$

Where C and D are the instantaneous molar concentration (mol/m^3) and the diffusivity (m^2/s) of moisture within the date flesh. Since that the transport phenomena are symmetric, a 2D axisymmetric domain was considered to represent date flesh as shown in Figure 2.

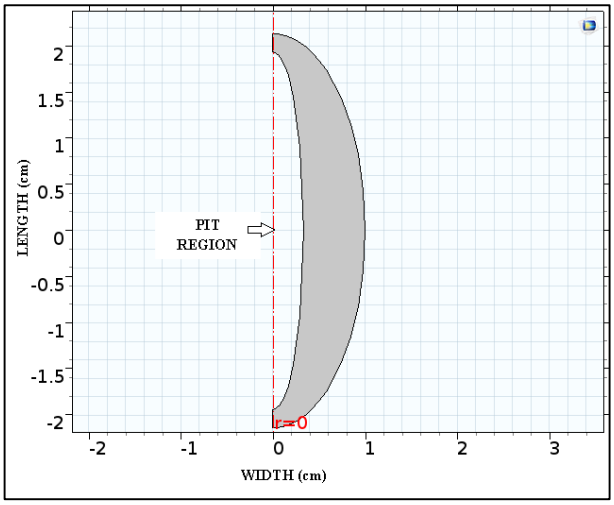

Figure 2: 2D Axisymmetric Domain

The initial and boundary conditions are as follows:

1. Uniform initial moisture molar concentration C_0 which is calculated from Eq.(2).

$$C_0 = \frac{X_0 \rho_0}{M_w} \quad (2)$$

Where X_0, ρ_0 and M_w are the initial average date flesh moisture content on humid basis (kg/kg), initial density of date flesh (kg/m^3) and the molecular mass of water (kg/mol).
ρ_0 is determined using Eq.(3).

$$\rho_0 = \frac{m_0}{V} \quad (3)$$

Where m_0 and v are the initial mass (kg) and the volume (m^3) of date flesh.
2. Null mass flux at the surface in contact with the date pit.
3. Natural mass convection at the outer surface in contact with the saturated air. The mass flux $N(mol.m^{-2}.s^{-1})$ of moisture inward date flesh is given by Eq. (4).

$$N = k_c(C_b - C_s) \quad (4)$$

Where k_c, C_b and C_S are convective mass transfer coefficient (m/s), bulk molar water vapor concentration (mol/m^3) and molar water vapor concentration in the air adjacent to the outer surface (mol/m^3).
C_b and C_S are determined using respectively Eq.(5) et Eq.(6).

$$C_b = \frac{P_{vs}}{RT} \quad (5)$$

$$C_s = \frac{P_{vs}}{RT} a_w \quad (6)$$

Where P_{vs}, R and a_w are saturated vapor pressure at the average absolute temperature T (K) of the air, ideal gas constant $(8.314\ J.mol^{-1}.K^{-1})$ and water activity of date flesh. Neglecting sorption hysteresis phenomenon, a_w was defined using the GAB model in Eq.(7) (Kechaou and Mâalej 1999; Kechaou and Mâalej 2000).

$$X = \frac{X_m C k a_w}{(1-ka_w)(1-ka_w+Cka_w)} \quad (7)$$

Where X is the instantaneous moisture content on dry basis(kg/kg). X_m, C and k are the constants of the model.
k_c is determined initially using the correlation for natural mass transfer coefficient around a sphere according to Eq.(8) (Cussler 2009).

$$\mathrm{Sh} = \frac{\mathrm{kcD_{eq}}}{\mathrm{D_{w,a}}} = 2 + 0.6(\mathrm{Gr})^{\frac{1}{4}}(\mathrm{Sc})^{\frac{1}{3}} \quad (8)$$

Where Sh, Gr and Sc are Sherwood, Grashof and Schmidt numbers. D_{eq} is the surface-equivalent sphere diameter of the date (m). $D_{w,a}$ is the diffusivity of the water vapor in air (m^2/s) which is estimated using Eq.(9) (Bolz and Tuve 1976).

$$\mathrm{D_{w,a}} = -2.775 \times 10^{-6} + 4.479 \times 10^{-8}\mathrm{T} + 1.656 \times 10^{-10}\ \mathrm{T^2} \quad (9)$$

The model was implemented in the software COMSOL®MultiPhysics release 5.1 which solves partial differential equations by using the finite element method. The computational domain is meshed using triangular elements. Date flesh moisture distribution is computed during hydration and the average moisture concentration is calculated as a function of time with the average coupling operator.
Then, by using the optimization module from COMSOL®, both moisture diffusivity and convective mass transfer coefficient at the surface were estimated by minimizing the least-square objective function

calculated from experimental and numerical mean moisture contents. Experimental values were implemented in COMSOL® using equations Eq.(10) and Eq.(11) similar to Eq.(2) and Eq.(3).

$$C_t = \frac{X_t \rho_t}{M_w} \quad (10)$$

Where X_t and ρ_t are the instantaneous average date flesh moisture content on humid basis (kg/kg) and density of date flesh (kg/m^3) . ρ_t is determined using Eq.(11).

$$\rho_t = \frac{m_t}{V} \quad (11)$$

Where m_t and v are the instantaneous mass (kg) and the volume (m^3) of date flesh which is considered constant and equal to the arithmetic mean of initial and hydrated date.

3. RESULTS

Although experiments were conducted for several types of Deglet Nour dates, only results for one type of dates which are slightly harder and drier than labeled Extra category dates are presented. The molar moisture concentration distribution is computed at times when average moisture contents were measured experimentally. Figure 3 illustrates molar moisture profile within the flesh of one date after 14640s (≈ 4h) of hydration at the average temperature of the air during hydration.

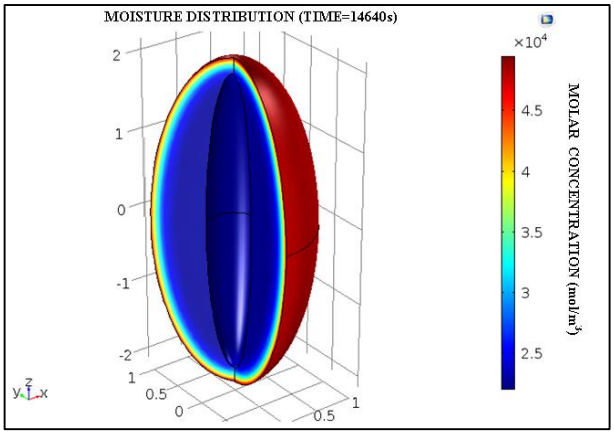

Figure 3: Moisture Concentration Distribution Within Date Flesh After 4h

As mentioned above, the mean water concentration is then computed. The estimation of both moisture diffusivity and mass transfer coefficient by minimizing the least square objective function using Levenberg-Marquardt optimization solver was undertaken as follows:

1. Effective mass diffusivity is estimated by taking initial mass transfer coefficient determined from the Eq.(8).
2. By considering the value of mass diffusivity found from the first run, a second optimization is performed to estimate the mass transfer coefficient.

Table 1 shows the estimated diffusivities and convective mass transfer coefficient for two dates from the considered type.

Table 1: Estimated Moisture Diffusivities and Mass Transfer Coefficients

Date Number	Date 1	Date 2
***D*(m²/s)**	5.54E-11	5.54E-11
***kc* (m/s)**	0.00123	0.00126

The values of estimated convective mass transfer coefficient which depend on the dimensions of dates are consistent with the values found using the correlation for natural convection (Eq.8).
Figure 4 and Figure 5 represent experimental and calculated moisture molar concentration data as a function of time using estimated mass diffusivity and convective coefficient.

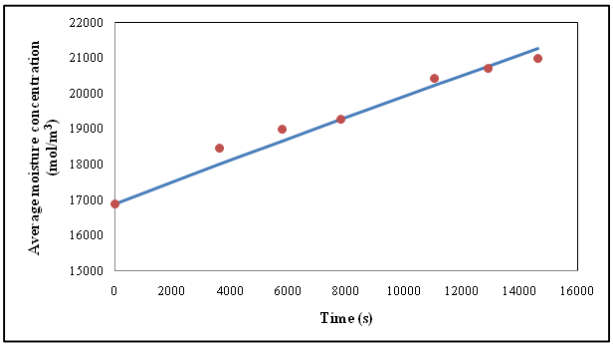

Figure 4: Experimental vs Calculated Average Moisture Concentration Of Date1

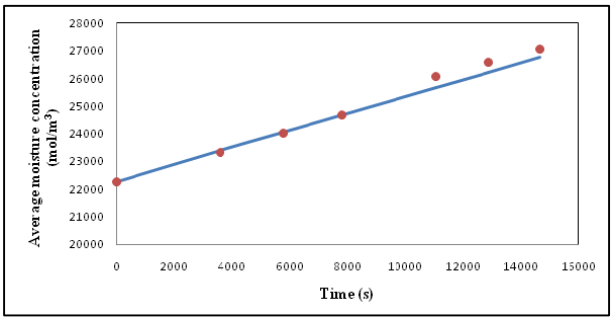

Figure 5: Experimental vs Calculated Average Moisture Concentration Of Date2

It is shown that there is a good agreement between calculated and experimental average moisture molar concentrations.
The root mean square difference (RMS) is also calculated from the Eq. 12 (Kechaou and Maâlej 2000).

$$RMS = \sqrt{\frac{\Sigma_i \left(\frac{Cav_{i,exp} - Cav_{i,cal}}{Cav_{i,exp}} \right)^2}{n-1}} . 100 \quad (12)$$

Where Cav_i is the average moisture molar concentration at the *i*-th experimental point.
Table 2 confirms the accuracy of the modeling since that root mean square differences (RMS) do not exceed the value of 1.39%.

Table 2: Root Mean Square Differences Between Experimental and Calculated Curves

Date Number	Date 1	Date 2
RMS (%)	1.39	0.97

It is also seen that the phase of decrease in moisture uptake rate is not observed. It could be explained by the relatively short times of hydration (in comparison to maximum processing times in industry).
The estimated moisture diffusivities and convective coefficients shown in Table 1, Figure 4 and Figure 5 indicate that these values do not vary greatly with the initial average moisture concentration. Therefore, this model can be used to predict times necessary to reach desired final moisture contents by taking into account the variability of raw material for this type of dates.

4. CONCLUSION

Hydration is the key unit operation in the industrial thermal process of dates. However there are a scarce data about the capacity of moisture uptake during hydration. In this work, a theoretical model was developed to describe mass transfer phenomena involved in this operation. The model enables to estimate moisture diffusivity and convective mass transfer coefficient using an investigation performed experimentally. This model can be used to simulate hydration of dates in order to predict and optimize this operation. In addition, the model could be used to optimize the maximum time of hydration. For current industrial applications, this operation often lasts during more than 4h. The proposed modeling approach may thus help for the optimization of this operation in order to enhance the mass transfer at the surface and to reduce the energy consumption during hydration.

REFERENCES

Bolz R.E. and Tuve G.L., 1976. Handbook of tables for Applied Engineering Science. 2nd ed. New York: CRC Press.

Cussler E.L.,2009. Diffusion mass transfer in fluid systems. 3rd ed. New York: Cambridge University Press.

El Arem A., Flamini G., Saafi E.B., Issaoui M., Zayene N., Ferchichi A., Hammami M., Helal A.N., Achour L., 2011. Chemical and aroma volatile compositions of date palm (*Phoenix dactylifera* L.) fruits at three maturation stages. Journal of Food Chemistry, 127, 1744-1754.

Kechaou N., Mâalej M., 1999. Desorption isotherms of the Tunisia deglet nour dates-Application of the GAB theory. Actes des 11èmes rencontres scientifiques et technologiques des industries alimentaires (AGORAL'99), pp.277-282. 31 mars et 1er avril, Nantes (France).

Kechaou N., Mâalej M., 2000. A simplified model for determination of moisture diffusivity of date from experimental drying curves. Journal of Drying Technology, 18 (4&5), 1109-1125.

Singh V., Guizani N., Al-Alawi A., Claereboudt M., Rahman M.S., 2013. Instrumental texture profile analysis (TPA) of date fruits as a function of its physic-chemical properties. Industrial Crops and Products, 50, 866-873.

POROVISCOELASTIC MODELING OF PROTEIN HYDROGELS

Ruben Mercadé-Prieto[(a)], Joaquim Lopez[(b)], Xiao Dong Chen[(c)]

[(a), (b), (c)] Suzhou Key Laboratory of Green Chemical Engineering, School of Chemical and Environmental Engineering, College of Chemistry, Chemical Engineering and Materials Science, Soochow University, Suzhou City, Jiangsu 215123, P.R. China
[(b)] IQS School of Engineering, Ramon Llull University, 08017 Barcelona, Spain

[(a)] ruben@suda.edu.cn, [(c)] xdchen@suda.edu.cn

ABSTRACT
Many solid food matrices contain high amounts of solvent, typically water. Hence, the structural behavior depends on its biphasic nature. The time dependent mechanical characterization of foods and hydrocoloid-based solids has typically been analyzed following a viscoelastic approach, omitting the effect of the solvent. However, in solvent rich solids the solvent flows internally as it is compressed, for example, which is typically understood using poroelastic theory. A poroelastic approach allows the determination of parameters, such as the Darcy's diffusivity or the intrinsic permeability, that have a physical meaning. The application of poroelasticity to materials has been traditionally limited due to the complex data analysis. Recently, it has been proposed for polymeric hydrogels a novel experimental methodology, based on relaxation after indentation that greatly simplifies the subsequent analysis. This methodology is applied here for the first time to a complex food-like matrix, to heat induced whey protein hydrogels.

Keywords: poroelasticity, finite elements analysis, hydrogel, whey proteins.

1. INTRODUCTION

Solvent rich soft materials, like hydrogels (Chan et al., 2012b) and cells (Trappmann et al., 2012), have recently been characterized using a novel poroelastic relaxation indentation methodology (Hu et al., 2010). The hydrogel, at swelling equilibrium, is indented a small fixed depth using a rigid probe. The relaxation force is measured with time and is subsequently analyzed using correlations obtained from poroelastic finite element analysis. The power of this novel methodology, despite the experimental simplicity, is that several material properties including the shear modulus, diffusion coefficient, average pore size and even the Flory-Huggings interaction parameter, could be obtained by a single experiment (Hu et al., 2011b).
This novel methodology, developed and tested initially for synthetic polymeric systems, has been recently expanded to biomaterials such as gelatin and agar (Strange and Oyen, 2012). We apply it here for the first time to protein hydrogels, and to whey proteins in particular due to their extensive use in research and commercial applications (Mercadé-Prieto et al., 2008). These initial tests were performed in a typical food lab rheometer with good normal force resolution, where the main limitation was that only one cylindrical indenter was available (Fig. 1). Subsequently it is summarized the mechanical analysis of indentation-relaxation tests with a cylindrical punch.

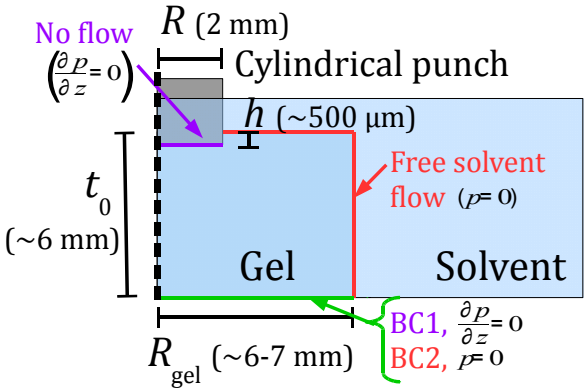

Figure 1. Schematic axisymmetric representation of a swollen protein hydrogel indented with a cylindrical punch. In the finite element analysis it was considered no solvent flow in the area in contact with the indenter (zero solvent flux in the vertical direction,), and free flow (zero pore pressure at the gel surface, $p = 0$) in the non-contact area. For the bottom area, that in contact with the substrate, two boundary conditions are considered: BC1 for no flow, and BC2 for diffusive equilibrium.

2. INDENTATION ANALYSIS

2.1. Elastic loading with a cylindrical punch

The force at an indentation depth h using a flat punch indenter in an elastic (E) sample (Fig. 1) is (Hu et al., 2010):

$$F_E = 8 G_E R h \Pi(R/t_0, \nu) \quad (1)$$

where G_E is the instantaneous shear modulus in a linear elastic material; R is the radius of the indenter, ν is the instantaneous Poisson's ratio, and $\Pi(R/t_0,\nu)$ is a dimensionless function needed to correct substrate effects, important for ratios of the indenter radius to the sample thickness $R/t_0 > 0.1$ (Cao et al., 2009). After loading, the indentation depth h is kept constant, resulting in a constant contact area. Because the indentation step is quick compared to the subsequent relaxation, it is typically treated the hydrogel as incompressible during loading (ν = 0.5).

2.2. Poroelastic (PE) relaxation

A purely elastic hydrogel does not show a force decrease with time t after indentation. A force relaxation in a hydrogel is typically due to the flow of the interstitial fluid through the polymer network – poroelasticity (PE) – and due to the intrinsic viscoelasticity (VE) of the polymer network (Strange et al., 2013). The force relaxation after indentation is first considered for a poroelastic material. Hu et al. (2010) have shown that the normalized relaxation force $F_{PE}(t)$ is only a function of the normalized time τ_{PE}:

$$\frac{F_{PE}(t)-F_{PE}(\infty)}{F_E-F_{PE}(\infty)}=f_{PE}(\tau_{PE}) \tag{2}$$

where $F_{PE}(\infty)$ is the force in the long-time limit. In a cylindrical punch, $\tau_{PE} = Dt/R^2$; where D is Darcy's law diffusivity. It is assumed that both the solvent and the solid matrix are incompressible. The function $f_{PE}(\tau_{PE})$ is found computationally for different indenter shapes and hydrogel configurations, such as different R/t_0 ratios (Hu et al., 2011a). The function $f_{PE}(\tau_{PE})$ is usually fitted to a series of exponential functions such as:

$$f_{PE}(\tau_{PE})=\sum_{i=1}^{N_{PE}} A_i e^{(B_i \tau_i^{C_i})} \tag{3}$$

where A_i, B_i, and C_i are regression constants, and N_{PE} is an integer typically 2 to 3. The extent of relaxation in PE is determined by the Poisson's ratio of the drained hydrogel, ν_d (Hu et al., 2010):

$$\frac{F_{PE}(\infty)}{F_E}=\frac{1}{2(1-\nu_d)} \tag{4}$$

Poroelastic properties of hydrogels are also typically described using the intrinsic permeability k:

$$k=\frac{(1-2\nu_d)D\eta}{2(1-\nu_d)G} \tag{5}$$

2.3. Viscoelastic (VE) relaxation

The viscoelastic relaxation of a material is usually described empirically using a series of exponentials, known as Prony series, of the shear modulus (Cao et al., 2009):

$$G_{VE}(t)=G_E\left(1-\sum_{j=1}^{N_{VE}} g_{VEj}\left(1-e^{(-t/\tau_{VEj})}\right)\right) \tag{6}$$

where g_{VEj} and τ_{VEj} are the relative shear modulus and the relaxation time of the viscoelastic deformation, and N_{VE} is an integer typically between 1 to 4. The normalized relaxation force with time due to viscoelasticity is therefore

$$\frac{F_{VE}(t)}{F_E}=1-\sum_{j=1}^{N_{VE}} g_{VEj}\left(1-e^{(-t/\tau_{VEj})}\right) \tag{7}$$

2.4. Poroviscoelastic (PVE) relaxation

Both relaxation methods, PE and VE, can occur simultaneously resulting in a poroviscoelastic (PVE) relaxation. Both phenomena have been suggested that can be decoupled to compute the overall PVE relaxation (Strange et al., 2013), such as:

$$F_{PVE}(t)=\frac{F_{VE}(t)F_{PE}(t)}{F_E} \tag{8}$$

The extent of relaxation in PVE is expected to be:

$$\frac{F_{PVE}(\infty)}{F_E}=\left(1-\sum_{j=1}^{N_{VE}} g_{VEj}\right)\left(\frac{1}{2(1-\nu_d)}\right) \tag{9}$$

In this paper we implement the above relaxation models to swollen protein hydrogels and discuss their validity.

3. INDENTATION OF PROTEIN HYDROGELS

3.1. Whey protein hydrogels

Heat-induced hydrogels were formed as reported previously (Mercadé-Prieto et al., 2007b), using commercial whey protein isolate powder (BiPro, Davisco, USA). Protein solutions at 15 wt%, with 0.1% sodium azide, were heated inside plastic test tubes for 20 min at 80°C. Gels were stored overnight at 4°C prior being cut in ~6 mm height cylinders, which were then submerged in water solutions at either 0.1, 0.2 or 0.3 M NaCl. The swelling ratio $SR = (m_{sw}/m_0 - 1)$ was calculated from the gels mass difference after swelling equilibrium was achieved (Mercadé-Prieto et al., 2007b).

3.2. Indentation

The swollen hydrogels were placed during testing on a glass petri dish with the corresponding salt solution. Indentation was performed using a rheometer with good normal force resolution, <0.001 N (Malvern Kinexus, UK), with a 2 mm cylindrical indenter. The indenter was placed close to, but not in contact with, the hydrogel surface. Thereafter, the gel was compressed by modifying the gap; the actual indentation depth h was determined a posteriori during the loading analysis.

Gels were allowed to relax for one hour or until no force change was noticeable.

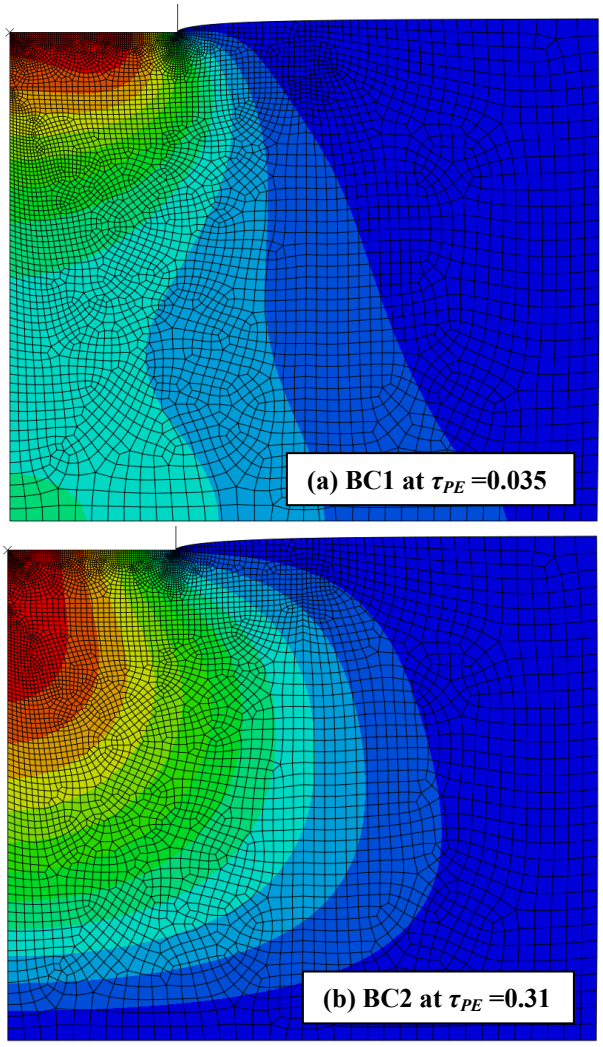

Figure 2. Finite element simulations of the pore pressure inside a swollen hydrogel using $\nu_d = 0$.

4. FINITE ELEMENT ANALYSIS OF INDENTATION RELAXATION

Finite element analysis of the indentation problem shown in Fig. 1 was performed as described by several previous researchers (Hu et al., 2011b; Lin and Hu, 2006; Strange et al., 2013). The main novelty in the present work is that we model small hydrogels using a flat cylindrical indenter, and that we verify PVE eq. 8 using finite elements also for a flat indenter. Although tested gels had some size variations in thickness and diameter, for instance due to the different extent of swelling, the variations where too small to justify using different finite element geometries for each particular gel. For example, the key parameter R/t_0 was 0.32 ± 0.02 (SD) for 0.1 M NaCl gels, 0.32 ± 0.01 at 0.2 M NaCl, and 0.34 ± 0.09 at 0.3 M NaCl, hence an average value of $R/t_0 = 0.333$ was considered in the simulations. In the same way, the diameter of the simulation hydrogel was chosen as $R/R_{gel} = 0.286$. The indentation depth simulated was very small, $h/t_0 < 0.03$, although results where highly insensitive to h up to large values after normalization.

In previous studies, it was assumed no solvent flow through the bottom of the hydrogel, this boundary condition is termed BC1 here (see Fig. 1). In BC1, the pore pressure does increase with time at the gel bottom, shown in Fig. 2(a). This boundary conditions seemed unlikely in our experiments. Hence, simulations were also performed allowing solvent flow in all directions except the area in contact with the rigid indenter (termed model BC2), Fig. 2(b). PE simulations were fitted to eq. 3 with $N_{PE} = 2$; that equation was then used to calculate D from normalized experimental relaxations, as reported in the literature. For PVE analysis, using $N_{VE} = 1$, three parameters where optimized: D, g_{VE1} and τ_{VE1}. The parameter D was optimized using the simplex search method, function *fminsearch* in Matlab, whereas the last two parameters were optimized within fixed bounds, using the function *fminbnd* in Matlab, in order to assure convergence and a physical meaning ($0 < g_{VE1} < 0.25$; $0.5 \text{ s} < \tau_{VE1} < 100$ s). The parameters were optimized one at a time, iteratively, until the mean square error (MSE) did not improve further. All the numerical analysis was performed in Matlab.

5. RELAXATION SIMULATIONS

5.1. Poroelastic simulations

The normalized force for PE given in eq. 2 is very useful to determine the solvent diffusivity D because the shape of $f_{PE}(\tau_{PE})$ does not change with the other material parameters, such as G_E and ν_d, or the extent of indentation h. However, the shape of $f_{PE}(\tau_{PE})$ does depend on size of the indenter in proportion to the hydrogel size, R/t_0, as shown elsewhere for a spherical indenter (Hu et al., 2011a). Figure 3 shows the finite element analysis results for the testing geometry shown in Fig. 1, for the two boundary conditions considered, which is faster compared to a semi-infinite sample, as shown from the results by Hu et al. (2010).

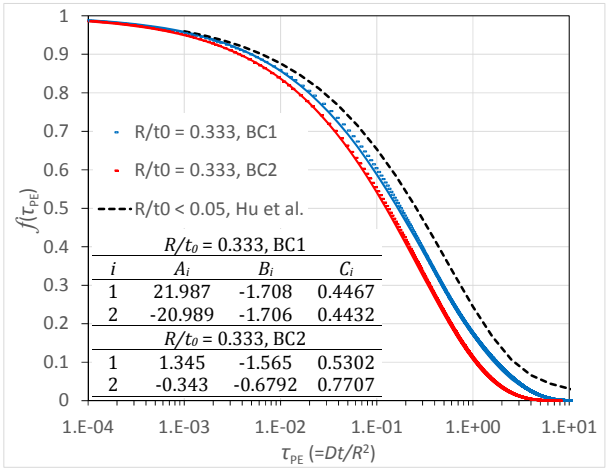

R/t_0 = 0.333, BC1

i	A_i	B_i	C_i
1	21.987	-1.708	0.4467
2	-20.989	-1.706	0.4432

R/t_0 = 0.333, BC2

1	1.345	-1.565	0.5302
2	-0.343	-0.6792	0.7707

Figure 3. Finite element simulations for the PE relaxation for the geometry shown in Fig. 1, and comparison with the results of Hu et al. (2010) for a

semi-infinite hydrogel. Continuous lines are the best fit exponential regressions eq. 3; inset table shows the regression coefficients for $N_{PE} = 2$.

5.2. Poroviscoelastic simulations

The fitting of the experimental relaxation curves in PVE was performed in analogy to that of PE, after normalizing the force as $(F(t) - F(\infty))/(F_E - F(\infty))$. However, if the shape of PE $f_{PE}(\tau_{PE})$ only depends on D for a fixed indenter and sample geometry, in PVE it also depends on the VE parameters g_{VEj} and τ_{VEj}. Here, only one exponential term was needed to model the additional viscoelastic relaxation, i.e. $N_{VE} = 1$. In addition, the PVE relaxation profile also depends on the drained Poisson's ratio ν_d, as it determines the extent of the PE relaxation, see Fig. 4. The drained Poisson's ratio used for PVE fitting was that calculated from the PE analysis; small ν_d modifications due to g_{VE1} during the overall fitting process where not considered for simplicity. The decoupled eq. 8 can describe the PVE relaxation satisfactorily in the experimental range of $0.2 > \nu_d > -0.2$ (Table 1); and the final $F_{PVE}(\infty)/F_E$ using eq. 9 was also well predicted from simulations for the typical parameters considered here, with errors <3%.

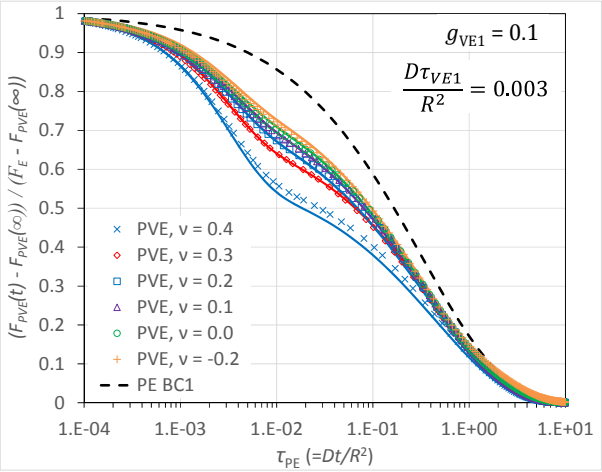

Figure 4. Normalized PVE force at fixed VE conditions and for different drained Poisson's ratio ν_d. Points are results from finite element analysis for the BC1 model, lines are calculated using eq. 8. Note that most experimental results were obtained for $0.2 > \nu_d > -0.2$, hence the relaxation profile does not change significantly.

6. RESULTS

6.1. Hydrogels indentation

Heat induced whey protein gels were soaked in water with three different NaCl concentration to achieve different degrees of equilibrium swelling ratios SR (Table 1). The indentation tests include a loading and a relaxation step at a fixed indentation depth h. From the loading step, the elastic shear modulus G_E was determined assuming a linear-elastic response, eq. 1. The contact point, required to calculate h was determined as shown in Fig. 5. An average corrective value of 1.42 was chosen for $\Pi(R/t_0,\nu)$ in eq. 1 for all experiments. The average G_E found, summarized in Table 1, are comparable to those reported previously for unswollen whey protein gels at similar protein concentrations using a different indentation technique (Özkan et al., 2002).

Table 1. Best fit relaxation parameters for whey protein gels at swelling equilibrium with different salt concentrations (± SD). Different superscripts show significant difference ($p < 0.05$): Latin letters for row comparisons, Greek letters for column comparisons of the same propriety.

	[NaCl] / M	0.1	0.2	0.3
	SR	$0.123^{a} \pm 0.017$	$-0.091^{b} \pm 0.02$	$-0.134^{c} \pm 0.02$
	# tests	34	19	28
	G_E / kPa	$15^{a} \pm 3$	$32^{b} \pm 5$	$36^{c} \pm 7$
	$F(\infty)/F_E$	$0.59^{a} \pm 0.06$	$0.50^{b} \pm 0.07$	$0.44^{c} \pm 0.08$
PE	ν_d	$0.14^{a\alpha} \pm 0.09$	$-0.01^{b\alpha} \pm 0.2$	$-0.2^{c\alpha} \pm 0.3$
PE BC1	D / 10^{-9} m^2 s^{-1}	$8.0^{a\alpha} \pm 3.5$	$6.4^{ab\alpha} \pm 3$	$5.8^{b\alpha} \pm 2$
	Av. MSE	$3.7\text{x}10^{-4\ a\alpha}$	$4.1\text{x}10^{-4\ a\alpha}$	$3.1\text{x}10^{-4\ a\alpha}$
PE BC2	D / 10^{-9} m^2 s^{-1}	$5.0^{a\beta} \pm 3.7$	$4.2^{ab\beta} \pm 2$	$3.9^{b\beta} \pm 1.3$
	Av. MSE	$5.7\text{x}10^{-4\ a\beta}$	$6.7\text{x}10^{-4\ a\alpha}$	$4.8\text{x}10^{-4\ a\beta}$
PVE BC1	D / 10^{-9} m^2 s^{-1}	$6.6^{a\alpha} \pm 3$	$5.3^{ab\alpha\beta} \pm 3$	$5.0^{b\alpha} \pm 1.9$
	g_{VE1}	$0.05^{a\alpha} \pm 0.03$	$0.079^{a\alpha} \pm 0.05$	$0.06^{a\alpha} \pm 0.04$
	τ_{VE1} / s	$8^{a\alpha} \pm 5$	$7.7^{a\alpha} \pm 4$	$6^{a\alpha} \pm 3$
	ν_d	$0.19^{a\alpha\beta} \pm 0.09$	$0.06^{b\alpha} \pm 0.2$	$-0.13^{c\alpha} \pm 0.3$
	Av. MSE	$1.7\text{x}10^{-4\ a\gamma}$	$1.1\text{x}10^{-4\ a\beta}$	$1.5\text{x}10^{-4\ a\gamma}$
PVE BC2	D / 10^{-9} m^2 s^{-1}	$4.0^{a\gamma} \pm 2$	$3.2^{ab\beta} \pm 1.7$	$3.0^{b\gamma} \pm 1.1$
	g_{VE1}	$0.082^{a\beta} \pm 0.04$	$0.12^{b\alpha} \pm 0.06$	$0.10^{ab\beta} \pm 0.04$
	τ_{VE1} / s	$13^{a\beta} \pm 6$	$12^{a\beta} \pm 5$	$11^{a\beta} \pm 4$
	ν_d	$0.21^{a\beta} \pm 0.1$	$0.10^{b\alpha} \pm 0.2$	$-0.08^{c\alpha} \pm 0.3$
	Av. MSE	$1.1\text{x}10^{-4\ a\delta}$	$6.5\text{x}10^{-5\ b\beta}$	$7.8\text{x}10^{-5\ ab\delta}$

6.2. Viscoelastic relaxation analysis

The relaxation of food matrices, such as cheese (Lucey et al., 2003) or yoghurt (Puvanenthiran et al., 2002), has been typically been modeled as an empirical viscoelastic process (Gallegos and Franco, 1999), where the estimated VE parameters do not have a strong physical meaning. A viscoelastic analysis, using eq. 6, was also be applied to the force relaxation of whey protein gels. A value of $N_{VE} = 3$ was required to fit the relaxation data well (Fig. 6); best fit values are shown in Table 2.

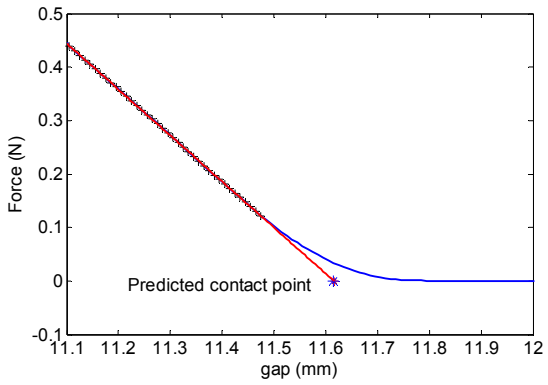

Figure 5. Example of loading step for a hydrogel swollen in 0.3 M NaCl. Red line is the best fit using eq. 1, used to calculate G_E at about 38 kPa here. The predicted contact point, used to determine h, is also shown.

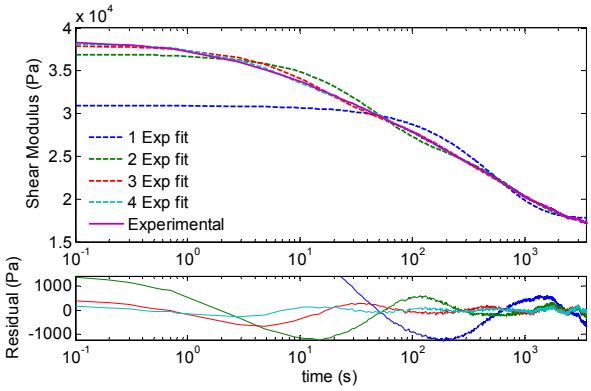

Figure 6. VE analysis with different N_{VE} values for the indentation shown in Fig. 5.

Table 2. Best fit viscoelastic parameters for N_{VE} = 3, estimated using nonlinear regressions of eq. 6.

[NaCl] / M	g_{VE1}	τ_{VE1} / s	g_{VE2}	τ_{VE3} / s	g_{VE3}	τ_{VE3} / s	Av. MSE
0.1	0.12[a] ± 0.03	10[a] ± 3	0.13[a] ± 0.02	107[a] ± 40	0.17[a] ± 0.05	860[a] ± 360	5x10^{-5}
0.2	0.15[b] ± 0.03	10[a] ± 3	0.15[b] ± 0.02	130[ab] ± 45	0.20[a] ± 0.06	1100[ab] ± 400	2x10^{-5}
0.3	0.17[b] ± 0.02	10[a] ± 2.5	0.17[c] ± 0.01	125[b] ± 30	0.25[b] ± 0.07	1000[b] ± 220	2x10^{-5}

6.3. Poroelastic relaxation analysis

The normalized relaxation force for whey protein hydrogels swollen at different salt concentrations was fitted to the PE $f_{PE}(\tau_{PE})$ eq. 3 functions to estimate D. The average D values for the three swelling conditions tested are given in Table 1, with D decreasing slightly with higher salt concentrations, although only the values at 0.1 and 0.3 M NaCl are statistically different. The selection of the model BC1 or BC2 is important as statistically different values are estimated, with BC2 resulting obviously in smaller D values.

The D values estimated are higher than for the water self-diffusion in a comparable whey protein gel (~1.5x10-9 m2 s-1 at 20°C (Colsenet et al., 2005) or in pure water. This result is reasonable because the average pore size of the whey protein hydrogels, estimated at ~20 nm using the PE data, is much larger than the dimension of the water molecule. Consequently, water is expected to flow more by convection rather than by diffusion (Hu et al., 2011b). The intrinsic permeability k of the whey protein gels made is calculated at (0.8–2)x10^{-16} m2, comparable to that reported for agar and acrylamide hydrogels but here for much higher solid concentrations (Oyen, 2014). In fact, the biomaterial more similar to whey protein hydrogels in terms of G_E and k, at similar solid concentrations, would be gelatin (Strange and Oyen, 2012).

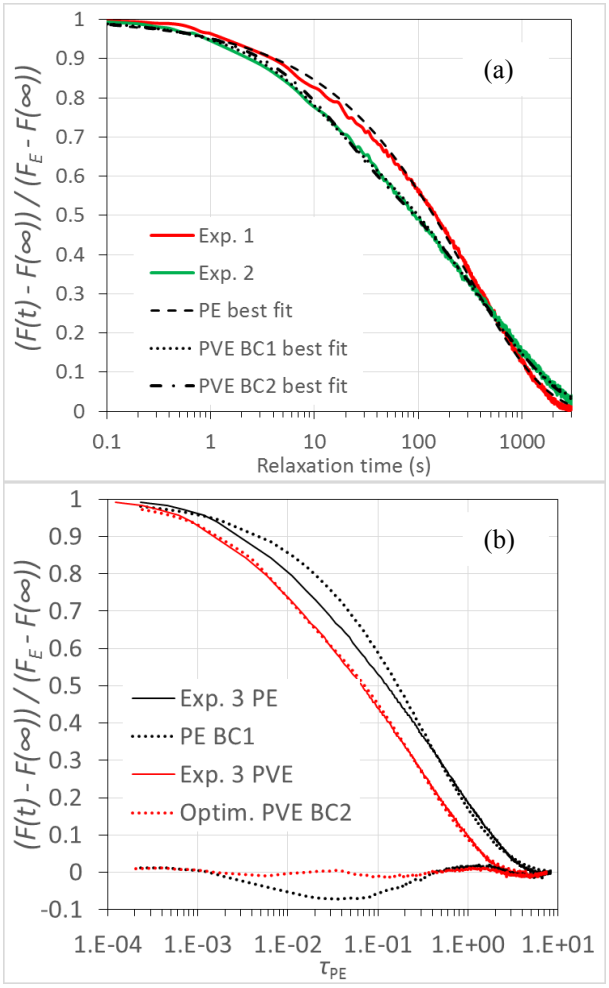

Figure 7. (a) Two representative relaxations of whey protein gels at swelling equilibrium in 0.1 M NaCl. In experiment 1 a PE relaxation fits well (best fit using BC2 model with D = 3.6x10^{-9} m^2 s^{-1}), and little improvement is achieved by considering PVE. Experiment 2 represents the more common tests where fitting is substantially improved by considering PVE relaxation (best fit PVE BC1: D = 4x10^{-9} m^2 s^{-1}, g_{VE1} = 0.074, τ_{VE1} = 10 s, and using PVE BC2: D = 2.4x10^{-9} m^2 s^{-1}, g_{VE1} = 0.11, τ_{VE1} = 16 s). (b) Normalized relaxation

of a hydrogel in 0.3 M NaCl and the best fit using PE BC 1 (black) and PVE BC2 (red) models, D = 9.3x10^{-9} m^2 s^{-1} and D = 4.9x10^{-9} m^2 s^{-1}, g_{VE1} = 0.10, τ_{VE1} = 6 s; respectively. Note that as the estimated D are different, the experimental data (continuous lines) have different τ_{PE} values depending on the model considered.

Experiment 1 in Fig. 7(a) shows one of the few examples (<9% of all tests) where PE could represent well the whole relaxation. The majority of the tests showed a poor agreement with the PE models at 10-100 s, see Exp. 2. This is clearly seen in another test shown in Fig. 7(b), where the residuals of the PE fit show a systematic over prediction at τ_{PE} ~0.01-0.1. Similar relaxation profiles have been reported in the literature, such as for chemically crosslinked polyethylene glycolmethacrylate (PEGMA) (Chan et al., 2012a), and have been explained by considering an additional viscoelastic relaxation, therefore a PVE model.

6.4. Poroviscoelastic relaxation analysis

Two examples of PVE regressions are shown in Fig. 7. The average PVE parameters found are summarized in Table 1. The addition of a viscoelastic relaxation results in lower D estimates, where again are lower using the BC2 model compared to BC1. On absolute terms, the D values estimated are similar to the self-diffusivity of free water (~2x10^{-9} m^2 s^{-1}), particularly using the BC2 model. The viscoelastic parameters g_{VE1} and τ_{VE1} calculated were not affected by the swelling degree. We note that the overall g_{VE1} and τ_{VE1} obtained from PVE are comparable to those found using a VE analysis only (g_{VE1} ~0.15 and τ_{VE1} = 10 s, Table 2). The use of model BC2 was hardly justified for PE analysis as the average MSE was indeed worse compared to BC1. However, for PVE analysis, BC2 fits better the experimental data, validating its use for comparison, and suggesting that solvent equilibration could be possible from the bottom of the hydrogels. The quality of the BC2 model fit, as shown by the average MSE values, is comparable to that of a pure VE analysis with N_{VE} = 3 (Table 2), but with half the number of adjustable parameters. The selection of the model did statistically influence the estimated g_{VE1} and τ_{VE1}, which is likely due to the smaller D estimated with model BC2. We observed a strong a correlation between the estimated D and the VE parameters, not shown. In any case, the values of τ_{VE1} at 6-13 s are comparable to those found for PEGMA hydrogels in an analogous PVE analysis, at 6-20 s (Chan et al., 2012a).

7. DISCUSSION

It was unexpected that the main difference between the whey protein hydrogels soaked at different salt concentrations, other than G_E which is directly related to the extent of swelling, was $F(\infty)/F_E$ and therefore ν_d (Table 1). In addition, it appears that the calculated D correlate with $F(\infty)/F_E$: tests with high $F(\infty)/F_E$ ratios show comparatively high D values (Fig. 8), as well as smaller g_{VE1} and τ_{VE1} for PVE fits.

Comparable small and negative ν_d values have been reported in the literature in agar-gelatin composite hydrogels when the hydrogels were more agar rich, with $0 > \nu_d > -1$ (Strange and Oyen, 2012); and with ν_d ~ -0.7 for pure agar hydrogels calculated with a PVE analysis (Strange et al., 2013). The reasons are unclear, and further tests are required to verify this finding. However, we note that if there were an additional VE relaxation with τ_{VE2} ~200 s, it would be impossible to discern from a PE relaxation in the current experimental setup.

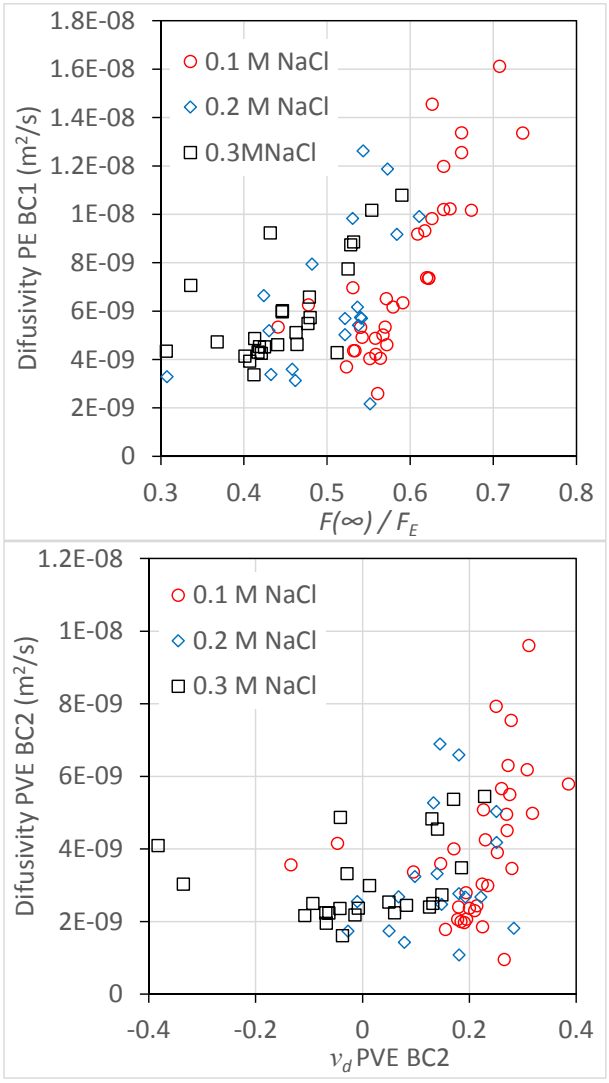

Figure 8. Diffusivites calculated assuming (a) poroelastic relaxation with no solvent flow from the bottom of the gel (BC1), and (b) poroviscoelastic relaxation with solvent flow from the bottom (BC2). Note the different y-axis scale.

One of the advantages of indentation testing to characterize hydrogels is that VE relaxation is independent of the indenter size R, whereas PE relaxation is strongly dependent on R (Wang et al., 2014). Hence, it is theoretically possible to perform experiments with different size indenters to elucidate the validity of the g_{VE1} and τ_{VE1} estimated here.

Unfortunately, only one indenter size was currently available in the rheometer used. In order to decouple more both relaxations in time, there are two options: (*i*) increase the indenter size to $R > 1$ cm, larger than the current size of the gels R_{gel}. Keeping the same indenter – hydrogel proportions than used here, the protein hydrogels should be $R_{gel} > 3$ cm and $t_0 > 3$ cm, which are highly impractical and expensive to make for routine testing. If the hydrogel dimensions were not so large for $R > 1$ cm, then the PE relaxation will occur much faster due to the closer boundary surfaces (Hu, Chan, et al., 2011), canceling the time decoupling effect of increasing R. Option (*ii*) would be to reduce significantly the indenter size, as in nanoindentation (Oyen, 2015). With very small indenters, the PE relaxation would occur before the VE one; for the conditions used here, it is predicted $R < 30$ μm to clearly see both relaxations. $R < 100$ μm should be used to check if there is a VE relaxation with τ_{VE2} ~200 s as discussed above. Different indentation techniques, such as AFM where PE relaxation occurs in the order of seconds or faster (Kalcioglu et al., 2012), would have to be used for such experiments.

The poroelastic indentation methodology has been further used in polymer hydrogels to obtain reasonable estimates of the Flory-Huggings interaction parameter χ (Hu et al., 2011b). It would be very convenient to be able to perform such analysis, despite its many limitations and simplifications, to other more complex food based systems, such as the protein hydrogels considered here. It is known from swelling experiments that χ for whey protein gels is ~0.5 (ideal or Θ conditions) (Mercadé-Prieto et al., 2007a). Yet, according to the figures provided by Hu et al. (2011b), such reasonable χ can only be obtained from indentation data for $0.25 < \nu_d < 0.3$, much higher than determined here. Previous studies on whey protein gels highlight that the extent of relaxation $F(\infty)/F_E$ after indentation is yet poorly understood, as it depends significantly on the gelation conditions for instance (Shim and Mulvaney, 2001). Future work is needed to validate ν_d with a different methodology, to check if a VE relaxation overlaps in time with the PE relaxation, or if a different theoretical framework is required.

8. CONCLUSIONS

We have applied the experimental methodology of indentation-relaxation developed to characterize biomaterials to protein hydrogels. A poroelastic (PE) analysis, where the relaxation is sorely caused by the internal flow of solvent in the hydrogel, provides reasonably good fits of the experimental data, yet it is significantly improved (as extra regression parameters are used) if a small viscoelastic relaxation at short times is considered. The calculated diffusivity D and intrinsic permeabilities k are reasonable and comparable to other hydrogels in the literature. Extensive indentation experiments were conducted with whey protein gels in swelling equilibrium with solutions with different salt concentrations, thus at different swelling ratios. The estimated D increased slightly in more swollen gels, as expected, but it was unexpected that the drained Poisson's ratio ν_d decreased at high salt concentrations to values equal to zero or even negative, which requires further investigation. The proposed PE analysis considers for the first time that solvent equilibrium can also occur from the bottom of the hydrogel (BC2 model), reasonable from an experimental point of view, which improves the PVE relaxation fits and yields D values slightly higher than that of the self-diffusion of free water.

ACKNOWLEDGEMENTS

This work was supported by the project funding from the Priority Academic Program Development (PAPD) of Jiangsu Higher Education Institutions and the "Jiangsu Specially-Appointed Professors Program" of China, and the Youth Fund of Natural Science Foundation of Jiangsu Province of China (No. BK20140343).

REFERENCES

Cao, Y., Ma, D., Raabe, D., 2009. The use of flat punch indentation to determine the viscoelastic properties in the time and frequency domains of a soft layer bonded to a rigid substrate. Acta Biomater. 5, 240–248.

Chan, E.P., Deeyaa, B., Johnson, P.M., Stafford, C.M., 2012a. Poroelastic relaxation of polymer-loaded hydrogels. Soft Matter 8, 8234–8240.

Chan, E.P., Hu, Y., Johnson, P.M., Suo, Z., Stafford, C.M., 2012b. Spherical indentation testing of poroelastic relaxations in thin hydrogel layers. Soft Matter 8, 1492–1498.

Colsenet, R., Mariette, F., Cambert, M., 2005. NMR relaxation and water self-diffusion studies in whey protein solutions and gels. J. Agric. Food Chem. 53, 6784–6790.

Gallegos, C., Franco, J.M., 1999. Rheology of food, cosmetics and pharmaceuticals. Curr. Opin. Colloid Interface Sci. 4, 288–293. doi:10.1016/S1359-0294(99)00003-5

Hu, Y., Chan, E.P., Vlassak, J.J., Suo, Z., 2011a. Poroelastic relaxation indentation of thin layers of gels. J. Appl. Phys. 110, 086103.

Hu, Y., Chen, X., Whitesides, G.M., Vlassak, J.J., Suo, Z., 2011b. Indentation of polydimethylsiloxane submerged in organic solvents. J. Mater. Res. 26, 785–795.

Hu, Y., Zhao, X., Vlassak, J.J., Suo, Z., 2010. Using indentation to characterize the poroelasticity of gels. Appl. Phys. Lett. 96, 121904.

Kalcioglu, Z.I., Mahmoodian, R., Hu, Y., Suo, Z., Van Vliet, K.J., 2012. From macro-to microscale poroelastic characterization of polymeric hydrogels via indentation. Soft Matter 8, 3393–3398.

Lin, Y.-Y., Hu, B.-W., 2006. Load relaxation of a flat rigid circular indenter on a gel half space. J. Non-Cryst. Solids 352, 4034–4040.

Lucey, J.A., Johnson, M.E., Horne, D.S., 2003. Invited Review: Perspectives on the Basis of the Rheology and Texture Properties of Cheese. J. Dairy Sci. 86, 2725–2743. doi:10.3168/jds.S0022-0302(03)73869-7

Mercadé-Prieto, R., Falconer, R.J., Paterson, W.R., Wilson, D.I., 2007a. Swelling and dissolution of β-lactoglobulin gels in alkali. Biomacromolecules 8, 469–476.

Mercadé-Prieto, R., Sahoo, P.K., Falconer, R.J., Paterson, W.R., Wilson, D.I., 2007b. Polyelectrolyte screening effects on the dissolution of whey protein gels at high pH conditions. Food Hydrocoll. 21, 1275–1284.

Mercadé-Prieto, R., Wilson, D., Paterson, W.R., 2008. Effect of the NaOH concentration and temperature on the dissolution mechanisms of ß-lactoglobulin gels in alkali. Int. J. Food Eng. 4.

Oyen, M., 2014. Mechanical characterisation of hydrogel materials. Int. Mater. Rev. 59, 44–59.

Oyen, M.L., 2015. Nanoindentation of hydrated materials and tissues. Curr. Opin. Solid State Mater. Sci.

Özkan, N., Xin, H., Chen, X.D., 2002. Application of a depth sensing indentation hardness test to evaluate the mechanical properties of food materials. J. Food Sci. 67, 1814–1820.

Puvanenthiran, A., Williams, R., Augustin, M., 2002. Structure and visco-elastic properties of set yoghurt with altered casein to whey protein ratios. Int. Dairy J. 12, 383–391.

Shim, J., Mulvaney, S.J., 2001. Effect of heating temperature, pH, concentration and starch/whey protein ratio on the viscoelastic properties of corn starch/whey protein mixed gels. J. Sci. Food Agric. 81, 706–717.

Strange, D.G., Fletcher, T.L., Tonsomboon, K., Brawn, H., Zhao, X., Oyen, M.L., 2013. Separating poroviscoelastic deformation mechanisms in hydrogels. Appl. Phys. Lett. 102, 031913.

Strange, D.G., Oyen, M.L., 2012. Composite hydrogels for nucleus pulposus tissue engineering. J. Mech. Behav. Biomed. Mater. 11, 16–26.

Trappmann, B., Gautrot, J.E., Connelly, J.T., Strange, D.G., Li, Y., Oyen, M.L., Stuart, M.A.C., Boehm, H., Li, B., Vogel, V., 2012. Extracellular-matrix tethering regulates stem-cell fate. Nat. Mater. 11, 642–649.

Wang, Q.-M., Mohan, A.C., Oyen, M.L., Zhao, X.-H., 2014. Separating viscoelasticity and poroelasticity of gels with different length and time scales. Acta Mech. Sin. 30, 20–27.

AUTHORS BIOGRAPHY

Prof. Ruben Mercadé-Prieto

Ruben Mercadé-Prieto graduated in Chemical Engineering at the IQS School of Engineering, Ramon Llull University, in Barcelona, Spain (2002); while he was also studying Economics at the University of Barcelona. Postgraduate research diploma on protein fouling and cleaning with Prof. Xiao Dong Chen at the University of Auckland, NZ (2003). PhD in Chemical Engineering at the University of Cambridge, UK (2007) with Dr. Ian Wilson on protein gelation and dissolution in reactive conditions. He took a postdoctoral position at the University of Wisconsin – Madison, USA, with Prof. S. Gunasekaran working of food rheology (2008). He came back to UK, to the University of Birmingham, for two postdoctoral positions for projects sponsored by the UK government EPSRC and Procter & Gamble (2009-2013). In 2013 he moved to Suzhou, China, to the new School of Chemical and Environmental Enginnering at Soochow University. He was awarded the Jiangsu specially appointed Professor (2013). He has published 33 refereed journal articles, 26 of them as first author, and one book chapter.

His main research areas are soft matter and food engineering, combining chemical engineering principles with polymer physics, protein chemistry, computational simulation, and whatever is needed. In particular, he is interested in understanding reactive processes with biomacromolecules, as in food fouling and cleaning.

Joaquim Lopez

Joaquim Lopez graduated in Chemical Engineering and Bioprocesses at the IQS School of Engineering, Ramon Llull University, in Barcelona, Spain (2013). Winner of the price-scholarship granted by TECHNIP for the best incoming student for the Master's degree in Chemical Engineering. Currently he is pursuing a Master degree in Chemical Engineering at IQS School of Engineering. He recently came to Soochow University as a visiting student pursuing his Master's final year project.

Prof. Xiao Dong Chen

Xiao Dong Chen graduated in Engineering Mechanics from Tsinghua University (1987). PhD in Chemical and Process Engineering from Canterbury University in NZ (1991). MSc in Mathematics from University of New South Wales in Australia (2014). After working for Fonterra NZ for 2.5 years on food particle technology, he took up a lectureship at The University of Auckland, NZ. He was made a Personal Chair of Chemical Engineering in 2001 at The University of Auckland. In 2006, he was appointed to the Chair of Biotechnology and Professor of Chemical Engineering at Monash University, Melbourne, Australia. He has published over 440 refereed journal articles and 220 conference papers (over 30 were Keynote or Plenary

Lectures), 3 books, 20 book chapters, and over 50 reports on industrial consulting projects. From early 2010 to the end of 2012, he held a 1000-Talent National Chair Professor of Chemical Engineering and the Executive Headship of Chemical and Biochemical Engineering at Xiamen University. He is an Elected Fellow of Royal Society of New Zealand since 2001 and an Elected Fellow of Australian Academy of Technological Sciences and Engineering since 2007, and is a Fellow of IChemE (UK) from 2001.

His main areas of research are in bio-inspired chemical engineering, food engineering and biotechnology, separation processes including drying and membrane processing, heat transfer and mass transfer including fouling, cleaning and drying, safety processes including spontaneous combustion of solid materials, powder technology and powder functionality including food and pharmaceutical particulates.

In January 2013, he has begun his role as the University Distinguished Professor and Head of School at Soochow University (Suzhou, PR China). He has established a new School of Chemical and Environmental Engineering there. He has remained as Adjunct Professors at Xiamen University (China) and Monash University (Australia).

VIRTUALIZATION STRATEGIES FOR MODELING THE ENERGY TRANSFER IN A FOOD UNDERGOING RF HEATING

Tesfaye Faye Bedane[(a)], Francesco Marra[(b)]

[(a),(b)] Università degli studi di Salerno, Dipartimento di Ingegneria Industriale

[(a)]tbedane@unisa.it, [(b)]fmarra@unisa.it

ABSTRACT

Heating uniformity in radiofrequency (RF) heating of agricultural and food commodities is a challenge to overcome for the development and dissemination of commercial RF heating systems at industrial scale. Different experimental studies have been carried out to test the effectiveness of RF heating in different food processing techniques. Modeling and simulation remains as one of the best tool used to virtualize the challenges of heating non-uniformity and effective tool to analyze and characterize the heating patterns during RF heating. Different strategies used to build-up virtualization of RF heating were briefly discussed in this paper. Dielectric and thermos-physical properties of the product subjected RF heating the key-factors to link the fundamental modeling approach with the data related to the investigated food material. The energy transfer across the food sample due to the RF heating and external convection effects have been discussed. Alternatively, using representative food samples like tylose with known thermo-physical and dielectric properties are also another strategy to be used to describe RF heating system.

Keywords: modelling, RF heating, energy transfer, food heating

1. INTRODUCTION

In recent years, the application of radio-frequency (RF) heating in agro-food processing has got wide applications due to the advantage of fast heating. Recently, a lot of interesting studies have been carried out on the application of RF heating in meat processing (Farag et al., 2008 and 2011; Marra et al., 2007; Uyar et al., 2014 and 2015), in post-harvest treatment and disinfestation of fruits (Birla et al, 2004; Wang et al., 2002, 2003 and 2006a; Alfaifi et al., 2012 and 2015).

In RF heating applications in agricultural and food processing technologies, the heating non-uniformity is mainly dependent on the power absorption capacity of the material subjected to heating. This heating non-uniformity remains a challenge to be solved to widen the application of RF heating commercially in industrial scale.

Different authors have been studied different methods and strategies to improve the heating uniformity during RF heating. For example, Birla et.al. (2008) reported that placing the sample at the center point between two parallel electrodes improved heating uniformity during RF disinfestation of fruits. Similar strategy was also proposed and used by Tiwari et al. (2011a) and Liu et. al. (2013). The use of forced air surface heating, mixing and product movement to improve heating uniformity during RF treatment of walnuts was also promising strategy proposed and applied by Wang et. al. (2005 and 2007). In their recent study, Wang et.al. (2014) also demonstrated a systematic means to evaluate RF heating uniformity by using polyurethane foams in drying of agricultural commodities.

The use of model materials such as tylose with consistent and stable properties to replace more complicated heterogeneous materials is the first step to gain insights about the RF heating patterns during RF assisted heating of food products.

2. COMPUTER VIRTUALIZATION OF RF HEATING

Computer virtualization of processes is a powerful tool which can be used as virtual laboratory to get insights of heating patterns and to during RF heating. The mathematical modeling of RF heating systems has been discussed by (Neophytou and Metaxas, 1998; Yang et al., 2003; Chan et al., 2004; Marra et al., 2007 and 2009; Birla et al., 2008; Romano and Marra, 2008; Tiwari et al., 2011; Wang et al., 2012; Uyar et al., 2015; Llave et al., 2015) for different types of products in different heating systems. The heating system in RF heating fall into two categories of energy transfer, which are the heat transfer within the material subjected to RF heating and the electric and magnetic fields.

The mathematical description of heat transfer in the food product which is placed between two electrodes is given by unsteady state heat equation with a generation term derived from electromagnetic equations.

The heat equation is given by:

$$\rho\, C_p\, \frac{dT}{dt} = \underline{\nabla} \cdot k\underline{\nabla}T + P_{abs} \qquad (1)$$

where T is the temperature within the sample, t is the time, k is thermal conductivity, ρ is the density, C_p is the heat capacity and P_{abs} is the power absorbed due to RF.

The power density or power dissipation per unit volume:

$$P_{abs} = 2\,\pi\,f\,\varepsilon_0\,\varepsilon_r''\,\left|\underline{E}\right|^2 \qquad (2)$$

The power density absorbed by lossy dielectric material is proportional to the frequency applied and the dielectric loss factor and proportional to the square of electric field.
The prediction of electromagnetic field distribution in RF heating is important to determine the power absorption density within the food product. Hence Maxwell's equations which relate the electric charge density, ρ_c; electric field, $\underline{E}$; electric displacement, $\underline{D}$; current, $\underline{J}$; magnetic field intensity, $\underline{H}$ and magnetic flux density, $\underline{B}$.

$$\underline{\nabla} \times \underline{H} = \underline{J} + \frac{\partial \underline{D}}{\partial t} \qquad (3)$$

$$\underline{\nabla} \times \underline{E} = -\frac{\partial \underline{B}}{\partial t} \qquad (4)$$

$$\underline{\nabla} \cdot \underline{D} = \rho_c \qquad (5)$$

$$\underline{\nabla} \cdot \underline{H} = 0 \qquad (6)$$

Based on the assumption of fields to be time-harmonic (Neophytou and Metaxas, 1998), combination of Maxwell's equation could be reduced to the following wave equation in frequency domain (Marra et al., 2009).

$$\underline{\nabla} \times \frac{1}{\mu_r} \underline{\nabla} \times \underline{E} - \omega^2\,\mu_0\,\varepsilon_0\,\varepsilon_r\,\underline{E} = 0 \qquad (7)$$

When a quasi-static approach is assumed, equation (5) could be reduced to the following:

$$\underline{\nabla} \cdot \left[(\sigma + j\,\omega\,\varepsilon)\underline{\nabla} V\right] = 0 \qquad (8)$$

where the electric potential, V is related to the electric field by:

$$\underline{E} = -\underline{\nabla} V \qquad (9)$$

The solution of the both heat equation and electromagnetic field equation are subjected assigning appropriate to initial and boundary conditions to come up with consistent and valid mathematical simulation of the process. The common initial and boundary conditions (BCs) used in solving heat equation are, uniform initial temperature of product and convection heat transfer on the boundaries of the product subjected to RF heating respectively. For the case of electromagnetic field distribution, an electric potential value or distribution is applied to the upper electrode while the bottom electrode is at ground condition. The RF applicator walls are also electrically insulated. Figure 1, where typical configuration of parallel electrode RF system is shown, allow to better focus on the whole domain representation and to visualize where the previously discussed BCs are applied.

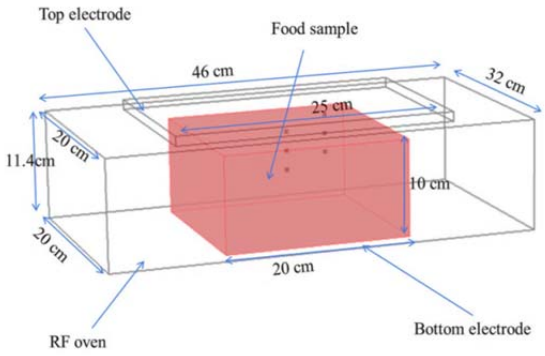

Figure 1: Typical configuration of parallel electrode RF system (adapted from Uyar et al., 2015)

3. VIRTUALIZATION STRATEGIES IN RF HEATING

Modeling of RF heating involves characterization of possible parameters and consideration of best configurations in the RF heating system. Different virtualization strategies have been proposed by different researchers since the first 3D FEM based mathematical model of RF heating by Neophytou and Metaxas, (1998). These strategies involve a number of issues which arise when processes assisted by RF are considered. Before modeling RF heating of foods, a number of questions require proper answers:

a) In order to describe the electric field displacement, it is necessary to consider the whole set of Maxwell's equations?
b) When the so called quasi-static approach is allowed?
c) It is possible to use constant values of dielectric (and thermos-physical) properties? Or it is always recommended to use empirical values/expressions as functions of the local temperature?
d) In the last case of point c), it is sufficient to consider the dielectric and thermos-physical properties as functions of the temperature, or also their dependence on moisture content (and, in some cases, in ionic concentration)?
e) What is the importance (and the role) of mass transfer? In other words, it is always sufficient to consider the set of equations previously introduced or also mass transfer equation(s) must be considered?
f) If also mass transfer has to be considered, what mass component is the more relevant? Moisture content? Ionic content? Fraction of free water with respect to bounded water?

g) If also moisture transfer has to be considered, what is the more appropriate mass transfer approach? The porous media approach (Datta, 2007)? The kinetic like approach (Marra et al., 2010)?
h) What happens when phase change has to be considered?
i) What about boundary conditions? When external convective heat transfer should be taken into account by solving the momentum transfer and the heat and mass transfer in the environment surrounding the food sample?
j) What about validation?

The answers to the questions listed above are not unique and the strategy of virtualization must be driven by the objective(s) of the research. Some examples are discussed below.

Under the hypothesis of quasi-static approach, Marra et al. (2007) solved coupled heat transfer and electromagnetic equations for a cylindrical shaped meat batters and demonstrated that quasi-static hypothesis to be successful in lab scale RF system. Different strategies have been applied by different researchers to find out how to improve the heating uniformity of the RF heating. Moving or rotating in water surrounding system has been proposed and used in modeling/experimental study about RF heating of high water content commodities like fruits (Birla et al., 2008) and for low moisture foods, use of polyetherimide (PEI) blocks, hot air assistance, intermittent stirring, electrode configuration and use of plastic sheets surrounding the product to enhance heating (Jiao et al, 2015; Alfaifi et al., 2014).

Virtualization of the processes also includes the assumptions and specific considerations about numerical parameters and also about process parameters involved in it. When a rough solution is sufficient for a preliminary analysis, one may choose to work with a coarse mesh, in order to deal with a numerical procedure less demanding in terms of computing power. The same strategy is not acceptable when the goal of virtualization is to have a model which is independent by the mesh grid. Another example, the latent heat peak during thawing of foods needs special consideration in order to simplify simulation complexities and time. Uyar et al. (2015) used apparent specific heat method in virtualization of lean beef meat undergoing thawing assisted by RF heating. The following section is about this topic.

As mentioned above, the virtualization strategy should include also a motivated decision on the set of BCs to be considered. In case of relevant convective contributions from the external environment toward the food product, the model should take into account (and, thus, should include) also the heat and mass transfer in the surrounding environment, and with it the momentum transfer too.

3.1 An example: meat thawing assisted by RF

In food processing industries tempering and thawing are the two main processes involved in heating frozen food products to required temperature for further processing or to make it ready for consumption. Tempering is considered as pre-thawing process, since it is used to increase the temperature of the product from frozen state to a temperature point where it is usable without causing harm to subsequent processing operations. Thawing is increasing frozen product temperature to melted or unfrozen state. RF assisted tempering and thawing have been experimentally studied and models were also developed to virtualize the heating patterns as well as to allocate the hot and cold spots during the process (Farag et al., 2008 and 2011; Llave et al., 2015; Uyar et al., 2015).

As shown in figure 2, where the temperature distribution (in °C) in a sample of beef meat during RF thawing is reported, the thawing process cannot be followed as a simple problem of monitoring the cold spot (which is located in the heart of the sample) but also in terms of a problem of overheating (as it happens in the areas colored in brown-red). Thus, here the virtualization strategy cannot ignore complex mechanisms happening at boundaries (at corners especially). These areas undergo phase change with subsequent severe changes in thermos-physical and dielectric properties.

Determination of RF power density (P_{abs}) distribution in the sample during the process is a key-step as well. Figure 3 shows the power density (in W/m^3) distribution (at side slice) in lean beef thawed by RF assisted heating at early stage of the process. In this figure it is possible to appreciate the great variability of power density values. At same time, it is possible to appreciate that in the strategy of virtualization – in this case – is to have a preliminary rough solution, being the mesh grid quite coarse.

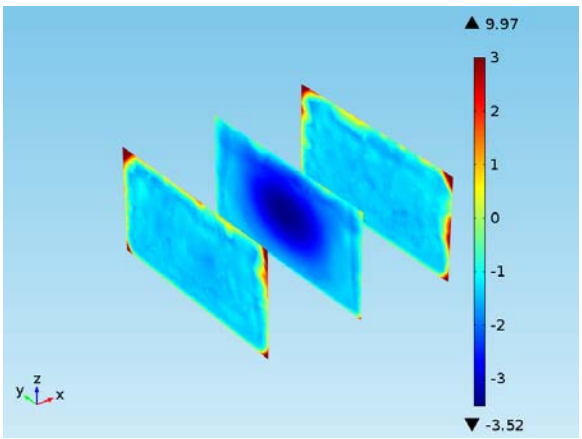

Figure 2: Temperature distribution [°C] in the sample during RF thawing of beef meat.

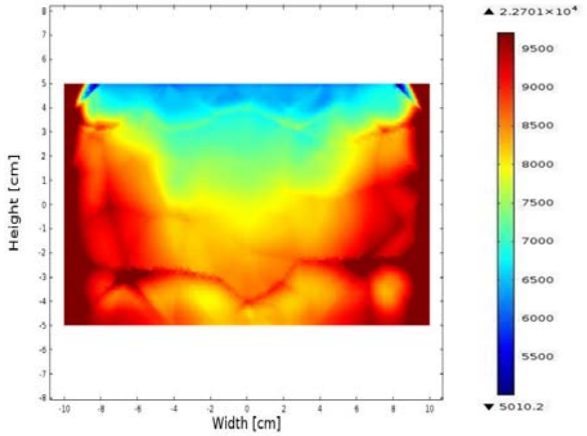

Figure 3: Power density [W/m^3] distribution (at side slice) in lean beef thawed by RF assisted heating, after 1 minute of processing.

4. CONCLUSIONS

Virtualization of complex processes, such as food heating assisted by radio-frequencies, should be based on a strategy which includes a number of steps related to what is simulated (definition of the process), where it is simulated (definition of a domain), how it is simulated (definition of the equations' set and of the solution procedure). A number of essential questions as been proposed and example of virtualization strategy have been discussed, with a focus on RF thawing of foods.

5. REFERENCES

Alfaifi, B., Tang, J., Jiao, Y., Wang, S., Raso, B., Jiao, S., Sablani, S. 2014, Radiofrequency disinfestation treatment for dries fruit: model development and validation. Journal of Food Engineering. 120: 268-276.

Birla, S.L., Wang, S., Tang, J. 2008. Computer simulation of radio frequency heating of model fruit immersed in water. Journal of Food Engineering. 84: 270–280.

Datta, A.K. 2007. Porous media approaches to studying simultaneous heat and mass transfer in food processes. I: Problem formulations. Journal of Food engineering, 80 (1): 80-95.

Farag, K.W., Lyng, J.G., Morgan, D.J. and Cronin, D.A. 2008a. A comparison of conventional and radio frequency tempering of beef meats: effects on product temperature distribution. Meat Science. 80: 488-495.

Farag, K.W., Lyng, J.G., Morgan, D.J. and Cronin, D.A. 2011. A comparison of conventional and radio frequency thawing of beef meats: effects on product temperature distribution. Food and Bioprocess Technology. 4: 1128-1136.

Jiao, Y., Tang, J., Wang, S. and Koral, T. 2014. Influence of dielectric properties on the heating rate in free-running oscillator radio frequency systems. Journal of Food Engineering. 120: 197-203.

Liu, Y., Wang, S., Mao, Z., Tang, J., Tiwari, G. 2013. Heating patterns of white bread loaf in combined radiofrequency and hot air treatment.

Llave, Y., Liu, S., Fukoka, M., Sakai, N. 2015. Computer simulation of radiofrequency defrosting of frozen foods. Journal of Food Engineering. 152:32-42.

Marra, F., Lyng, J., Romano, V. and McKenna, B. 2007. Radio-frequency heating of foodstuff: solution and validation of a mathematical model. Journal of Food Engineering. 79: 998–1006.

Marra, F., Zhang, L., Lyng, J.G. 2009. Radio frequency treatment of foods: Review of recent advances. Journal of Food Engineering. 91:497-508.

Neophytou, R.I., Metaxas, A.C., 1998. Combined 3D FE and circuit modeling of radiofrequency heating systems. Journal of Microwave Power and Electromagnetic Energy 33 (4), 243–262.

Tiwari, G., Wang, S., Tang, J. and Birla, S.L. 2011. Computer simulation model development and validation for radio frequency (RF) heating of dry food materials. Journal of Food Engineering. 105: 48–55.

Uyar, R., Bedane, T.F., Erdogdu, F., Palazoglu, T.K., Farag, K.W., Marra, F. 2015. Radio-frequency thawing of food products-Acomputational study. Journal of Food Engineering. 146:163-171.

Uyar, R., Erdogdu, F, and Marra, F. 2014. Effect of volume on power absorption and temperature evolution during radio-frequency heating of meat cubes: a computational study. Food and Bio-products Processing. 92:243-251.

Wang, S., Monzon, M., Johnson, J.A., Mitcham, E.J., Tang, J. 2007. Industrial-scale radiofrequency treatments for insect control in walnuts I: Heating uniformity and energy efficiency. Postharvest Biology and Technology. 45:240-246.

Wang, S., Yue, J., Tang, J., Chen, B. 2005. Mathematical modelling of heating uniformity for in-shell walnuts subjected to radiofrequency treatments within intermittent stirrings. Postharvest Biology and Technology. 35:97-107.

Wang, Y., Zhang, L., Gao, M., Tang, J., Wang, S. 2014. Evaluating radiofrequency heating uniformity using polyurethane foams. Journal of Food Engineering. 136:28-33.

REACTION ENGINEERING METHODOLOGY AS AN EFFECTIVE APPROACH TO MODEL DRYING, BAKING AND WATER VAPOR SORPTION PROCESSES

Aditya Putranto, Xiao Dong Chen[(a)], Ruben Mercadé-Prieto[(b)]

Affiliation Suzhou Key Lab of Green Chemical Engineering, School of Chemical and Environmental Engineering, College of Chemistry, Chemical Engineering and Material Science, Soochow University, Jiangsu Province, China

[(a)] xdchen@suda.edu.cn, [(b)]ruben@suda.edu.cn ,

ABSTRACT

An effective model of simultaneous heat and mass transfer processes is useful to assist in process design, optimization of existing processes and monitoring product quality. Previously, the lumped reaction engineering approach (L-REA) has been shown to model the global drying rate of several heat and mass transfer processes very well. Here, the REA framework is implemented to model the local evaporation/condensation rate in drying of non-food materials, baking and water vapor sorption. The REA is combined with a set of equations of conservation of heat and mass transfer to yield the S-REA (spatial reaction engineering approach) to model these processes. For modeling each process, the activation energy is generated from one accurate run and evaluated according to environmental temperature and humidity. The relative activation energy implemented in the L-REA is implemented in the S-REA by applying local variables. The results indicate that the S-REA is accurate to describe baking, drying and water vapor sorption process, which shows the applicability of the REA to model the local evaporation/condensation rate of these processes. The S-REA is readily implemented to assist in process design, evaluation of existing processes and maintenance of product quality. In near future, by coupling with solid mechanics, the REA may be employed to predict material deformation and shape change during heat and mass transfer processes by coupling with solid mechanics. The development of the REA to describe migration of volatiles inside materials undergoing heat and mass transfer processes is also underway.

Keywords: reaction engineering approach, drying, baking, water vapor sorption, model

1. INTRODUCTION

Several heat and mass transfer processes including drying, baking and water vapor sorption are commonly applied in industry. For process design of new equipment and evaluation of current processes, a reliable mathematical model is useful. The model may also be used to predict product quality during the processes. The reaction engineering approach (REA), a semi-empirical approach, was proposed in 1996 and initially used to model thin layer drying of food materials (Chen and Lin, 2005; Lin and Chen, 2006; 2007). The model accurately captures the major physics of drying. The relative activation energy, a material characteristic, basically expresses the difficulty to remove the moisture from the materials. The removal of both free and bound moisture is captured by the relative activation energy. The REA has advantages of simplicity, accuracy and effectiveness with respect to generating the drying parameters. Only one accurate drying run is required to generate the parameters (Chen, 2008). The REA in its lumped format, later called as the lumped reaction engineering approach (L-REA), has accurately modeled several challenging heat and mass transfer processes. In this study, the REA is combined with a set of equations of conservation of heat and mass transfer to yield the S-REA to model drying of non-food materials, baking and water vapor sorption. This study aims to develop S-REA and implement it in the study of several heat and mass transfer processes. Its accuracy is examined by benchmarking model results against high quality experimental data reported in the literature.

2. MATHEMATICAL MODELING

For drying, the applicability of the S-REA to describe the drying processes was benchmarked towards the experimental data of drying of honeycomb (Dhall et al, 2012) while for baking and water vapor sorption, the validity of the S-REA is tested towards Zhang and Chen (2014) and Li et al (2014), respectively. The S-REA consists of a set of equations of microscopic heat and mass balance in which the REA is used to describe the local evaporation/condensation rate. For drying of honeycomb (Dhall et al, 2012), the mass balance of liquid water in Lagrangian coordinate, which allows expansion and contraction of the matrix, is written as (Putranto and Chen, 2013a,b):

$$\frac{\partial(C_s X)}{\partial t} = \frac{1}{r}\frac{\partial}{\partial r}\left(D_w r \frac{\partial(C_s X)}{\partial r}\right) - \dot{I} \qquad (1)$$

where Dw is the local surface diffusivity (m2 s-1), X is the concentration of liquid water (kg H2O kg dry solids-1), Cs is the solids concentration (kg dry solids m-3)

which can change if the structure changes, is the evaporation or condensation rate (kg H2O m-3 s-1) and is positive when evaporation occurs locally.

The mass balance of water in the vapor phase (water vapor) in spherical coordinate system is expressed as (Putranto and Chen, 2013a,b):

$$\frac{\partial C_v}{\partial t} = \frac{1}{r}\frac{\partial}{\partial r}(D_v r \frac{\partial C_v}{\partial r}) + \dot{I} \quad (2)$$

where D_v is the local effective vapor diffusivity ($m^2\ s^{-1}$) and C_v is the concentration of water vapor (kg H_2O m^{-3}).

The heat balance is represented by the following equation (Putranto and Chen, 2013[a,b]):

$$\rho\ C_p\ \frac{\partial T}{\partial t} = \frac{1}{r}\frac{\partial}{\partial r}(k\ r\ \frac{\partial T}{\partial r}) - \dot{I}\ \Delta H_v \quad (3)$$

where T is the sample temperature (K), k is the local thermal conductivity of sample (W m^{-1} K^{-1}), ΔH_v is the water vaporization heat (J kg^{-1}), C_p is the local specific heat of sample (W m^{-1} K^{-1}) and ρ is the local sample density (kg m^{-3}).

The initial and boundary conditions for equations (1) to (3) are:

$$t=0,\ X=X_o,\ C_v=C_{vo},\ T=T_o \quad (4)$$

$$r=0,\ \frac{dX}{dr}=0\ ,\ \frac{dC_v}{dr}=0\ ,\ \frac{dT}{dr}=0 \quad (5)$$

$r=R$,

$$-C_s D_w \frac{dX}{dr} = h_m \varepsilon_w (\frac{C_{v,s}}{\varepsilon} - \rho_{v,b}) \quad (7)$$

$$-D_v \frac{dC_v}{dr} = h_m \varepsilon_v (\frac{C_{v,s}}{\varepsilon} - \rho_{v,b}) \quad (8)$$

$$k\frac{dT}{dr} = h(T_b - T) \quad (9)$$

where R is the sample radius (m), h is the heat transfer coefficient ($W.m^{-2}.K^{-1}$), ε_w and ε_v are fraction of surface area influenced by liquid water and water vapor respectively.

I is the local evaporation/condensation rate within the solid structure described as (Putranto and Chen, 2013a,b):

$$\dot{I} = h_{m_{in}} A_{in} (C_{v,s} - C_v) \quad (9)$$

where $h_{m,in}$ is the internal mass transfer coefficient (m.s-1), A_{in} is the total internal surface area available for phase change ($m^2.m^{-3}$ $C_{v,s}$ is the internal-solid-surface water vapor concentration (kg.m-3). Although the void space inside the samples may be large enough, the incorporation of the advection term in the S-REA is not necessary since its term has been captured by the local evaporation/condensation term as represented by equation (9).

By implementing the REA, the internal-surface water vapor concentration can be written as (Putranto and Chen, 2013a,b):

$$C_{v,s} = \exp(\frac{-\Delta E_v}{RT}) C_{v,sat} \quad (10)$$

where $C_{v,sat}$ is the internal-saturated water vapor concentration (kg m^{-3}).

Therefore, the local evaporation rate can be expressed as (Putranto and Chen, 2013[a,b]):

$$\dot{I} = h_{m_{in}} A_{in} [\exp(\frac{-\Delta E_v}{RT}) C_{v,sat} - C_v] \quad (11)$$

The relative activation energy of honeycombs is generated from one accurate drying run at temperature of 103 °C. The relationship between the relative activation energy and average moisture content is assumed to be represented by simple mathematical equation obtained by least square method using Microsoft Excel®. The relative activation energy was found to be suitably fitted as:

$$\frac{\Delta E_v}{\Delta E_{v,b}} = -138685(X - X_b)^5 + 50405(X - X_b)^4 - 6953.5(X - X_b)^3 + 466.12(X - X_b)^2 - 17.616(X - X_b) + 1.0053 \quad (12)$$

For baking and water vapor sorption, the S-REA, similar to the ones written in equations (1) to (3) are setup and implemented. This is then combined with appropriate relative activation energies of dough during baking (Zhang and Chen, 2014) and silica gel during water vapor sorption (Li et al, 2007). The relative activation energy of dough can be written as:

$$\frac{\Delta E_v}{\Delta E_{v,b}} = -55.754(\overline{X} - X_b)^5 + 113.95(\overline{X} - X_b)^4 - 96.768(\overline{X} - X_b)^3 + 40.609(\overline{X} - X_b)^2 - 8.385(\overline{X} - X_b) + 1.006 \quad (13)$$

While the relative activation energy of silica gel can be expressed as:

$$\frac{\Delta E_v}{\Delta E_{v,b}} = -4.19(\overline{X} - X_b)^4 - 15.66(\overline{X} - X_b)^3 + 3.192(\overline{X} - X_b)^2 - 10.063(\overline{X} - X_b) + 1 \quad (14)$$

In order to yield the spatial profiles of moisture content, concentration of water vapor and temperature, equations (1) to (3) are solved simultaneously in conjunction with the initial and boundary conditions (shown in equations (4) to (8) and the appropriate relative activation energy.

3. RESULTS AND DISCUSSION

For convective drying of honeycombs, as suggested by Dhall et al (2012), the liquid diffusivity of 10^{-10} $m^2.s^{-1}$ is used. Interestingly, as shown in Figure 1, the liquid

diffusivity of lower than $1x10^{-10}$ m^2s^{-1} does not result in any noticeable differences in the moisture content and temperature profiles. This may indicate that the modeling is independent on surface diffusivity and hence the surface diffusion term may be neglected in the modeling. Without incorporating the surface diffusion term, the results of modeling of drying of honeycombs at temperature of 103 and 137 °C are shown in Figures 2 and 3. A good agreement towards the experimental data is shown (R^2 of higher than 0.998 for moisture content and R^2 of higher than 0.993 for temperature). Benchmarks against the modeling implemented by Dhall et al (2012) shows that the S-REA yields closer agreement to the experimental data. The S-REA is accurate to model both moisture content and temperature profiles at drying air temperature of 103 and 137 °C.

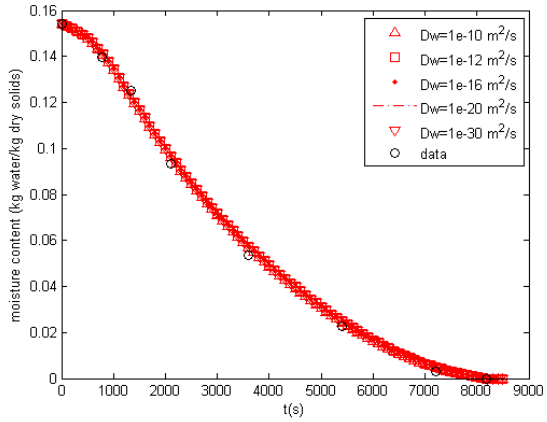

Figure 1. Sensitivity of effective liquid diffusivity towards profiles of moisture content during drying of honeycombs at temperature of 137 °C (Putranto and Chen, 2015)

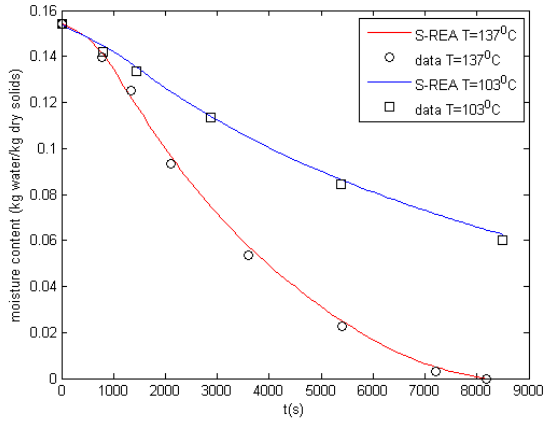

Figure 2. Profiles of moisture content during drying of honeycombs at temperature of 103 and 137 °C (Putranto and Chen, 2015)

For baking, the moisture content profiles during baking of 0.5 and 1 g bread are shown in Figure 4. A good agreement towards the experimental data is shown (R^2 of 0.992 and 0.988 for 0.5 and 1 g bread, respectively). Figure 5 shows the spatial profiles of moisture content during baking of 1 g of bread at baking temperature of 235 °C. The profiles at the outer part of the samples are lower than those at the inner part which indicate that the moisture migrate outwards during baking. The profiles decrease during baking time since the moisture in the samples depletes as baking progresses. The S-REA models well the baking process which could be due to the applicability of the REA to represent the local evaporation/condensation rate during baking. The relative activation energy seems to be sufficiently accurate to capture the local evaporation/condensation inside the samples coupled with starch gelatization, protein denaturation and browning.

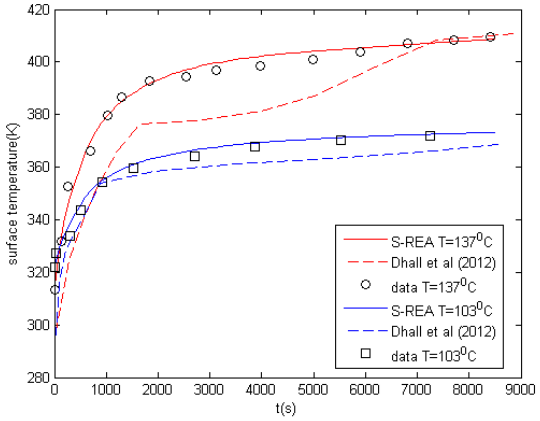

Figure 3. Profiles of surface temperature during drying of honeycombs at temperature of 103 and 137 °C (Putranto and Chen, 2015).

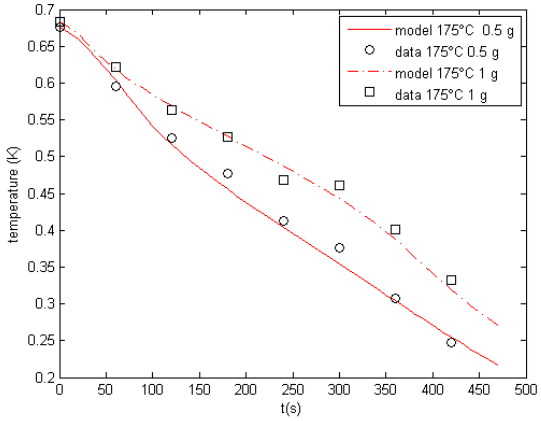

Figure 4. Profiles of average moisture content during baking of bread at baking temperature of 175 °C (Putranto and Chen, 2015)

For water vapor sorption, similar to the convective drying of honeycombs, the varied values of surface diffusivity do not give any noticeable differences in the profiles. Without using the surface diffusion term, the profiles of average moisture content are shown in Figure 6 while the profiles of spatial one are indicated in Figure 7. The S-REA models accurately the water vapor sorption which may be because the REA describes well the local condensation rate. The applicability of the REA indicates that the relative

activation energy used to model the global wetting rate (refer to equation (16)) (Putranto and Chen, 2014) is also applicable to model the local wetting rate of water vapor sorption.

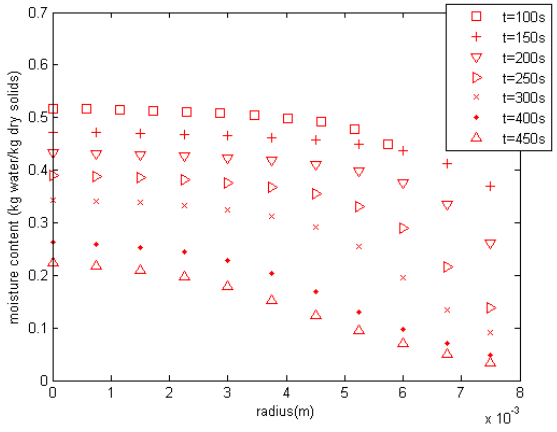

Figure 5. Spatial profiles of moisture content during bread baking of 1 g of bread at baking temperature of 235 °C (Putranto and Chen, 2015)

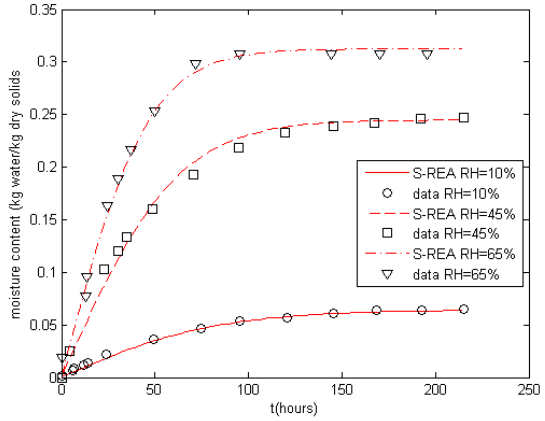

Figure 6. Profiles of moisture content during water vapor sorption at various relative humidity (Putranto and Chen, 2015)

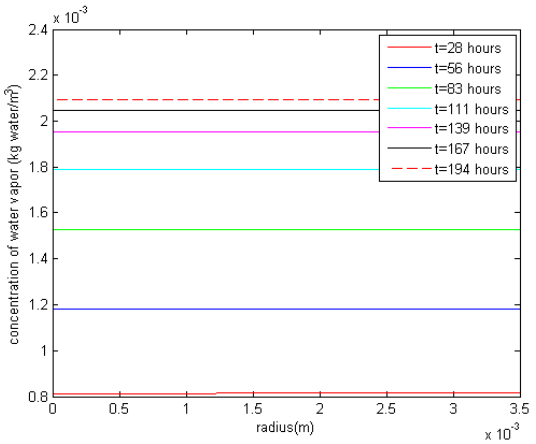

Figure 7. Spatial profiles of concentration of water vapor inside silica gel during water vapor sorption at relative humidity of 10% (Putranto and Chen, 2015)

4. CONCLUSIONS

In this study, the applicability of the S-REA to describe several simultaneous heat and mass transfer processes is demonstrated. The S-REA is accurate to model the convective drying, baking and water vapor sorption. This accuracy indicates that the REA is applicable to model the local evaporation/condensation rates during the processes. The combination of relative and equilibrium activation energy results in a unique relationship of activation energy which can describe the local structural changes during the simultaneous heat and mass transfer processes, as affected by the environmental conditions.

REFERENCES

Chen, X.D., 2008. The basics of a reaction engineering approach to modeling air drying of small droplets or thin layer materials, Drying Technology 26, 627-639.

Chen, X.D., Lin, S.X.Q., 2005. Air drying of milk droplet under constant and time dependent conditions, AIChE Journal 51, 1790-1799.

Chen, X.D., Putranto, A., 2013. Modeling Drying Processes: A Reaction Engineering Approach. Cambridge University Press, U.K.

Dhall, A., Squier, G., Geremew, M., Wood, W.A., George, J., Datta, A.K., 2012. Modeling of Multiphase Transport during Drying of Honeycomb Ceramic Substrates. Drying Technology, 30: 607–618.

Li, X., Li, Z., Xia, Q., Xi, H., 2007. Effects of pore sizes of porous silica gels on desorption activation energy of water vapour. Applied Thermal Engineering 27, 869–876.

Lin, S.X.Q., Chen, X.D., 2006. A model for drying of an aqueous lactose droplet using the reaction engineering approach. Drying Technology 24, 1329-1334.

Lin, S.X.Q., Chen, X.D., 2007. The reaction engineering approach to modeling the cream and whey protein concentrate droplet drying. Chemical Engineering and Processing 46, 437-443.

Putranto, A., Chen, X.D., 2013[a]. Spatial reaction engineering approach (S-REA) as an alternative for non-equilibrium multiphase mass transfer model for drying of food and biological materials. AIChE Journal 59, 55-67.

Putranto, A., Chen, X.D., 2013[b]. Multiphase drying modeling of intermittent drying using the spatial reaction engineering approach (S-REA). Chemical Engineering and Processing: Process Intensification 70, 169-183.

Putranto, A., Chen, X.D., 2014. Modeling of water vapor sorption process by employing the reaction engineering approach (REA). Separation and Purification Technology 122, 456-461.

Putranto, A., Chen, X.D., 2015. Spatial reaction engineering approach (S-REA): an effective approach to model drying, baking and water vapor sorption process. Chemical Engineering Research

and Design (accepted on 4 May 2015, http://dx.doi.org/10.1016/j.cherd.2015.05.004)
Zhang, L., Chen, X.D., 2014. Bakery products in China. Bakery Products: Science and Technology 2nd edition. John Wiley&Sons, New York

AUTHORS BIOGRAPHY

Xiao Dong Chen was born in Beijing in 1965. BE in Engineering Mechanics from Tsinghua University (1987). PhD in Chemical and Process Engineering from Canterbury University in NZ (1991). MSc in Mathematics from University of New South Wales in Australia (2014). After working for Fonterra NZ for 2.5 years on food particle technology, he took up a lectureship at The University of Auckland, NZ. He was made a Personal Chair of Chemical Engineering in 2001 at The University of Auckland. In 2006, he was appointed to the Chair of Biotechnology and Professor of Chemical Engineering at Monash University, Melbourne, Australia. He has published over 440 refereed journal articles and 220 conference papers (over 30 were Keynote or Plenary Lectures), 3 books, 20 book chapters, and over 50 reports on industrial consulting projects. From early 2010 to the end of 2012, he held a 1000-Talent National Chair Professor of Chemical Engineering and the Executive Headship of Chemical and Biochemical Engineering at Xiamen University. He is an Elected Fellow of Royal Society of New Zealand since 2001 and an Elected Fellow of Australian Academy of Technological Sciences and Engineering since 2007, and is a Fellow of IChemE (UK) from 2001.

His main areas of research are in bio-inspired chemical engineering, food engineering and biotechnology, separation processes including drying and membrane processing, heat transfer and mass transfer including fouling, cleaning and drying, safety processes including spontaneous combustion of solid materials, powder technology and powder functionality including food and pharmaceutical particulates.

In January 2013, he has begun his role as the University Distinguished Professor and Head of School at Soochow University (Suzhou, PR China). He has established a new School of Chemical and Environmental Engineering there. He has remained as Adjunct Professors at Xiamen University (China) and Monash University (Australia).

Author's Index